Towards the elucidation of voriconazole pharmacokinetics: quantitative insights into distribution and metabolism processes in humans

Inaugural-Dissertation

to obtain the academic degree

Doctor rerum naturalium (Dr. rer. nat.)

submitted to the Department of Biology, Chemistry, Pharmacy

of Freie Universität Berlin

by

Josefine Schulz

2022

Declaration of authorship

I hereby confirm that I have authored the submitted dissertation independently and that I have not used any sources and aids other than those indicated by me.

This dissertation was prepared from 2018 to 2022 under the supervision of Prof. Dr. Charlotte Kloft at the Institute of Pharmacy, Freie Universität Berlin.

1st Reviewer: Prof. Dr. Charlotte Kloft

2nd Reviewer: Prof. Dr. Markus Zeitlinger

Date of defense: 11 July 2022

Abstract

Invasive fungal infections are an increasing threat to the global public health causing approximately 1.5 million deaths worldwide every year. As the emergence and spread of resistance to antimycotics is expanding and the development of new antifungal agents is lagging behind this epidemiological burden, one important aspect is the rational use of existing drugs, such as voriconazole (VRC). Despite its long-term and frequent application in humans, VRC pharmacokinetics (PK) are still not fully understood revealing large intra- and interindividual variability as well as therapy failures and adverse events. The main source of variability is assumed to derive from the extensive metabolism of VRC involving the cytochrome P450 (CYP) isoenzymes 2C19, 2C9 and 3A4. Furthermore, the target site of VRC, i.e. the interstitial space fluid (ISF), is more relevant for PK investigations in contrast to the usually determined plasma concentrations. A powerful tool for ISF investigations is the minimally-invasive sampling technique microdialysis, which allows the continuous sampling of protein-unbound drug over time.

Therefore, the present thesis aimed at contributing to the elucidation of VRC PK by generating mechanistic and quantitative insights into its distribution and metabolism processes in humans to ultimately support the optimisation of VRC dosing strategies. To achieve this objective, research in three main areas was performed. First, a versatile bioanalytical liquid chromatography-tandem mass spectrometry (LC-MS/MS) assay was developed and validated for the quantification of VRC and its metabolites in various biological matrices. Second, *in vitro* metabolism investigations were performed for a comprehensive characterisation of VRC and its metabolites as substrates and inhibitors of CYP2C19, CYP2C9 and CYP3A4. Third, *in vitro* and *in vivo* microdialysis investigations were performed evaluating the application of simultaneous microdialysis of VRC and its potentially toxic metabolite, voriconazole *N*-oxide (NO) in humans.

The developed bioanalytical LC-MS/MS assay enabled the simultaneous quantification of VRC, NO and hydroxyvoriconazole (OH-VRC) in human plasma, ultrafiltrate and microdialysate as well as in the *in vitro* matrices of human liver/intestine microsomes (HLM/HIM) and recombinant human CYP (rhCYP) isoenzymes. In a first step, the assay was fully validated according to the European Medicines Agency guideline on bioanalytical method validation for the quantification of VRC and NO in plasma and microdialysate. Overall, the quantification was rapid, simple and feasible for clinically relevant concentrations of VRC and NO from 5 to 5000 ng/mL in plasma and ultrafiltrate as well as from 4 to 4000 ng/mL in microdialysate. Due to the high sensitivity of the assay, only 20 µL of plasma or ultrafiltrate and 5 µL of microdialysate were required. For VRC and NO in plasma and microdialysate, between-run accuracy was high with a maximum mean deviation of 7.0% from the nominal concentration and between-run precision was

demonstrated by ≤11.8% coefficient of variation. Stability under various conditions was demonstrated for both compounds. In a second step, the assay was successfully adapted for PK analyses in *in vitro* experiments covering a concentration range of 0.1 to 500 ng/mL for NO and of 1.0 to 500 ng/mL for OH-VRC at a sample volume of 20 µL. Overall, by reducing the required sample volume, the bioanalytical method allowed for an increased number of plasma samples in vulnerable populations and enabled the generation of concentration-time profiles with a higher temporal resolution in microdialysis studies.

In vitro metabolism investigations revealed NO formation to follow Michaelis-Menten kinetics and was mediated by the CYP isoenzymes 2C19, 2C9 and 3A4 as determined by incubation of VRC with HLM, HIM and rhCYP. The kinetic parameters of the reaction, i.e. Michaelis-Menten constant (K_M), maximum reaction velocity (V_{max}) and intrinsic clearance (CL_{int}), were derived and an *in vitro in vivo* extrapolation using the well-stirred liver model demonstrated their validity by comparison to *in vivo* data. In contrast, no OH-VRC formation was detected in any of the metabolic systems, suggesting a different metabolic pathway of formation. The contribution of the individual isoenzymes to NO formation was 63.1% for CYP2C19, 13.2% for CYP2C9 and 29.5% for CYP3A4 as determined by specific CYP inhibition in HLM and application of intersystem extrapolation factors to scale the metabolism in rhCYP. The type of inhibition and inhibitory potential of VRC, NO and OH-VRC were evaluated in HLM by their effects on CYP specific marker reactions for CYP2C19, CYP2C9 and CYP3A4. Regarding the half maximum inhibitory concentration (IC_{50}), NO was the weakest and VRC and OH-VRC comparably strong inhibitors of CYP2C9 and CYP3A4. CYP2C19 was significantly inhibited by VRC only. Time-independent inhibition by VRC, NO and OH-VRC was demonstrated by the absence of an IC_{50} shift when a pre-incubation step of inhibitor and enzyme in the absence or presence of NADPH re-generating system was performed. Lastly, the assessment of the inhibitory constant (K_i) confirmed the observations of inhibitory potential from IC_{50} investigations, as well as revealed competitive inhibition of CYP2C19 by VRC and OH-VRC and non-competitive inhibition by NO. Inhibition of CYP2C9 was competitive while inhibition of CYP3A4 was non-competitive for VRC, NO and OH-VRC.

As a prerequisite for the assessment of target-site exposure of VRC and NO, the feasibility of simultaneous microdialysis of VRC and NO was first explored *in vitro* by investigating the relative recovery (RR) of both compounds in the absence and presence of the other. Dependencies of RR on compound combination, compound concentration, microdialysis catheter and study day were evaluated and quantified by a linear mixed-effects model. Median RR of VRC and NO during individual microdialysis were high with 87.6% and 91.1%, respectively. During simultaneous microdialysis of VRC and NO, median RR did not change relevantly being 87.9% and 91.1%, respectively. The linear mixed-effects model confirmed the graphically presumed

absence of significant differences between RR of VRC and NO during individual and simultaneous microdialysis as well as between the two compounds ($p>0.05$). No impact of the investigated clinically relevant compound concentration on RR was found ($p=0.284$). The study day was the main source of variability (46.3%), while the microdialysis catheter had a minor impact (4.33%). VRC retrodialysis was a feasible catheter calibration method to derive ISF concentrations of VRC *and* NO simultaneously.

Hereinafter, to assess the *in vivo* feasibility and clinical applicability of the simultaneous microdialysis of VRC and NO, plasma, ultrafiltrate and ISF samples, obtained in a clinical microdialysis trial investigating VRC PK after administration of an approved VRC dosing regimen, were analysed. Concentration-time profiles, exposure assessed as area under the concentration-time curve (AUC) and metabolic ratios ($concentration_{NO}/concentration_{VRC}$) of four healthy male adults in plasma, ultrafiltrate and ISF were evaluated regarding the impact of multiple dosing and the CYP2C19 genotype-predicted phenotype. VRC and NO revealed distribution into ISF with AUC being up to 2.82- and 17.7-fold lower compared to plasma. Intraindividual variability of metabolic ratios was largest after the first VRC dose administration while interindividual differences increased with multiple dosing. The CYP2C19 genotype-predicted phenotype influenced interindividual differences with a maximum 6- and 24-fold larger AUC ratio (AUC_{NO}/AUC_{VRC}) between the intermediate and rapid metaboliser in plasma and ISF, respectively. VRC metabolism was saturated or auto-inhibited, indicated by decreasing metabolic ratios with increasing VRC concentrations.

Overall, the present thesis advanced the elucidation of VRC PK by generating mechanistic and quantitative insights into distribution and metabolism processes in humans. The application of the newly established bioanalytical LC-MS/MS assay enabled the thorough characterisation of VRC and its metabolites as substrates and inhibitors of the CYP isoenzymes 2C19, 2C9 and 3A4. Moreover, *in vitro* microdialysis feasibility investigations provided the basis for the evaluation of simultaneous microdialysis of VRC and NO *in vivo*. Thus, the exploratory PK analysis highlighted the potential sources of intra- and interindividual differences observed in the context of VRC treatment in humans. Ultimately, a thorough understanding of VRC target-site PK and metabolism is key to the optimisation of personalised VRC dosing regimens.

Zusammenfassung

Invasive Pilzinfektionen stellen eine zunehmende Bedrohung für die globale öffentliche Gesundheit dar und verursachen jedes Jahr weltweit etwa 1.5 Millionen Todesfälle. Da die Entstehung und Ausbreitung von Resistenzen gegen Antimykotika zunimmt und die Entwicklung neuer antimykotischer Wirkstoffe hinter dieser epidemiologischen Belastung zurückbleibt, ist ein wichtiger Aspekt der rationale Einsatz vorhandener Arzneimittel wie z. B. Voriconazol (VRC). Trotz der langjährigen und häufigen Anwendung am Menschen ist die Pharmakokinetik (PK) von VRC noch immer nicht vollständig verstanden, was sich in einer großen intra- und interindividuellen Variabilität sowie in Therapieversagen und unerwünschten Arzneimittelwirkungen zeigt. Es wird angenommen, dass die Hauptursache für die Variabilität im komplexen Metabolismus von VRC liegt, an dem die Cytochrom P450 (CYP)-Isoenzyme 2C19, 2C9 und 3A4 beteiligt sind. Darüber hinaus ist der Zielort von VRC, d. h. die interstitielle Flüssigkeit (ISF), für PK-Untersuchungen relevanter als die üblicherweise bestimmten Plasmakonzentrationen. Eine leistungsfähige Methode für ISF-Untersuchungen ist die minimal-invasive Probenahmetechnik der Mikrodialyse, die eine kontinuierliche Probenahme von nicht proteingebundenen Arzneistoffmolekülen über einen bestimmten Zeitraum ermöglicht.

Ziel der vorliegenden Arbeit war daher, einen Beitrag zur Aufklärung der VRC PK zu leisten, indem mechanistische und quantitative Einblicke in die Verteilung und die Stoffwechselprozesse beim Menschen gewonnen werden, um letztendlich die Optimierung der Dosierungsstrategien für VRC zu unterstützen. Um dieses Ziel zu erreichen, wurden Untersuchungen in drei Hauptforschungsgebieten durchgeführt. Erstens wurde ein vielseitiger bioanalytischer Flüssigchromatographie-Tandem-Massenspektrometrie-Assay (LC-MS/MS) für die Quantifizierung von VRC und seinen Metaboliten in verschiedenen biologischen Matrices entwickelt und validiert. Zweitens wurden *In-vitro*-Metabolismusuntersuchungen zur umfassenden Charakterisierung von VRC und seinen Metaboliten als Substrate und Inhibitoren von CYP2C19, CYP2C9 und CYP3A4 durchgeführt. Drittens wurden *In-vitro*- und *In-vivo*-Mikrodialyse-Untersuchungen durchgeführt, um die Anwendung der gleichzeitige Mikrodialyse von VRC und dem potenziell toxischen Metaboliten, Voriconazol-*N*-Oxid (NO), beim Menschen zu bewerten.

Der entwickelte bioanalytische LC-MS/MS-Assay ermöglichte die gleichzeitige Quantifizierung von VRC, NO und Hydroxyvoriconazol (OH-VRC) in menschlichem Plasma, Ultrafiltrat und Mikrodialysat sowie in den *In-vitro*-Matrices menschlicher Leber-/Darm-Mikrosomen (HLM/HIM) und rekombinanter menschlicher CYP-Isoenzyme (rhCYP). In einem ersten Schritt wurde der Assay gemäß der Leitlinie zur „Validierung bioanalytischer Methoden für die Quantifizierung“ der Europäischen Arzneimittelagentur für VRC und NO in Plasma und Mikrodialysat vollständig validiert. Insgesamt war die Quantifizierung schnell, unkompliziert

und verwendbar für klinisch relevante Konzentrationen von VRC und NO von 5 bis 5000 ng/mL in Plasma und Ultrafiltrat sowie von 4 bis 4000 ng/mL in Mikrodialysat. Aufgrund der hohen Sensitivität des Assays wurden nur 20 µL Plasma oder Ultrafiltrat und 5 µL Mikrodialysat benötigt. Für VRC und NO in Plasma und Mikrodialysat war die Richtigkeit zwischen den Messsequenzen mit einer maximalen mittleren Abweichung von 7.0 % von der Nennkonzentration hoch und die Präzision zwischen den Messsequenzen wurde mit einem Variationskoeffizienten von ≤11.8 % bestätigt. Beide Substanzen erwiesen sich unter verschiedenen Bedingungen als stabil. In einem zweiten Schritt wurde der Assay erfolgreich für PK-Analysen in *In-vitro*-Experimenten angepasst, die einen Konzentrationsbereich von 0.1 bis 500 ng/mL für NO und von 1.0 bis 500 ng/mL für OH-VRC bei einem Probenvolumen von nur 20 µL abdeckten. Insgesamt ermöglichte die bioanalytische Methode durch die Verringerung des erforderlichen Probenvolumens eine größere Anzahl von Plasmaproben in vulnerablen Bevölkerungsgruppen und die Erstellung von Konzentrations-Zeitprofilen mit einer höheren zeitlichen Auflösung in Mikrodialysestudien.

In-vitro-Metabolismusuntersuchungen ergaben, dass die NO-Bildung einer Michaelis-Menten-Kinetik folgt und durch die CYP-Isoenzyme 2C19, 2C9 und 3A4 vermittelt wird, wie durch Inkubation von VRC mit HLM, HIM und rhCYP festgestellt wurde. Die kinetischen Parameter der Reaktion, d. h. die Michaelis-Menten-Konstante (K_M), die maximale Reaktionsgeschwindigkeit (V_{max}) und die intrinsische Clearance (CL_{int}), wurden bestimmt und deren Gültigkeit durch eine *In-vitro-in-vivo*-Extrapolation unter Verwendung des „well-stirred"-Lebermodells und den Vergleich mit *In-vivo*-Daten gezeigt. Im Gegensatz dazu wurde in keinem der Enzymsysteme eine Bildung von OH-VRC festgestellt, was auf einen anderen Stoffwechselweg der Bildung hindeutet. Der Beitrag der einzelnen Isoenzyme zur NO-Bildung betrug 63.1 % für CYP2C19, 13.2 % für CYP2C9 und 29.5 % für CYP3A4, wie durch spezifische CYP-Hemmung in HLM und Anwendung von Intersystem-Extrapolationsfaktoren zur Skalierung des Metabolismus in rhCYP ermittelt wurde. Die Art der Inhibition und das hemmende Potenzial von VRC, NO und OH-VRC wurden in HLM durch ihre Auswirkungen auf CYP-spezifische Markerreaktionen für CYP2C19, CYP2C9 und CYP3A4 bewertet. Hinsichtlich der halbmaximalen Hemmkonzentration (IC_{50}) waren NO der schwächste und VRC und OH-VRC vergleichsweise starke Inhibitoren von CYP2C9 und CYP3A4. CYP2C19 wurde nur durch VRC signifikant gehemmt. Die zeitunabhängige Inhibition durch VRC, NO und OH-VRC wurde durch das Fehlen einer IC_{50}-Verschiebung nachgewiesen, wenn ein Vorinkubationsschritt von Inhibitor und Enzym in Abwesenheit oder Anwesenheit eines NADPH-regenerierenden Systems durchgeführt wurde. Schließlich bestätigte die Bewertung der Inhibitionskonstanten (K_i) die Beobachtungen des inhibitorischen Potenzials aus den IC_{50}-Untersuchungen und zeigte eine kompetitive Hemmung von CYP2C19 durch VRC und OH-VRC sowie eine nicht-kompetitive

Hemmung durch NO. Die Hemmung von CYP2C9 war kompetitiv, während die Hemmung von CYP3A4 nicht-kompetitiv für VRC, NO und OH-VRC war.

Als Voraussetzung für die Bestimmung der VRC und NO Exposition am Zielort, wurde zunächst die Durchführbarkeit der gleichzeitigen Mikrodialyse von VRC und NO *in vitro* untersucht, indem die relative Wiederfindung (RR) beider Substanzen in Abwesenheit und Anwesenheit der jeweils anderen bestimmt wurde. Die Abhängigkeiten der RR von der Substanzkombination, der Konzentration der Substanz, dem Mikrodialysekatheter und dem Studientag wurden mit einem linearen gemischten Modell bewertet und quantifiziert. Die mediane RR von VRC und NO während der individuellen Mikrodialyse war mit 87.6 % bzw. 91.1 % hoch. Bei gleichzeitiger Mikrodialyse von VRC und NO änderte sich die mediane RR mit 87.9 % bzw. 91.1 % nicht wesentlich. Das lineare gemischte Modell bestätigte die grafisch vermutete Abwesenheit signifikanter Unterschiede zwischen der RR von VRC und NO bei individueller und gleichzeitiger Mikrodialyse sowie zwischen den beiden Substanzen ($p>0.05$). Es wurde kein Einfluss der untersuchten klinisch relevanten Konzentrationen der Substanzen auf die RR festgestellt ($p=0.284$). Der Studientag war die Hauptursache der Variabilität (46.3 %), während der Mikrodialysekatheter einen geringen Einfluss hatte (4.33 %). Die Retrodialyse mit VRC war als Katheterkalibrierungsmethode zur gleichzeitigen Bestimmung der ISF-Konzentrationen von VRC *und* NO geeignet.

Um die *In-vivo*-Durchführbarkeit und klinische Anwendbarkeit der gleichzeitigen Mikrodialyse von VRC und NO zu bewerten, wurden Plasma-, Ultrafiltrat- und ISF-Proben analysiert, die in einer klinischen Mikrodialysestudie zur Untersuchung der PK von VRC nach Verabreichung eines zugelassenen VRC-Dosierungsschemas gewonnen wurden. Die Konzentrations-Zeitprofile, die als Fläche unter der Konzentrations-Zeitkurve (AUC) bewertete Exposition und die metabolischen Quotienten ($Konzentration_{NO}/Konzentration_{VRC}$) von vier gesunden männlichen Erwachsenen in Plasma, Ultrafiltrat und ISF wurden im Hinblick auf die Auswirkung der Mehrfachdosierung und des vom CYP2C19-Genotyp vorhergesagten Phänotyps bewertet. VRC und NO zeigten eine Verteilung in die ISF, wobei die AUC im Vergleich zum Plasma bis zu 2.82- bzw. 17.7-mal niedriger war. Die intraindividuelle Variabilität der metabolischen Verhältnisse war nach der ersten Verabreichung von VRC am größten, während die interindividuellen Unterschiede bei mehrfacher Verabreichung zunahmen. Der vom CYP2C19-Genotyp vorhergesagte Phänotyp beeinflusste die interindividuellen Unterschiede mit einem maximal 6- bzw. 24-fach größeren AUC-Verhältnis (AUC_{NO}/AUC_{VRC}) zwischen dem intermediären und dem schnellen Metabolisierer im Plasma bzw. in der ISF. Der VRC-Metabolismus war gesättigt oder auto-inhibiert, was durch abnehmende metabolische Verhältnisse bei steigenden VRC-Konzentrationen ersichtlich wurde.

Insgesamt hat die vorliegende Arbeit einen Beitrag zur Aufklärung der PK von VRC geleistet, indem sie mechanistische und quantitative Erkenntnisse über die Verteilungs- und Stoffwechselprozesse beim Menschen lieferte. Die Anwendung des neu etablierten bioanalytischen LC-MS/MS-Assays ermöglichte die umfangreiche Charakterisierung von VRC und der Metabolite als Substrate und Inhibitoren der CYP-Isoenzyme 2C19, 2C9 und 3A4. Darüber hinaus formten die *In-vitro*-Mikrodialyse-Machbarkeitsuntersuchungen die Grundlage für die Bewertung der gleichzeitigen Mikrodialyse von VRC und NO *in vivo*. Die explorative PK-Analyse hat somit mögliche Ursachen der intra- und interindividuellen Unterschiede aufgezeigt, die im Zusammenhang mit der VRC-Behandlung beim Menschen beobachtet wurden. Letztendlich ist ein umfassendes Verständnis der Zielort-PK und des Metabolismus von VRC der Schlüssel zur Optimierung personalisierter VRC-Dosierungsschemata.

Acknowledgements

I would like to take this opportunity to thank all the people who have accompanied and supported me over the past years and who have shaped the scientific and social environment during this unique time as doctoral student at the Department of Clinical Pharmacy and Biochemistry at the Institute of Pharmacy at Freie Universität Berlin.

In particular, I want to express my sincere gratitude to my supervisor *Prof. Dr. Charlotte Kloft*. Thank you, for giving me the opportunity to perform my doctoral research in such an extraordinary environment, for your curiosity and enthusiasm in every scientific detail as well as for your (scientific and non-scientific) guidance, trust and backing in good and more challenging times. Finally, thank you for the freedom to work on research and teaching related ideas and projects I was interested in.

Thank you, *Dr. Robin Michelet* for giving the impulse to perform research on voriconazole metabolism, your curiosity and (contagious) passion in everything science related. Thanks for sharing your expertise with me, giving valuable feedback and last but not least for believing in me and my progress.

Thank you, *Prof. Dr. Markus Zeitlinger*, from the Department of Clinical Pharmacology, Medical University Vienna, for fruitful discussions and sharing your enthusiasm about microdialysis, as well as for reviewing this thesis and being a member of the doctoral committee.

Thank you, *Prof. Dr. Gerd Mikus* for the extensive scientific discussions throughout my doctoral studies, your interest in my projects as well as your invaluable feedback for all abstracts, presentations and manuscripts.

Thank you, *Dr. Jan Joseph* and *Dr. Fabian Schumacher* for the smooth coordination of PharmaMS, your support in all bioanalytical questions, your great commitment to quickly troubleshoot the instruments as well as your interest in scientific discussions.

Thanks to *Tania Fuhrmann-Selter* and *Corinna Schmidt* for your very valuable support in the lab. Over the years, you have not only helped prepare and perform countless experiments but have always been welcome company in the lab to talk about current events, scientific or otherwise. Thank you, *Dr. Ingo Siebenbrodt* for the organisation of all teaching-related activities, for your inspiring interest in everything pharmacy-related and all the entertaining exam correction and review sessions. Thank you *Hacer Bayram* and *Gabriela Karsubke* for managing so much behind the scenes.

Thank you, *Dr. Johanna Seeger* for your companionship and valuable and honest opinions from the very beginning. It was a pleasure having you next door for short laughs as well as longer, philosophical-like scientific discussions. Our mutual view on many topics gave me strength and confidence. Thank you, *Nicole Zimmermann* for being a confidant and your matter-of-fact views on complex situations. I appreciated your listening, your understanding and your eagerness to cheer me up by sharing photos and stories of your dog Jimmy. Thanks, *Dr. Sebastian Franck* for sympathizing with my MS challenges and offering target-oriented solutions. Thank you, *Viktoria Stachanow* and *Ayatallah Saleh* for your friendship and trustful scientific exchange.

Thank you, *Antonia Thomas* for your interest in my research project, your trust in my guidance and your enthusiasm to do "all the experiments". It was a pleasure to grow alongside you and see your hard work finalised in a Diploma thesis and a shared publication.

Sincere credit also goes to *Nicole Zimmermann*, *Amrei Konrad*, *Ayatallah Saleh*, *Alix Démaris*, *Franz Weber*, *Banafshe Pourshacheraghi* and *Johanna Seeger*, who reviewed parts of this thesis. Thank you for your excellent input.

It was a pleasure to spend my time with great colleagues and friends from "AK Kloft", during lunchbreaks, Lidl walks, conferences and many other activities. Thanks *Alix Démaris*, *Amrei Konrad*, *Banafshe Pourshacheraghi*, *Dr. Lisa Schmitt*, *Franziska Kluwe*, *Luis Ilia*, *Dr. Anna Mc Laughlin*, *Ferdinand Weinelt*, *David Busse*, *Dr. Ana-Marija Gričić*, *Dr. Francis Ojara*, *Davide Bindellini*, *Felix Müller*, *Franz Weber*, *Yomna Nassar*, *Dr. Carlos Montefusco-Pereira*, *Ella Widigson Winterkvist*, *Malin Andersson*, *Maike Petersen*, *Dr. Eva Göbgen* and *Dr. Christine Weiser* for contributing to a great environment during, between and after work.

Thank you also to "*AK Parr*", who welcomed me in their labs in "KöLu", included me for lunchbreaks, gave a helping hand and shared frustrations about "Karl" and "Becky".

Thank you to all the eager and interested pharmacy students who continuously renewed my enthusiasm for pharmacy, research and science. In particular, thanks to my elective students *Jakob Kirmse*, *Emma Fröling*, *Julia Wind*, *Therese Gölling*, as well as the incredible "WPF KOM" and "WPF KOM2" groups.

Finally, I thank my *family* and *friends* who supported me and provided welcome distractions from the scientific work. Most importantly, thank you *Felix* for your encouragements, support, patience and understanding, in brief, for making this possible.

Table of contents

Abbreviations

AIC	Akaike information criterion
AUC	Area under the concentration-time curve
BP	Blood-to-plasma ratio
BSA	Bovine serum albumin
$C_{\mu D}$	Concentration in microdialysate
CAL	Calibrator(s)
C_{Enzyme}	Enzyme concentration
C_I	Inhibitor concentration
CI	Confidence interval(s)
C_{ISF}	Concentration in interstitial space fluid
$CL_{hepatic}$	Hepatic clearance
CL_{int}	Intrinsic clearance
CL_R	Renal clearance
C_{max}	Maximum concentration
C_{Medium}	Concentration in medium
C_{Met}	Concentration of metabolite
C_{min}	Minimum concentration
C_{Nom}	Nominal concentration
$C_{Retrodialysate}$	Concentration in retrodialysate
$C_{Retroperfusate}$	Concentration in retroperfusate
C_S	Substrate concentration
CV	Coefficient of variation
CYP	Cytochrome P450
dMRM	Dynamic multiple reaction monitoring
DMSO	Dimethyl sulfoxide
EMA	European Medicines Agency
ESI	Electrospray ionisation
FA	Formic acid
$FAD/FADH_2$	Oxidated/reduced form of flavin adenine dinucleotide
FDA	Food and Drug Administration
FMO	Flavin containing monooxygenase(s)
f_u	Fraction unbound

H	Hill factor
HIM	Human intestine microsomes
HIV	Human immunodeficiency virus
HLM	Human liver microsomes
HPLC	High-performance liquid chromatography
i.v.	Intravenous
IC_{50}	Half maximum inhibitory concentration
IM	Intermediate metaboliser(s)
IQR	Interquartile range(s)
IS	Internal standard
ISEF	Intersystem extrapolation factor(s)
ISF	Interstitial space fluid
IVIVE	*In vitro in vivo* extrapolation
K_i	Inhibitory constant
K_M	Michaelis-Menten constant
LC	Liquid chromatography
LLE	Liquid-liquid extraction
LLOQ	Lower limit of quantification
LME	Linear mixed-effects
LOD	Limit of detection
m/z	Mass-to-charge ratio
MeOH	Methanol
MF	Matrix factor(s)
MPPGL	Microsomal protein per gram liver
MS	Mass spectrometry
$NADP^+$/NADPH	Oxidated/reduced form of nicotinamide adenine dinucleotide phosphate
NM	Normal metaboliser(s)
NO	Voriconazole *N*-oxide
NO-D_3	Deuterated voriconazole *N*-oxide
OH-DIC	4-Hydroxydiclofenac
OH-MDZ	1-Hydroxymidazolam
OH-MEP	4-Hydroxymephenytoin
OH-VRC	Hydroxyvoriconazole

p.o.	Peroral
PAES	Polyarylethersulphone
PBPK	Physiologically-based pharmacokinetic
PD	Pharmacodynamic(s)
PK	Pharmacokinetic(s)
PM	Poor metaboliser(s)
PPB	Potassium phosphate buffer
QC	Quality control
Q_H	Hepatic blood flow
QQQ	Triple quadrupole
R^2	Coefficient of determination
rD	Relative delivery
R-H	Initial state of substrate
rhCYP	Recombinant human cytochrome P450
RM	Rapid metaboliser(s)
R-OH	Oxidated state of substrate, i.e. hydroxylated substrate
RR	Relative recovery
RS	Ringer's solution
SD	Standard deviation
SIL	Stable isotope labelled
sIVMS	Static *in vitro* microdialysis system
SPE	Solid-phase extraction
SS_{res}	Sum of square residuals
$t_{1/2}$	Half-life
TDM	Therapeutic Drug Monitoring
t_{max}	Time at maximum concentration
t_{reac}	Reaction time
TRIS	Trishydroxymethylaminomethane
UGT	Uridine 5'-diphospho-glucuronosyltransferase
UHPLC	Ultrahigh-performance liquid chromatography
ULOQ	Upper limit of quantification
UM	Ultrarapid metaboliser(s)
UP	Ultra-pure

UV	Ultraviolet
V	Reaction velocity
$V_{con.}$	Reaction velocity of the control
$V_{inh.}$	Reaction velocity in the presence of inhibitor
V_{max}	Maximum reaction velocity
VRC	Voriconazole
VRC-D_3	Deuterated voriconazole
WHO	World Health Organization

1 Introduction

1.1 Infectious diseases

In human history, infectious diseases were the major cause of death for centuries. The lack of knowledge on the sources, prevention, spread and cure of infections was the main accelerator of mortality and low life expectancy. Therefore, it is not surprising that several pandemics, e.g. typhus, cholera, syphilis and smallpox, mark human history. One of the largest was the plague, also referred to as the "Black Death", killing approximately 100 million people in the fourteenth century corresponding to approximately 25% of the world's population at this time [1–3].

1.1.1 Anti-infective therapy: opportunities and pitfalls

The first breakthrough discoveries in the fight against infectious diseases were made in the 19th century following the invention of microscopy and the discovery of microorganisms as causes of diseases [3]. However, only in 1929 Alexander Flemming described that contaminating mould caused the lysis of bacterial cultures. Although only years later the structure of the active agent, penicillin, was discovered and the purified drug used in therapy, this observation marked the beginning of the antibiotic era [3]. Since then, antiinfectives, including antibiotics, antivirals, antimycotics and antiparasitics, are routinely used in the treatment of infectious diseases. In fact, due to the successful application of antiinfectives, in the last 100 years the global average human lifespan has increased by 23 years [4]. While in the USA in 1900 the three leading causes of death were pneumonia, tuberculosis and diarrhoea/enteritis in 1997 the share of overall deaths by infectious diseases (i.e. pneumonia, influenza and human immunodeficiency virus (HIV)) decreased to 4.7%. Instead, heart diseases and cancer are the major causes of death in the USA and Germany nowadays [5–7]. Considering the great importance of antiinfectives for the sustainment of human health and wellbeing, it is alarming to witness the growing incidence of antimicrobial resistance. Already today 700,000 people worldwide are dying each year from resistant infections. A number that might rise to 10 million people per year in 2050 if no drastic actions are taken to fight antimicrobial resistance [8]. Hence, it is not surprising, that the World Health Organization (WHO) has declared antimicrobial resistance to one of the top ten global public health threats [9].

In a first step, it is essential to understand the emergence and driving forces of resistance evolution mechanisms. Overall, the more susceptible pathogens are exposed to antiinfectives the more likely they are to develop resistance. Thus, the excessive and inappropriate use of drugs leads to a natural selection of resistant variants, which can occur spontaneously or by horizontal gene transfer, erasing drug-sensitive competitor pathogens. Furthermore, the extensive agricultural use presents a large problem. Livestock is treated worldwide prophylactically with antibiotics to

increase yields and prevent quickly spreading diseases due to the type of husbandry. Similarly antifungal agents are used to protect crops and augmenting the harvest. As a consequence, through food, humans get in contact either directly with those antiinfectives or with the resistant pathogens that emerged in the animals/plants and which subsequently can infect them [10–12].

In a second step, awareness of the global challenge needs to be aroused and joint actions taken. On the World Health Assembly in 2015 the attending countries committed to a Global Action Plan on antimicrobial resistance including five major objectives: (i) raising awareness and expanding the knowledge of antimicrobial resistance by education and training, (ii) fostering surveillance and research, (iii) reduction of infection incidences through improved sanitation and hygiene, (iv) *promotion of the rational use of antiinfectives in humans and animals* and (v) increasing the investment in the development of new drugs, diagnostics, vaccines and interventions [13]. Nowadays, common knowledge about the risk of bacterial infections and antibiotic resistance exists among the general population. However, other pathogens, such as fungi, pose a similar threat to the global public health but have not yet received much attention.

1.1.2 Invasive fungal infections

Fungal infections affect approximately 1.7 billion people worldwide with superficial infections of the skin and nails being the most frequent. Although the incidence of *invasive* fungal infections is much lower, mortality by those infections is an underappreciated threat. More than 1.5 million people die from invasive fungal infections worldwide every year. Thus, deaths due to invasive fungal infections outnumber those of tuberculosis whose epidemiological burden is more recognised [14–16]. Indeed, only in 2020 the first meeting of the WHO antifungal expert group took place recognising the increased burden on the public health by invasive fungal infections. The efforts made by the WHO lie within the ‘Global Action Plan on Antimicrobial Resistance’ to organise, foster and observe research and development activities within the field [13,17]. This action plan was presented already in 2015 but mainly focussed on antibiotic-resistant bacteria and new antibiotic treatments. In a comparable approach, priority fungal pathogens were now identified for a target-oriented development of new antimycotics [13,17]. Most pathogenic fungi are opportunistic, i.e. although fungi belong to the commensal flora of humans, the immune system of healthy individuals effectively prevents infections. Therefore, the main reason for an increasing prevalence of invasive fungal infections is the rising number of immunocompromised patients. This includes infections with HIV, cancer and/or chemotherapy as well as patients receiving immune suppressive drugs e.g. because of solid organ or haematopoietic stem cell transplantation [14,18,19].

The vast majority of invasive fungal infections, i.e. >90%, are caused by four genera: *Cryptococcus*, *Candida*, *Aspergillus* and *Pneumocystis* [14]. In intensive care patients *Candida*

spp. and *Aspergillus* spp. have been described as major pathogens causing invasive fungal infections [20]. The mortality rates of invasive fungal infections are high and were reported to be 30%-95% for aspergillosis, 46%-75% for candidiasis, 20%-70% for cryptococcosis and 20-80% for pneumocystis [14]. One reason for those high mortality rates is the complicated and often delayed diagnosis [21]. In fact, based on autopsy reports, estimates suggest that only 50% of patients are diagnosed with invasive fungal infections before death [22]. Overall, invasive fungal infections cause unspecific symptoms such as fever, chills and chest pain in those affected. The available diagnostics include x-rays, computed tomography-scans as well as blood tests, but often lack specificity, sensitivity or are not affordable in resource-limited countries [14,23]. Compared to bacteria, culturing of fungi by blood cultures is complex, insensitive and slow. For invasive candidiasis, for instance, blood culture has a sensitivity of approximately 50% and 0% for aspergillosis [14]. More recently, point-of-care tests have been developed and are currently the standard of care in the diagnosing of cryptococcal meningitis [23]. Based on the immune-chromatography principle also tests for the *Histoplasma* antigen and immunoglobulin G to diagnose chronic aspergillosis and coccidioidomycosis are under development. Lastly, nucleic acids of fungi are detectable by polymerase chain reaction but there is a need for standardisation and clinical validation [23].

Currently, four classes of antifungal agents are used for the treatment of invasive fungal infections: polyenes, azoles, echinocandins and pyrimidine analogues [12,24]. Amphotericin B, the most prominent polyene, binds to ergosterol in the fungal cell wall and provokes a disruption in cell integrity. Also the azoles, such as voriconazole (VRC), target the fungal cell wall by inhibition of the lanosterol 14α-demethylase and hence inhibiting the biosynthesis of ergosterol. Echinocandins, e.g. anidulafungin or caspofungin, constrain the 1,3-β-glucan synthase, which is a main component of the fungal cell wall, and as a consequence cause the lysis of the cell. Lastly, 5-fluorocytosin as a pyrimidine analogue blocks the pyrimidine metabolism and DNA synthesis [12,24,25]. However, within the last two decades only one new class of antifungal drugs (the echinocandins) has been introduced to the market. Indeed, in the last ten years even only one new antifungal drug (isavuconazole) has been approved [26]. Consequently, as new antimycotics are scarce and the number of regularly used antifungals is limited, antifungal resistance is an increasing challenge [12,27–29]. In particular the emergence of multidrug resistance is a rising threat, some species such as *Candida auris*, that was first described in 2009, is now resistant to all clinical antifungals [12,27]. The classification into susceptible or resistant fungi populations is commonly based on reports of the European Committee on Antimicrobial Susceptibility Testing (EUCAST) who provides guidance for standardised *in vitro* methods for the determination of minimum inhibitory concentrations of moulds and yeasts and publishes clinical breakpoints for *Candida spp*. and *Aspergillus spp.* [30–32]. A variety of resistance mechanisms

has been described. Among the most common for fungi are the conformational change, overexpression or absence of the target structure, the overexpression of efflux pumps back-transporting the antifungal agent, the regulation of stress response pathways as well as genomic plasticity by aneuploidy or hypermutation [12,27].

On the upside, the awareness of the threat by invasive fungal infections and evolved resistance against antifungal agents has increased in recent years and is accompanied by intensified research and development efforts. Thus, several new antifungal agents for clinical use are currently in (pre)clinical testing. In fact, even a new class of antimycotics is under development, the orotomides, with the first representative olorofim being in the early stages of clinical investigations. The orotomides target the dihydroorotate dehydrogenase, an enzyme involved in the synthesis of pyrimidine which is essential for the formation of nucleic acids of the fungi [24,33,34]. Other pathways being investigated as potential targets for future antifungal agents include the mitochondrial turnover of the fungi, the glyoxylate cycle, the calcineurin pathway or the sphingolipid pathway [34]. Also the repurposing of existing drugs, such as sertraline or tamoxifen as well as the development of vaccines might play a role in the fight against invasive fungal infections and the emerging resistance to current antimycotics [12,34].

However, until novel treatment options are available and routinely established, the sustainment of the effectiveness of frequently used antifungal drugs is key. This antifungal stewardship includes, but is not limited to, the improvement of the diagnostic process, the education of medical and pharmaceutical personnel, surveillance approaches as well as personalised therapies choosing the right drug and dosing regimen for each patient-pathogen interplay [21].

1.2 Characterisation of voriconazole

VRC, (2R,3S)-2-(2,4-difluorophenyl)-3-(5-fluoropyrimidin-4-yl)-1-(1H-1,2,4-triazol-1-yl)butan-2-ol, is a broad-spectrum, second-generation triazole antifungal agent first approved as VFEND® by the European Medicines Agency (EMA) in 2002 and by the U.S. Food and Drug Administration (FDA) in 2003. The WHO has listed VRC as an essential medicine for adults and children as it is available worldwide at low costs [35,36]. VRC is applicable as lyophilised powder for solution for intravenous (i.v.) infusion, film-coated tablets for oral administration and as powder for oral suspension [37,38]. Based on the structure of fluconazole, VRC is a more lipophilic compound (logP 1.8) of poor solubility in water with a molar mass of 349.317 g/mol [39].

1.2.1 Indication, pharmacokinetic and pharmacodynamic properties

VRC is used in first-line treatment of invasive fungal infections in adults and children older than two years such as aspergillosis or candidaemia in non-neutropenic patients, as well as for

prophylaxis in high-risk allogeneic hematopoietic stem cell transplant recipients [38,40–42]. Further areas of application include fluconazole-resistant invasive *Candida* infections as well as serious infections caused by *Scedosporium spp.* and *Fusarium spp.* [38]. As an azole antifungal agent, VRC is inhibiting the ergosterol biosynthesis of the fungal cell wall. The specific target is the 14α-demethylase, an enzyme belonging to the cytochrome P450 family (CYP51) [43,44].

Therapy with VRC in adults is initiated according to the summary of product characteristics by a loading dose to quickly reach steady state concentrations [38]. This is either a weight adapted i.v. dose of 6 mg/kg body weight every 12 h on day one or a peroral (p.o.) dose of 400 or 200 mg tablets twice daily for patients >40 kg or <40 kg, respectively. The maintenance dose, that is given from day two onwards, comprises either 4 mg/kg i.v. dosing, 200 mg (>40 kg body weight) or 100 mg (<40 kg body weight) tablets twice daily. As bioavailability is high, a switch between i.v. and p.o. dose administration is feasible. Children (2 to <12 years) and young adolescents with low body weight (12-14 years and <50 kg) receive higher doses of 9 mg/kg i.v. in the first 24 h and 8 mg/kg i.v. twice daily after the first 24 h [38].

After p.o. dosing VRC is absorbed almost completely according to the manufacturer Pfizer who reports a bioavailability of 96%. In fact, bioavailability was found to be reduced in patients (45.9%, 83.0% and 58.0%) [45–47], in CYP2C19 normal metabolisers (NM, 75.2%) compared to poor metabolisers (PM, 94.4%) [48] and children (44.6%) [49]. The maximum plasma concentration (C_{max}) occurs 1-2 h after dose administration and is, similar to the area under the concentration-time curve (AUC), reduced when VRC is administered with high fat meals [38,50]. Absorption is however, not affected by increased gastric pH. The volume of distribution for VRC was reported as 4.6 L/kg indicating an extensive distribution outside the vascular space [38]. Furthermore, VRC distribution into various tissues and tissue fluids has been described [51] including cerebrospinal fluid and brain tissue [52,53], synovial fluid and bone tissue [54], liver, kidney, lung, spleen and myocardial tissue [53] as well as pleural tissue [55,56]. Plasma protein binding of VRC was originally reported by Pfizer as 58% [38]. However, more extensive studies found plasma protein binding of 47.6% (*in vitro*) and 49.6% (*in vivo*, intensive care unit patients) [57], 53.0% and 58.3% using different ultrafiltration devices [58] as well as 67.7% and 77.1% (*in vitro* and *in vivo*) [59]. The major binding partner is albumin (25.5% of total plasma protein binding), to a lesser extent α_1-acid glycoprotein (4.8% of total plasma protein binding) while the remaining plasma protein binding is unexplained [57].

VRC is an intensely metabolised drug: only 2% is excreted unchanged whilst 98% undergoes mainly oxidative metabolism [60]. Thus, a large spectrum of metabolites and metabolic pathways are known to occur in humans. Metabolising enzymes thereby include CYP enzymes 2C19, 2C9 and 3A4. Whereas CYP3A4 genes are mostly conserved [61], genes of CYP2C9 and CYP2C19 express different genotypes leading to phenotypes of NM (CYP2C9*1/*1, CYP2C19*1/*1) –

previously classified as extensive metabolisers [62] – , PM (CYP2C9*2/*2, *3/*3, *2/*3; CYP2C19*2/*2, *3/*3, *2/*3), intermediate metabolisers (IM, CYP2C9*1/*2, *1/*3; CYP2C19*1/*2, *1/*3, *2/*17), rapid metabolisers (RM, CYP2C19*1/*17) or ultrarapid metabolisers (UM CYP2C19*17/*17) [63,64]. In Figure 1.1 the reported metabolites of VRC and their proposed pathways and metabolic enzymes are summarised. Voriconazole *N*-oxide (NO) is the main observed circulating metabolite without contributing to the antifungal activity of VRC [38,60]. Nevertheless, NO is suspected to cause adverse events such as the phototoxicity regularly observed in the context of VRC treatment [65,66]. Numerous other metabolites, with lesser proportions in VRC metabolism, have been mainly detected in urine, e.g. hydroxyvoriconazole (OH-VRC), dihydroxyvoriconazole and 4-hydroxyvoriconazole [37,48,60,67–69]. Different phase I and II metabolic enzymes are involved in the formation of the respective metabolites. NO was, based on *in vitro* investigation in human liver microsomes (HLM), recombinant human cytochrome P450 (rhCYP) isoenzymes and recombinant flavin containing monooxygenases (FMO), suggested to be formed by CYP2C19, CYP2C9, CYP3A4 and FMO [69–71]. 4-hydroxyvoriconazole was reported to emerge from incubations of rhCYP3A4 [69]. So far, no *in vitro* experiments were reported to enlighten the metabolic enzymes responsible for the (di-)hydroxylation of the fluoropyrimidine moiety of VRC. Nevertheless, it has been claimed that this hydroxylation pathway is influenced by the CYP2C19 genotype [48]. Further glucuronidation of phase I metabolites has been reported by different authors without investigations on the UDP-glucuronosyl-transferases (UGT) involved [48,60,67]. Furthermore, direct *N*-glucuronidation by UGT1A4 of the triazole ring of VRC has been described. However, as the Michaelis-Menten constant (K_M) was found to be very high (550 µM), this direct glucuronidation is probably of lesser relevance *in vivo* [72].

Elimination of VRC occurs mainly in the form of metabolites. After the administration of radiolabelled VRC, carrying two ^{14}C in the triazole moiety, 83% of radioactivity is recovered in urine and after 96 h most of the total radioactivity is excreted (>94%) [38,60]. The terminal half-life ($t_{1/2}$) of VRC is dose dependent and estimated to be approximately 6 h after the p.o. administration of 200 mg. Furthermore, VRC is displaying nonlinear pharmacokinetics (PK) in adults [38]. Several factors influence the PK of VRC. Among the polymorphisms of the described metabolising enzymes, influences of sex, age, body weight and inflammation were described [37,38,73–77]. Additionally, saturation and auto-inhibition mechanisms of VRC on its own metabolism might play a role in its observed nonlinear PK [68,78].

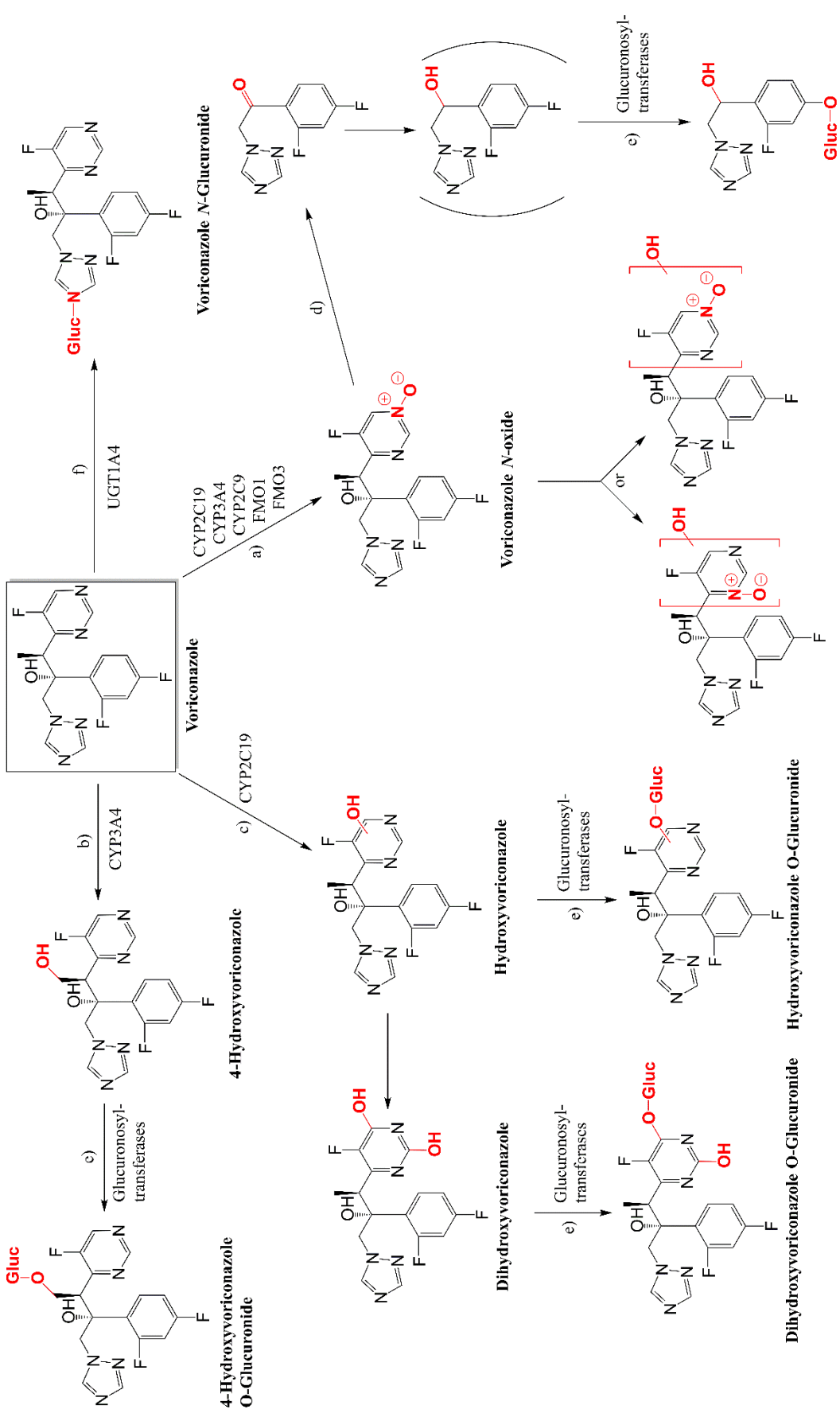

Figure 1.1: Proposed metabolic pathways of voriconazole in humans. (a) Fluoropyrimidine *N*-oxidation, (b) ethyl-hydroxylation, (c) fluoropyrimidine-hydroxylation, (d) loss of fluoropyrimidine, (e) O-glucuronide conjugation, (f) *N*-glucuronide conjugation.

1.2.2 Drug interactions and safety

VRC is a substrate of CYP2C19, CYP2C9 and CYP3A4, but also a potent inhibitor of diverse CYP isoenzymes [79]. Hence, there are numerous described drug-drug interactions with VRC related to CYP isoenzyme kinetics [38,80]. However, it has been shown that VRC does not significantly inhibit P-glycoprotein and UGT [38,81]. The inhibitory effect of VRC has been studied *in vitro* on various CYP isoenzymes including CYP1A2, CYP2A6, CYP2B6, CYP2C8, CYP2C9, CYP2C19, CYP2D6, CYP2E1, CYP3A4 and CYP3A5 using enzyme-specific probe substrates. In these experiments, VRC reduced the metabolism of probe substrates in incubations with CYP2B6, CYP3A4 and CYP3A5, CYP2C9 and CYP2C19 (order in decreasing inhibition) whereas no inhibition was observed in the other CYP isoenzymes. As a result, interactions with substrates of these enzymes and VRC are expected to occur also *in vivo* [82–85]. Drug-drug interactions investigated *in vitro* include amongst other interactions with tacrolimus and the analgesics buprenorphine, methadone and oxycodone [86–88]. The main circulating metabolite of VRC, the *N*-oxide, was also evaluated for its inhibitory potential on CYP enzymes and found to inhibit CYP2C9, CYP3A4 and CYP2C19 [38,68,89]. Furthermore, a vast number of patient cases and clinical studies is available on the influence of VRC on the plasma concentration-time profiles of drugs metabolised by enzymes inhibited by VRC. Invasive aspergillosis is often occurring in patients treated with immunosuppressant drugs after i.e. solid organ transplantations or hematopoietic stem cell transplantation. Therefore, drug-drug interactions between sirolimus, tacrolimus and cyclosporin and VRC are of high clinical relevance [90]. Serious adverse events might as well occur in patients treated concomitantly with VRC and warfarin. VRC was shown to lengthen the prothrombin time, already prolonged by warfarin, thus risking major bleedings [91]. Recently developed physiologically-based pharmacokinetic (PBPK) models found that concomitant VRC administration is also capable to increase plasma concentrations of tamoxifen, glucocorticoids (dexamethasone, methylprednisolone) and non-steroidal anti-inflammatory drugs (ibuprofen, celecoxib) [92–94]. In contrast, also VRC concentrations can be influenced when it is co-administered with other drugs. Proton pump inhibitors like (es)omeprazole are among the strongest CYP2C19 inhibitors and have been described to inhibit the metabolism of VRC [95,96], an effect also used as “booster” in patients with subtherapeutic plasma concentrations [97,98]. As different CYP enzymes metabolise VRC, lower plasma concentrations are expected when it is co-administered with CYP inducers. This has been demonstrated for St. John’s wort, rifampin, rifabutin and phenytoin, among others [99–102]. Lastly, also VRC itself is suspected to influence its own metabolism. Besides the discussion about auto-inhibition [68,78], also cases of auto-induction have been reported [98,103].

A variety of adverse events is observed under VRC treatment. This includes reversible visual impairments such as blurred vision or photophobia, which is often observed shortly after infusion,

indicating a dependency on VRC concentration [38,104]. Further common adverse reactions are dermatological issues, e.g. mild to moderate rashes as well as photosensitivity during longer treatments. Less frequent adverse events involve severe cutaneous reactions such as Stevens-Johnson syndrome or squamous cell carcinoma [38,105]. VRC has been observed to prolong the QTc interval and thus rare cases of torsades de pointe arrhythmia were reported. Consequently, VRC should be administered with caution to high-risk cardiac patients and those with a congenital QTc prolongation or patients with concomitant drugs known to prolong the QTc interval [38]. Moreover, hepatic and renal toxicity or dysfunction were described in the context of VRC treatment and led to the recommendation of continued hepatic and renal function monitoring [38,105]. Further observed rather unspecific adverse events comprise nausea, vomiting, diarrhoea, headache and abdominal pain [38]. Overall, in particular longer VRC treatment should be based on an appropriate individual benefit-risk assessment and in case of severe events VRC treatment must be discontinued [38].

1.3 Human cytochrome P450 system

The metabolism or biotransformation of exogenous substances, i.e. xenobiotics including active pharmaceutical agents, is a physiological process and an essential component for the description of the PK of a drug. In particular lipophilic compounds experience intensive metabolic transformations which entail the generation of hydrophilic metabolites that can be more easily renally excreted and thus avoiding accumulation in the body with potentially toxic effects. The central organ of biotransformation is the liver, however among others also the intestine, lung, kidney and blood can be involved in metabolism processes. In general, biotransformation is catalysed by enzymes and can be distinguished in phase I and II reactions. Phase I reactions comprise oxidation, reduction, hydrolysis and decarboxylation reactions of compounds while phase II reactions describe the conjugation of compounds, i.e. glucuronidation, sulphation, acetylation, methylation and coupling with glycine or glutathione. Additionally, phase II reactions can occur subsequently to a phase I transformation. In the metabolism of drugs, the CYP isoenzymes are a major contributor, catalysing the oxidative reactions of phase I metabolism [106,107].

1.3.1 Mechanism of action and clinical relevance

Approximately 60% of drugs are metabolised via microsomal monooxygenases containing the haemoprotein cytochrome P450 (CYP). CYP enzymes depict a superfamily with individual enzymes revealing unique amino acid sequences and hence a particular substrate specificity. The large variety of CYP enzymes is classified in families, subfamilies and isoforms. CYP enzymes of the same family share the same first number and are >40% identical in their amino acid sequence. The following letter designates the respective subfamily, which shares >59% sequence

identity. Lastly, the second number defines the CYP isoform [106]. The majority of drugs is metabolised by enzymes belonging to the families 1, 2 and 3. In detail, the isoforms 3A4/5, 2D6 and 2C9 metabolise 30.2%, 20.0% and 12.8% of the clinically used drugs, respectively. Further important isoenzymes in human drug biotransformation encompass 1A2 (8.9%), 2B6 (7.2%), 2C19 (6.8%), 2C8 (4.7%), 2A6 (3.4%), 2E1 (3%) and 2J2 (3%) [108].

The transformation of a substrate (R-H) by monooxygenases starts by its binding to the CYP with a trivalent iron ion. Subsequently, the iron ion is reduced by the transfer of an electron from an electron transfer chain involving nicotinamide adenine dinucleotide phosphate ($NADP^+$) and flavin adenine dinucleotide (FAD, Figure 1.2, centre) and hence converted to a bivalent iron ion. In the following, elemental oxygen as well as another electron are taken up and the enzyme substrate complex decomposes into the hydroxylated substrate (R-OH) and one molecule of water under regeneration of the enzyme (Figure 1.2). Overall, this results in the following net reaction (Eq. 1.1) [109]:

$$R\text{-}H + O_2 + NADPH + H^+ \rightarrow R\text{-}OH + H_2O + NADP^+ \qquad (1.1)$$

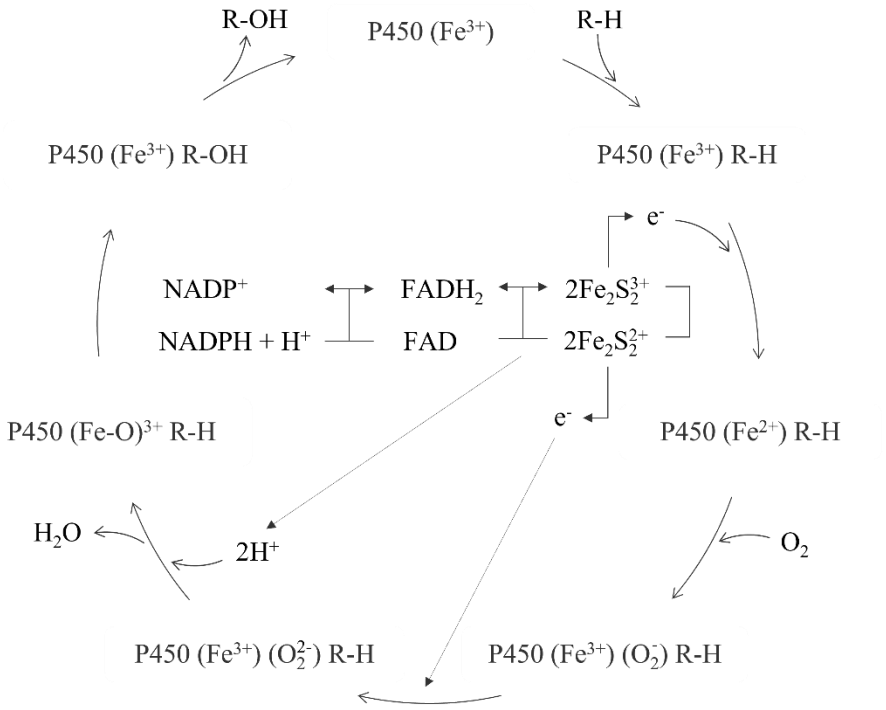

Figure 1.2: Mechanism of action of cytochrome P450 enzymes. For a detailed description of the cascade, see main text. Modified from [109].

R-H, initial state of the substrate; R-OH, oxidated state of the substrate, i.e. hydroxylated substrate; $NADP^+$, nicotinamide adenine dinucleotide phosphate; NADPH, reduced form of nicotinamide adenine dinucleotide phosphate; FAD, flavin adenine dinucleotide; $FADH_2$, reduced form of flavin adenine dinucleotide.

The clinical relevance of CYP enzymes manifests itself in several ways. Primarily, CYP enzymes are essential in the detoxification of drugs. The oxidation of a molecule makes it more hydrophilic, improving its ability to be renally excreted. Hence, in most cases the biotransformation of a drug leads to its loss in pharmacological activity. However, in some cases also the metabolites of a compound show pharmacological effects. This can either be wanted, i.e. supporting the therapeutic effect of the parent compound, or unwanted, i.e. causing adverse events. The latter is in the strict sense against the purpose of the biological function. Furthermore, in the case of prodrugs the enzymatic system is involved in the therapeutic principle as prodrugs have themselves no or only minor pharmacological activity but are activated to potent compounds by the respective metabolic enzymes.

Additionally, many clinically observed drug-drug interactions are based on inhibition or induction of CYP enzymes [109,110]. When an enzyme is inhibited, the biotransformation of the respective substrates is decelerated resulting in an increase in plasma concentrations and a prolonged $t_{1/2}$. Consequently, adverse events associated with drug treatment become more likely, or in the case of prodrugs, the anticipated pharmacological effects remain absent. From a mechanistic point of view, inhibition can be reversible or irreversible. Additionally, reversible inhibitors can be differentiated in competitive, non-competitive, uncompetitive and mixed competitive/non-competitive inhibitors by the nature of their interaction with the enzyme or enzyme-substrate complex [110,111]. Competitive inhibitors compete with the substrate for the same enzyme binding site, i.e. the active site, and hence when the substrate concentration is (largely) increased the maximum reaction velocity can be reached as the inhibitor is completely displaced. In contrast, non-competitive inhibitors do not bind to the active site but a secondary binding site (allosteric binding) and can equally interact with the enzyme and the enzyme-substrate complex. Thus, inhibitor binding has no influence on substrate binding but appears as a reduction in the amount of metabolising enzyme. Lastly, uncompetitive inhibitors bind to the enzyme-substrate complexes only, removing them from the system and thus leading simultaneously to a decreased reaction velocity and affinity for the substrate [110]. Irreversible inhibitors lead to a permanent removal of metabolising enzymes and hence entail long-lasting drug-drug interaction potential as only the biosynthesis of new enzymes revitalise the full functionality of the metabolic system [110]. Often, irreversible inhibition is referred to as “mechanism-based inhibition” or even “suicide inhibition” as the inactivation is caused by the generation of reactive electrophiles which bind covalently to the CYP enzyme, e.g. its haem group, in an $NADP^+$ dependent manner [111,112]. In contrast to inhibition, CYP enzymes can be activated as well as induced by xenobiotics. As a result, substrates of the respective enzymes are metabolised faster, shortening the time of pharmacological efficacy, potentially leading to subtherapeutic concentrations and hence therapy failure. In the case of prodrugs, opposite effects are likely, i.e. increased

concentrations of the pharmacologically active metabolite and hence the occurrence of adverse drug reactions. Mechanistically, activation is conveyed by a binding to the allosteric site of the CYP enzyme causing a conformational change and consequently an improved binding and conversion of the substrate. Induction on the other hand is mediated by an increased biosynthesis of enzyme molecules due to an adapted transcription of the encoding CYP enzyme genes [109,111].

Lastly, for many essential CYP isoenzymes polymorphisms, i.e. genetic variants, have been described. The most common mutation of CYP genes are single-nucleotide polymorphisms which can result in gain- and loss-of-function alleles [108,113]. Hence, the respective phenotypes are described as UM and RM, when two or one gain-of function alleles are present, respectively, NM, when two of the wild-type alleles are observed, as well as IM and PM, when one or two loss-of-function alleles are detected, respectively [108,113]. The phenotypic distribution in the population is dependent on the respective CYP isoenzyme and the ethnicity [113,114]. The clinical impact is comparable as described for inhibition and induction: the presence of loss-of-function alleles results in an impeded metabolism and inactivation of drugs, causing adverse events and toxic effects due to increased drug exposure. In contrast, gain-of-function alleles accelerate the metabolic turnover, entailing subtherapeutical exposures and hence the absence or reduction of therapeutic efficacy. For prodrugs, the effects are vice versa [108,113].

1.3.2 *In vitro* metabolic systems

A large variety of metabolic systems exist for *in vitro* investigations on human metabolism. The choice of the respective system is dependent on the research question as all systems have advantages and disadvantages. The most frequently used cellular and subcellular fractions are directly derived from human tissue. In Figure 1.3 the extraction procedure is illustrated for the liver, although subcellular fractions such as microsomes can also be acquired from other organs, e.g. the intestine or the kidneys. The human tissue is procured from discarded transplants, split liver transplants as well as waste material from liver surgeries [110,115]. Primary hepatocytes can be isolated from these tissues and used freshly or cryopreserved applying specific protocols to maintain cell viability [116,117]. As procedures of cryopreservation have been improved in the last decades and thus ameliorated the general availability of hepatocytes for research purposes, the popularity of hepatocytes for *in vitro* metabolism studies is increasing. The primary advantage of hepatocyte cultures is the integrity of the networks of metabolic pathways including all metabolic enzymes and their cofactors. In particular, investigations can elucidate the involvement of transporters and the potential of a compound to be an enzyme inducer. Consequently, enzyme kinetics determined in hepatocytes are assumed to be closest to the *in vivo* situation [116]. However, as cultivation and experimental procedures are cumbersome and time intensive,

subcellular fractions are still of high importance. They are obtained by homogenisation of liver tissue and gradual centrifugation with increasing centrifugal force to clear the homogenate from cell organelles, e.g. nuclei and mitochondria, and other cell debris (Figure 1.3). The supernatant that is available after the second centrifugation iteration is the so-called S9 fraction which contains besides the endoplasmic reticulum subcellular fraction also the cytosolic enzyme fraction. The latter includes enzymes such as aldehyde oxidase, xanthin oxidase, sulfotransferases, methyltransferases, *N*-acetyl transferases and glutathione transferases [118]. Therefore, the diversity in available enzymes is a benefit compared to microsomes. However, the dilution of the enzymes potentially hampers the detection of compound turnover or metabolite formation. Additionally, compared to hepatocytes, the addition of cofactors such as NADPH is necessary [118].

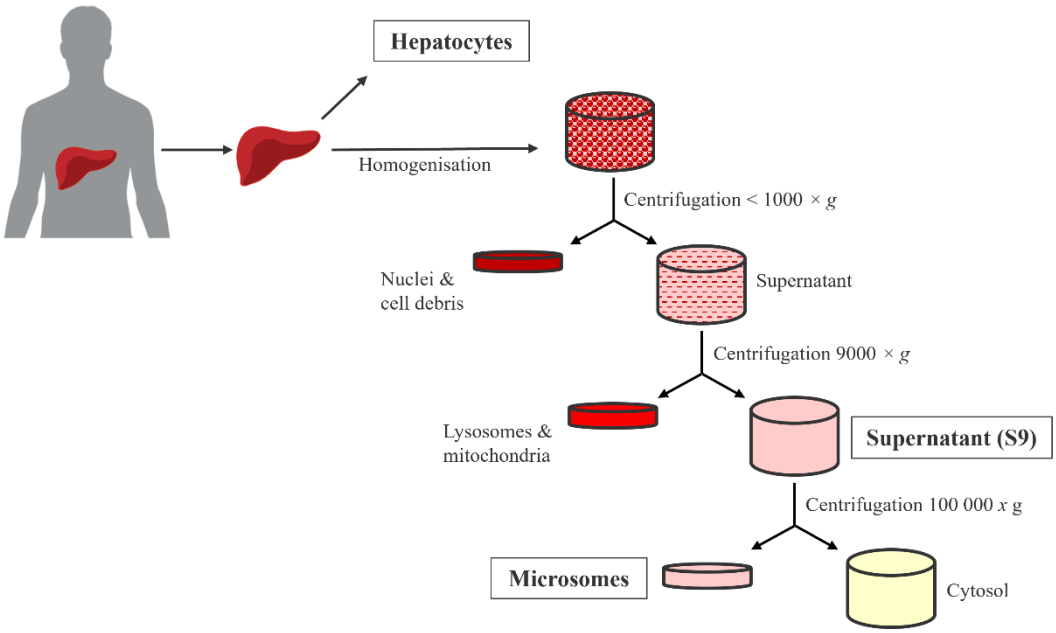

Figure 1.3: Schematic overview of the extraction of cellular and subcellular fractions from human liver to obtain the *in vitro* applicable metabolic systems of hepatocytes, S9-mixture and microsomes (boxes). Modified from [118].

Lastly, if the S9 supernatant is further centrifuged with high centrifugal force (100 000 × *g*), the remaining pellet depicts the microsomal fraction. Microsomes contain enzymes that are bound to the membrane of the endoplasmic reticulum including CYP enzymes as well as UGT. Microsomes are in comparison to hepatocytes easy to prepare and use as well as very robust regarding storage. Additionally, they contain CYP enzymes at a high concentration, ensuring in general sufficient compound turnover and metabolite formation. Accessory enzymes, such as the NADPH-cytochrome P450 reductase are conserved, however, similar to the S9 fraction, cofactors such as NADPH have to be added to *in vitro* incubations [110,118].

Besides the described cellular and subcellular fractions, also recombinant enzymes can be used for *in vitro* metabolism investigations. Although they are artificial in nature, which complicates the *in vitro* prediction of reaction kinetics, they have the large advantage of being a single enzyme system [110]. Hence, the involvement of individual enzymes can be determined, which is why they are commonly used for reaction phenotyping studies. Frequently applied expression systems comprise mammalian cells, insect cells, yeast and bacteria which yield a large variety of enzyme expression levels [119,120].

1.3.3 Michaelis-Menten kinetics

The most commonly applied model for the qualitative and quantitative description of metabolising enzyme kinetics is the Michaelis-Menten model, which characterises enzymatic processes at steady state and is based on the following assumptions. First, the binding of enzyme (E) and substrate (S) to an enzyme-substrate complex (ES), which is described by the rate constant k_1, is fast, resulting in a rapid attainment of steady state conditions. Second, each enzyme molecule binds one substrate molecule, i.e. cooperative or allosteric binding is negligible. Third, at steady state the concentration of the reactive intermediate of the reaction, i.e. the enzyme-substrate complex, is constant. Fourth, the dissociation of enzyme-substrate complex back to the individual components is faster than the formation of the product (P), i.e. the metabolite ($k_{-1} > k_2$). Fifth, the change in substrate concentration is negligible, i.e. the formation of enzyme-substrate complexes as well as product formation does not deplete the system of a relevant amount of substrate (<10%). This implies that substrate concentration is correspondingly higher than the enzyme concentration (Eq. 1.2) [106,110].

$$E + S \underset{k_{-1}}{\overset{k_1}{\rightleftarrows}} ES \xrightarrow{k_2} E + P \tag{1.2}$$

The Michaelis-Menten equation considers the reaction velocity (V) in relation to the substrate concentration (C_S), deriving two kinetic parameters: the maximum reaction velocity (V_{max}) and the Michaelis-Menten constant (K_M). V_{max} represents a rate, i.e. change in concentration per time, which is commonly normalised to the enzyme concentration, and K_M is defined as the substrate concentration at half-maximum reaction velocity (1/2 V_{max}, Eq. 1.3).

$$V = V_{max} \cdot \frac{C_S}{K_M + C_S} \tag{1.3}$$

The resulting hyperbolic concentration-reaction velocity function is shown in Figure 1.4. In the initial phase, at low substrate concentrations, reaction velocity is increasing linearly with increasing substrate concentrations. However, a saturation effect is observed at high substrate concentrations (>K_M), as a further increase in substrate concentration does not lead to

proportionally higher reaction velocities. Hence, the reaction velocity approaches asymptotically V_{max} [106,110].

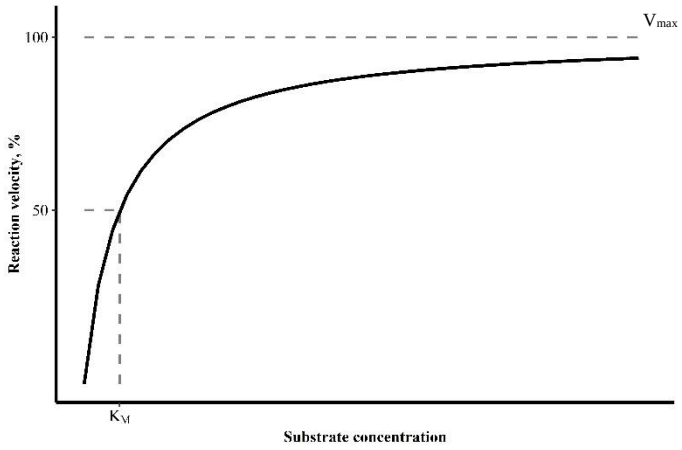

Figure 1.4: Exemplary representation of a hyperbolic function of the Michaelis-Menten equation, which relates substrate concentration to reaction velocity and the derivation of the Michaelis-Menten constant (K_M) and maximum reaction velocity (V_{max}).

To the most popular transformations of the Michaelis-Menten equation belong the linearisations by Lineweaver-Burk and Eadie-Hofstee. The Lineweaver-Burk plot is a double reciprocal plot, showing the relation of 1/V and $1/C_S$, hence the slope depicts the ratio K_M/V_{max} and the y-intercept $1/V_{max}$. The transformation by Eadie-Hofstee is based on the relation of V to the ratio of V/C_S and thus results in a linear function with the slope representing $-K_M$ and the y-intercept equalling V_{max}. Although the kinetic parameters of K_M and V_{max} can be derived from these linearisations, a nonlinear regression analysis is superior regarding accuracy and precision of the determined parameters. Hence, nowadays they are only used as diagnostic plots to detect atypical kinetics, which become apparent as deviations from linearity [110].

1.4 Target-site exposure assessment by microdialysis

PK investigations in clinical trials mainly focus on total drug concentrations determined in plasma. Yet, pathogens usually reside in extravascular spaces, i.e. the interstitial space fluid (ISF), representing the target site for anti-infective drugs [51,121–123]. As plasma and ISF concentrations have been observed to differ extensively [51,124], regulatory agencies reinforced recommendations to assess target-site concentrations in non-homogenate tissue [125]. A powerful tool for this aim is the minimally-invasive sampling technique microdialysis. In contrast to biopsies [126], it allows continuous sampling of the protein-unbound fraction over time as well as the determination of extracellular concentrations [127–129]. First descriptions of the microdialysis technique date back until the 1960s, although it gained popularity only approximately 20 years later. While these first studies were mainly conducted in the field of

neurosciences, today, microdialysis is applied for all kinds of endogenous and exogenous compounds and drugs in a large variety of tissues and fluids [130].

1.4.1 Principle of microdialysis

The microdialysis system consists of three major components: a high precision pump, the microdialysis catheter and a microvial for sample collection [127]. During the microdialysis process, the pump is continuously conveying a fluid, the so-called perfusate, through the attached microdialysis catheter at a flow rate of usually 1-2 µL/min [131,132]. The microdialysis catheter is, at its tip, equipped with a selectively permeable membrane, that is inserted into the tissue fluid to sample e.g. interstitial space or cerebrospinal fluid. In case of recovery investigations, the concentration of the respective compound is higher in ISF than in the perfusate. Thus, following the concentration gradient, molecules diffuse across the membrane into the perfusate, which is subsequently collected as microdialysate in the microvial (Figure 1.5, left). To avoid an excessive diffusion of fluids, the perfusate commonly consist of an aqueous solution mimicking the surrounding medium to prevent osmotic differences [127]. As the microdialysis catheter is continuously perfused, an equilibrium between concentration in ISF and perfusate is never reached, resulting in the need to determine a relative recovery (RR) value. The RR of a compound describes the fraction of the ISF concentration determined in microdialysate and is required to convert microdialysate concentrations to ISF concentrations [127–130].

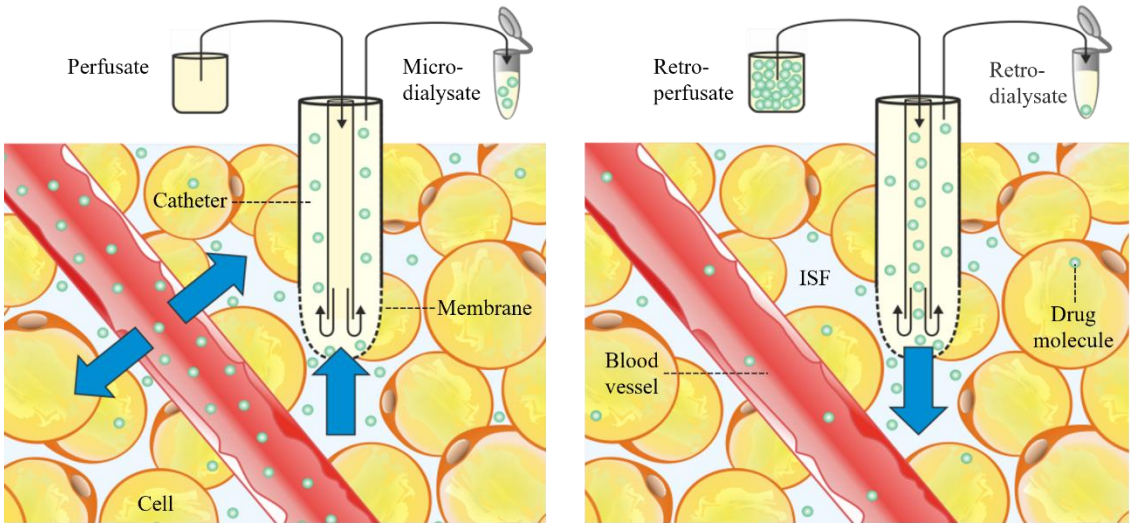

Figure 1.5: The principle of microdialysis for recovery (left) and delivery investigations (right), exemplified for a microdialysis catheter inserted into subcutaneous adipose tissue for investigations on interstitial space fluid (ISF).

The RR value is dependent on various parameters. First, the choice of the used microdialysis catheter considering inlet and outlet tubings as well as membrane characteristics, e.g. its molecular mass cut-off, dimensions and materials. The decision on the microdialysis catheter is

mainly dependent on the tissue fluid of interest, as different specialised catheters such as brain, gastrointestinal or i.v. microdialysis catheters exist. Furthermore, two different types of microdialysis catheters, concentric and linear, are applied in clinical practice. While in concentric catheters the inlet and outlet tubing are combined, linear catheters have separate inlet and outlet tubings. The core component of a microdialysis catheter is its membrane. Most membranes are made of polyarylethersulphone (PAES) an unreactive synthetic material that has been demonstrated to be appropriate for the sampling of most endogenous and exogenous compounds. However, a large variety of molecular mass cut-offs is available, ranging from typically 20 to 100 kDa and thus enabling the sampling of small molecule drugs as well as macromolecules. Moreover, the surface area of the membrane is essential with diameters of 0.5 to 0.6 mm and lengths of 10 to 30 mm the area available for diffusion processes differs relevantly [127,133]. Second, with increasing flow rate, the RR is decreasing [134]. Consequently, concentrations in microdialysate are low, potentially challenging the bioanalytical quantification. In contrast, lower flow rates result in a higher RR, but entail longer sampling intervals to obtain the necessary volume for bioanalysis and therefore impair the generation of high-resolution concentration-time profiles. Hence, the best compromise must be made for the aim of the respective investigation [127,134]. Third, RR is highly dependent on the compound of interest itself. As a general rule, the molecular mass of the compound should not be larger than one fourth of the membrane cut-off of the microdialysis catheter. However, charge, lipophilicity and sterical configurations play an additional role [128]. In particular highly lipophilic drugs have been described to show non-specific binding to the different components of the microdialysis system, e.g. membrane and tubings [129,135]. As a result, microdialysate concentrations do not reflect ISF concentrations as a time delay might be observed. In order to enable microdialysis of these compounds, albumin can be added to the perfusate or catheters precoated ensuring saturation of the nonspecific binding sites before the start of the investigations. However, as a consequence the behaviour of recovery might be altered, impeding the evaluation of the results [129,135,136]. Here, profound *in vitro* preliminary investigations are essential. Fourth and last, when comparing *in vitro* and *in vivo* RR values the latter will be in most cases decreased due to the tortuosity, i.e. the increased diffusion path of the molecules caused by the presence of cell structures and extracellular matrix [127,129].

1.4.2 Calibration of microdialysis catheters

A calibration of microdialysis catheters is necessary to determine the RR and thus to transform concentrations in microdialysate to ISF concentrations. This calibration is typically performed *in vivo* individually for each compound and catheter as due to the tortuosity, *in vitro* determinations of RR are not transferable to an *in vivo* situation. For this purpose, a variety of approaches have been developed for the calibration of microdialysis catheters exploiting in particular the dependence of recovery on flow rate and concentration [127–129].

First, as RR is increasing with decreasing flow rates, the extrapolation to zero approach uses the relation of RR to flow rate to deduce the RR at a flow rate of zero which equals the condition of equilibrium. A reasonable approximation is the method of low flow rates which assumes the formation of an equilibrium when very low flow rates are applied. Second, the no-net-flux approach is based on the absence of diffusion of the compound across the membrane when the concentration in ISF equals the concentration in the perfusate. Therefore, the respective compound is added to the perfusate at different concentrations and the concentration difference between perfusate and microdialysate determined. Is this difference described as a function of the perfusate concentration, the ISF concentration can be deduced as the perfusate concentration at a difference of zero. However, the no-net-flux method can only be applied at steady-state conditions and is time and labour intensive. Third, endogenous compounds such as urea can be used as a reference in recovery investigations. The assumptions taken are, that urea is a freely diffusible molecule, the concentration in ISF is constant over time and that the RR ratio of two compounds is transferable from *in vitro* to *in vivo* [127–129]. Fourth, the retrodialysis method which is the most frequently used due to its easy and time efficient application. This approach applies the microdialysis principle in reverse: a minimum 20-fold higher concentration of drug compared to expected ISF concentrations is added to the perfusate (now the so-called retroperfusate) leading to a diffusion of drug molecules into the ISF (Figure 1.5, right). Consequently, the decrease in concentration in microdialysate (or retrodialysate) compared to the retroperfusate can be determined and enables the calculation of relative delivery (rD). RR is assumed equal to rD as diffusion across the microdialysis membrane is supposedly independent of the direction [127–129]. Fifth, the calibration by internal standard (IS), which is based on the retrodialysis principle but continuously applies a second compound, with optimally identical behaviour in microdialysis, in the perfusate and assumes that the loss of the IS equals the recovery of the compound of interest [127].

Overall, the described calibration approaches reach their boundaries when besides the compound of interest also its metabolites are to be investigated. While it is common practice to administer the metabolite directly to animals, this is prohibited for humans as metabolites are chemical substances not licensed for human administration [60]. Consequently, different approaches have to be found.

1.4.3 Static *in vitro* microdialysis system

Although *in vitro* determined RR cannot be directly transferred to *in vivo* studies, *in vitro* investigations are essential to characterise the compound of interest in microdialysis sampling [129]. Thereby, the suitability of a compound for the performance of microdialysis sampling can be determined in the first place. In particular highly lipophilic drugs have been observed to adsorb

to the membrane or other materials of the microdialysis system. Consequently, recovery can be optimised *in vitro* before the conduction of clinical trials. Furthermore, a general RR can be derived supporting the decision on flow rates for *in vivo* investigations and subsequently guide the study design, i.e. the duration of sampling intervals appropriate for bioanalytical quantification.

Nevertheless, to achieve reliable predictions, a standardised *in vitro* approach, mimicking the *in vivo* situation, is crucial. Therefore, a static *in vitro* microdialysis system (sIVMS) has been developed and validated [137]. In brief, it is composed of a pump module, ensuring the sound placement of the *in vitro* microdialysis pumps, a catheter module, allowing the safe fixation of medium containers, microdialysis catheters and collection vials during the investigation, a stirring module, ensuring the constant flow of the catheter-surrounding medium and lastly, the thermo module, heating the medium to 37°C to mimic body temperature. Furthermore, the setup allows for a constant monitoring of the microdialysis procedure. The containers holding the catheter-surrounding medium are made of glass, enabling the check for air bubbles at the catheter membrane which potentially pose a diffusion barrier. Additionally, the medium containers are freely accessible, enabling the easy sampling of the catheter-surrounding medium. Besides the constant stirring of the fluid and a temperature of 37°C, a physiological-like solution, such as Ringer's solution (RS), is applied as catheter-surrounding medium to overall mimic the *in vivo* conditions as best as possible [134,135,137].

1.5 Quantitative aspects of pharmacokinetic investigations

PK investigations focus on the concentration-time course of a drug and its metabolites in different tissues and body fluids. The absorption, distribution, metabolism and excretion of a compound is highly dependent on the individual study participant's characteristics such as age, weight, body composition, organ function, health condition, concomitant medication, as well as on drug-specific features, e.g. its physicochemical properties or the administered dose. Hence, to satisfactorily describe the PK of a drug and its metabolites, accurate and precise quantification methods are needed for diverse matrices of variable available volumes.

In most PK investigations, drug and metabolite concentrations are routinely determined in plasma as it can be easily obtained from whole blood. In human adults, numerous blood samples of 5-10 mL can be drawn daily, and hence the available volume for quantification is not limiting the PK investigation. This is different for paediatric or animal studies. Here, only a limited volume of blood can be acquired and consequently higher demands on quantification methods are imposed. For the investigation of target-site concentrations, i.e. ISF concentrations, the application of microdialysis is feasible. As for the perfusion of the microdialysis catheter often low flow rates (1-2 µL/min) are used, also in this case, the available volume for bioanalytical

quantification is limited [127]. Indeed, the less volume is needed for bioanalysis, shorter sampling intervals are feasible, resulting in the generation of high-resolution concentration-time profiles.

The volume needed for bioanalysis is also highly dependent on the necessary sample pre-treatment procedure. Microdialysate is already free of protein and thus can be directly subjected to quantification. In contrast, plasma has to be cleared of its proteins, e.g. by precipitation with organic solvents such as acetonitrile or methanol (MeOH). Depending on the compound of interest and the bioanalytical method, also more sophisticated approaches as liquid-liquid extraction (LLE) or solid-phase extraction (SPE) might be necessary. Hence, more volume of the original sample might be needed. The same holds true, when plasma is to be further processed, e.g. by ultrafiltration, to obtain the unbound fraction of the drug in plasma. Similar to microdialysis, ultrafiltration is based on the principle, that (protein) unbound molecules can cross a selectively-permeable membrane. However, ultrafiltration applies centrifugation force for separation. Naturally, the processing of the sample often results in a dilution of the original concentration, requiring consequently a higher sensitivity in detection and quantification.

In recent years therefore, liquid chromatography-tandem mass spectrometry (LC-MS/MS) became the routine method for quantification in PK investigations. In a first step, the LC part, the compounds of interest are separated from each other as well as from matrix constituents by application of an appropriate column, suitable eluents, their respective gradient and a justified temperature. Subsequently, a mass spectrometer detects the arriving molecules by ionisation, e.g. by an electrospray technique. As for PK investigations often a high specificity is needed, commonly tandem MS with a triple quadrupole (QQQ) is used. This technique selects a precursor ion with a defined mass-to-charge ratio (*m/z*) in the first quadrupole which is subsequently fragmented in the second quadrupole, also called the collision cell. In the third quadrupole one or multiple product ions with specified *m/z* are singled out for detection. The specificity is hence given by the pre-selection of the compounds molecular mass as well as its unique fragmentation pattern [138]. Moreover, the described procedure reduces background noises caused by various components in complex matrices to a minimum. As a result, very low concentrations are detectable and even quantifiable. This in turn, allows for a decreased injection volume and hence less required volume of the original sample.

Lastly, determinations of PK investigations have to be accurate, precise and reproducible. Therefore, drug regulatory agencies such as the EMA and the FDA have published guidelines specifying procedures and compliance criteria for bioanalytical method development and validation [139,140]. Although those guidelines are addressed to the pharmaceutical industry preparing clinical studies for market authorisation of new drugs, the specifications provide a solid scientific basis also for other applications. Among the parameters that are to be investigated are selectivity, matrix effects, accuracy, precision and stability.

1.6 Objectives

The increasing global prevalence of invasive fungal infections is a rising, but an underappreciated threat to the public health. As the development of new antifungal agents is lagging behind this epidemiological burden, one important aspect is the stewardship of existing antifungal drugs, such as VRC. Despite its long-term and frequent application in humans, large intra- and interindividual variability in VRC PK is observed, resulting in inadequate dosing and hence therapy failures and adverse events. The underlying mechanisms of the high variability, in particular its complex metabolism are not yet fully understood and require a thorough comprehension in order to adjust VRC dosing for an optimised risk-benefit ratio in each patient.

This thesis therefore aimed at contributing to the elucidation of the PK of VRC by investigations of distribution and metabolism processes in humans. For this purpose, the research objectives of this thesis were located in three major areas (Figure 1.6). As an essential prerequisite for comprehensive *in vitro* and *in vivo* PK investigations of VRC and its metabolites, a versatile and sensitive bioanalytical method, covering a variety of human matrices, was aimed for. Furthermore, striving for a broader comprehension of the complex metabolism of VRC, *in vitro* metabolism investigations were identified as valuable instruments and thorough quantitative and mechanistic characterisations were intended. Lastly, aiming at amalgamating the knowledge on PK of VRC that can be gained by microdialysis investigations and simultaneous drug and metabolite assessment, an *in vitro* and an *in vivo* investigation for the simultaneous microdialysis of VRC and NO was targeted.

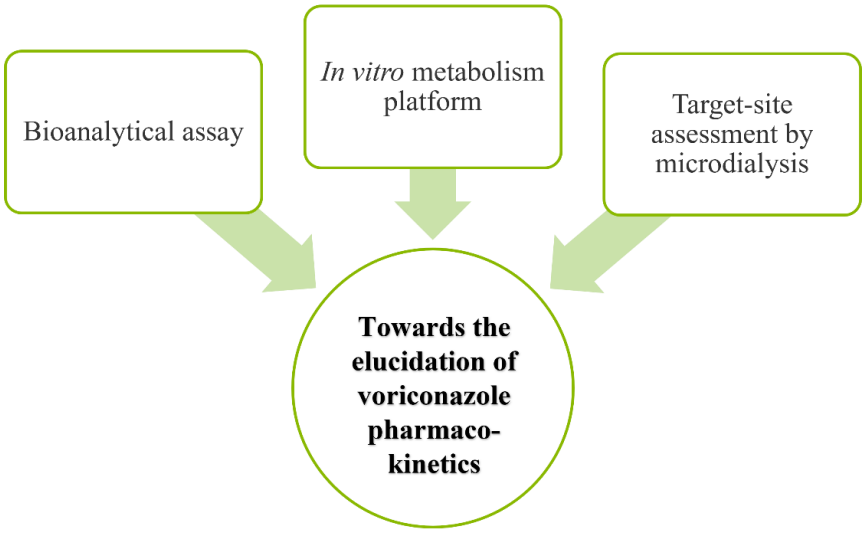

Figure 1.6: Overview of the three main research areas covered in this thesis to achieve the overarching objective.

The first research pillar, comprising the establishment of a bioanalytical quantification method enabling more profound *in vivo* and *in vitro* PK investigations of VRC, pursued the following detailed objectives:

- Development of a bioanalytical LC-MS/MS assay for the simultaneous quantification of VRC, NO and OH-VRC in small sample volumes of plasma, ultrafiltrate and microdialysate.
- Validation of this bioanalytical assay according to international guidelines for the simultaneous determination of VRC and NO in human plasma and microdialysate.
- Adaptation of the bioanalytical assay for quantification of NO and OH-VRC in *in vitro* metabolism experiments.

In the second research pillar, the focus was on the comprehensive, quantitative and mechanistic characterisation of VRC and its metabolites as substrates and inhibitors of the CYP isoenzymes 2C19, 2C9 and 3A4, aiming concretely at:

- Establishment of an *in vitro* metabolism platform optimised for the reliable characterisation of VRC in the enzymatic systems of HLM, human intestine microsomes (HIM) and rhCYP.
- Characterisation of Michaelis-Menten kinetics for the *N*-oxidation of VRC in HLM, HIM and rhCYP2C19, 2C9 and 3A4.
- Assessment of the contribution of the CYP isoenzymes 2C19, 2C9 and 3A4 to the overall *N*-oxidation of VRC.
- Performance of *in vitro in vivo* extrapolation (IVIVE) to assess the *in vivo* human hepatic clearance by VRC *N*-oxidation.
- Determination of the metabolic stability of NO and OH-VRC.
- Quantitative and mechanistic assessment of the inhibitory potential of VRC, NO and OH-VRC on the CYP isoenzymes 2C19, 2C9 and 3A4.

The third research pillar involved the exploration of distribution processes of VRC and its *N*-oxide metabolite into ISF using the technique of microdialysis considering the following aims:

- Assessment of the feasibility of simultaneous microdialysis sampling of VRC and NO by comprehensive *in vitro* investigations.
- Determination and quantification of the impact of experimental parameters on the *in vitro* RR of VRC and NO.

- Proposal of an *in vivo* applicable approach for microdialysis catheter calibration allowing the deduction of ISF concentrations of NO.
- Assessment of the *in vivo* feasibility of simultaneous microdialysis of VRC and NO in humans by quantification of clinical microdialysis samples.
- Exploratory PK analysis of VRC and NO total and unbound plasma as well as ISF concentrations of four healthy volunteers and assessment of the impact of the CYP2C19 genotype-predicted phenotype and number of administered doses on intra- and interindividual differences.

2 Materials and methods

2.1 Materials

2.1.1 Chemicals, drugs, reagents and biological materials

1-Hydroxymidazolam, LOT: 0589923	Cayman Chemical, Ann Arbor, Michigan, United States of America
4-Hydroxydiclofenac, LOT: 0522547	Cayman Chemical, Ann Arbor, Michigan, United States of America
4-Hydroxymephenytoin, LOT: 0550849	Cayman Chemical, Ann Arbor, Michigan, United States of America
Albumin Fraction V (from bovine serum), LOT: 399288924	Carl Roth GmbH, Karlsruhe, Germany
Corning© UltraPool™ HLM 150, LOT: 38292, 38294, 38295	Corning Inc., New York, United States of America
Corning® Gentest™ NADPH Regenerating System Solution A, 26 mM $NADP^+$, 66 mM Glucose-6-phosphate, 66 mM Magnesium chloride, LOT: 0344003, 1046001	Corning Inc., New York, United States of America
Corning® Gentest™ NADPH Regenerating System Solution B, 40 U/mL Glucose-6-phosphate dehydrogenase in 5 mM sodium citrate, LOT: 0342002, 1095005	Corning Inc., New York, United States of America
Corning® Gentest™ pooled human intestine microsomes, LOT: 8193001	Corning Inc., New York, United States of America
D-Glucose-6-phosphate dipotassium salt hydrate, LOT: SLBT8385	Sigma-Aldrich, Saint Louis, Missouri, United States of America
Diazepam in methanol, 1 mg/mL solution, LOT: FE12021903	Cerilliant Corporation, Round Rock, Texas, United States of America

Diclofenac sodium salt, LOT: BCCB7633	Sigma-Aldrich, Saint Louis, Missouri, United States of America
Dipotassium hydrogen phosphate trihydrate, LOT: 6319483	Merck KGaA, Darmstadt, Germany
Formic acid, LC-MS grade, LOT: 200812	SERVA Electrophoresis GmbH, Heidelberg, Germany
Glucose-6-phosphate dehydrogenase, LOT: 128M4011V	Sigma-Aldrich, Saint Louis, Missouri, United States of America
Glucose-6-phosphate dehydrogenase, LOT: J61181	AlfaAesar™, Thermo Fisher Scientific Inc., Rochester, New York, United States of America
Human sodium citrate plasma	German Red Cross blood donation service, Berlin, Germany
Hydrochloric acid 37%, LOT: K47066817541	Merck KGaA, Darmstadt, Germany
Hydroxyvoriconazole, LOT: 7-NVG-146-1	Toronto Research Chemicals, Toronto, Canada
Ketoconazole, LOT: VRTIO	Tokyo Chemical Industry, Tokyo, Japan
Loratadine, LOT: YQ74L	Tokyo Chemical Industry, Tokyo, Japan
Magnesium chloride hexahydrate, LOT: 5273508	Merck KGaA, Darmstadt, Germany
Methanol, LC-MS grade, various LOTs	J.T. Baker™, Thermo Fisher Scientific Inc., Rochester, New York, United States of America
Midazolam in methanol, 1 mg/mL solution, LOT: FE04082004	Merck KGaA, Darmstadt, Germany
Milli-Q® water, purified by Milli-Q® Reference A+	Merck KGaA, Darmstadt, Germany
Nicotinamide adenine dinucleotide phosphate ($NADP^+$), LOT: 0495515	Cayman Chemical, Ann Arbor, Michigan, United States of America

Potassium dihydrogen phosphate, LOT: 1167701	Merck KGaA, Darmstadt, Germany
Ringer's solution for infusion, various LOTs	B. Braun, Melsungen, Germany
S-mephenytoin, LOT: 0575934	Cayman Chemical, Ann Arbor, Michigan, United States of America
Sulfaphenazole, LOT: 0545861	Cayman Chemical, Ann Arbor, Michigan, United States of America
Supersomes™, Human CYP2C19 + P450 Reductase, LOT: 9275001 Human CYP2C9*1 (Arg_{144}) + P450 Reductase LOT: 9277002 Human CYP3A4 + P450 Reductase, LOT: 9023001	Corning Inc., New York, United States of America
Trishydroxymethylaminomethane (TRIS), LOT: 2365376	Fluka™, Thermo Fisher Scientific Inc., Rochester, New York, United States of America
Ultra-pure water, purified by SG LaboStar™ 2-DI/UV	Evoqua Water Technologies, Eschborn, Germany
Voriconazole *N*-oxide, LOT: 7-DPM-64-3, 4-FBJ-47-4	Toronto Research Chemicals, Toronto, Canada
Voriconazole *N*-oxide, LOT: 0591435	Cayman Chemical, Ann Arbor, Michigan, United States of America
Voriconazole, LOT: 1-TTK-73-1	Toronto Research Chemicals, Toronto, Canada
Voriconazole, LOT: 052301-008-09	Pfizer, Kent, United Kingdom

2.1.2 Consumables

Centrifuge tubes (15 mL), various LOTs	VWR International, Darmstadt, Germany
Centrifuge tubes (50 mL), various LOTs	Carl Roth GmbH, Karlsruhe, Germany

CMA60 microdialysis catheters, Membrane: PAES Membrane length: 30 mm Cut-off: 20 kDa Shaft length: 20 mm Inlet: 400 mm Outlet: 105 mm LOT: T15382, T18205	CMA Microdialysis AB, Stockholm, Sweden
InfinityLab Poroshell 120 Phenyl Hexyl column (RP, 2.1 × 100 mM, 2.7 µM), various LOTs	Agilent Technologies, Waldbronn, Germany
Norm-Ject® 1 mL syringes (luer), various LOTs	Henke Sass Wolf, Tuttlingen, Germany
Nunc™ 96-well plates (polypropylene, conical bottom), various LOTs	Thermo Fisher Scientific Inc., Rochester, New York, United States of America
Nunc™ pre-slit well cap for 96-well plates, various LOTs	Thermo Fisher Scientific Inc., Rochester, New York, United States of America
Pipette tips, epT.I.P.S.® Standard (0.1 µL – 5 mL), various LOTs	Eppendorf AG, Hamburg, Germany
Safe-lock tubes (0.5 mL, 1.5 mL, 2.0 mL), various LOTs	Eppendorf AG, Hamburg Germany
Soft-Ject® 1 mL syringes (luer lock), various LOTs	Henke Sass Wolf, Tuttlingen, Germany
Sterican® cannulas (various sizes), various LOTs	B. Braun, Melsungen, Germany
UHPLC Guard 3PK, InfinityLab Poroshell 120 Phenyl Hexyl (2.1 × 4 mM, 2.7 µM), various LOTs	Agilent Technologies, Waldbronn, Germany
Ultrafiltration units (cut-off 30 kD, modified polyethersulfone membrane), LOT: FE1061	VWR International, Darmstadt, Germany

2.1.3 Laboratory devices and equipment

Agilent LC-MS/MS system: 1290 Infinity II LC system (Autosampler G7167B High speed pump G7120A Multicolumn thermostat G7116B), Triple quadrupole system G6495A	Agilent Technologies, Waldbronn, Germany
Analytical balance, BP221S	Sartorius AG, Göttingen, Germany
Analytical balance, R200D	Sartorius AG, Göttingen, Germany
Centrifuge, Eppendorf 5417R	Eppendorf AG, Hamburg, Germany
Centrifuge, Eppendorf 5430R	Eppendorf AG, Hamburg, Germany
CMA102® pumps	CMA Microdialysis AB, Stockholm, Sweden
Duran® glass bottles (various sizes)	Schott AG, Mainz, Germany
Eppendorf Thermomixer 5436	Eppendorf AG, Hamburg, Germany
Eppendorf Thermomixer 5437	Eppendorf AG, Hamburg, Germany
Glass equipment (volumetric flasks, measuring cylinders, funnels, beakers, Erlenmeyer flasks)	VWR International, Darmstadt, Germany
Magnetic stirrer RCT basic	IKA Labortechnik GmbH, Staufen, Germany
Magnetic stirring bars (various sizes)	VWR International, Darmstadt, Germany
pHenomenal™, pH-Meter pH 1000 L	VWR International, Darmstadt, Germany
Pipettes (0.5-10 µL, 2-20 µL, 10-100 µL, 20-200 µL, 100-1000 µL, 500-5000 µL) Eppendorf Research Eppendorf Research plus	Eppendorf AG, Hamburg, Germany
Vortexer, REAX2000	Heidolph Instruments GmbH & CO. KG, Schwabach, Germany

2.1.4 Software

The following software was used throughout all projects and applied to generate, process, analyse and evaluate data. Related packages, features and settings relevant for specific investigations are mentioned in the respective chapters.

Agilent MassHunter, version B.08.00 & B.10.00	Agilent Technologies, Waldbronn, Germany
ChemDraw®, version 18.1	PerkinElmer, Waltham, Massachusetts, United States of America
Microsoft® Office Excel®	Microsoft Corporation, Redmond, Washington, United States of America
R, version 3.6.0	R foundation for Statistical Computing, Vienna, Austria
RStudio®, version 1.3.1056	RStudio Inc., Boston, Massachusetts, United States of America

2.1.5 Preparation of buffers and solutions

For a better reproducibility and comparability of the results, all buffers and solutions were prepared in the same way throughout the investigations. In particular, whenever possible, the same products and batches were used.

2.1.5.1 Preparation of phosphate buffer

Potassium phosphate buffer (PPB), 50 mM and pH 7.4, was used as homogenisation buffer for dilutions of HLM, rhCYP and HIM [110,141,142]. For this purpose, 1.14 g of dipotassium hydrogen phosphate trihydrate and 0.680 g potassium dihydrogen phosphate were dissolved in 100 mL ultra-pure (UP) water each, resulting in 50 mM solutions. Afterwards, the potassium dihydrogen phosphate solution was added gradually to the dipotassium hydrogen phosphate solution under constant stirring until a pH of 7.4 was attained and stable for a minimum of 5 min.

2.1.5.2 Preparation of TRIS buffer

TRIS buffer, 250 mM and pH 7.5, was prepared by dissolving 3.03 g TRIS base in approximately 80 mL UP water and adding 2 N hydrochloric acid under constant stirring until a pH of 7.5 was reached and stable for a minimum of 5 min. Finally, the volume was filled up to 100 mL using a volumetric flask and the pH was verified. The concentrated TRIS buffer solution was diluted 1:5 in the final incubation mixture resulting in a 50 mM incubation buffer (chapter 2.3) [71,110,143].

2.1.5.3 Preparation of stock solutions

The concentrations of stock solutions must be accurate to enable reliable quantifications. Therefore, a minimum of 10 mg of drug substance was weighted to ensure an imprecision of ≤1% of the analytical balance used. If less than 10 mg of drug substance were purchased, the exact weight was requested from the manufacturer. All stock solutions were prepared accounting for the potency of the respective batch that encompassed the purity of the substance given by an appropriate assay (e.g. HPLC-MS), the water content as well as the reduction of the active fraction due to the presence of counter-ions of salts [144]. If the potency was not directly provided by the manufacturer, it was calculated according to equation 2.1. The respective volume of solvent was determined according to equation 2.2.

$$Potency = assay\ purity\ \cdot active\ fraction \cdot (1 - water\ content) \quad (2.1)$$

$$Volume\ (mL) = \frac{weight\ (mg) \cdot potency}{concentration\ \left(\frac{mg}{mL}\right)} \quad (2.2)$$

VRC and NO were dissolved in MeOH to obtain two independent stock solutions of 1 mg/mL each. Furthermore, a stock solution of VRC of 3.5 mg/mL in a premixed solution of water and MeOH (1:1 [V/V]) was prepared for all metabolism experiments (chapter 2.3.4). Stock solutions of OH-VRC, midazolam, diazepam and 4-hydroxydiclofenac (OH-DIC) were prepared at a concentration of 1 mg/mL in MeOH, of diclofenac and S-mephenytoin at a concentration of 10 mg/mL in MeOH, of 4-hydroxymephenytoin (OH-MEP) at a concentration of 5 mg/mL in MeOH and of 1-hydroxymidazolam (OH-MDZ) at a concentration of 0.5 mg/mL in MeOH, respectively. All stock solutions were stored at -80°C in aliquots of 1 mL or 100 µL depending on the initially prepared volume.

2.2 Bioanalytical assay for the simultaneous quantification of voriconazole, voriconazole *N*-oxide and hydroxyvoriconazole

For more profound research on VRC PK, a reliable and versatile bioanalytical assay for the quantification of VRC and its two major metabolites in various *in vitro* and *in vivo* matrices was aimed for. To cover its employment in all projects, applicability to the human matrices of plasma, ultrafiltrate and microdialysate as well as in matrices derived from *in vitro* experiments, i.e. *in vitro* microdialysis and incubations of HLM, rhCYP and HIM, was required. In order to ensure the best possible performance of the assay, the quality standards of the EMA guideline on bioanalytical method validation [139] were followed.

2.2.1 Development of the bioanalytical LC-MS/MS assay

The bioanalytical assay had to be suitable for a wide range of matrices and analytes. For an efficient application of the method, a stepwise approach was taken. Firstly, the method was optimised with regards to chromatographic separation and MS detection (chapter 2.2.1.1). Secondly, quantification of VRC and NO in plasma and microdialysate was established and subsequently also fully validated according to the EMA guideline (chapter 2.2.2) [139]. Thirdly, the method was expanded and if necessary, adapted to the quantification of VRC and NO in ultrafiltrate (chapter 2.2.3) and of NO in *in vitro* matrices (chapter 2.2.4).

2.2.1.1 Instrumentation and LC-MS/MS instrument setup

The LC-MS/MS system used for quantification was composed of an Agilent 1290 Infinity II LC system, including a multisampler, a high-speed pump and a multicolumn thermostat, and a QQQ MS/MS system. Agilent MassHunter software as well as R and RStudio® were used for adjusting instrument settings, data generation and processing.

For the prevention of degradation and maintenance of standardised conditions, samples were kept at 4°C in the autosampler until injection. An InfinityLab Poroshell 120 Phenyl Hexyl column (RP, 2.1 x 100 mM, 2.7 µM) was combined with an InfinityLab Poroshell 120 Phenyl Hexyl guard column (2.1 x 5 mM, 2.7 µM) and ensured chromatographic separation. As eluents, MeOH and UP water were utilised and the addition of 0.1% [V/V] formic acid (FA) in both solvents enhanced the ionisation process. For the optimisation of the elution and separation of VRC, NO and OH-VRC as well as the IS, a 1 µg/mL methanolic mixture was used and different gradient profiles with varying increases in the MeOH fraction, were investigated.

Ionisation in the MS system was accomplished by an electrospray ionisation (ESI) source. To explore the fragmentation of VRC, NO and OH-VRC as well as the IS, matrix-free individual methanolic solutions at concentrations of 10 µg/mL were directed to the MS. The Agilent Optimizer software performed the optimisation of the respective mass transitions from the precursor ions ($[M+H]^+$) of *m/z* 350 (VRC), *m/z* 366 (NO and OH-VRC) and *m/z* 285 (IS) by a series of different scan types [145]. This included, in the order given, an optimisation of the acquisition of product ions, the optimisation of the collision energy and the validation of the collision energy and masses determined in previous steps.

Finally, ion source parameters were optimised using the Agilent Optimizer Software by repeated injections of a mixture of VRC, NO, OH-VRC and the IS applying the final gradient chromatography method. For this purpose, the capillary voltage, nebulizer gas pressure, drying gas flow and temperature, sheath gas flow and temperature as well as iFunnel parameters were varied for every injection and the intensity of product ion formation monitored.

2.2.1.2 Preparation of matrix, calibrator, quality control and internal standard solutions

Calibrator (CAL) and quality control (QC) samples were prepared in matrices similar to future study samples. For this purpose, human sodium citrate plasma from four individual donors was pooled, aliquoted and stored at -80°C until usage. Pure ultrafiltrate was obtained from pooled plasma by centrifugation at 10000 × *g* for 60 min using centrifugal filters with a membrane of polyethersulfone and a molecular mass cut-off of 30 kDa. RS is regularly used as perfusate in clinical microdialysis studies [132,134,146] and was hence applied as artificial microdialysate matrix for bioanalytical method development and validation. For the quantification of NO and OH-VRC in the *in vitro* matrices of HLM, rhCYP and HIM, a surrogate incubation matrix was developed to avoid the routine preparation of CAL and QC samples in those rare matrices. Therefore, the HLM protein content was replaced by bovine serum albumin (BSA) which was dissolved in PPB (50 mM, pH 7.4) at a concentration of 4 mg/mL and diluted with TRIS buffer (250 mM, pH 7.5) and UP water to a concentration of 0.2 mg/mL. Due to simplicity, co-factors for the enzymatic reactions, such as $NADP^+$, glucose-6-phosphate and glucose-6-phosphate dehydrogenase were omitted in the surrogate matrix (compare chapter 2.3.1).

To maintain the specific characteristics of the matrices, a dilution with water or organic solvents during spiking had to be avoided. Thus, the addition of a volume fraction of maximum 5% was tolerated in the preparation of working solutions.

For the preparation of VRC and NO CAL and QC working solutions in plasma, ultrafiltrate and microdialysate the stock solutions of 1 mg/mL were used. For this purpose, the stock solution was diluted 100-fold with plasma, ultrafiltrate or microdialysate to acquire a working solution of 10 µg/mL which was further serially diluted with the respective matrix to concentrations of 1000 and 100 ng/mL. Independent sets of those three working solutions were used for the preparation of CAL or QC samples, respectively. Final CAL concentrations were 5, 10, 50, 100, 500, 2000 and 5000 ng/mL for plasma and 4, 10, 40, 100, 500, 1800 and 4000 ng/mL for microdialysate, while QC concentrations were 5, 15, 200, 1500 and 4000 ng/mL for plasma, 4, 8, 150, 1200 and 3000 ng/mL for microdialysate and 15 and 4000 ng/mL in ultrafiltrate.

CAL and QC samples of NO and OH-VRC in surrogate incubation matrix were prepared using a secondary stock solution of 100 µg/mL in MeOH. Based on this, working solutions of 1000 and 10 ng/mL were prepared in surrogate matrix to spike final CAL and QC samples. For NO, CAL samples at concentrations of 0.1, 0.25, 0.5, 2.5, 10, 50, 200 and 500 ng/mL and QC samples at concentrations of 0.1, 0.25, 0.5, 5, 100 and 400 ng/mL were prepared. CAL samples of OH-VRC were prepared at concentrations of 1, 2.5, 5, 20, 75, 120, 250 and 500 ng/mL and QC samples at concentrations of 50 and 400 ng/mL.

The IS solution was prepared by first diluting the diazepam stock solution 10-fold with MeOH to obtain a working solution of 100 µg/mL. For each batch a fresh IS solution was prepared by diluting the working solution with water to a concentration of 100 ng/mL.

2.2.1.3 Sample pre-treatment

Plasma, ultrafiltrate and surrogate incubation matrix contained proteins which had to be precipitated before injection into the LC system to avoid column clogging. Therefore, 20 µL of plasma, ultrafiltrate or surrogate incubation matrix were added to 80 µL of ice-cold MeOH, vortex-mixed and centrifuged for 15 min at 14000 × *g* at 4°C. Afterwards, in the case of plasma und ultrafiltrate, 20 µL of the supernatant were transferred to 140 µL IS solution while the supernatant of surrogate incubation matrix was added to 20 µL IS solution. As microdialysate was already protein free, sample pre-treatment consisted of a dilution step only, adding 5 µL to 155 µL IS solution. Zero samples were prepared accordingly using analyte-free matrix, while blank samples neither contained analyte nor the IS.

Final samples were vortex-mixed again, transferred to 96-well plates, covered with pre-slit well caps and stored at 4°C in the autosampler until injection.

2.2.2 Validation of the bioanalytical assay for the simultaneous quantification of voriconazole and its *N*-oxide metabolite in human plasma and microdialysate

For VRC and NO in plasma and microdialysate, the following criteria were investigated according to the EMA guideline's [139] specifications: selectivity, carry-over, calibration function, lower limit of quantification (LLOQ), accuracy, precision, matrix effects and stability.

2.2.2.1 Selectivity and carry-over

Six blank samples from six individual plasma donors were investigated for their interference at the retention times of VRC, NO and the IS. Selectivity of the method was assumed when the detector response was less than 20% of the response at the LLOQ of VRC and NO and less than 5% of the response for the IS of the same run. Microdialysate is a rare matrix, i.e. difficult to obtain in larger quantities and from numerous individuals. Thus, for microdialysate, six blank samples prepared from RS were investigated in a first step. For further examination, additionally four baseline microdialysate samples from healthy volunteers of a clinical microdialysis study were examined.

Carry-over effects occurred when the compounds remained in the LC system, e.g. in the injection needle or sample loop, and were transferred to the subsequently injected sample. Thus, for the assessment, high concentrated VRC or NO samples (≥3000 ng/mL) were injected followed by blank samples. The detector responses in the blank samples were compared to the mean LLOQ

response of the same run. Preliminary investigations indicated that carry-over might be unavoidable for VRC. Therefore, additional samples of pure solvent (MeOH:H_2O 90:10 [V/V]) were processed after the respective blank sample. The absence of carry-over was considered when the detector response in those injections was <20% of the response of VRC or NO LLOQ and <5% of the IS response, respectively.

2.2.2.2 Calibration function

VRC and NO concentrations were calculated based on linear regression. The ratio of the detector response for VRC or NO to the IS were explored in the dependence of the nominal concentration of VRC or NO, respectively. A weighting factor of 1/(concentration)² in the linear regression model increased the accuracy for samples in the lower concentration range [147]. A minimum of six calibration concentrations were required according to the EMA guideline [139]. However, to cover the large calibration range adequately, seven CAL levels were used in addition to a blank and a zero sample. Back calculated concentrations of the CAL samples were required to be within ±15% of their nominal value (±20% at the LLOQ) with a minimum of 75% of CAL samples fulfilling this criterion. In case of a rejected CAL sample, the calibration function was re-assessed without it, if a minimum of six CAL levels remained. The goodness of fit, assessed as coefficient of determination (R^2), was aimed to be >0.99.

2.2.2.3 Lower limit of quantification

The LLOQ had to be reliably quantified with an accuracy of ±20% of the nominal concentration and a precision of ≤20% coefficient of variation (CV). Furthermore, the detector response at the LLOQ was compared to the response of a blank sample and had to be at least five times higher. The limit of detection (LOD) was calculated based on the calibration functions, using the mean slope (S) of all validation runs and the standard deviation of the y-intercepts (SD) (Eq. 2.3) [148].

$$LOD = \frac{3.3 \cdot SD}{S} \tag{2.3}$$

2.2.2.4 Accuracy and precision

Five levels of QC samples with concentrations spanning the calibration range with five to six replicates per level were analysed on four days, in four independent runs. Within-run and between-run accuracy were assessed by comparing the mean concentration of each QC level >LLOQ to its nominal concentration. Deviations of ±15% were accepted. For the assessment of within-run and between-run precision the CV for each QC level was considered and had to be ≤15%.

2.2.2.5 Matrix effects

For the assessment of a possible matrix effect on VRC, NO and IS signals, matrix (plasma and microdialysate) as well as UP water were spiked in an identical manner with the analytes to obtain five to six replicates of a low (8 ng/mL microdialysate, 15 ng/mL plasma) and a high QC level (3000 ng/mL microdialysate, 4000 ng/mL plasma). Plasma was taken from six individual donors. Then, all samples prepared in matrix and water were treated equally as described in chapter 2.2.1.3. The absolute matrix factor (MF) was calculated by dividing the mean peak area of VRC, NO or the IS in the presence of matrix by the mean peak area of VRC, NO or the IS in the absence of matrix, respectively. Additionally, an IS-normalised MF was determined. The precision, calculated as CV, was compared to the criterion of ≤15% and indicated the absence of a relative matrix effect.

2.2.2.6 Stability investigations

Stability investigations of VRC and NO were performed using a bracketing approach, i.e. exposing QC samples of a low (8 ng/mL microdialysate, 15 ng/mL plasma) and a high (3000 ng/mL microdialysate, 4000 ng/mL plasma) concentration to various conditions relevant for future applications. For the assessment of autosampler stability, processed QC samples were re-injected after ≥24 h in the autosampler at 4°C. Freeze- and thaw-stability was determined by freezing QC samples for ≥12 h at -80°C and thawing them unassisted at room temperature. All samples underwent three freeze-thaw cycles. Short-term stability was explored by keeping sets of QC samples in the fridge at 4-8°C overnight. Long-term stability was evaluated by reanalysing spiked samples after ≥3-month storage at -80°C. Freshly prepared CAL samples were used to calculate the concentrations of all stability samples. Stability of VRC and NO in plasma and microdialysate was assumed when the deviation to the nominal concentration was ≤±15%.

Freeze-thaw, short-term and long-term stability of the stock solution were assessed under the same experimental conditions. For analysis, the stock solution was diluted to a low and high QC level as described before (chapter 2.2.1.2).

2.2.3 Simultaneous quantification of voriconazole and its *N*-oxide metabolite in ultrafiltrate

For VRC and NO in ultrafiltrate, not a full validation was performed but the hypothesis tested whether ultrafiltrate samples could be equated to plasma samples with regard to their matrix effect. This would enable a more time- and material-efficient quantification of VRC and NO.

For this purpose, pooled ultrafiltrate was spiked with VRC or NO, respectively, at a low and a high QC level and equally treated as plasma samples (chapters 2.2.1.2 and 2.2.1.3). Concentrations were calculated using the plasma calibration function of VRC or NO,

respectively. The determined concentrations were required to be within 85%-115% of their nominal concentration and imprecision needed to be ≤15% CV. Moreover, ultrafiltrate from six individual donors was prepared and evaluated for selectivity according to the criteria described above (chapter 2.2.2.1).

2.2.4 Quantification of voriconazole metabolites in *in vitro* matrices

In *in vitro* metabolism investigations a low concentration of the enzymatic system as well as a short reaction time were desired. However, this entailed low metabolite concentrations and thus imposed higher demands on the bioanalytical assay. Hence, to further optimise the quantification in the *in vitro* matrices, sample pre-treatment was adapted. While the protein precipitation step was identical to plasma and ultrafiltrate samples (20 µL sample added to 80 µL MeOH), the subsequent dilution of the supernatant was altered. Moreover, the injection volume was increased to overall evaluate the detector responses and define a corresponding LLOQ.

Matrix effect. For the quantification of NO formation in *in vitro* metabolism studies, the bioanalytical method was expanded to two metabolic systems: HLM and rhCYP (2C19, 2C9 and 3A4). Therefore, a surrogate incubation matrix was used for the routine preparation of CAL and QC samples (chapter 2.2.1.2). To demonstrate the feasibility of this matrix for unbiased quantification, it was compared to real incubation matrix. Therefore, HLM and rhCYP incubations were inactivated by heating them to 70°C for 5 min to avoid distortion by continued metabolic transformations. The surrogate incubation matrix was prepared at a protein concentration of 0.2 mg/mL BSA and hence resembled the HLM incubations which contained the same concentration of protein. Incubations of rhCYP (3A4, 2C19, 2C9) ranged from 0.0065 to 0.162 mg/mL protein concentration. However, for the sake of simplicity, the BSA concentration was not adapted to those concentrations but maintained at 0.2 mg/mL. In all cases, both the surrogate and heat-inactivated incubation matrix were spiked with identical NO solutions to obtain a concentration of 10 ng/mL and the detector responses compared. Matrix effects were found negligible if the IS corrected detector signals did not deviate more than ±15% between matrices and imprecision was ≤15% CV.

Analytical runs. Performance, i.e. accuracy and precision, of the adapted bioanalytical method was monitored in all analytical runs. Therefore, requirements for analytical runs defined by the EMA guideline on bioanalytical method validation were adhered to [139]. In all runs, calibration series, consisting of a minimum of six CAL, and QC samples were included. The number of QC samples was adjusted to the amount of study samples within the run, reflecting 5% of study samples or a minimum of three QC levels in duplicate, whichever was higher. A minimum of 75% of CAL had to be within ±15% of their nominal concentration (±20% at the LLOQ). In case of the rejection of a CAL sample, the calibration function was re-assessed without it provided that

a minimum of six CAL samples remained. For QC samples an accuracy of 85%-115% (80%-120% at the LLOQ) compared to their nominal concentration was required. A minimum of 67% of QC samples had to meet this criterion as well as a minimum of 50% per concentration level. Only if CAL and QC samples fulfilled those requirements the analytical run was accepted, and study samples evaluated. The overall performance was evaluated pooling the results of all QC samples and assessing the mean accuracy and precision of all accepted runs. Thereby, the same limits were applied for accuracy. Furthermore, precision was assessed as CV and was required to be ≤15% (≤20% at the LLOQ) for each concentration level.

2.3 *In vitro* metabolism studies for voriconazole and its metabolites

On the one hand, VRC has been described as a substrate of CYP2C19, CYP2C9 and CYP3A4 [37,38,69,71]. Thus, a profound quantitative analysis of the underlying kinetics was performed aiming for a better understanding of VRC metabolism in humans (chapter 2.3.4).

On the other hand, VRC has been discussed as a strong CYP inhibitor, potentially influencing its own metabolism [37,38,82,83,85]. Therefore, the inhibitory potential of VRC was evaluated and expanded to its *N*-oxide and hydroxy metabolite to generate an overarching picture (chapter 2.3.5).

2.3.1 Preparation of enzyme and co-factor solutions

HLM, HIM and rhCYP (2C19, 2C9 and 3A4) were purchased in a ready-to-use form and the respective enzyme source was selected depending on the investigation. HLM were a pooled batch from 150 donors with an equal gender distribution and HIM were prepared from duodenum and jejunum sections from seven donors and contained only mature enterocytes. The rhCYP were derived from baculovirus-infected insect cells. All enzyme stock solutions were stored as recommended by the manufacturer at -80°C and rapidly thawed at 37°C directly before usage [143]. After the withdrawal of the necessary volume, the enzyme solutions were immediately re-frozen to keep the loss in enzyme activity as low as possible. Overall, no stock solution was exposed to more than five freeze-thaw cycles.

Working solutions of HLM, rhCYP and HIM were prepared at a 20- to 25-fold higher concentration than in the final set-up by diluting the stock solution with PPB.

To prevent the depletion of NADPH and thus deviations in the enzyme kinetics, a NADPH re-generating system was applied to ensure the repeated production of NADPH *in situ*. This system was composed of two individual, subordinate solutions. Solution A consisted of $NADP^+$, glucose-6-phosphate and magnesium chloride while solution B contained glucose-6-phosphate dehydrogenase. Solution A and B were purchased as ready-made solutions, aliquoted and thawed

at the respective day of the investigation or prepared freshly from the individual components. All working solutions were kept on wet ice until needed in the experiment.

2.3.2 Incubation conditions and procedure

The incubation conditions should mimic the *in vivo* hepatocyte environment as closely as possible. Thus, all incubations were performed at 37°C and pH 7.5 in TRIS buffer under gentle, constant shaking in an Eppendorf Thermomixer®. Final incubations were prepared by mixing the different higher concentrated working solutions, i.e. TRIS buffer (250 mM, pH 7.5), NADPH re-generating system (solutions A and B), the respective substrate, enzyme system and where applicable the respective inhibitor, with the required volume of UP water to reach a total volume of 100 µL (Figure 2.1). This resulted in a final concentration of 50 mM TRIS buffer, 1.0 to 1.3 mM $NADP^+$, 3.3 to 5.0 mM glucose-6-phosphate, 3.3 mM magnesium chloride and 0.4 to 0.5 U/mL glucose-6-phosphate dehydrogenase. Final concentrations of the buffer and co-factors were kept constant between different investigations to ensure comparability. Dilutions and final concentrations of the respective substrates, enzyme systems and inhibitors were carried out in an adapted manner depending on the aim of the investigation and are therefore reported in the respective chapters. An overview of all individual experimental set-ups is presented in Table 7.1.

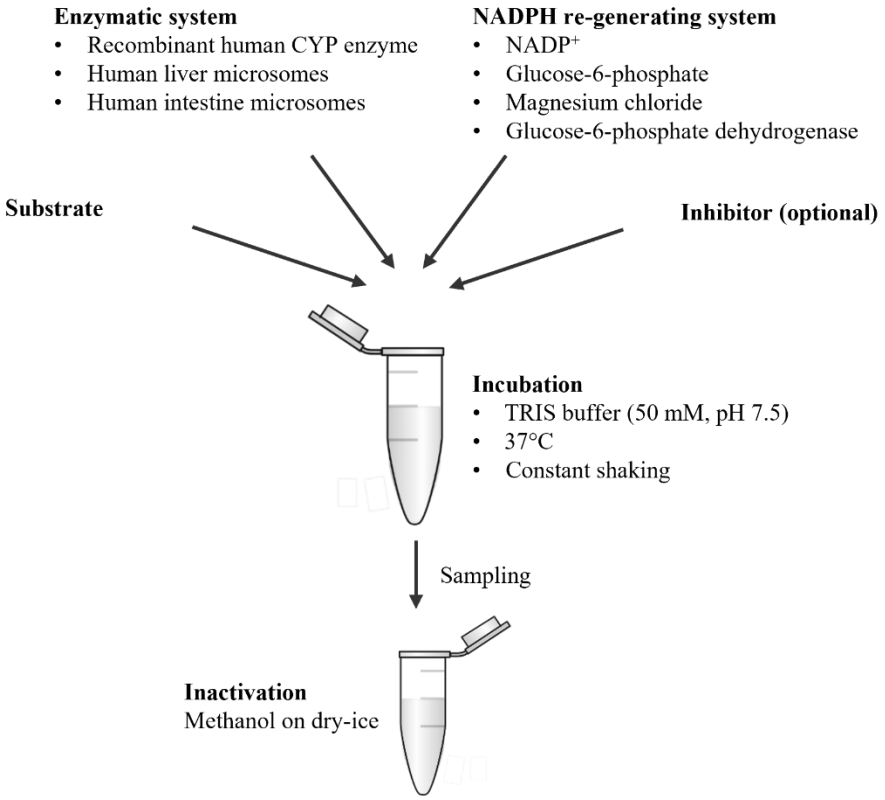

Figure 2.1: Schematic overview of the experimental set-up for *in vitro* metabolism investigations.

Time measurements for the adherence of the reaction time were started as soon as the mixture was complete, with the addition of NADPH re-generating system solution A or the enzyme working solution always being the last step. From all incubations, a minimum of two 20 µL samples at two different time points were taken and the enzymatic reaction was stopped by precipitation in 80 µL dry-ice-cold MeOH. All samples were vortex-mixed immediately and stored at -80°C until analysis.

2.3.3 Assessment of CYP2C19, CYP2C9 and CYP3A4 activity with marker reactions

Marker reactions, i.e. metabolic transformations catalysed by a specific CYP isoenzyme, were required to assess the CYP enzyme activity *in vitro* in a standardised approach. In the framework of this thesis, marker reactions for CYP2C19, CYP2C9 and CYP3A4 were essential. The choice of marker reactions was made based on recommendations by international guidelines on the investigation of drug interactions by the EMA and FDA [149,150]. For all here described investigations, the activity of CYP2C19 was monitored by the 4-hydroxylation of S-mephenytoin, of CYP2C9 by the 4-hydroxylation of diclofenac and of CYP3A4 by the 1-hydroxylation of midazolam.

After implementing the marker reactions under laboratory-individual resources and conditions, their Michaelis-Menten kinetics were characterised in HLM and rhCYP (chapter 2.3.3.2). This was the prerequisite for the determination of intersystem extrapolation factors (ISEF), which were necessary for calculating the contribution of individual CYP enzymes to the overall formation of NO (chapter 2.3.4.3) as well as for the assessment of the inhibitory effects of VRC, NO and OH-VRC on the respective CYP isoenzymes (chapter 2.3.5).

2.3.3.1 Bioanalytical assay for the quantification of 4-hydroxymephenytoin, 4-hydroxydiclofenac and 1-hydroxymidazolam

A previously developed LC-MS/MS assay was applied for the quantification of OH-MEP, OH-DIC and OH-MDZ as well as for the detection of the substrates (S-mephenytoin, diclofenac, midazolam) and inhibitors (VRC, NO and OH-VRC) [151]. This assay was based on the bioanalytical method described in chapter 2.2 and adapted to enable and optimise the quantification of the three metabolites of the marker reactions. Thus, also the same instrumentation was used as described in chapter 2.2.1.1. Chromatographic separation was achieved by a Poroshell Phenyl Hexyl column (RP, 2.1 x 100 mM, 2.7 µM) combined with an InfinityLab Poroshell 120 Phenyl Hexyl guard column (2.1 x 5 mM, 2.7 µM) at 30°C. As eluents, UP water and MeOH were used. Both contained 0.1% [V/V] FA and were combined according to the gradient method in Table 2.1. The flow rate was set to 0.350 mL/min and the injection volume adapted to the current sensitivity of the MS with volumes ranging from 5-18 µL. The total run time encompassed 6.9 min and included a 1.6 min postrun and 15 s needle wash time.

Table 2.1: Mobile phase composition of the LC-MS/MS gradient method.

Interval	Time [min]	Ultrapure water + 0.1% formic acid, %	Methanol + 0.1% formic acid, %
0	0.00	95	5
1	0.50	50	50
2	1.00	50	50
3	3.00	30	70
4	3.05	2	98
5	4.70	2	98
6	4.80	95	5
7	6.90	95	5

The ESI source was operated in positive ionisation mode and ion acquisition was performed in dynamic multiple reaction monitoring (dMRM) mode with a 2 min retention time window. In the final settings, transitions of ten different compounds were monitored. The respective precursor and product ions for the ten analytes as well as the collision energy and retention times are listed in Table 2.2. The final optimised source parameters were a capillary voltage of 3000 V, nebulizer gas pressure of 35 psi, drying gas and sheath gas flow of 19 and 12 L/min of nitrogen, drying gas and sheath gas temperature 210 and 400 °C.

Table 2.2: Precursor and product ions, as well as corresponding collision energy, fragmentor voltage, cell accelerator voltage and retention times, of all compounds included in the bioanalytical assay used for the quantification of the metabolites of the marker reactions for CYP2C19 (S-mephenytoin 4-hydroxylation), CYP2C9 (diclofenac 4-hydroxylation) and CYP3A4 (midazolam 1-hydroxylation) in the presence or absence of voriconazole and its two metabolites, voriconazole *N*-oxide and hydroxyvoriconazole. The mass transitions used for quantification are marked in **bold**.

Compound	Precursor ion *m/z* $[M+H]^+$	Product ion *m/z*	Collision energy [eV]	Fragmentor voltage [V]	Cell accelerator voltage [V]	Retention time [min]
4-Hydroxy-mephenytoin	235	**150**	16	380	5	2.3
	235	105	36	380	5	2.3
	235	56	40	380	5	2.3
4-Hydroxy-diclofenac	312	266	8	380	5	4.2
	312	**230**	32	380	5	4.2
	312	195	64	380	5	4.2

Table 2.2: continued

1-Hydroxy-midazolam	342	**324**	20	380	5	3.5
	342	203	32	380	5	3.5
	342	168	44	380	5	3.5
S-Mephenytoin	219	134	20	380	5	3.3
	219	115	44	380	5	3.3
	219	56	40	380	5	3.3
Diclofenac	296	250	8	380	5	4.4
	296	215	24	380	5	4.4
	296	214	40	380	5	4.4
Midazolam	326	291	28	380	5	3.2
	326	249	44	380	5	3.2
	326	222	56	380	5	3.2
Voriconazole	350	281	17	380	5	4.1
	350	224	13	380	5	4.1
	350	127	41	380	5	4.1
Voriconazole *N*-oxide	366	224	13	380	5	3.4
	366	143	9	380	5	3.4
Hydroxy-voriconazole	366	297	16	380	5	3.7
	366	143	24	380	5	3.7
	366	127	55	380	5	3.7
Internal standard (diazepam)	285	222	36	380	5	4.4
	285	**193**	36	380	5	4.4
	285	154	32	380	5	4.4

m/z, mass-to-charge ratio

CAL and QC samples for the quantification of OH-MEP, OH-DIC and OH-MDZ were prepared in the same surrogate incubation matrix as described for NO (chapter 2.2.1.2). The BSA content was adjusted to the protein content of the HLM incubation of the individual marker reaction and the respective experiment. Hence, it was 0.2 mg/mL for OH-MEP (CYP2C19), 0.04 mg/mL (or 0.08 mg/mL) for OH-DIC (CYP2C9) and 0.05 mg/mL for OH-MDZ (CYP3A4, Table 7.1). From the original stock solutions (chapter 2.1.5.3) secondary stock solutions of 100 µg/mL were prepared in MeOH. The latter were diluted 100-fold with surrogate incubation matrix to obtain a working solution that could be further serially diluted with matrix. Finally, a set of three

individual working solutions was obtained for each metabolite as well as CAL and QC samples, spanning a concentration range of 10^3. Final CAL and QC concentrations were adapted according to the type of the experiment and the expected metabolite concentrations, as recommended in the EMA guideline for bioanalytical method validation [139]. Thus, for experiments determining un-inhibited kinetics of the marker reactions, calibration ranges were shifted to higher concentration ranges while in investigations expecting high inhibitory effects on the marker reactions, calibration ranges were adapted to cover lower concentrations. At all times, the CAL series were composed of a blank and a zero sample plus eight CAL levels that ranged from 0.5 to 400 ng/mL for OH-MEP, from 1 to 1000 ng/mL for OH-DIC and from 0.1 to 1000 ng/mL for OH-MDZ, respectively. Additionally, three QC concentration levels at a low, medium and high concentration with regard to the calibration range, were investigated in all analytical runs. As IS diazepam was used and the IS solution prepared by spiking 20 mL of UP water with 20 or 4 µL of IS working solution (10 µg/mL in MeOH), respectively. This resulted in final IS solutions of 2 or 10 ng/mL.

Sample pre-treatment consisted of a protein precipitation step by adding 20 µL of the respective sample to 80 µL ice-cold MeOH. After vortex-mixing, all samples were centrifuged at 14000 × *g* for 15 min at 4°C. 20 µL of the supernatant were transferred to 20 µL of the IS solution or in the case of blank samples, to 20 µL of UP water and vortex-mixed again.

Final samples were transferred to a 96-well plate, covered with a pre-slit well cap and stored at 4°C in the autosampler until injection.

The respective metabolite concentrations were calculated based on linear regression of the ratio of the detector response for the metabolite to the IS versus the nominal concentration of the metabolite. A weighting factor of $1/(\text{concentration})^2$ in the linear regression model increased the accuracy for samples in the lower concentration range [147]. Back-calculated concentrations of CAL samples were required to be within ±15% of their nominal concentration (±20% at the LLOQ) with a minimum of 75% being accurate and a minimum of six CAL per calibration row. Furthermore, 67% of QC samples of each run had to fulfil the accuracy criteria with a minimum of 50% per concentration level. Overall method performance was evaluated by the determination of an overarching accuracy and precision, pooling all QC samples from all analytical runs. Here, the mean concentration of all QC samples was required to be within ±15% of the nominal concentration (±20% at the LLOQ) and precision ≤15% CV (≤20% at the LLOQ).

2.3.3.2 Michaelis-Menten kinetics of the 4-hydroxylation of S-mephenytoin, 4-hydroxylation of diclofenac and 1-hydroxylation of midazolam

Essential preliminary investigations, e.g. the examination of reaction linearity and absence of substrate depletion, were performed previously in the same laboratory under identical conditions

or based on the manufacturer's information [151–154]. Additionally, in literature reported kinetic parameters for the respective marker reactions were considered to optimise the study design with regard to enzyme and substrate concentration as well as reaction times [155–157].

Building upon this knowledge, experiments for the determination of Michaelis-Menten kinetics in HLM were performed at protein concentrations of 0.2, 0.04 and 0.05 mg/mL for the marker reactions of CYP2C19, CYP2C9 and CYP3A4, respectively. Two samples were taken from each incubation after 15 and 25 min for CYP2C19, after 5 and 10 min for CYP2C9 and after 7 and 12 min for CYP3A4, respectively. Those settings ensured sufficient metabolite formation for quantification while maintaining short reaction times and HLM concentrations. For each marker reaction, eight substrate concentrations were chosen to cover all phases of the Michaelis-Menten kinetics. In detail, S-mephenytoin concentrations of 4.58, 9.16, 13.7, 18.3, 36.7, 45.8, 91.6 and 458 µM, diclofenac concentrations of 1.69, 3.38, 6.75, 10.1, 13.5, 27.0, 67.5 and 169 µM and midazolam concentrations of 0.307, 0.767, 1.53, 3.07, 6.14, 9.21, 20.0 and 30.7 µM were applied (n=3 each).

For investigations in rhCYP concentrations of 2.5 pmol/mL rhCYP2C19 (n=3), 2 pmol/mL rhCYP2C9 (n=6) and 12.5 and 25 pmol/mL rhCYP3A4 (n=3 each) were applied, respectively. Sampling time points were identical to those in HLM as were substrate concentrations of S-mephenytoin and midazolam. For diclofenac, a lower substrate concentration of 0.844 µM was included in exchange for the 10.1 µM level.

The reaction velocity (V in pmol/(min·mg) for HLM and HIM and in pmol/(min·pmol) for rhCYP) was determined for each sample as the concentration of the respective metabolite (C_{Met} in pmol/mL) divided by the respective reaction time (t_{reac} in min) and concentration of HLM/HIM or rhCYP (C_{Enyzme} in mg/mL for HLM and in pmol/mL for rhCYP, Eq. 2.4), respectively.

$$V = \frac{C_{Met}}{C_{Enzyme} \cdot t_{reac}} \tag{2.4}$$

For the evaluation of the enzyme kinetics, the reaction velocity of metabolite formation (V) was considered in dependence of the added substrate concentration (C_S in µM) applying the Michaelis-Menten equation (Eq. 2.5). Kinetic parameters, i.e. the K_M (in µM) and V_{max} (in pmol/(min·mg) for HLM and HIM and in pmol/(min·pmol) for rhCYP), were estimated by nonlinear regression using the "nls" function in R and RStudio®.

$$V = V_{Max} \cdot \frac{C_S}{K_M + C_S} \tag{2.5}$$

Furthermore, the intrinsic clearance value (CL_{int} in µL/(min·mg) for HLM and HIM and in µL/(min·pmol) for rhCYP) was determined as the respective ratio of V_{max} and K_M (Eq. 2.6).

$$CL_{int} = \frac{V_{max}}{K_M} \quad (2.6)$$

2.3.4 Voriconazole and its metabolites as substrates

With the objective to generate a comprehensive overview of VRC metabolism, different approaches were chosen to characterise the observed kinetics quantitatively. These included the assessment of the kinetics in different metabolic systems, i.e. in HLM, HIM and rhCYP (chapter 2.3.4.2), determination of the respective enzyme contributions (chapter 2.3.4.3), as well as the inspection of the plausibility of the respective *in vitro* results by a transformation to an *in vivo* situation (chapter 2.3.4.4). Furthermore, investigations of the metabolic stability of the formed metabolites were conducted (chapter 2.3.4.5).

2.3.4.1 Reaction linearity, voriconazole stability and substrate depletion

As a prerequisite for the characterisation of the Michaelis-Menten kinetics in HLM, rhCYP and HIM linearity of metabolite formation with respect to incubation time and enzyme concentration was assessed. This ensured the validity of future investigations because the kinetic parameter V_{max} represented a rate, i.e. formation of metabolite in relation to time and enzyme concentration.

For linearity investigation in HLM, the stock solution was diluted to final protein concentrations of 0.05, 0.1, 0.2 and 0.5 mg/mL. VRC solutions were prepared from the 3.5 mg/mL stock solution by serial dilutions with UP water and resulted in final substrate concentrations of 1, 10, 20 and 100 µM. Each VRC substrate concentration was combined with each HLM dilution, and every combination was investigated in duplicate. As for the linearity assessment over time, 20 µL aliquots were needed at seven different time points, the overall volume of the incubation was increased to 500 µL. Samples were taken after 5, 10, 15, 20, 30, 60 and 120 min.

For rhCYP2C19, rhCYP2C9 and rhCYP3A4, linearity investigations were performed in a similar way. Here, final enzyme concentrations amounted to 1, 5, 10 and 20 pmol/mL for rhCYP2C19, 5, 20, 40, 60 and 80 pmol/mL for rhCYP2C9 and 5, 20, 40 and 80 pmol/mL for rhCYP3A4. The substrate VRC was added to all rhCYP solutions at concentrations of 1, 10 and 100 µM (n=2-4, Table 7.1). Reaction times of 5, 10, 15, 20, 30 and 60 min were investigated, and hence, the total volume of the incubation was raised to 200 µL.

For HIM, only linearity over time was determined as the low CYP activity did not allow a reduction of protein concentration to maintain quantifiable NO concentrations during bioanalysis. Therefore, all incubations were carried out at a concentration of 0.5 mg/mL HIM. Substrate concentrations of 1, 5, 10 and 100 µM VRC were investigated, and reactions stopped after 5, 15, 25 and 60 min (n=3).

Linearity was in all cases evaluated with a linear regression model that related the metabolite concentration to the reaction time or protein/enzyme concentration, respectively. The goodness of linearity was assessed by the coefficient of determination (R^2).

Additionally, control incubations were performed that lacked the NADPH re-generating system (solution A and B) to explore the CYP specificity of the reaction as well as the stability of VRC under incubation conditions.

Finally, not only the metabolite formation was investigated, but also the disappearance of VRC over time. To avoid a distortion of the kinetics, it was aimed at keeping the substrate concentration constant over the whole reaction time. A maximum depletion of 10% VRC was deemed negligible.

2.3.4.2 Michaelis-Menten kinetics of the *N*-oxidation of voriconazole

For the assessment of the kinetic parameters, i.e. K_M, V_{max} and CL_{int}, of VRC *N*-oxidation in HLM, a protein concentration of 0.2 mg/mL was chosen considering a low protein concentration but sufficient NO formation for bioanalysis. The substrate VRC was added in a wide concentration range to cover all phases of the Michaelis-Menten curve. Final concentrations were 0.5, 2, 3, 4, 5, 8, 10, 15, 20, 30, 60 and 100 µM (n=3). After 10, 20 and 30 min, a 20 µL sample was taken to ensure evaluable results in case of experimental variabilities.

Investigations in recombinant systems were performed at enzyme concentrations of 5 (n=3) and 15 pmol/mL (n=6) for rhCYP2C19, 100 pmol/mL (n=5) for rhCYP2C9 and 20 (n=3) and 40 pmol/mL (n=6) for rhCYP3A4, respectively. VRC concentrations of 0.5, 1, 2, 3, 4, 8, 30 and 100 µM were applied to describe the trajectory of the Michaelis-Menten curve satisfactorily. All incubations were sampled twice, after 15 and 25 min, respectively.

Michaelis-Menten kinetics in HIM were assessed at a protein concentration of 0.5 mg/mL, applying VRC substrate concentrations of 0.5, 1, 2, 3, 4, 5, 8, 10, 15, 30, 60 and 100 µM (n=3). Samples were taken, and the reaction terminated after 5, 15 and 25 min.

Reaction velocities as well as K_M, V_{max} and CL_{int} were determined as described for the marker reactions (chapter 2.3.3.2) using equations 2.4 to 2.6.

Furthermore, a Lineweaver-Burk linearisation was performed by determination of the reciprocal of the mean of the reaction velocity and the respective substrate concentration. The transformed data were subjected to linear regression analysis and the results were evaluated graphically in a Lineweaver-Burk plot.

2.3.4.3 Contribution of individual CYP isoenzymes to voriconazole *N*-oxidation

Further research focussed on the contribution of individual CYP isoenzymes to the overall formation of NO in HLM. Therefore, two different approaches were explored. First, CYP enzymes in the complex system of HLM were individually inhibited to determine the remaining metabolism. Second, kinetic parameters determined in recombinant systems were transformed to reflect the metabolism in HLM.

Specific enzyme inhibition in human liver microsomes. To identify the involved CYP isoenzymes in VRC *N*-oxidation, experiments with specific CYP inhibitors were performed. For this purpose, VRC concentrations of 0.5, 1, 2, 3, 4, 8, 30 and 100 µM were incubated with HLM at a concentration of 0.2 mg/mL. Additionally, the CYP specific inhibitors loratadine (CYP2C19), sulfaphenazole (CYP2C9) and ketoconazole (CYP3A4), as well as a mixture of the three, were added to the incubation [149,150,158]. The specificity of the inhibition is highly dependent on the concentration of the inhibitor, thus based on literature, concentrations of 10 µM loratadine, 10 µM sulfaphenazole and 0.1 µM ketoconazole were used [159–162]. Control incubations were performed without inhibitor, instead the same volume of inhibitor-free solvent was added. The enzymatic reaction was stopped by addition of 20 µL of the incubation mixture to 80 µL MeOH after 15 and 25 min. The reaction velocities at the respective substrate concentration in the presence and absence of the inhibitor were determined according to equation 2.4. The contribution of a single enzyme to the overall VRC *N*-oxidation was calculated as the deviation to 100% of the ratio of the respective reaction velocity of incubations in the presence of inhibitor ($V_{inh.}$) and the reaction velocity at the same concentration level of the control ($V_{con.}$, Eq. 2.7).

$$Contribution_{CYPi}, \% = 100\% - \frac{V_{inh.}}{V_{con.}} \cdot 100\% \qquad (2.7)$$

In order to control for the specificity of the enzyme inhibition, the inhibitors loratadine, sulfaphenazole and ketoconazole were tested on marker reactions specific for the respective CYP isoenzymes (chapter 2.3.3). For this purpose, S-mephenytoin (CYP2C19), diclofenac (CYP2C9) and midazolam (CYP3A4) were used as probe substrates at concentrations close to their K_M, i.e. 45.8, 10.1 and 6.1 µM, respectively, and incubated with HLM at a concentration of 0.2 mg/mL for 15 and 25 min. Each probe substrate was incubated in the presence of each inhibitor. The reaction velocity, calculated according to equation 2.4, was determined in the presence of each inhibitor and compared to the reaction velocity in an uninhibited control. The latter was derived during the determination of the Michaelis-Menten kinetics of the marker reactions as described in chapter 2.3.3.2.

Extrapolation from recombinant human CYP enzymes. Individual CL_{int} of VRC *N*-oxidation determined in the recombinant human isoenzymes 2C19, 2C9 and 3A4 ($CL_{int,rhCYPi}$) were extrapolated to the CL_{int} of the respective isoenzyme in HLM by taking the CYP abundance in HLM into account (Eq. 2.8). Consequently, the CL_{int} of each isoenzyme ($CL_{int,CYPi,HLM}$) was either related to (i) the overall observed CL_{int} in HLM ($CL_{int,HLM}$, Eq. 2.9) or (ii) to the sum of the individual converted CL_{int} to determine the contributions of the respective CYP isoenzymes (Eq. 2.10).

$$CL_{int,CYPi,HLM} = CL_{int,rhCYPi} \cdot P450i\ abundance \tag{2.8}$$

$$Contribution_{CYPi},\% = \frac{CL_{int,CYPi,HLM}}{CL_{int,HLM}} \cdot 100\% \tag{2.9}$$

$$Contribution_{CYPi},\% = \frac{CL_{int,CYPi,HLM}}{\sum CL_{int,CYPi,HLM}} \cdot 100\% \tag{2.10}$$

However, as rhCYP are artificially expressed systems, the use of ISEF were considered to account for activity differences in the two metabolic systems [163,164]. ISEF were derived by the assessment of Michaelis-Menten kinetics of marker reactions, which are specific for one enzyme, in HLM and rhCYP (chapter 2.3.3). Subsequently, the ISEF was calculated by two different approaches. First, as the ratio of V_{max} of the respective marker reaction ($V_{max,MR}$) in HLM and rhCYP (chapter 2.3.3.2) corrected for CYP abundance in HLM (P450*i* $abundance_{HLM}$) under the assumption that the K_M was constant in the two systems (Eq. 2.11). Second, as the ratio of CL_{int} of the respective marker reaction ($CL_{int,MR}$) in HLM and rhCYP (chapter 2.3.3.2) corrected for CYP abundance in HLM and thus allowing for a different K_M in the two systems (Eq. 2.12).

$$ISEF_{V_{max},CYPi} = \frac{V_{max,MR,HLM}}{V_{max,MR,rhCYP} \cdot P450i\ abundance_{HLM}} \tag{2.11}$$

$$ISEF_{CL_{int},CYPi} = \frac{CL_{int,MR,HLM}}{CL_{int,MR,rhCYP} \cdot P450i\ abundance_{HLM}} \tag{2.12}$$

The individual isoenzyme CL_{int} of VRC *N*-oxidation in HLM ($CL_{int,CYPi,HLM,ISEF}$) were then calculated by using the individual CL_{int} determined in the respective rhCYP ($CL_{int,rhCYPi}$) and converting them, taking into account the individual CYP abundances in HLM as well as the respective ISEF (Eq. 2.13). CYP abundances per milligram liver were taken from literature [165] and are reported in Table 7.2.

$$CL_{int,CYPi,HLM,ISEF} = ISEF_{CYPi} \cdot CL_{int,rhCYPi} \cdot P450i\ abundance \tag{2.13}$$

Lastly, the individual CL_{int} of each isoenzyme was either related to (i) the overall CL_{int} observed in HLM ($CL_{int,HLM}$) (Eq. 2.9) or (ii) the sum of the individual converted CL_{int} corrected by the ISEF approach (Eq. 2.10), and hence the contribution determined.

2.3.4.4 *In vitro in vivo* extrapolation

CL_{int} determined in *in vitro* metabolic systems can be extrapolated to *in vivo* hepatic CL_{int} ($CL_{int,hepatic,invivo}$) by multiplication with the microsomal protein per gram liver (MPPGL in mg/g) and the mean human liver weight (Eq. 2.14) [164].

$$CL_{int,hepatic,invivo} = MPPGL \cdot liver\ weight \cdot CL_{int,\ invitro} \quad (2.14)$$

Furthermore, by applying the well-stirred liver model [164,166,167], that takes hepatic blood flow (Q_H in mL/min), the fraction unbound in plasma (fu_p) and the blood-plasma-ratio (BP) into account, an *in vivo* hepatic clearance ($CL_{hepatic}$ in mL/min) was calculated (Eq. 2.15).

$$CL_{hepatic} = \frac{Q_H \cdot \frac{fu_p}{BP} \cdot CL_{int,hepatic,invivo}}{Q_H + \frac{fu_p}{BP} \cdot CL_{int,hepatic,invivo}} \quad (2.15)$$

Respective values for MPPLG, liver weight, Q_H, fu_P and BP were taken from literature and are collected in Table 7.2.

2.3.4.5 Metabolic stability of voriconazole *N*-oxide and hydroxyvoriconazole

For investigations of NO and OH-VRC stability in HLM incubations, continued metabolism to secondary VRC metabolites and degradation, both compounds were directly incubated with HLM. The depletion of NO and OH-VRC at a low (0.137 µM) and a high (1.10 µM) concentration was assessed over time in incubations containing 0.2 mg/mL HLM. After 5, 15, 30 and 60 min samples were taken and the respective concentration of NO or OH-VRC was determined (n=2). An incubation that contained PPB only instead of an HLM dilution, served as a control and was used for normalisation (n=1).

2.3.5 Voriconazole and its metabolites as enzyme inhibitors

VRC and its two main metabolites, NO and OH-VRC, were investigated for their inhibitory potential as well as their inhibitory properties characterised in more detail. Overall, a thorough picture of the effects of VRC on its own metabolising enzymes, i.e. CYP2C19, CYP2C9 and CYP3A4, was aimed for.

2.3.5.1 Inhibitory potential of voriconazole, voriconazole *N*-oxide and hydroxyvoriconazole

For the assessment of the inhibitory potential of VRC, NO and OH-VRC, the previously described marker reactions (chapter 2.3.3) were used at a substrate concentration close to the respective K_M of the reaction, which was 55.0 µM for S-mephenytoin, 4.73 µM for diclofenac and 4.60 µM for midazolam. Additionally, five test compound (VRC, NO, OH-VRC) concentrations plus a control containing only the solvent of the test compound dilution (UP water) were added to the

incubations (n=2). The sampling time points were kept constant as described before (chapter 2.3.3.2). However, the HLM concentration for the CYP2C9 marker reaction of diclofenac 4-hydroxylation was increased to 0.08 mg/mL to ensure the formation of sufficient metabolite for bioanalysis even at a potential 95% inhibition. VRC was investigated as inhibitor at concentrations of 0.10, 1.0, 5.0, 10.0 and 100 µM while for NO and OH-VRC due to limited solubility concentrations of 0.0958, 0.958, 3.83, 9.58 and 34.2 µM were used.

Concentrations of OH-MEP (CYP2C19), OH-DIC (CYP2C9) and OH-MDZ (CYP3A4) were determined in the incubations and reaction velocities calculated according to equation 2.4. Reaction velocities derived from metabolic transformations in the presence of an inhibitor ($V_{inh.}$) were related to the reaction velocities of the uninhibited control ($V_{con.}$) and thus the percentage of remaining activity (A) determined (Eq. 2.16).

$$A,\% = \frac{V_{inh.}}{V_{con.}} \cdot 100\% \qquad (2.16)$$

The concentration at which VRC, NO and OH-VRC displayed their half maximal inhibitory effect (IC_{50} in µM) under the applied conditions as well as the Hill factor, i.e. the steepness of the inhibition curve (H), were estimated by fitting the four-parameter inhibition model to the experimental data (Eq. 2.17) [110]. Maximum (A_{max}) and minimum activity (A_0) were fixed to 100% and 0%, respectively.

$$A,\% = A_0 + \frac{(A_{max} - A_0)}{1 + \left(\frac{log(C_I)}{log(IC_{50})}\right)^H} \qquad (2.17)$$

In addition, in a sensitivity analysis, A_{max} and A_0 were estimated one at a time as well as simultaneously in the model, allowing the evaluation of their impact on IC_{50}.

2.3.5.2 Time-dependent inhibition

Time-dependent inactivation of CYP2C19, CYP2C9 and CYP3A4 by VRC, NO and OH-VRC was investigated performing an IC_{50} shift assay. The proceedings of this assay were identical to the IC_{50} determination (chapter 2.3.5.1) despite a pre-incubation time of 30 min before the addition of the respective substrate of the marker reaction. In this pre-incubation step, VRC, NO or OH-VRC were incubated at 37°C together with HLM in the presence or absence of the NADPH re-generating system and the remaining activity compared to a control that contained inhibitor-free solvent (Eq. 2.16). IC_{50} calculations were performed according to equation 2.17 setting A_{max} to 100% and A_0 to 0%. In case of time-dependent inhibition, IC_{50} values were expected to shift to lower values and shifts of >1.5-fold have been previously described to be physiologically relevant [168].

2.3.5.3 Type of reversible inhibition

For the assessment of the type of reversible inhibition the previous experiments were extended and six substrate concentrations of the marker reactions were combined with five concentrations of VRC, NO or OH-VRC plus the uninhibited control. The concentrations of VRC, NO and OH-VRC were identical to those in IC_{50} investigations (chapter 2.3.5.1). For CYP2C19, CYP2C9 and CYP3A4 S-mephenytoin concentrations of 9.16, 13.7, 18.3, 55.0, 91.6 and 458 µM, diclofenac concentrations of 1.69, 3.38, 4.73, 6.75, 27.0 and 169 µM and midazolam concentrations of 0.767, 1.53, 3.07, 4.60, 9.21 and 30.7 µM were used, respectively. Hence, substrate concentrations ranged across the full kinetic profile of the respective marker reaction. All incubations were carried out in duplicate and two samples taken from each incubation at the previously defined time points (chapter 2.3.3.2). Reaction velocities and their precision were determined (Eq. 2.4) and investigated in relation to the substrate (C_S) and inhibitor (C_I in µM) concentration to determine K_M and V_{max} as well as the inhibitory constant (K_i in µM) of the reaction. The obtained data were used to fit the three main models of reversible inhibition, i.e. competitive (Eq. 2.18), non-competitive (Eq. 2.19) and uncompetitive (Eq. 2.20) using the "nls" function in R [110]. The type of inhibition was determined according to the best model fit assessed with the Akaike's information criteria (AIC) [169]. Models with a lower AIC were considered superior to models with a higher AIC. A model was deemed to be significantly better when the difference in AIC exceeded 2. All estimated model parameters were evaluated for their precision and plausibility.

$$V = \frac{V_{max}}{1 + \frac{K_M}{C_S}\left(1 + \frac{C_I}{K_i}\right)} \tag{2.18}$$

$$V = \frac{V_{max}}{\left(1 + \frac{K_M}{C_S}\right)\left(1 + \frac{C_I}{K_i}\right)} \tag{2.19}$$

$$V = \frac{V_{max}}{\left(1 + \frac{K_M}{C_S} + \frac{C_I}{K_i}\right)} \tag{2.20}$$

Lastly, also a Lineweaver-Burk linearisation of the data was performed by determination of the reciprocals of the reaction velocities and the substrate concentrations. Subsequently, a linear regression analysis was performed for each inhibitor as well as inhibitor level on the CYP isoenzymes 2C19, 2C9 and 3A4. In case of competitive inhibition, individual linear functions were expected to share a common intersection on the y-axis of the Lineweaver-Burk plot (the V_{max}) while in the case of non-competitive inhibition the common intersection would lie on the x-axis of the plot (the K_M). Uncompetitive inhibition was concluded when the linear regression functions present themselves as parallel lines (identical slopes) [110].

2.4 *In vitro* microdialysis feasibility studies for voriconazole and its *N*-oxide metabolite

The feasibility of the simultaneous microdialysis of VRC and NO was explored *in vitro* under standardised conditions before the investigation of clinical trial samples. For this purpose, in a first step VRC and NO RR were assessed in the absence of the respective other across a large concentration range (chapter 2.4.4). Afterwards, combinations of VRC and NO at different concentration levels were evaluated (chapter 2.4.5) as well as all data simultaneously analysed applying a linear mixed-effects (LME) model (chapter 2.4.6). Finally, the catheter calibration method of retrodialysis was explored to test its feasibility for determination of ISF concentrations for VRC *and* NO (chapter 2.4.7).

2.4.1 Preparation of *in vitro* microdialysis solutions

VRC and NO solutions for *in vitro* microdialysis investigations, i.e. catheter-surrounding medium and retroperfusate, were prepared using the 1 mg/mL methanolic stock solutions (chapter 2.1.5.3). By a 100-fold dilution of the stock solution with RS, a 10 µg/mL working solution of VRC and NO was prepared. The final catheter-surrounding medium was prepared by spiking RS with the VRC and/or NO stock or working solution, respectively, to obtain the final concentrations as described in the following sections. A total volume of 14 mL was needed to adequately surround microdialysis catheters with medium in the sIVMS (chapter 1.4.3).

For VRC retroperfusate, the same stock solution was used to spike RS to obtain a concentration of 60 µg/mL. A total volume of 5 mL was prepared as identical solutions were applied for the parallel use of up to four microdialysis catheters.

2.4.2 *In vitro* microdialysis procedure

The previously developed and validated sIVMS [134] was used to perform all *in vitro* microdialysis experiments under standardised conditions and enable the parallel use of up to four microdialysis catheters. To optimally mimic the ISF, the catheter-surrounding medium, consisting of RS, was constantly stirred and maintained at 37°C. For all recovery investigations, the catheter-surrounding medium was spiked with the respective compound(s), VRC, NO or a combination, at different concentrations. Microdialysis catheters were perfused with RS at a flow rate of 2 µL/min, which was identical to flow rates of previously performed *in vivo* investigations [132,146]. For the purpose of reproducibility and uniformity, all experiments were conducted according to a standardised procedure. First, syringes holding the perfusate and containers for the catheter-surrounding medium were filled with MilliQ® water and microdialysis catheters perfused for 15 min while gradually increasing the flow rate and flushing finally at 15 µL/min for one minute. Secondly, syringes and medium containers were filled with compound-free RS and the procedure was repeated. Afterwards the flow rate was set to the final 2 µL/min and the system

was equilibrated for 15 min. Two baseline samples were taken by collecting microdialysate for 15 min each in an Eppendorf tube while pure RS was in the syringes and medium containers. This procedure ensured that no VRC or NO from previous experiments were left in the catheters and the flushing procedure had been successful. After the baseline samples, the catheter-surrounding medium was exchanged to medium spiked with VRC, NO or a combination, and another 15 min equilibrated to assure the steadiness of concentrations in the tubing system. Recovery investigations started thereafter. One sample period lasted 7.5 min to collect enough volume of microdialysate for quantification. Depending on the study day, up to ten microdialysate samples were taken consecutively. The catheter-surrounding medium was sampled directly after preparation and then after every second microdialysis interval for calculation of RR values (Figure 2.2).

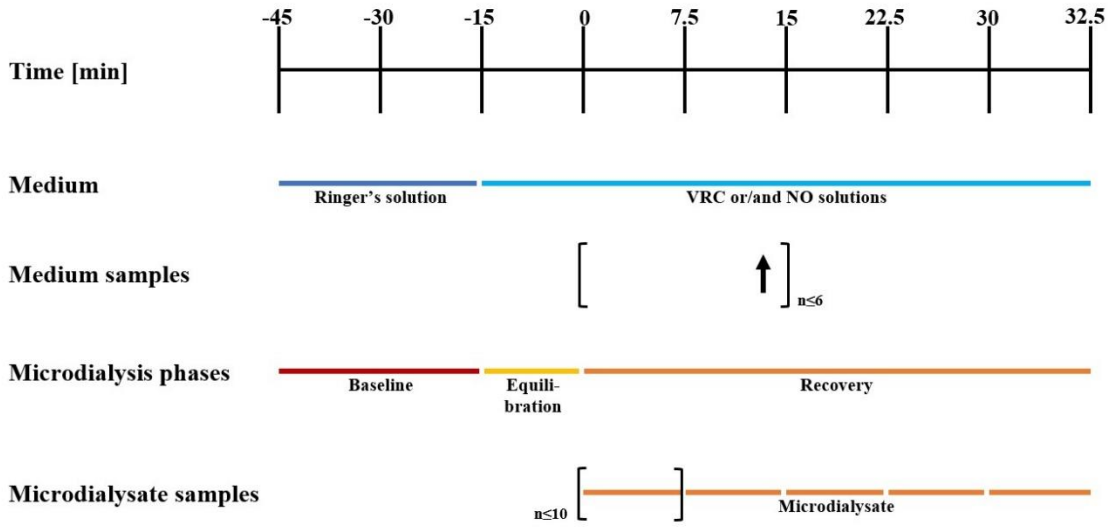

Figure 2.2: Experimental procedure and sampling schedule for the determination of relative recovery of voriconazole (VRC) and its *N*-oxide metabolite (NO) in a validated *in vitro* microdialysis system. Times are given relatively to the start of recovery investigations.

2.4.3 Stability of voriconazole *N*-oxide under *in vitro* microdialysis conditions

As a prerequisite for reliable microdialysis investigations NO needed to be stable at a temperature of 37°C for an adequate time of approximately 4 h. Therefore, two NO solutions at a low and a high concentration (0.01 and 4.0 µg/mL), were prepared in duplicate in RS and kept at 37°C in a constantly shaking Eppendorf ThermoMixer®. Aliquots for analysis were taken immediately after preparation and every 20 min afterwards for a total of 4 h and quantified with freshly prepared calibration samples (chapter 2.2). The metabolite was deemed stable if no degradation tendencies were observable and the deviation from the nominal concentration was less than ±15% as predefined by the EMA guideline on bioanalytical method validation [139].

2.4.4 Relative recovery of voriconazole and its *N*-oxide metabolite during individual microdialysis

The RR of VRC and NO in the absence of the respective other was investigated using five concentrations (0.01, 0.1, 0.2, 0.5 and 3 µg/mL) for VRC and four (0.01, 0.1, 0.5 and 3 µg/mL) for NO in the catheter-surrounding medium. For VRC, investigations were performed on five study days using five different microdialysis catheters and for NO on three days using four catheters. Microdialysate samples were collected over a period of 7.5 min with up to ten intervals consecutively on each study day with the same catheter. Additionally, the catheter-surrounding medium was sampled up to six times throughout the experiment (Figure 2.2). RR was assessed as ratio of the individual microdialysate concentration ($C_{\mu D}$) and mean medium concentration (C_{Medium}) (Eq. 2.21).

$$RR, \% = \frac{C_{\mu D}}{C_{Medium}} \cdot 100\% \qquad (2.21)$$

RR values were graphically explored to evaluate their dependency on concentration, the used microdialysis catheter and the study day. Thereby, the respective other parameters were omitted.

2.4.5 Relative recovery of voriconazole and its *N*-oxide metabolite during simultaneous microdialysis

Simultaneous microdialysis of VRC and NO was investigated using four catheters on three study days. In total, five different solutions combining VRC plus NO were examined: 0.01 + 0.01, 0.2 + 0.5, 0.5 + 0.5, 3 + 0.01 and 3 + 3 µg/mL, respectively. Combinations of high NO and low VRC concentrations were not feasible due to the impurity of the NO reference standard containing approximately 2% of VRC. Medium samples were taken throughout each experiment and used to calculate RR according to equation 2.21. The obtained RR values were evaluated graphically to assess changes in RR compared to individual microdialysis. Additionally, the influence of the concomitant concentration of the second compound was explored.

2.4.6 Linear mixed-effects modelling

For a comprehensive evaluation, a LME model was built, applying the "lme4" package in R and RStudio® [170], to *simultaneously* assess the impact of experimental factors on RR as well as to explore the difference between RR of VRC, NO and their combination. Investigated experimental factors comprised the VRC and NO concentration, the used individual microdialysis catheter and the respective study day. The RR of VRC and NO were set as dependent variable and the corresponding nominal concentration (C_{Nom}) as well as the scenario were defined as fixed terms. In total, RR corresponded to four different scenarios, which were integrated in the model as categorial variables (Figure 2.3).

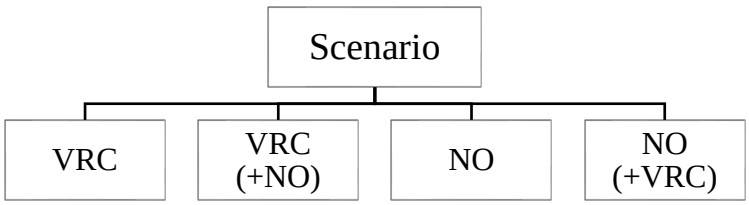

Figure 2.3: The four investigated scenarios for the determination of relative recovery of voriconazole (VRC), its *N*-oxide metabolite (NO) individually or in the presence of the respective other (given in brackets).

RR of the individual microdialysis of VRC was thereby the reference scenario and estimated as the coefficient a_0 (Eq. 2.22) corresponding to the y-intercept of the linear model. The RR of the other three scenarios were estimated as absolute deviation from RR of VRC as coefficient a_1 for each of the remaining three scenarios (Eq. 2.22). The slope of the linear regression for each scenario was described by the impact of C_{Nom} and its coefficient a_2. Furthermore, the individual microdialysis catheter (n=5) and the study day (n=7) were defined in the model as crossed random effects as they were assumed to contribute to the observed variance (σ) in the data whereas ε depicted the remaining unexplained variance (Eq. 2.22).

$$RR = a_0 + a_1 * Scenario + a_2 * C_{Nom} + \sigma(Catheter) + \sigma(Study\ day) + \varepsilon \qquad (2.22)$$

All fixed effects were tested for statistical significance applying an F-statistic using Satterthwaite's approximation for the degrees of freedom, using the lmerTest package [171] in the software R. The result was considered statistically significant with the 95% confidence interval (CI) excluding zero and p-values ≤0.05.

2.4.7 *In vitro* retrodialysis

Retrodialysis with VRC was performed at the end of two recovery investigations using a 20-fold higher VRC concentration in perfusate (60 µg/mL) as the highest VRC concentration in medium. This ensured an unsaturated diffusion across the membrane of the microdialysis catheter as the concentration in the catheter-surrounding medium was negligibly compared to retroperfusate [137]. Three retrodialysate samples were collected per microdialysis catheter for 10 min each while retroperfusate samples were taken at the beginning (n=1) and the end of retrodialysis (n=2) (Figure 2.4).

Relative delivery (rD) was calculated as difference to 100% of the ratio of the VRC concentration in retrodialysate ($C_{Retrodialysate}$) and the concentration in retroperfusate ($C_{Retroperfusate}$) (Eq. 2.23) and used to determine the concentration of VRC and NO in the catheter-surrounding medium (Eq. 2.24).

$$rD, \% = 100\% - \left(\frac{C_{Retrodialysate}}{C_{Retroperfusate}}\right) \cdot 100\% \quad (2.23)$$

$$C_{Medium\ or\ ISF} = \frac{C_{\mu D}}{rD, \%} \cdot 100\% \quad (2.24)$$

The performance of VRC retrodialysis was assessed by comparing these calculated VRC and NO concentrations to the direct measurements in the catheter-surrounding medium (n=6).

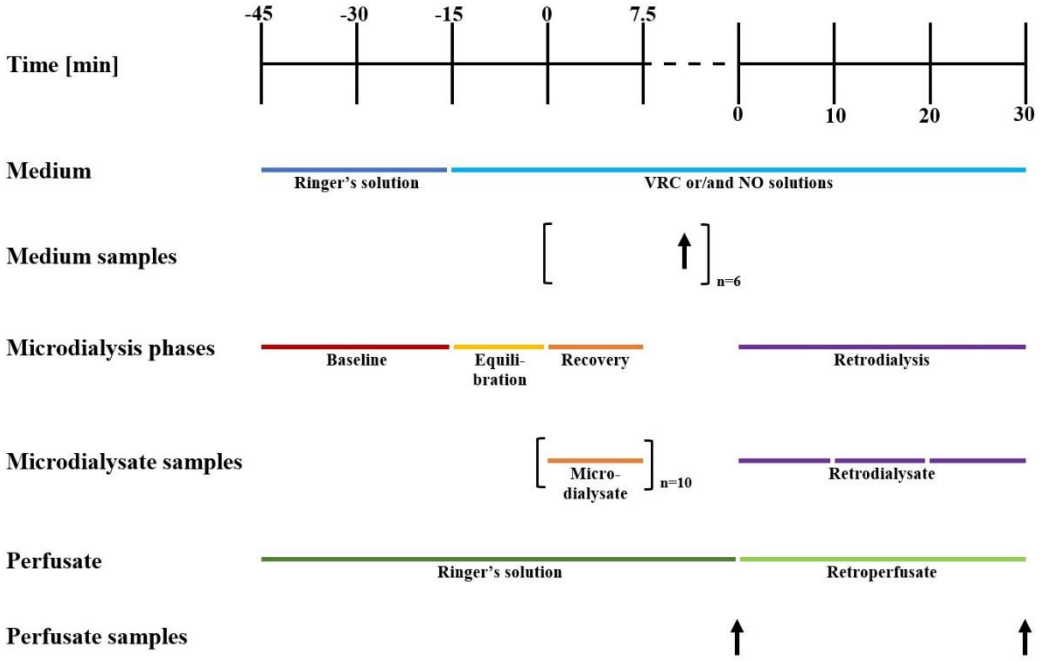

Figure 2.4: Experimental procedure and sampling schedule for the determination of relative recovery of voriconazole (VRC) and its *N*-oxide metabolite (NO) in a validated *in vitro* microdialysis system including retrodialysis. Times are given relatively to the start of recovery investigations and start of retrodialysis, respectively.

2.5 Clinical microdialysis trial for the determination of voriconazole and its *N*-oxide metabolite concentrations in plasma, ultrafiltrate and interstitial space fluid

Aiming at amalgamating the knowledge on VRC PK that can be gained by microdialysis investigations and the simultaneous assessment of drug and metabolite, plasma, ultrafiltrate and microdialysate samples from a clinical trial were assessed for their VRC and NO concentrations and differences in the PK profiles were investigated.

2.5.1 Clinical trial design and study schedule

From 2009 to 2013, a clinical microdialysis study (ClinicalTrials.gov identifier NCT01539330; EudraCT No. 2008-008524-32) was conducted at the Medical University Vienna. The trial was approved by the Ethics Committee of the university, the competent federal authority (BASG) and

performed according to the Declaration of Helsinki as amended in Seoul 2008 [172], the ICH guideline for good clinical practice, as well as local regulatory requirements at the Department of Clinical Pharmacology, Medical University Vienna, Austria. Healthy male volunteers were enrolled in the prospective, open-labelled and uncontrolled trial. All received twice daily an approved VRC standard dosing of 6 mg/kg body weight i.v. as a 2 h infusion on day one, 4 mg/kg i.v. as a 1.3 h infusion on day two and 200 mg tablets on day three and four [38].

Microdialysis catheters were inserted into ISF of the abdominal subcutaneous adipose tissue for a total of four days and microdialysate as well as plasma samples were collected according to a prespecified schedule. After the first, fifth and seventh dose, intensive sampling was performed by taking 16 plasma samples (0, 0.5, 1, 1.5, 1.75, 2, 2.25, 2.5, 3.25, 4.5, 6, 8, 9, 10, 11, 12 h) as well as collecting microdialysate samples in 16 intervals (0-0.5, 0.5-1, 1-1.5, 1.5-2, 2-2.5, 2.5-3, 3-3.5, 3.5-4, 4-5, 5-6, 6-7, 7-8, 8-9, 9-10, 10-11, 11-12 h) after VRC administration. Sparse sampling was performed after the second, third and fourth VRC dose administration taking plasma samples at the end of the infusion (2 h on day 1, 1.3 h on day 2 and 3) and after 12 h as well as collecting microdialysis samples in 0.33 h intervals until the end of the infusion. After the sixth dose (tablet) on day 3, only after 12 h, a plasma sample was taken [132]. Ultrafiltrate was acquired by centrifugation of 1 mL plasma in a Centrifree® ultrafiltration device at 2000 × *g* at room temperature for 20 min.

To individually calibrate microdialysis catheters, retrodialysis was performed twice, subsequently to the third and last (seventh) dosing interval. Therefore, catheters were perfused with RS containing VRC at a concentration of 200 µg/mL and two retrodialysate samples were collected for 15 min after a 10 min equilibration. Perfusate as well as retrodialysate samples were evaluated individually for every volunteer [173]: rD was assessed by relating the concentration in retrodialysate ($C_{Retrodialysate}$) to the concentration in retroperfusate ($C_{Retroperfusate}$) as presented in equation 2.23 and assumed equal to RR. Thus, based on rD determinations, concentrations of VRC and NO in ISF (C_{ISF}) were determined from microdialysate concentrations ($C_{\mu D}$) as described in equation 2.24.

2.5.2 Study population

The described clinical trial was evaluated previously for VRC concentrations alone in ultrafiltrate and microdialysate [132,173]. The current analysis focussed on *all* available matrices, i.e. plasma, ultrafiltrate and microdialysate, from four individuals of this trial to simultaneously assess the concentrations of VRC and NO. The investigated healthy volunteers were all male, between 22 and 28 years old and had a body mass index of 20.5 to 23.4 kg/m². Despite their similar demographic characteristics, they all showed a different CYP2C19 genotype-predicted phenotype. According to the recommendations of the Clinical Pharmacogenetics Implementation

Consortium (CPIC®), one individual was thus classified as a RM (CYP2C19 *1/*17), one as a NM (CYP2C19 *1/*1) and two as IM (CYP2C19 *1/*2 and CYP2C19 *2/*17) [63]. However, for better differentiation, the CYP2C19 *2/*17 genotype will be referred to as a RM/PM.

2.5.3 Bioanalysis of study samples

Bioanalysis was performed according to the validated LC-MS/MS assay described in chapter 2.2. Each analytical run was conducted and evaluated as recommended by the EMA guideline on bioanalytical method validation [139]. Therefore, each run contained, besides the clinical samples, CAL samples, including a blank and a zero sample, and QC samples. For each analyte, VRC and NO, separate CAL and QC samples were prepared. Four QC levels were assessed at least in duplicate and evenly increased to equal or exceed 5% of the number of study samples. Overall, four bioanalytical runs were carried out, two for microdialysate and two for plasma and ultrafiltrate samples. Thereby, the ultrafiltrate samples obtained during the first evaluation of the clinical trial were used and plasma samples not submitted to a new ultrafiltration procedure. Samples from the CYP2C19 RM and NM as well as the CYP2C19 IM and RM/PM were combined for the respective analytical runs.

An analytical run was accepted if the back-calculated concentrations of the CAL samples were within ±15% of their nominal value (±20% for the LLOQ). In total, a minimum of 75% of CAL samples had to fulfil this criterion. If a CAL sample was outside those limits, it was rejected and the linear regression re-assessed without it. A minimum of six CAL concentrations had to remain in the calibration function to permit its application to study samples. In case the LLOQ or upper limit of quantification (ULOQ) had to be rejected, the calibration range was adapted for this run if all QC levels were still covered by it. However, when replicate CAL concentrations were used and only one sample at the LLOQ or ULOQ failed, the range remained unchanged. Furthermore, more than 67% of QC samples in each run had to be accurate, indicated by a maximum deviation of ±15% of their nominal value. At least 50% of QC samples per level had to conform to this limit. An overall accuracy and precision of VRC and NO quantification was determined for plasma and microdialysate by combining the respective QC measurements of all runs. Good performance was demonstrated if the mean concentration per QC level was within ±15% of the nominal value and the imprecision ≤15% CV [139].

2.5.4 Pharmacokinetic data analysis for clinical study samples in plasma, ultrafiltrate and interstitial space fluid

The obtained clinical data of VRC and NO from plasma, ultrafiltrate and microdialysate were subjected to an exploratory PK analysis. This analysis focussed on several aspects: the plasma protein binding (chapter 2.5.4.1), the concentration-time profiles (chapter 2.5.4.2), the total exposure (chapter 2.5.4.3) as well as the metabolic ratios (chapter 2.5.4.4) of VRC and NO.

Therefore, the four individuals were assessed individually considering their CYP2C19 genotype-predicted phenotype and changes in PK analysed regarding the number of VRC dose administrations. In particular, PK after the first VRC dose administration (first dosing interval on day one, i.e. considered as single dosing), which reflected an i.v. administration, after the fifth dose (fifth dosing interval on day three, i.e. multiple dosing), which reflected the first p.o. dosing and after the seventh and last dose of the clinical trial (seventh dosing interval on day four, i.e. multiple dosing), was evaluated. Further, differences in PK between plasma, ultrafiltrate and ISF were explored.

2.5.4.1 Fraction unbound in plasma of voriconazole and its *N*-oxide metabolite

The fraction unbound (f_u) of VRC and NO was investigated by relating the unbound plasma concentrations determined in ultrafiltrate to the total plasma concentrations assessed in plasma. The dependencies of VRC and NO plasma protein binding were investigated by relating f_u to the total concentration of the respective compound as well as to the time after the first VRC dose administration. Furthermore, the differences between the individuals with different CYP2C19 genotype-predicted phenotypes was evaluated.

2.5.4.2 Concentration-time profiles and pharmacokinetic target attainment

VRC and NO concentration-time profiles were investigated in plasma, ultrafiltrate and ISF. While concentrations of VRC and NO in plasma samples reflected *total* plasma concentrations, ultrafiltrate samples represented the protein-unbound concentrations in plasma. Concentrations determined in microdialysate samples were transformed to ISF concentrations by application of retrodialysis data. Diffusion processes across the microdialysis membrane were considered equal in both directions, thus VRC rD determined by retrodialysis was presumed equivalent to RR and used to calculate VRC concentrations in ISF. NO concentrations were calculated in the same way, using VRC retrodialysis as a surrogate based on *in vitro* feasibility investigations (chapters 2.4.7 and 3.3.5). Lastly, midtime points of the microdialysis sampling intervals were considered for graphical evaluations.

Maximum and minimum plasma, ultrafiltrate and ISF concentrations (C_{max} and C_{min}) as well as time points for the occurrence of C_{max} (t_{max}) in all matrices were determined for VRC and NO, respectively. As a PK target, C_{min} of VRC in plasma is typically considered, targeting concentrations of minimum 1-2 µg/mL (2.86 – 5.73 µmol/L) while not exceeding 4.5-6 µg/mL (12.9 – 17.2 µmol/L) [174]. Consequently, also the attainment of C_{min} was explored for each individual.

2.5.4.3 Total exposure of voriconazole and its *N*-oxide metabolite in plasma, ultrafiltrate and interstitial space fluid

To assess the exposure over time, the AUC was determined for VRC and NO in plasma, ultrafiltrate and ISF after the first, fifth and seventh VRC dose as in those dosing intervals intensive sampling was performed. The AUC was determined by the linear-up/log-down trapezoidal method from time point 0 to the time point of the last positive concentration, i.e. quantified concentration, using the "pkr" package in R [175]. For this purpose, while concentrations were increasing, a linear interpolation between two successive measurements (C_i and C_{i+1} with their measurement time points t_i and t_{i+1}) was applied and the emerging trapezia summed up (Eq. 2.25). When concentrations were decreasing, a logarithmic interpolation between two successive measurements was used and the emerging trapezia summed up (Eq. 2.26).

$$AUC_{t_i - t_{i+1}} = \sum_{i=1}^{n} \frac{C_i + C_{i+1}}{2} \cdot (t_{i+1} - t_i) \tag{2.25}$$

$$AUC_{t_i - t_{i+1}} = \sum_{i=1}^{n} \frac{C_i - C_{i+1}}{\ln\left(\frac{C_i}{C_{i+1}}\right)} \cdot (t_{i+1} - t_i) \tag{2.26}$$

The extent of tissue fluid exposure was furthermore assessed by the ratio of AUC in ISF to the AUC in plasma or ultrafiltrate for VRC and NO, respectively.

2.5.4.4 Metabolic ratios

For the assessment of the total observed differences between the four individuals as well as to investigate the extent of metabolism, ratios of the VRC and NO concentrations were evaluated. For this purpose, in a first step, metabolic ratios of NO to VRC molar concentrations were calculated for every individual plasma, ultrafiltrate and ISF sample and investigated for changes across time and VRC concentration.

In a second step, also the metabolic ratios of the molar AUC of NO to VRC were explored for the different CYP2C19 genotype-predicted phenotypes, the respective dosing interval as well as for the three different matrices.

2.6 Statistics

All generated data were subjected to various statistical analyses. Specific numerical evaluations, e.g. quantification of enzyme kinetics (chapter 2.3) or LME modelling (chapter 2.4.6), were introduced in the preceding chapters. In the following general statistical parameters and methods that were applied throughout this thesis are presented. The respective calculations were performed with R and RStudio® or Microsoft Excel®.

2.6.1 Descriptive statistics

Central tendency parameters. The arithmetic mean (Eq. 2.27) was applied as a measure of central tendency whenever data were symmetrically distributed. As the median (Eq. 2.28) is less prone to outliers it was used when the number of data points was small or the distribution of the data unknown [176]. In particular for box plots data were assessed based on quartiles ordering the values from smallest to largest and dividing the number of data points into equally sized quarters. The first quartile (Q_1) thereby represented the middle value between the minimum and the median indicating that 25% of the data are lower than this value (25th percentile). The third quartile (Q_3) reflected the middle value between the median and the maximum and indicated that 25% of the data are larger than this value (75th percentile). The second quartile (Q_2) equalled the median.

$$\bar{x} = \frac{1}{n} \cdot \sum_{i=1}^{n} x_i \tag{2.27}$$

$$\textit{For uneven n:} \quad \tilde{x} = x_{\frac{n+1}{2}} \tag{2.28}$$

$$\textit{For even n:} \quad \tilde{x} = \frac{1}{2} \cdot \left(x_{\frac{n}{2}} + x_{\frac{n}{2}+1} \right)$$

Dispersion parameters. Variability and hence the precision of the generated data was assessed with dispersion parameters such as the range (Eq. 2.29), variance (σ^2, Eq. 2.30), standard deviation (SD, Eq. 2.31) or the coefficient of variation (CV, Eq. 2.32). Additionally, the 95% confidence interval (CI) was applied, describing the lower and upper limit of the range the estimated point falls with a probability of 95%. The interquartile range (IQR) was defined as the difference between Q_3 and Q_1 and was represented by the upper and lower border of the box in boxplots. Additionally, the upper whisker of the boxplots extended to the largest value but no further than 1.5-fold IQR, the lower whisker extended to the smallest value at most 1.5-fold IQR.

$$Range = x_{maximum} - x_{minimum} \tag{2.29}$$

$$\sigma^2 = \frac{1}{n-1} \sum_{i=1}^{n} (x_i - \bar{x})^2 \tag{2.30}$$

$$SD = \sqrt{\sigma^2} \tag{2.31}$$

$$CV, \% = \frac{SD}{\bar{x}} \cdot 100 \tag{2.32}$$

2.6.2 Linear regression analysis

Regression analyses were performed to explore the relation between two continuous variables [177]. Thereby, the change of a dependent variable y_i (e.g. concentration of metabolite formed) was observed as an independent variable x_i (e.g. time) changed. In the case of a linear regression, the assumption of a linear relationship between the dependent and independent variable was made, resulting in the estimation of the model parameters β_0 (intercept with the y-axis) and β_1 (slope of the function) (Eq. 2.33). The term ε_i described an error term.

$$y_i = \beta_0 + \beta_1 \cdot x_i + \varepsilon_i \tag{2.33}$$

The sum of square residuals (SS_{res}) of the observed to the predicted dependent variables was aimed to be minimised (Eq. 2.34). The goodness of fit was evaluated based on the coefficient of determination (R^2, Eq. 2.36), which was determined as the ratio of SS_{res} (Eq. 2.34) to the total sum of squares (SS_{tot}, Eq. 2.35). A value of R^2 of 1 represented a perfect fit. All linear regression analyses were carried out with R and RStudio® using the "lm" function of the package "stats".

$$SS_{res} = \sum_{i=1}^{n} (y_i - (\beta_0 + \beta_1 \cdot x_i))^2 \tag{2.34}$$

$$SS_{tot} = \sum_{i=1}^{n} (y_i - \bar{y})^2 \tag{2.35}$$

$$R^2 = 1 - \frac{SS_{res}}{SS_{tot}} \tag{2.36}$$

3 Results

3.1 Bioanalytical assay for the simultaneous quantification of voriconazole, voriconazole *N*-oxide and hydroxyvoriconazole

For all *in vitro* and *in vivo* PK investigations, a reliable and versatile bioanalytical assay was developed that enabled the simultaneous determination of VRC, NO and OH-VRC (chapter 3.1.1). The LC-MS/MS assay was furthermore fully validated for VRC and NO in two matrices, plasma and microdialysate (chapter 3.1.2). The feasibility of the bioanalytical assay for quantifications in ultrafiltrate (chapter 3.1.3) and the *in vitro* matrices of HLM and rhCYP was demonstrated and the performance of the latter continuously evaluated (chapter 3.1.4) [178].

3.1.1 Development of the bioanalytical assay

The best chromatographic results were achieved by maintaining the phenyl-hexyl column at 30°C and sustaining a flow rate of the mobile phase of 0.350 mL/min. The analytes, i.e. VRC, NO and OH-VRC, as well as the IS were highly lipophilic, requiring a high proportion of organic solvent for elution from the column during chromatography. Thus, starting from a baseline eluent composition of 95% UP water plus 5% MeOH, the MeOH fraction was linearly increased to 50% over 0.5 min and kept at this level for another 0.5 min. Afterwards, the MeOH fraction was first gradually increased to 70% over 2 min followed by a steep rise to 98% over 0.05 min. This condition was kept constant for 1.65 min before the mobile phase composition was reset to baseline conditions within 0.1 min and maintained until the next injection (Figure 3.1). The injection volume was set to 2 µL and the injection needle washed with a solution of MeOH/UP water (90:10 [V/V]) to minimise carry-over.

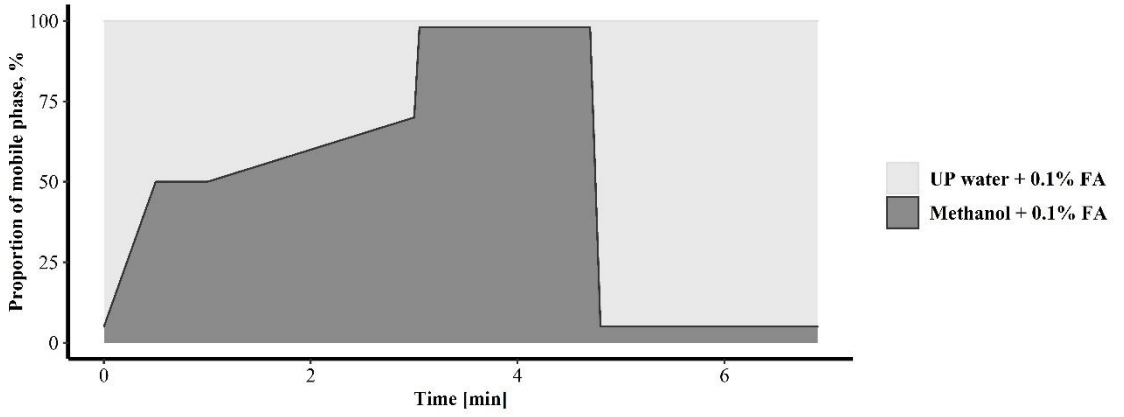

Figure 3.1: Mobile phase composition over time for the elution of voriconazole and its *N*-oxide and hydroxy metabolite. Mobile phase A and B consisted of ultrapure (UP) water and methanol, respectively, both containing 0.1% formic acid (FA) [V/V].

The overall short run time of 6.9 min included a postrun of 1.6 min as well as a needle wash time of 20 s. All eluents were directed to the waste before 2.4 min to avoid a contamination of the ion source with non-evaporable inorganic salts and thus a decrease in sensitivity during longer analytical runs. The described gradient method resulted in retention times of 3.4 min for NO, 3.7 min for OH-VRC, 4.1 min for VRC and 4.4 min for the IS, diazepam (Figure 3.2).

In the final MS settings, the ESI source was operated in positive ionisation mode and ion acquisition was performed in dMRM mode. Three mass transitions were monitored for VRC, OH-VRC and the IS and two for NO. The transition with the highest intensity and smallest background noise in blank samples was chosen as the quantifier. All mass transitions with the corresponding collision energies are presented in Table 3.1. The qualifier to quantifier relative response was 32.8% *(m/z* 350 → 224) and 92.1% *(m/z* 350 → 127) for VRC, 80.0% for NO (*m/z* 366 → 143), 34.0% (*m/z* 366 → 143) and 68.4% (*m/z* 366 → 127) for OH-VRC and 50.0% *(m/z* 285 → 222) and 102% *(m/z* 285 → 154) for the IS, respectively. The qualifier to quantifier ratio was monitored in all runs, allowing for an uncertainty of ±25%. Only few individual samples revealed a ratio close outside the allowed range. However, overall the ratios were maintained during all runs and study days indicating a reproducible identification of the compounds.

Table 3.1: Precursor ions of voriconazole, its *N*-oxide and hydroxy metabolite as well as the internal standard diazepam including the product ions with corresponding applied collision energy. Transitions used for quantification are marked in **bold**.

Compound	Precursor ion *m/z* $[M+H]^+$	Product ion *m/z*	Collision energy [eV]	Fragmentor voltage [V]	Cell accelerator voltage [V]	Polarity
Voriconazole	350	**281**	17	380	5	Positive
	350	224	13	380	5	Positive
	350	127	41	380	5	Positive
Voriconazole *N*-oxide	366	**224**	13	380	5	Positive
	366	143	9	380	5	Positive
Hydroxy-voriconazole	366	**297**	16	380	5	Positive
	366	143	24	380	5	Positive
	366	127	56	380	5	Positive
Internal standard (diazepam)	285	222	36	380	5	Positive
	285	**193**	36	380	5	Positive
	285	154	32	380	5	Positive

m/z, mass-to-charge ratio

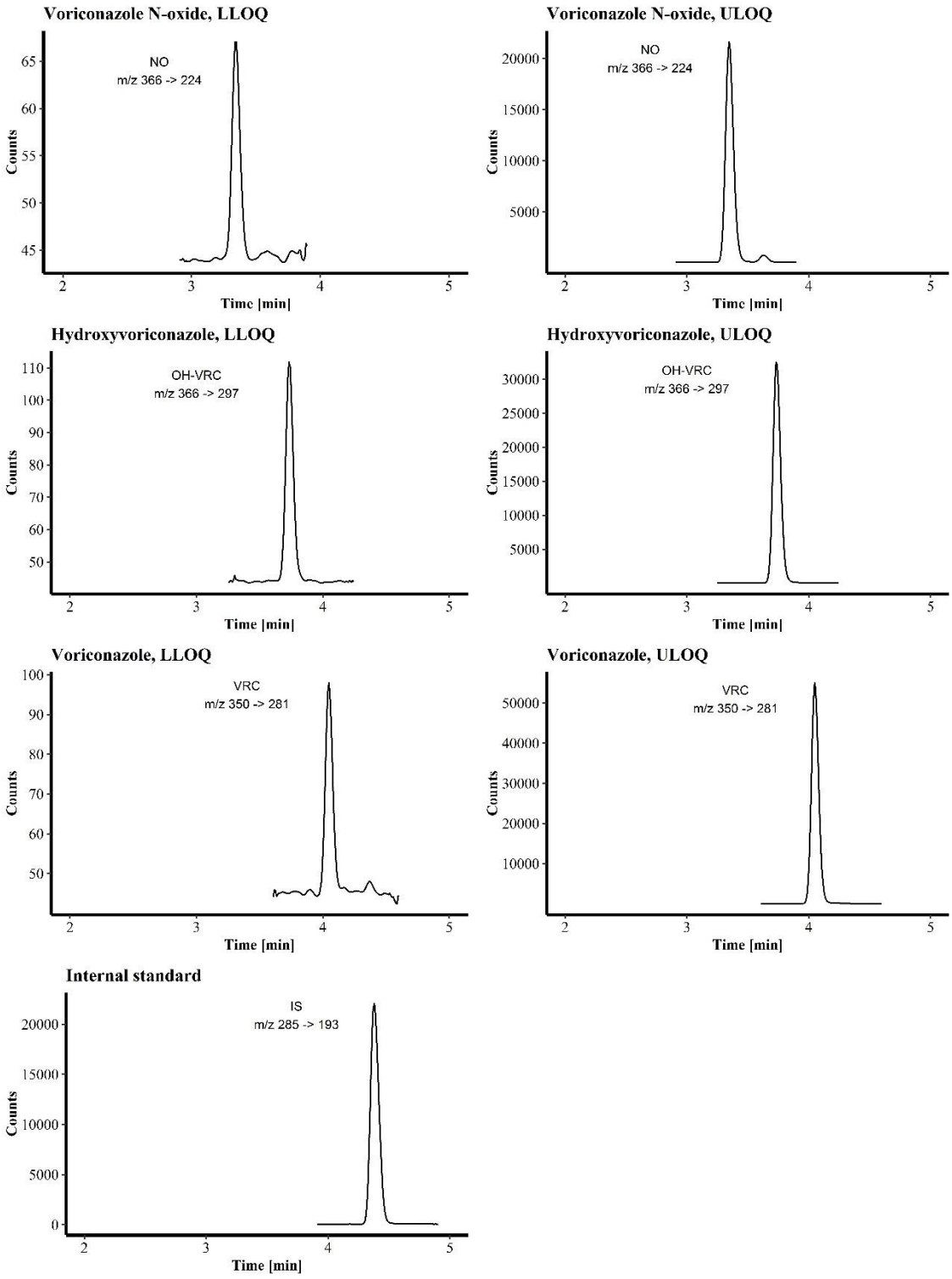

Figure 3.2: Typical chromatograms of the quantifier mass-to-charge (*m/z*) transitions at the lower (LLOQ) and upper (ULOQ) limit of quantification for voriconazole *N*-oxide (NO), hydroxyvoriconazole (OH-VRC), voriconazole (VRC) and the internal standard (IS).

As NO and OH-VRC had identical precursor ions and shared equal product ions, a chromatographic separation was essential. The final chromatographic and MS settings provided for this requirement and led to sharp and clear detector responses for VRC, NO, OH-VRC and

the IS (Figure 3.2). Ion source parameters were primarily optimised for NO and OH-VRC ionisation as here the lowest concentrations were expected. The final ion source parameters are listed in Table 3.2.

Table 3.2: Ion source parameters of the mass spectrometer.

Parameter	Value
Capillary voltage	2500 V
Nebulizer gas pressure	40 psi
Drying gas flow	13 L/min of nitrogen
Drying gas temperature	120 °C
Sheath gas flow	12 L/min of nitrogen
Sheath gas temperature	350 °C
iFunnel	RFH 60 V/RFL 90 V

RFH, radio frequency voltage high pressure; RFL, radio frequency voltage low pressure

3.1.2 Validation of the bioanalytical assay for the simultaneous quantification of voriconazole and its *N*-oxide metabolite in human plasma and microdialysate

The developed method was successfully validated for the quantification of VRC and NO in plasma and microdialysate according to the following parameters of the EMA guideline on bioanalytical method validation [139].

3.1.2.1 Selectivity and carry-over

Blank samples prepared from six individual plasma donors were investigated for interferences at the retention times of VRC and NO. The EMA guidelines criteria (<20% of the LLOQ response) were met with a maximum response of 8.18% for VRC and 1.96% for NO, respectively. As microdialysate is a rare matrix, no blank matrices from six individuals were available. Thus, in a first step six blank samples prepared from pure RS, which is used in clinical settings for the perfusion of the microdialysis catheter, were investigated and resulted in a maximum response of 4.58% for VRC and 5.02% for NO, respectively. However, additional microdialysate samples, collected from four healthy volunteers before VRC administration, were inspected and showed a maximum detector response of 12.3% for VRC and 6.94% for NO compared to the LLOQ, which additionally confirmed the selectivity of the method. The IS achieved a maximum response of 0.0842% in blank samples, supporting the selectivity.

Carry-over was initially not avoidable for VRC in plasma and microdialysate due to its high lipophilicity and the large concentration range. Despite the optimisation of the needle wash composition and increased needle washing time, the maximum detector response of a blank

sample following a high VRC concentration was 44.8% of the response at the LLOQ and thus not acceptable. The second blank sample after a high concentration occasionally showed (3 of 20 samples) too high responses (max. 26.0%) as well. For NO in plasma and microdialysate carry-over was not as pronounced. Only 2 of 17 blank samples following a high concentration showed a response >20% (max. 28.3%) compared to the LLOQ. Consequently, a full randomisation of the sample order was not possible and in case of expected high VRC or NO concentrations, additional blank samples were processed. In contrast, for the IS no carry-over effect was detectable with a maximum response across all matrices of 0.339% in blank samples following an IS containing sample compared to the mean IS detector response.

3.1.2.2 Calibration function

In plasma, linearity was assessed over a concentration range from 5 to 5000 ng/mL. Resulting R^2 values were ≥0.9924 for VRC and ≥0.9973 for NO, respectively (Table 3.3, Figure 7.1). None of the back-calculated CAL concentrations were outside the accuracy limits of ±15% of their nominal value (±20% at the LLOQ). Overall accuracy of CAL samples in plasma ranged from 85.4% to 109% of their nominal value for VRC and from 92.1% to 106% for NO (Figure 3.3).

Table 3.3: Parameters (slope, intercept, R^2) of voriconazole and voriconazole *N*-oxide calibration functions in human plasma and microdialysate on the four different days of validation.

Compound		**Plasma**			**Microdialysate**		
	Day	Slope	Intercept	R^2	Slope	Intercept	R^2
Vori-conazole	1	$5.57 \cdot 10^{-4}$	$3.14 \cdot 10^{-4}$	0.9962	$8.28 \cdot 10^{-4}$	$-2.85 \cdot 10^{-4}$	0.9924
	2	$5.68 \cdot 10^{-4}$	$2.36 \cdot 10^{-4}$	0.9993	$7.67 \cdot 10^{-4}$	$4.49 \cdot 10^{-4}$	0.9986
	3	$5.56 \cdot 10^{-4}$	$2.53 \cdot 10^{-4}$	0.9978	$6.26 \cdot 10^{-4}$	$-0.359 \cdot 10^{-4}$	0.9946
	4	$8.35 \cdot 10^{-4}$	$-0.743 \cdot 10^{-4}$	0.9924	$7.19 \cdot 10^{-4}$	$2.45 \cdot 10^{-4}$	0.9918
Vori-conazole *N*-oxide	1	$2.65 \cdot 10^{-4}$	$-0.094 \cdot 10^{-4}$	0.9973	$2.73 \cdot 10^{-4}$	$1.11 \cdot 10^{-4}$	0.9988
	2	$2.54 \cdot 10^{-4}$	$0.177 \cdot 10^{-4}$	0.9988	$3.10 \cdot 10^{-4}$	$-0.0569 \cdot 10^{-4}$	0.9980
	3	$3.03 \cdot 10^{-4}$	$0.104 \cdot 10^{-4}$	0.9995	$2.69 \cdot 10^{-4}$	$-0.844 \cdot 10^{-4}$	0.9910
	4	$2.63 \cdot 10^{-4}$	$-0.0156 \cdot 10^{-4}$	0.9987	$3.01 \cdot 10^{-4}$	$1.57 \cdot 10^{-4}$	0.9973

The calibration functions of VRC and NO in microdialysate showed good linearity over a range of 4 – 4000 ng/mL indicated by a R^2 of ≥0.9918 for VRC and R^2 of ≥0.9910 for NO, respectively (Table 3.3, Figure 7.1). Back-calculated concentrations of CAL samples in microdialysate were 100% accurate for VRC (n=28) and 96.4% accurate for NO (n=28). The one inaccurate NO CAL sample was excluded and the respective calibration function of this run re-assessed. Subsequently, the remaining six CAL levels met the required accuracies and the function was thus used for the evaluation of the run. In total the concentrations of CAL samples applied during the validation

process in microdialysate ranged from 87.3% to 111% of their nominal value for VRC and from 84.9% to 114% for NO (Figure 3.3).

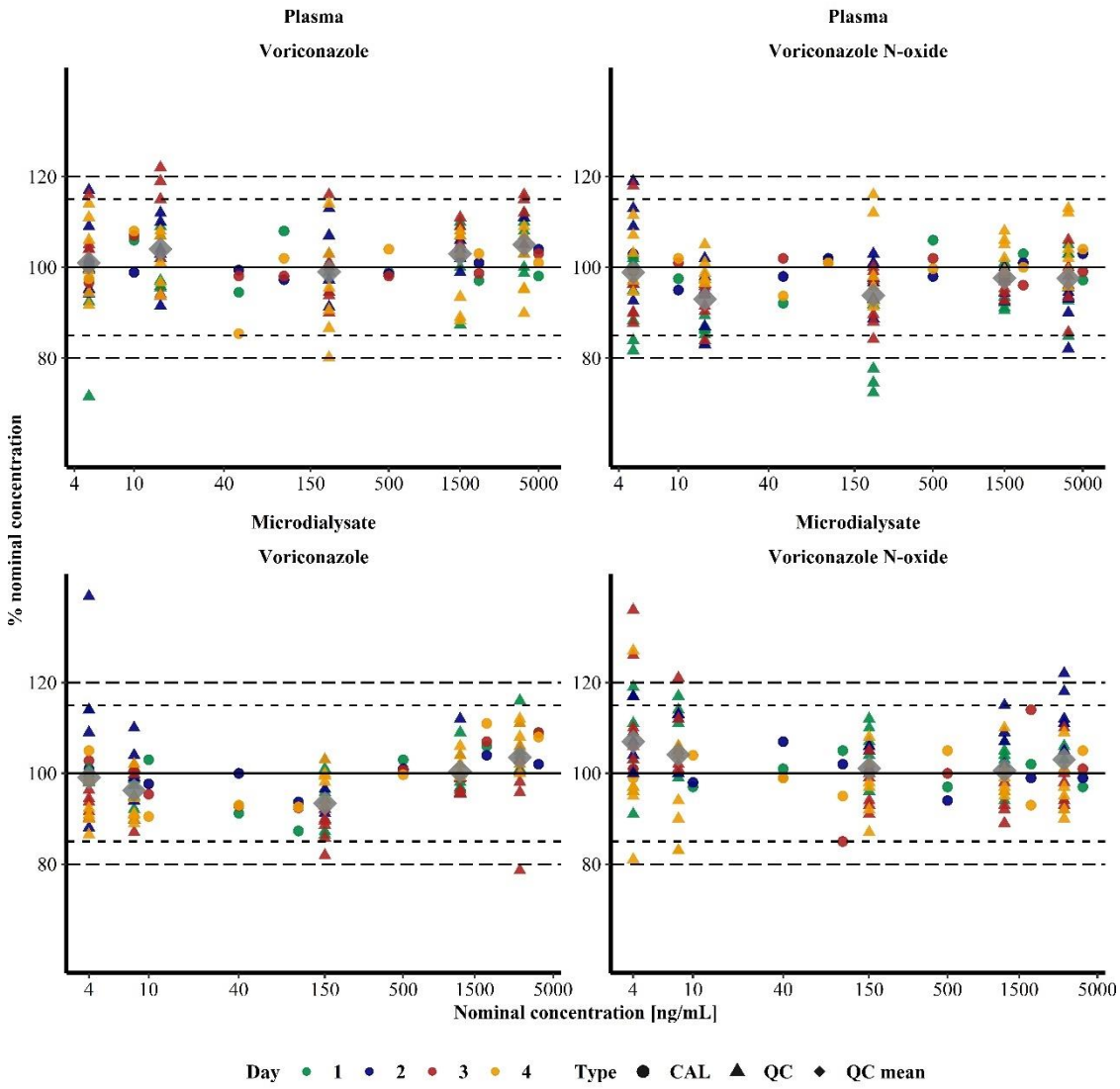

Figure 3.3: Accuracy of voriconazole (left panel) and voriconazole *N*-oxide (right panel) calibration (CAL) and quality control (QC) samples in plasma (upper panel) and microdialysate (lower panel). Data was acquired on four independent days (n=5-6 per concentration and day) and is presented as percentage of its nominal concentration. Dashed lines indicate the required accuracies of ±15% and ±20% for the lower limit of quantification.

3.1.2.3 Lower limit of quantification

The detector response at the LLOQ of VRC and NO was, in both matrices and at all study days, more than five times higher than the response of the preceding blank or zero sample and therefore met the EMA guideline's criteria [139]. Within-run accuracy at the LLOQ (5 ng/mL) ranged from 94.7% to 105% and from 92.0% to 105% for VRC and NO in plasma, respectively. In microdialysate within-run accuracy of the LLOQ (4 ng/mL) was 92.8%-110% for VRC and

98.8%-115% for NO (Figure 3.3, Table 7.3). Imprecision calculated as CV was ≤12.6% and ≤11.5% for VRC and NO in plasma and ≤17.5% and ≤15.3% for VRC and NO in microdialysate (Table 7.3). Thus, the set criteria of an inaccuracy and imprecision of ≤20% at the LLOQ were met. The calculated LOD for VRC and NO was 0.914 ng/mL and 0.912 ng/mL in plasma, and 1.70 ng/mL and 1.26 ng/mL in microdialysate, respectively.

3.1.2.4 Accuracy and precision

To cover the large concentration range of the calibration function, the EMA guideline's requirements for QC sample levels were expanded and four QC levels plus the LLOQ were investigated. For VRC in plasma, a within-run mean accuracy from 94.9% to 110% and a CV of ≤12.8% was achieved for samples above the LLOQ. Investigations of NO QC samples >LLOQ resulted in a within-run mean accuracy of 84.5%-104% and an imprecision of ≤12.8% (Figure 3.3, Table 7.3). Between-run accuracy for VRC and NO in plasma ranged from 99.0% to 105% and from 93.0% to 97.6% while between-run precision resulted in a CV ≤8.58% for VRC and ≤10.8% for NO, respectively (Table 3.4). Overall, 95.0% of all VRC plasma QC samples (n=120) were within ±15% of their nominal value (±20% at the LLOQ) and 92.5% of all NO plasma QC samples (n=120).

In microdialysate, within-run mean accuracy for VRC QC samples >LLOQ fluctuated between 88.0% and 106% of the nominal value and within-run imprecision ranged from 1.79% to 9.49% CV and thus fulfilled the set criteria (Figure 3.3, Table 7.3). The same applied to between-run accuracy and precision that ranged from 93.4% to 104% of the nominal value and from 4.39% to 7.12% CV, respectively (Table 3.4). Overall, 96.4% of individual VRC microdialysate QC samples (n=110) were within ±15% or ±20% at the LLOQ of their nominal value. For NO in microdialysate, within-run mean accuracy of QC samples >LLOQ was between 93.3% and 111% while precision investigations resulted in a CV of ≤10.6% (Table 7.3). Between-run accuracy for NO microdialysate samples >LLOQ ranged from 101% to 104% and imprecision was ≤9.28% CV (Table 3.4). Only nine of 120 individual QC samples were outside the defined criteria, representing 92.5% accuracy.

Table 3.4: Between-run accuracy and precision (n=22-24 per concentration level) for voriconazole and voriconazole *N*-oxide quality control samples in human plasma and microdialysate. Precision is presented as the coefficient of variation (CV) and accuracy as mean concentration compared to the nominal concentration (C_{Nom}).

Matrix and compound	C_{Nom} [ng/mL]	X_{mean} ± SD [ng/mL]	Accuracy, %	CV, %
Plasma				
Voriconazole	5	5.07 ± 0.474	101	9.35
	15	15.6 ± 1.22	104	7.87
	200	198 ± 17.0	99.0	8.58
	1500	1547 ± 105	103	6.77
	4000	4216 ± 250	105	5.92
Voriconazole *N*-oxide	5	4.94 ± 0.501	98.9	10.1
	15	13.9 ± 0.938	93.0	6.73
	200	188 ± 20.3	93.8	10.8
	1500	1464 ± 68.8	97.6	4.70
	4000	3903 ± 311	97.6	7.96
Microdialysate				
Voriconazole	4	3.97 ± 0.464	99.1	11.7
	8	7.70 ± 0.476	96.3	6.18
	150	140 ± 8.62	93.4	6.16
	1200	1205 ± 52.8	100	4.39
	3000	3106 ± 221	104	7.12
Voriconazole *N*-oxide	4	4.27 ± 0.502	107	11.8
	8	8.33 ± 0.773	104	9.28
	150	152 ± 9.51	101	6.27
	1200	1207 ± 78.3	101	6.49
	3000	3077 ± 257	103	8.36

X_{mean}, mean concentration; SD, standard deviation

3.1.2.5 Matrix effects

Overall, matrix effects were not very distinct and did not differ remarkably between the low and high investigated concentration. For VRC and NO in plasma, MF of 1.17 and 1.08 as well as 0.89 and 0.97 were determined for the low and the high concentration, respectively (n=6 each). In microdialysate, the MF for the low and high concentration were 1.16 and 1.12 for VRC and 1.10

and 1.13 for NO. Furthermore, the required precision of ≤15% CV was accomplished for VRC and NO in both matrices. In detail, at the low and high plasma concentration (15 ng/mL and 4000 ng/mL), the CV was 8.07% and 6.70% for VRC and 9.33% and 7.61% for NO, respectively. In microdialysate concentrations of 8 and 3000 ng/mL were investigated and resulted in CV of 7.61% and 3.31% for VRC and 5.14% and 7.07% for NO.

3.1.2.6 Stability

Due to previously reported instabilities of VRC and NO, stability investigations were approached with particular care. However, VRC proved stable under all applied conditions in both matrices (Table 3.5). Freeze-thaw stability, autosampler stability, short-term stability and long-term stability were indicated by high recoveries in QC samples of a low and high concentration ranging from 88.0% to 112% and from 91.9% to 107%, respectively. The imprecision was at all times ≤11.7% CV. Furthermore, NO was stable under most conditions according to the defined criteria (Table 3.5). Only the third freeze-thaw cycle of the lower concentration resulted in a recovery of only 81.0%. However, as the original samples were with a mean accuracy of 87.5% already close to the lower accuracy limit of 85%, this might be a coincidence and not a proof of degradation. Except this observation, recoveries for NO ranged between 95.5% and 107% for the low QC and between 92.9% and 107% for the high QC concentration. All measurements were precise with a maximum CV of 12.6%.

The stock solution of 1 mg/mL VRC in MeOH was stable under all investigated conditions. Short-term stability was demonstrated by a recovery of 103% and 107% after dilution to a low (8 ng/mL in microdialysate) and high (3000 ng/mL in microdialysate) QC level. The precision of the investigation was given by a CV of 9.18% and 0.874% (n=5 each). After three freeze-thaw cycles VRC stock solution did not show degradation with recoveries of 102% (3.35% CV) and 109% (1.77% CV) after dilution to a low (8 ng/mL in microdialysate) and high QC concentration (3000 ng/mL in microdialysate, n=5 each). Lastly, also a three-month storage at -80°C had no observable effects on VRC stock solution stability indicated by a recovery of 98.8% (9.06% CV) and 108% (2.63% CV) after dilution to a low (8 ng/mL in microdialysate) and high (3000 ng/mL in microdialysate) QC level (n=5 each). NO stock solution of 1 mg/mL in MeOH was stable short-term as overnight storage at 4-8°C in the fridge resulted in recoveries of 93.8% (2.65% CV) and 92.0% (2.58% CV) after dilution to a low (8 ng/mL in microdialysate) and high (3000 ng/mL in microdialysate) QC concentration, respectively (n=6 each). Freeze-thaw stability of NO stock solution was demonstrated by three freeze-thaw cycles and recoveries of 85.4% (7.15% CV) and 102% (1.48% CV) at the low (15 ng/mL in plasma) and high QC level (4000 ng/mL in plasma, n=3 each). Finally, the stock solution of NO was also stable long-term. After three-month storage

at -80°C and a dilution to a low (15 ng/mL in plasma) and a high (4000 ng/mL in plasma) QC concentration level recoveries of 95.0% (8.27% CV) and 109% (5.63% CV) were determined.

Overall, a rapid and targeted handling of all VRC and NO samples was recommended to forestall degradation processes. Wherever possible samples should be kept chilled, e.g. in the autosampler or the centrifuge, and on ice during preparation.

Table 3.5: Freeze-thaw, autosampler, short-term and long-term stability of voriconazole (VRC) and voriconazole *N*-oxide (NO) quality control samples in human plasma and microdialysate at a low and high concentration under specified conditions (n=5-6, except long-term stability n=3-5).

Com-pound	C_{Nom} [ng/mL]	Freeze-thaw stability [a]		Autosampler stability [b]		Short-term stability [c]		Long-term stability [d]	
		RV, %	CV, %	RV, %	CV, %	RV, %	CV, %	RV, %	CV, %
Plasma									
VRC	15	112	4.76	99.5	5.13	95.0	11.7	102*	8.82*
	4000	102	4.67	105	3.25	102	9.33	98.7*	4.86*
NO	15	81.0	7.80	104	8.22	96.4	6.42	97.2	6.09
	4000	92.9	3.29	113	9.67	100	2.03	107	2.23
Microdialysate									
VRC	8	88.0	2.10	99.5	5.25	93.1	6.80	93.4*	6.30*
	3000	104	1.21	107	10.6	107	2.38	91.9*	2.52*
NO	8	106	6.60	99.0	5.68	95.5	12.6	107	6.34
	3000	99.1	1.83	103	2.31	100	0.99	98.7	4.81

C_{Nom}, nominal concentration; CV, coefficient of variation; RV, recovery

[a] 3 cycles of freezing (>12 h at -80°C) and thawing (4-8°C); [b] >24 h at 4°C; [c] >12 h at 4-8°C; [d] >3 months at -80°C; *long-term stability of VRC was investigated at concentrations of 10 and 4000 ng/mL

3.1.3 Simultaneous quantification of voriconazole and its *N*-oxide metabolite in ultrafiltrate

Selectivity for VRC and NO in ultrafiltrate blank samples prepared from six individual donors was supported by a maximum detector response of 13.9% for VRC and 3.46% for NO compared to the mean response of LLOQ samples of the same run. The IS reached a maximum of 0.0222% interference and thus equally fulfilled the defined criteria. Spiked ultrafiltrate samples were reliably quantifiable using the plasma calibration function. VRC ultrafiltrate samples of a concentration of 15 ng/mL and 4000 ng/mL reached an accuracy of 96.7% and 103% (n=6 each), respectively. The precision of the determination was high, with a respective CV of 2.99% and 2.80% for the low and high QC level. For NO, accuracy was 99.2% for the low QC concentration

and 95.7% for the high, while the precision assessed as CV was 5.95% and 3.49%, respectively. Consequently, it was concluded that plasma and ultrafiltrate caused similar matrix effects and that plasma CAL and QC samples can be applied to ultrafiltrate samples. Thus, no additional CAL and QC solutions were needed for the quantification of unbound VRC and NO.

3.1.4 Quantification of voriconazole metabolites in *in vitro* matrices

For the quantification of NO and OH-VRC in all *in vitro* matrices, sample pre-treatment was adapted to allow a decrease in the LLOQ. The final 1:2 dilution was carried out by adding 20 µL of the supernatant after protein precipitation to 20 µL IS solution. By an increase of the injection volume to a minimum of 5 µL, the LLOQ for NO and OH-VRC could be lowered to 0.1 and 1 ng/mL, respectively. Due to pronounced fluctuations in sensitivity of the MS system, the injection volume was adjusted for the individual run, ranging between 5 and 18 µL. The aim was to keep the intensity of the detector response at a constant value between study days and hence maintain the LLOQ.

Matrix effect. Conformity of NO detector responses in the surrogate incubation (n=4) and HLM matrix (n=8) was high and resulted in a deviation of only 4.13%. Also, imprecision was comparable in the two matrices, being 7.09% in surrogate incubation and 6.61% CV in HLM matrix. The same observation was made for the surrogate incubation matrix (n=8) and the three rhCYP systems 2C19, 2C9 and 3A4 (n=12 each). For rhCYP2C19, rhCYP2C9 and rhCYP3A4 the deviation was 7.3%, 11.3% and 8.1%, respectively. In all cases, detector responses were higher in the surrogate incubation matrix. The imprecision, assessed as CV, was similar between the different matrices with 4.95% in surrogate incubation and 7.98% in rhCYP2C19 matrix, 8.85% in surrogate incubation and 10.4% in rhCYP2C9 matrix as well as 8.36% in surrogate incubation and 8.91% in rhCYP3A4 matrix.

Analytical runs. In total seven analytical runs were performed for the quantification of NO and all met the set criteria of the EMA guideline on bioanalytical method validation resulting in the acceptance of the runs [139]. Only four individual CAL samples were rejected, yielding a 93.0% accuracy. The maximum deviation was 155% of the nominal concentration, most likely originating in a mistake during spiking or sample pre-treatment, e.g. by setting an incorrect pipetting volume. All accepted CAL samples ranged between 86.4% and 115% accuracy. From a total number of 111 QC samples, seven failed the ±15% (±20% at the LLOQ) accuracy limits resulting in an overall accuracy of 93.7%. However, three individual QC samples not meeting the necessary limits were in retrospective assessment exposed as handling errors and therefore excluded from the overall evaluation. The LLOQ of 0.1 ng/mL showed a mean accuracy of 105% and a precision of 6.53% CV (n=7). At a concentration of 0.25 (n=21) and 0.5 ng/mL (n=14) mean accuracy amounted to 101% and 99.4% while imprecision was 12.1% and 7.14% CV,

respectively. The higher QC levels of 5, 100 and 400 ng/mL (n=22 each) reached mean accuracies of 100%, 96.0 % and 95.6% as well as precisions of 7.72%, 6.32% and 6.02% CV, respectively. Consequently, all EMA guideline requirements were accomplished and thus the performance of the adapted bioanalytical method demonstrated.

3.2 *In vitro* metabolism studies for voriconazole and its metabolites

Prior to the examination of VRC and its metabolites, a characterisation of marker reactions for the CYP isoenzymes 2C19, 2C9 and 3A4 was performed (chapter 3.2.1) to enable the generation of ISEF and the assessment of inhibitory potentials. Afterwards, a coherent framework of VRC metabolism was established by assessing the three compounds as substrates (chapter 3.2.2) as well as inhibitors (chapter 3.2.3) of the enzymes CYP2C19, CYP2C9 and CYP3A4 [179].

3.2.1 Assessment of CYP2C19, CYP2C9 and CYP3A4 activity with marker reactions

The activity of CYP2C19, CYP2C9 and CYP3A4 was assessed using marker reactions with high specificity for the respective enzyme as recommended by EMA and FDA guidelines on the investigation of drug interactions [149,150]. For CYP2C19, the 4-hydroxylation of S-mephenytoin, for CYP2C9, the 4-hydroxylation of diclofenac and for CYP3A4, the 1-hydroxylation of midazolam was monitored. All kinetic parameters were derived from the quantification of the formation of the respective metabolites in the enzymatic incubations.

3.2.1.1 Bioanalytical assay for the quantification of 4-hydroxymephenytoin, 4-hydroxydiclofenac and 1-hydroxymidazolam

A previously developed bioanalytical LC-MS/MS assay was applied to quantify the concentrations of OH-MEP, OH-DIC and OH-MDZ in incubations of HLM and rhCYP [151]. The performance of the assay was continuously controlled by the evaluation of CAL and QC samples of the respective runs. Overall, four analytical runs were performed for the quantification of OH-MEP and five each for OH-DIC and OH-MDZ.

From 32 CAL samples of OH-MEP, all were accurate, indicated by a deviation from their nominal value of less than ±15% (±20% at the LLOQ). The minimum and maximum accuracy achieved were 85.5% and 115%, respectively. In 98.0% of the cases, individual QC samples were correctly quantified, with only one sample of 51 being outside the ±15% accuracy limits. For individual QC levels of OH-MEP, the overall mean accuracy and precision of all runs were determined: accuracies ranged from 96.8% at a concentration of 1.5 ng/mL to 106% at a concentration of 300 ng/mL. Imprecision calculated as CV was on all QC levels ≤9.20%.

The 40 CAL samples of OH-DIC met the accuracy limits with a minimum of 88.3% and a maximum of 114% of their nominal concentration, respectively. The QC samples (n=60) were

93.3% accurate and ranged from 72.6% to 118% of their nominal value. Mean accuracy and precision of the individual QC concentration levels were demonstrated by a maximum deviation of -4.2% from the nominal value at a concentration of 75 ng/mL and a CV of ≤11.8%, respectively.

Overall, 100% of OH-MDZ CAL samples (n=41) were within ±15% of their nominal concentration, ranging from 85.4% to 110%. From the total 66 OH-MDZ QC samples, 87.9% were accurate according to the set requirements. One individual QC sample was excluded from the evaluation as an error during preparation was detected in retrospect. All other QC samples varied between 86.8% and 148% of their nominal concentration. The mean accuracy for the individual QC levels was high, with a maximum deviation of +6% of the nominal concentration at the 40 ng/mL concentration level. The imprecision was highest at the lowest concentration of 0.3 ng/mL with a CV of 14.8%.

3.2.1.2 Michaelis-Menten kinetics of the 4-hydroxylation of S-mephenytoin, 4-hydroxylation of diclofenac and 1-hydroxylation of midazolam

The Michaelis-Menten kinetics of the marker reactions, i.e. the respective K_M, V_{max} and CL_{int}, were assessed in HLM and the respective rhCYP under laboratory-individual conditions as a prerequisite for further investigations with VRC and its metabolites.

Human liver microsomes. The 4-hydroxylation of S-mephenytoin by CYP2C19 was characterised by a slow metabolic turnover. Therefore, after 15 and 25 min a sample was taken from each incubation (n=3) to ensure quantifiable concentrations of OH-MEP. The K_M of the reaction resulted in 53.0 µM (95% CI: 45.6 – 60.4 µM) while V_{max} reached 44.7 pmol/(min·mg) (95% CI: 42.3 – 47.2 pmol/(min·mg)) and was based on six observations of the reaction velocity per substrate concentration. Thus, the CL_{int} amounted to 0.845 µL/(min·mg). Overall, the chosen substrate concentrations spread from approximately $1/10^{th}$ to 10-fold the K_M and represented all phases of the Michaelis-Menten kinetics well (Figure 3.4, Table 7.4).

The formation of OH-DIC by CYP2C9 was distinguished by a rapid metabolism. Reaction times of 5 and 10 min were sufficient to reach quantifiable OH-DIC concentrations. The underlying Michaelis-Menten kinetics were described by a K_M of 4.15 µM (95% CI: 3.61 – 4.70 µM) and V_{max} of 1693 pmol/(min·mg) (95% CI: 1639 – 1746 pmol/(min·mg)). The CL_{int} was hence determined as 408 µL/(min·mg). Diclofenac concentrations ranged from approximately half the K_M to 40-fold K_M, representing disproportionally the higher substrate concentrations (Figure 3.4, Table 7.4).

Lastly, the 1-hydroxylation of midazolam by CYP3A4 was described by a moderately pronounced metabolic turnover. Three incubations were carried out per substrate concentration, taking samples after 7 and 12 min reaction time. This yielded in Michaelis-Menten kinetics

described by a K_M of 4.45 µM (95% CI: 3.56 – 5.35 µM) and a V_{max} of 559 pmol/(min·mg) (95% CI: 523 – 595 pmol/(min·mg)). CL_{int} consequently resulted in 126 µL/(min·mg). The applied midazolam concentrations ranged from approximately 1/15th to 7-fold K_M, capturing all phases of the kinetic profile well (Figure 3.4, Table 7.4).

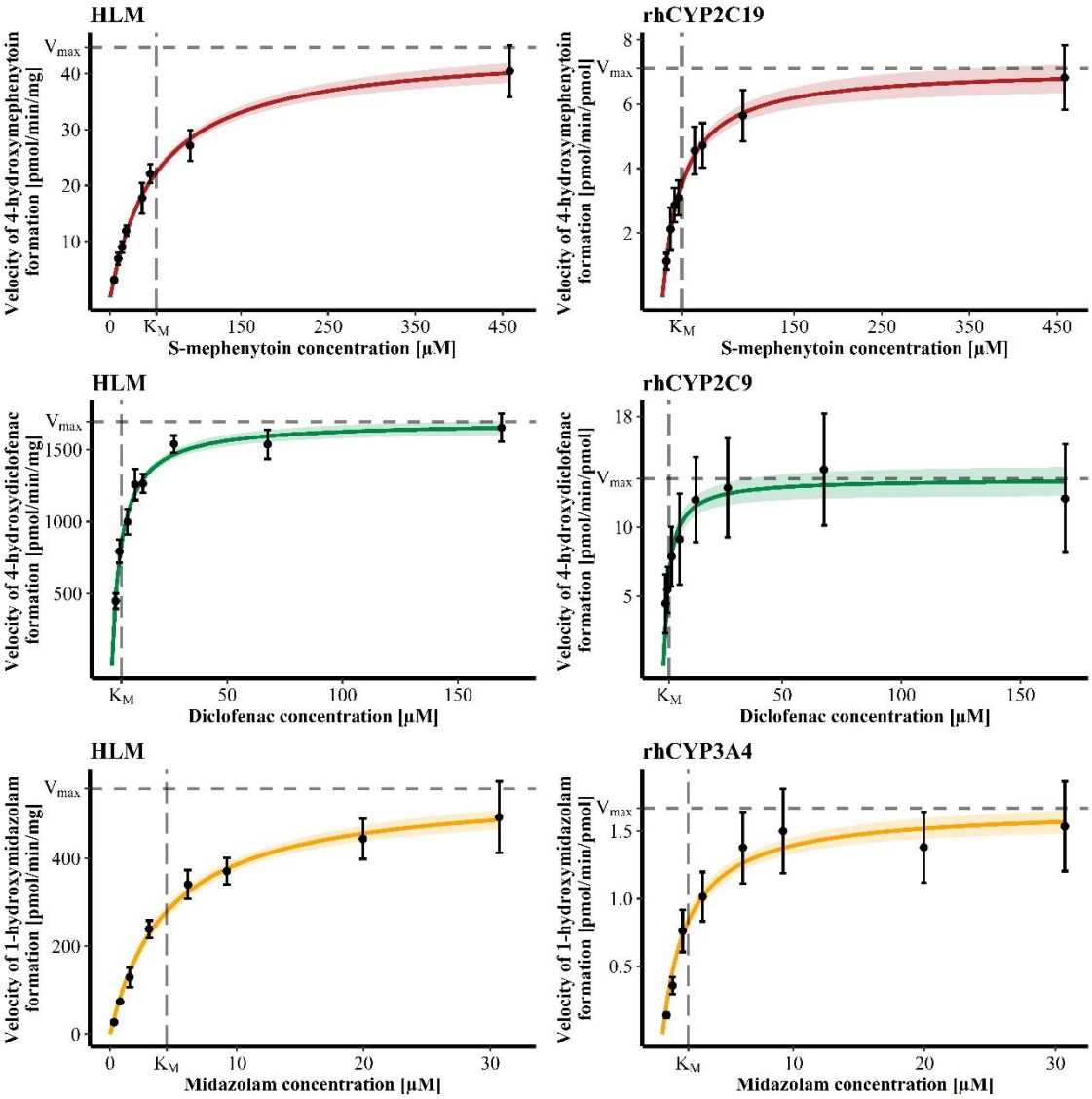

Figure 3.4: Michaelis-Menten kinetics of the 4-hydroxylation of S-mephenytoin (upper panel), 4-hydroxylation of diclofenac (middle panel) and 1-hydroxylation of midazolam (lower panel) in human liver microsomes (HLM, left panel, n=5-6 each) and the recombinant human cytochrome P450 isoenzymes (rhCYP) 2C19 (n=6), 2C9 (n=12) and 3A4 (right panel, n=12).
Data points: mean reaction velocity; error bars: standard deviation of reaction velocity; solid line: estimated enzyme kinetics; shaded area: 95% confidence interval of the estimation; dashed lines: estimated Michaelis-Menten constant (K_M) and maximum reaction velocity (V_{max}).

Recombinant human CYP. Michaelis-Menten kinetics for the 4-hydroxylation of S-mephenytoin, 4-hydroxylation of diclofenac and the 1-hydroxylation of midazolam were similarly determined in recombinant enzyme systems.

The formation of OH-MEP in rhCYP2C19 was assessed by triplicate determinations per substrate concentration, taking a sample each after 15 and 25 min reaction time (n=6). As a result, kinetics were determined with a K_M of 22.1 µM (95% CI: 17.2 – 27.0 µM) and a V_{max} of 7.10 pmol/(min·pmol) (95% CI: 6.59 – 7.62 pmol/(min·pmol)). From this, a CL_{int} of 0.321 µL/(min·pmol) was derived (Figure 3.4, Table 7.4).

The 4-hydroxylation of diclofenac was determined on two different study days performing three replicates each and sampling each incubation twice. Thus, the kinetic profile was based on twelve individual reaction velocity determinations per substrate concentration. The resulting K_M, V_{max} and CL_{int} were 2.29 µM (95% CI: 1.40 – 3.17 µM), 13.5 pmol/(min·pmol) (95% CI: 12.4 – 14.6 pmol/(min·pmol)) and 5.89 µL/(min·pmol), respectively (Figure 3.4, Table 7.4).

The 1-hydroxylation of midazolam was investigated on two separate study days, using triplicate incubations and sampling each after 7 and 12 min reaction time. This resulted in a twelve-fold determination of the reaction velocity for each substrate concentration. The overall kinetics for the reaction were characterised by a K_M of 1.96 µM (95% CI: 1.49 – 2.44 µM) and a V_{max} of 1.67 pmol/(min·pmol) (95% CI: 1.56 – 1.78 pmol/(min·pmol)). CL_{int} was hence determined as 0.850 µL/(min·pmol) (Figure 3.4, Table 7.4).

3.2.2 Voriconazole and its metabolites as substrates

The interaction of VRC with CYP2C19, CYP2C9 and CYP3A4 was investigated in a stepwise approach. First, as a prerequisite for kinetic investigations, optimal experimental conditions were determined by evaluation of the linearity of NO formation and the reaction's enzyme dependence (chapter 3.2.2.1). Second, the reaction kinetics of VRC *N*-oxidation in different enzyme systems were analysed (chapter 3.2.2.2). Third, the contribution of the three CYP isoenzymes to NO formation was assessed by different established methods (chapter 3.2.2.3). Fourth, IVIVE was performed to gauge *in vivo* relevance of VRC *N*-oxidation (chapter 3.2.2.4). Last, secondary metabolic pathways of VRC were explored by investigating the VRC metabolites, NO and OH-VRC, as substrates (chapter 3.2.2.5).

3.2.2.1 Reaction linearity, voriconazole stability and substrate depletion

To assess the reaction kinetics of VRC metabolite formation, the determination of the reaction velocity at the respective substrate concentration was essential. The reaction velocity was determined as metabolite concentration per reaction time and protein (for HLM and HIM) or enzyme (for rhCYP) concentration. Hence, metabolite formation had to be linear until the sampling time point and applied protein/enzyme concentration. Additionally, the transformation to NO and OH-VRC had to be solely enzyme-dependent without spontaneous NO or OH-VRC

production and the depletion of VRC kept to a minimum (<10%) to avoid a distortion of reaction kinetics.

In all the following described investigations, also the formation of OH-VRC was monitored. However, OH-VRC was not detected. Consequently, also no kinetic evaluations were performable, and VRC *N*-oxidation was focussed on.

Human liver microsomes. The formation of NO in HLM was linear for up to 120 min for all four investigated protein concentrations as well as for all four substrate concentrations. R^2 yielded values of ≥0.9781 (maximum 0.9952) in all cases, confirming the graphically suggested linearity of NO formation across reaction time. Moreover, linearity of NO formation across protein concentration was demonstrated for all seven reaction times by R^2 values of ≥0.9713 (maximum 0.9998). The results of the linearity investigations are shown in Figure 3.5 and Figure 3.6 for VRC concentrations of 1 and 100 µM. In none of the control incubations without NADPH re-generating system, NO was formed and VRC concentrations did not decrease across time, indicating the specificity of the reaction and VRC stability in HLM incubations.

In most incubations, VRC did not show depletion indicated by a recovery of 90%-110% compared to a control incubated without NADPH re-generating system. The only exceptions were incubations with the highest protein concentration (0.5 mg/mL) combined with the lowest VRC substrate concentration (1 µM) after 60 and 120 min reaction time. After 60 min, -13.0% and -18.1% VRC were observed in the two replicates compared to the control and after 120 min -23.8% and -12.5%, respectively. A mean loss of 18.1% after 120 min equalled 139 pmol/mL VRC. At the same time, 108 pmol/mL NO were formed, indicating that a high percentage of 77.7% of the depleted VRC was transformed to NO.

Recombinant human CYP. For rhCYP2C19, all performed incubations led to quantifiable NO concentrations, except for the second replicate at a rhCYP2C19 enzyme concentration of 10 pmol/mL where a handling error during the experiment led to unusable results. Firstly, the linearity of NO formation in rhCYP2C19 was acceptable until 60 min reaction time with R^2 ≥0.6861 (maximum 0.9905) (Figure 3.5). The lowest R^2 value of NO formation across time was found for the lowest enzyme concentration (1 pmol/mL) in combination with the lowest substrate concentration (1 µM). However, the second lowest R^2 value was 0.8469, indicating an informative relation. Furthermore, the graphical evaluation displayed a decrease in NO formation after 60 min. Thus, this time point was excluded and linearity re-assessed without it. Consequently, R^2 increased to ≥0.8617 (maximum 0.9920). Secondly, the linearity of NO formation across rhCYP2C19 enzyme concentrations was demonstrated with R^2 ≥0.8991 (maximum 0.9944) (Figure 3.6). Control incubations without NADPH re-generating system did not form NO, demonstrating the rhCYP2C19 dependence of the formation. Relevant depletion

was observed in incubations with 20 pmol/mL rhCYP2C19 and a VRC concentration of 1 µM. After 60 min, the VRC concentration compared to the control was decreased by -54.3% and -57.1% in the two replicates, respectively. The loss in VRC (458 and 430 pmol/mL) was, within the precision limits of the bioanalytical method, equal to the amount of NO formed (457 and 461 pmol/mL), suggesting VRC *N*-oxidation as the sole metabolic pathway of CYP2C19.

In rhCYP2C9, NO formation was very low, yielding non-evaluable results for enzyme concentrations ≤40 pmol/mL as those incubations only narrowly exceeded the LLOQ for NO after 15 min reaction time with a substrate concentration of 100 µM and only after 60 min with 10 µM VRC. Consequently, the investigation was extended to rhCYP2C9 concentrations of 60 and 80 pmol/mL using VRC concentrations of 10 and 100 µM. Nevertheless, incubations with 60 pmol/mL rhCYP2C9 and 10 µM VRC still revealed NO concentrations below the LLOQ at earlier time points. However, the evaluation of incubations with NO concentrations above the LLOQ resulted in acceptable linearity across reaction time until 60 min with R^2 of ≥0.7459 (maximum 0.9719) (Figure 3.5). A quantitative assessment of linearity across enzyme concentration was not feasible with two enzyme concentrations (Figure 3.6). In all control incubations without NADPH re-generating system, no NO was detectable. Additionally, there was no depletion of VRC in any incubation observed across time.

Finally, also in rhCYP3A4, VRC turnover was unexpectedly low. Incubations of 5 pmol/mL rhCYP3A4 did not produce high enough NO concentrations for linearity investigations with regards to reaction time. Here, only in incubations with 100 µM VRC, NO was detectable after 15 min reaction time. Also at 20 pmol/mL rhCYP3A4 and a substrate concentration of 1 µM, the NO concentration was below the LLOQ after 5 min reaction time. Additionally, due to an error during the execution of the experiment, the second replicate of the enzyme concentration of 80 pmol/mL at all VRC concentrations was unavailable. However, linearity of VRC *N*-oxidation across time in rhCYP3A4 was demonstrated until 60 min reaction time by R^2 of ≥0.8566 (maximum 0.9887) (Figure 3.5). The graphical evaluation suggested a flattening of NO formation at 60 min reaction time. Hence, linearity across time was re-assessed until 30 min, revealing higher linearity indicated by an R^2 of ≥0.8812 (maximum 0.9943). For the assessment of linearity of NO formation across enzyme concentration, only three rhCYP3A4 concentrations were available. Evaluations resulted in R^2 values of ≥0.7783 (maximum 0.9994), indicating a sufficient linearity in particular as the lowest relation was found at the already unfavourable reaction time of 60 min. In none of the control incubations without NADPH re-generating system NO formation was observable, suggesting the specificity of the reaction. Lastly, no depletion of the substrate VRC was detected, being in line with the observed low turnover and stability of VRC in rhCYP3A4 incubations.

Human intestine microsomes. The linearity of VRC *N*-oxidation across reaction time in HIM was demonstrated until 60 min by R^2 of ≥0.9124 (maximum 0.9537). However, the graphical assessment suggested a decreased formation of NO at 60 min (Figure 3.5). The linearity evaluation without this time point resulted in higher R^2 values of ≥0.9204 (maximum 0.9887). Linearity across protein concentration was not determinable as CYP concentrations in HIM were low, not allowing for a further decrease in concentration and simultaneously maintaining NO formation in the quantifiable range of the bioanalytical assay. Control incubations without NADPH re-generating system showed no NO formation, and VRC concentrations were stable until the last measurement at 60 min. Overall, VRC turnover was low in HIM, matching with the absence of VRC depletion in all incubations across time.

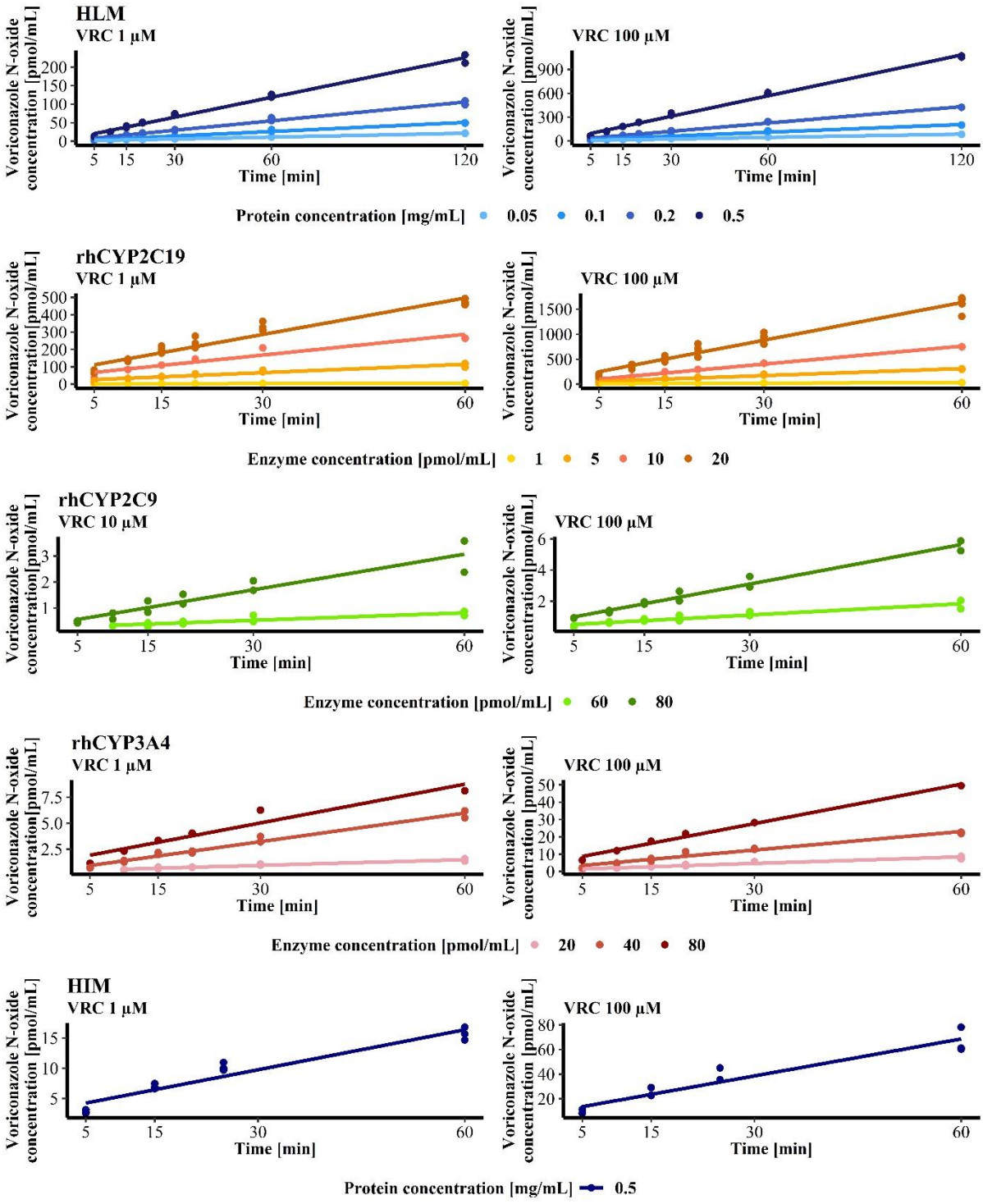

Figure 3.5: Voriconazole (VRC) *N*-oxide formation across time in human liver microsomes (HLM, n=2, top row), recombinant human cytochrome P450 (rhCYP) isoenzymes 2C19 (n=1-4, second row), 2C9 (n=2, middle row) and 3A4 (n=1-2, second last row) and human intestine microsomes (HIM, n=3, bottom row) at a low (1 or 10 µM, left) and high (100 µM, right) VRC concentration.

Data points: individual determinations of VRC *N*-oxide concentrations; solid line: linear model describing the VRC *N*-oxide concentration as function of reaction time.

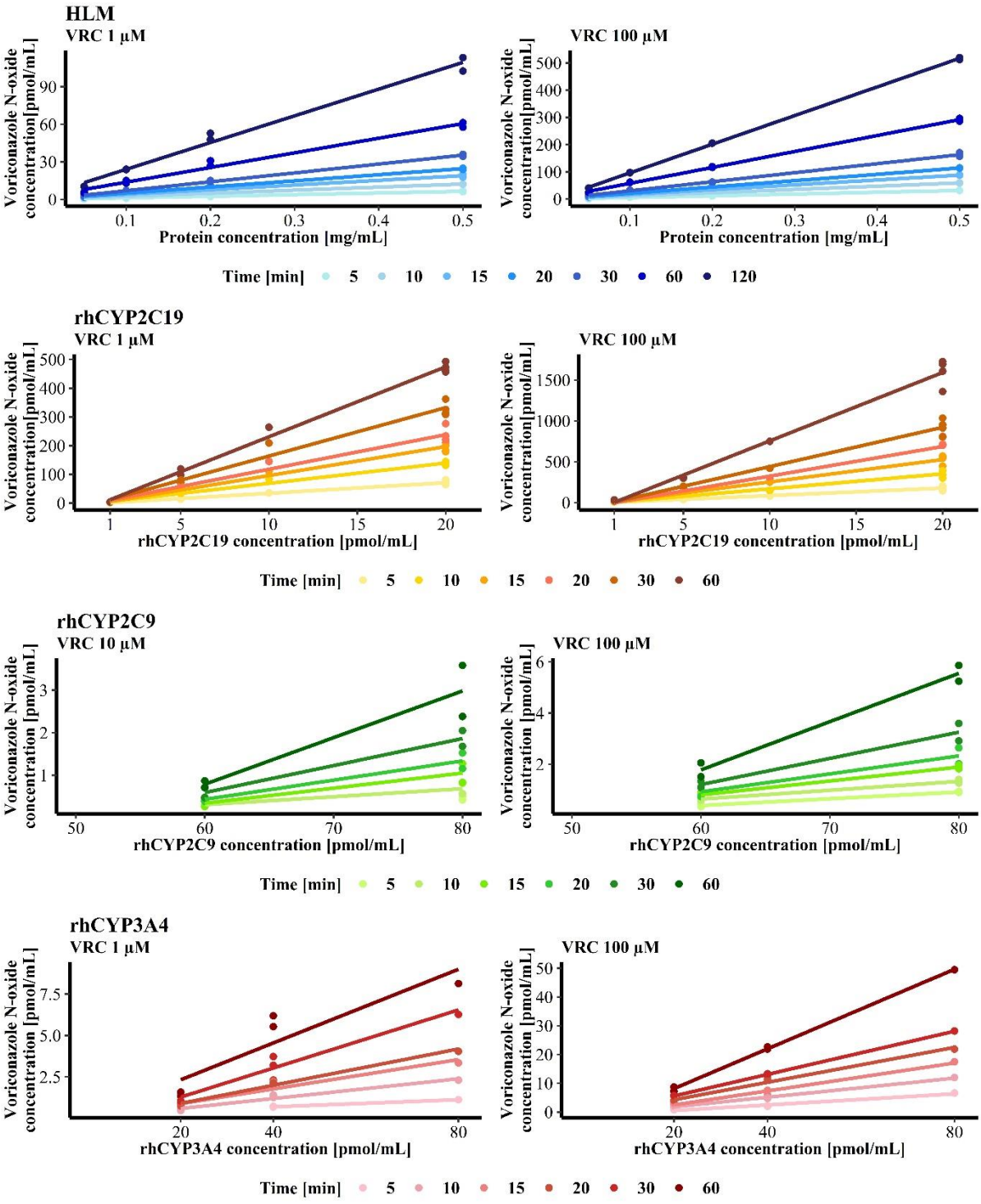

Figure 3.6: Voriconazole (VRC) *N*-oxide formation across protein concentration in human liver microsomes (HLM, n=2, top row), and enzyme concentration in recombinant human cytochrome P450 (rhCYP) isoenzymes 2C19 (n=2-4, second row), 2C9 (n=2, second last row) and 3A4 (n=1-2, bottom row) at a low (1 or 10 µM) and high (100 µM) VRC concentration.

Data points: individual determinations of VRC *N*-oxide concentrations; solid line: linear model describing the VRC *N*-oxide concentration in function of protein/enzyme concentration.

3.2.2.2 Michaelis-Menten kinetics of the *N*-oxidation of voriconazole

VRC *N*-oxidation was characterised by Michaelis-Menten kinetics in all investigated enzymatic systems (HLM, HIM and rhCYP, Figure 3.7). As HLM and HIM were multi-enzyme systems, i.e. more than one CYP isoenzyme might have been involved in the transformation of a substrate, only apparent kinetics could be determined.

The estimated kinetic parameters, i.e. K_M, V_{max} and CL_{int}, are summarised in Table 3.6. Overall, the K_M in HLM and HIM was in a similar range, while V_{max} was 6.78-fold higher in HLM. Furthermore, the K_M in rhCYP2C19 and rhCYP3A4 was in a comparable range but was approximately 3-fold higher in rhCYP2C9. V_{max} was highest in rhCYP2C19 and 233- and 184-fold lower in rhCYP2C9 and rhCYP3A4, respectively.

Table 3.6: Estimated Michaelis-Menten kinetic parameters, i.e. the Michaelis-Menten constant (K_M), maximum reaction velocity (V_{max}) and the resulting intrinsic clearance (CL_{int}), including their 95% confidence interval (CI), of the *N*-oxidation of voriconazole determined in human liver microsomes (HLM), human intestine microsomes (HIM) and recombinant human cytochrome P450 enzymes 2C19, 2C9 and 3A4 (rhCYP).

Enzymatic system	**K_M (95% CI) [µM]**	**$V_{max,HLM/HIM}$ (95% CI) [pmol/(min·mg)] or $V_{max,rhCYP}$ (95% CI) [pmol/(min·pmol)]**	**$CL_{int,HLM/HIM}$ (95% CI) [µL/(min·mg)] or $CL_{int,rhCYP}$ (95% CI) [µL/(min·pmol)]**
HLM	2.98 (2.63 – 3.33)	26.1 (25.4 – 26.8)	8.76 (7.63 – 10.2)
HIM	2.53 (2.15 – 2.92)	3.85 (3.70 – 4.00)	1.52 (1.27 – 1.86)
rhCYP2C19	1.31 (0.862 – 1.75)	1.64 (1.50 – 1.77)	1.25 (0.857 – 2.05)
rhCYP2C9	4.06 (3.32 – 4.81)	0.00705 (0.00665 – 0.00744)	0.00173 (0.00138 – 0.00224)
rhCYP3A4	1.20 (0.830 – 1.58)	0.00893 (0.00827 – 0.00958)	0.00742 (0.00523 – 0.0115)

Consequently, in HLM a CL_{int} of VRC *N*-oxidation of 8.76 µL/(min·mg) (7.63 – 10.2 µL/(min·mg)) was determined. HIM also relevantly metabolised VRC to NO. The reaction kinetics were characterised by a CL_{int} of 1.52 µL/(min·mg) (1.27 – 1.86 µL/(min·mg)) and were thus 5.76-fold lower than CL_{int} observed in HLM. In recombinant enzymes, rhCYP2C19 showed the highest VRC turnover indicated by a CL_{int} of 1.25 µL/(min·pmol) (0.857 – 2.05 µL/(min·pmol)). Kinetics for rhCYP2C9 were determined with a CL_{int} of 0.00173 µL/(min·pmol) (0.00138 – 0.00224 µL/(min·pmol)) which was 723-fold lower than in

rhCYP2C19. Lastly, in rhCYP3A4, Michaelis-Menten kinetics of VRC *N*-oxidation were described by a CL_{int} of 0.00742 µL/(min·pmol) (0.00523 – 0.0115 µL/(min·pmol)) which was 168-fold lower and 4.29-fold higher than in rhCYP2C19 and rhCYP2C9, respectively (Table 3.6).

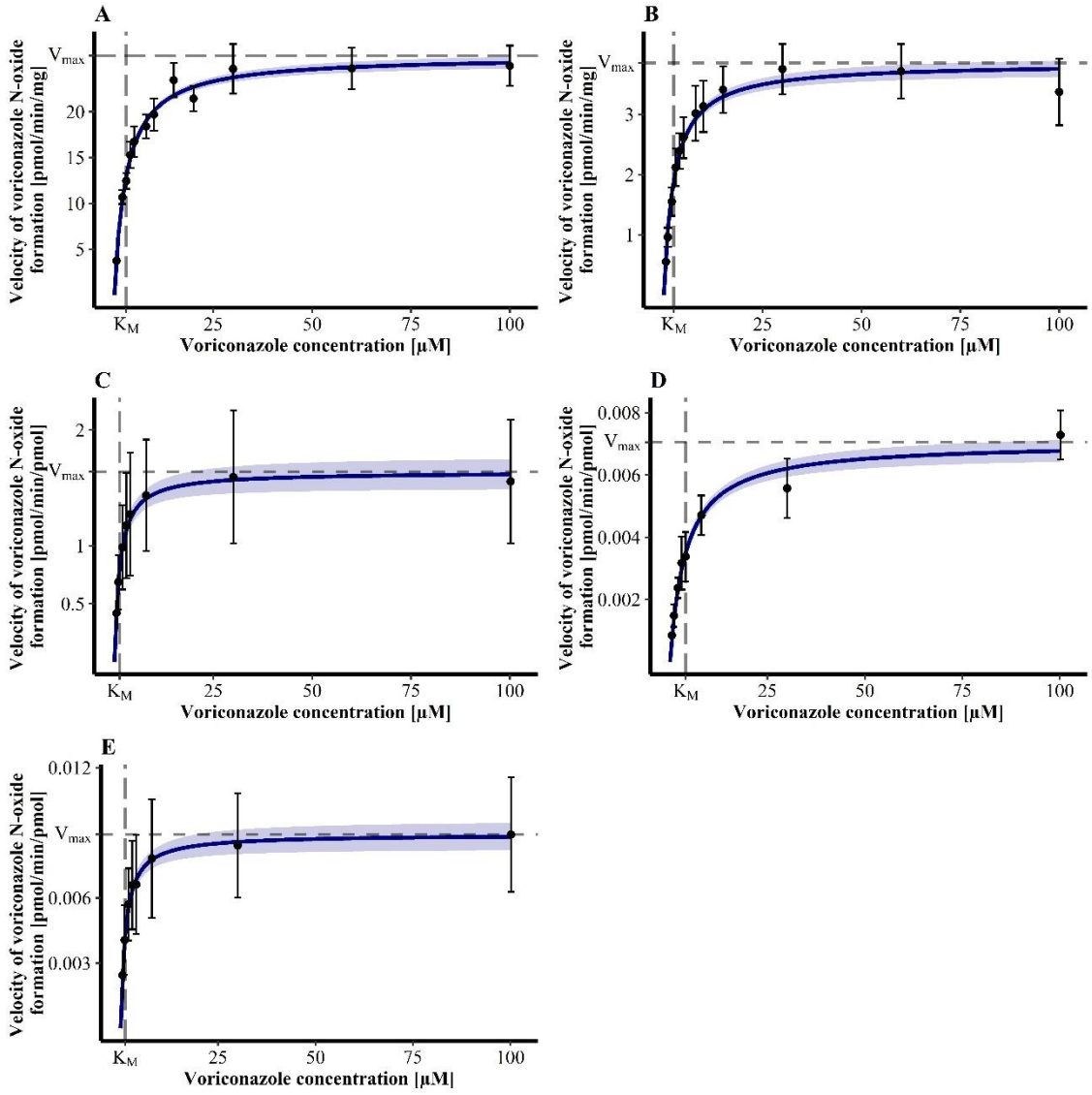

Figure 3.7: Michaelis-Menten kinetics of the *N*-oxidation of voriconazole in human liver microsomes (A, n=8-9), human intestine microsomes (B, n=9) and recombinant human cytochrome P450 isoenzymes 2C19 (C, n=18), 2C9 (D, n=10) and 3A4 (E, n=18).
Data points: mean reaction velocity; error bars: standard deviation of reaction velocity; solid line: estimated enzyme kinetics; shaded area: 95% confidence interval of the estimation; dashed lines: estimated Michaelis-Menten constant (K_M) and maximum reaction velocity (V_{max}).

Evaluations applying the Lineweaver-Burk transformation showed linear relations between the reciprocal of the reaction velocities and reciprocals of the substrate concentration (Figure 7.2). The absence of a noticeable disruption in the slope of the linear function contrasted with the presumption that more than one metabolic enzyme was involved in the formation of NO in HLM

and HIM. However, only isoenzymes with large differences in their K_M regarding the substrate could be detected by this approach.

3.2.2.3 Contribution of individual CYP isoenzymes to voriconazole *N*-oxidation

To assess the individual contribution of the CYP isoenzymes 2C19, 2C9 and 3A4 to the *N*-oxidation of VRC, two different experimental approaches were applied to detect potential biases in the determination.

Specific enzyme inhibition in human liver microsomes. First, the CYP isoenzymes 2C19, 2C9 and 3A4 were inhibited in HLM by loratadine, sulfaphenazole and ketoconazole, respectively. Inhibition on the reaction velocities of VRC *N*-oxidation was evaluated at VRC concentrations $\leq K_M$ (2.98 µM), in the linear phase of the Michaelis-Menten kinetics. CYP2C19 had the largest share in VRC *N*-oxidation with 61.8% and was followed by CYP3A4 with 47.6% and CYP2C9 with 36.2% (Table 3.7). VRC concentrations $>K_M$ were not included in the assessment of enzyme contributions as loratadine, sulfaphenazole and ketoconazole are competitive inhibitors and at increasing VRC concentrations a displacement of the inhibitors from the enzyme by the substrate was observable. This displacement was accompanied by a reduction in the contribution of the respective isoenzyme. Thus, if assessments were made at a VRC concentration of 100 µM a contribution of 56.5%, 24.4% and 21.4% for CYP2C19, CYP2C9 and CYP3A4 would have been determined.

Evidently, an inhibition of >100% in sum was implausible and indicated that the inhibitors were not sufficiently specific for the respective enzymes. Thus, they were tested on marker reactions catalysed by mainly one enzyme (chapter 3.2.1). Loratadine inhibited the formation of OH-MEP by CYP2C19 reliably with less than 5% of reaction velocity remaining compared to an uninhibited control. Additionally, it did not affect the 1-hydroxylation of midazolam by CYP3A4 with reaction velocities remaining unchanged in its presence. However, there was a cross-reaction with the 4-hydroxylation of diclofenac by CYP2C9 as its reaction velocity was decreased to 42% when loratadine was present. The observations made for sulfaphenazole, a CYP2C9 inhibitor, were comparable. Sulfaphenazole inhibited CYP2C9 almost completely as reaction velocities decreased to 6.3% compared to an uninhibited control. The CYP3A4 catalysed reaction of midazolam 1-hydroxylation was again not affected with a reaction velocity of 97% compared to the control incubation without sulfaphenazole. Yet, sulfaphenazole also inhibited CYP2C19 as reaction velocities were decreased to 77% compared to the uninhibited control. Lastly, ketoconazole had minor effects on CYP2C19 and CYP2C9 with 92% and 85% remaining metabolism compared to the uninhibited control but relevantly inhibited the 1-hydroxylation of midazolam by CYP3A4 as only a fraction 37% reaction velocity was observed in comparison to the non-inhibition control (Table 7.5).

Table 3.7: Reaction velocities of voriconazole *N*-oxidation in the absence and presence of cytochrome P450 (CYP) enzyme inhibitors and their proportion compared to the uninhibited control incubation and the resulting percentage of inhibition (n=6).

Voriconazole concentration [µM]	Mean (SD) reaction velocity [pmol/(min·mg)]	% of uninhibited control	Mean (SD) % of uninhibited control	% inhibition
Control incubation without inhibitor				
0.5	2.92 (0.288)	100		
1	5.34 (0.574)	100	100	0
2	7.79 (1.05)	100	(0)	
3	9.38 (1.11)	100		
Incubation with CYP2C19 inhibitor loratadine				
0.5	1.23 (0.118)	42.0		
1	2.01 (0.267)	37.7	38.2	61.8
2	2.86 (0.351)	36.7	(2.64)	
3	3.40 (0.311)	36.2		
Incubation with CYP2C9 inhibitor sulfaphenazole				
0.5	1.89 (0.124)	64.8		
1	3.24 (0.431)	60.7	63.8	36.2
2	4.88 (0.391)	62.6	(2.69)	
3	6.48 (0.839)	66.9		
Incubation with CYP3A4 inhibitor ketoconazole				
0.5	1.45 (0.140)	49.8		
1	2.58 (0.248)	48.4	52.4	47.6
2	4.17 (0.350)	53.6	(4.26)	
3	5.43 (0.393)	57.9		
Incubation with a mixture of the CYP2C19, 2C9 and 3A4 inhibitors loratadine, sulfaphenazole and ketoconazole				
0.5	0.249 (0.0151)	8.52		
1	0.525 (0.0442)	9.83	10.8	89.2
2	0.910 (0.111)	11.7	(2.02)	
3	1.23 (0.149)	13.1		

SD, standard deviation

Overall, the observed effect of the three combined inhibitors on VRC *N*-oxidation might be the most conclusive as specificity was of less importance. Here, 89.2% of the metabolism of VRC was inhibited indicating that the most relevant enzymes were detected – in particular considering that CYP3A4 inhibition was insufficient, potentially due to a too low ketoconazole concentration.

Extrapolation from recombinant human CYP enzymes. As all the investigated recombinant enzyme systems (rhCYP2C19, rhCYP2C9 and rhCYP3A4) revealed a distinct NO formation, an extrapolation of CL_{int} in rhCYP to HLM was performed.

First, only the respective CYP abundance in HLM (Table 7.2) was considered and the CL_{int} of VRC *N*-oxidation observed in rhCYP2C19 (1.25 µL/(min·pmol)), rhCYP2C9 (0.00173 µL/(min·pmol)) and rhCYP3A4 (0.00742 µL/(min·pmol)) was transformed. This resulted in $CL_{int,CYP2C19,HLM}$ of 13.8 µL/(min·mg), $CL_{int,CYP2C9,HLM}$ of 0.106 µL/(min·mg) and $CL_{int,CYP3A4,HLM}$ of 0.690 µL/(min·mg). Compared to the total CL_{int} of 8.76 µL/(min·mg) determined in HLM, this was a share of 157% for CYP2C19, 1.21% for CYP2C9 and 7.87% for CYP3A4. The sum of the individual CL_{int} of the isoenzymes resulted in 14.6 µL/(min·mg) and thus yielded in isoenzyme contributions of 94.5% for CYP2C19, 0.726% for CYP2C9 and 4.73% for CYP3A4.

Second, ISEF were determined to account for activity differences in the two metabolic systems, rhCYP and HLM. Michaelis-Menten kinetics of the marker reactions for CYP2C19, CYP2C9 and CYP3A4 were evaluated under laboratory-individual conditions in HLM and rhCYP (chapter 3.2.1.2). When V_{max} was used for ISEF determination, $ISEF_{Vmax}$ values resulted in 0.573, 2.06 and 3.60 for CYP2C19, CYP2C9 and CYP3A4, respectively. Consequently, extrapolated $CL_{int,CYPi,HLM}$ yielded 7.89, 0.218 and 2.48 µL/(min·mg) and respective contributions of 90.0%, 2.49% and 28.4% for CYP2C19, CYP2C9 and CYP3A4 in VRC *N*-oxidation when compared to the total CL_{int} observed in HLM. The sum of the individual clearances was in this approach 10.6 µL/(min·mg). Consequently, when the individual $CL_{int,CYPi,HLM,ISEF}$ were related to their sum, isoenzyme contributions resulted in 74.4% for CYP2C19, 2.06% for CYP2C9 and 23.4% for CYP3A4.

Third, ISEF was based on CL_{int} of the marker reactions and values of $ISEF_{CLint}$ of 0.239, 1.13 and 1.59 for CYP2C19, CYP2C9 and CYP3A4 were obtained. Hence, extrapolated $CL_{int,CYPi,HLM}$ for VRC *N*-oxidation yielded 3.30, 0.120 and 1.10 µL/(min·mg) for CYP2C19, CYP2C9 and CYP3A4, respectively. Based on this, enzyme contributions of CYP2C19, CYP2C9 and CYP3A4 were determined as 37.6%, 1.37% and 12.5% when compared to the determined $CL_{int,HLM}$ of 8.76 µL/(min·mg) or 73.0%, 2.65% and 24.3% when compared to the sum of $CL_{int,CYPi,HLM}$ of 4.52 µL/(min·mg).

Finally, a mean contribution was assessed, amalgamating the results from the inhibition experiment in HLM and the two ISEF approaches when $CL_{int,CYPi,HLM}$ was related to the measured CL_{int} in HLM (not the sum). This resulted in a mean contribution in the *N*-oxidation of VRC of 63.1% for CYP2C19, 13.2% for CYP2C9, 29.5% for CYP3A4 and a sum of 106% for the three isoenzymes, respectively.

3.2.2.4 *In vitro in vivo* extrapolation

IVIVE from VRC *N*-oxidation in HLM resulted in a $CL_{int,hepatic,invivo}$ of 540 mL/min (32.4 L/h) and applying the well-stirred liver model in a $CL_{hepatic}$ of 227 mL/min (13.6 L/h). When individual CL_{int} of VRC *N*-oxidation in rhCYP were summed up, $CL_{int,hepatic,invivo}$ of 652 and 278 mL/min (39.1 and 16.7 L/h) were obtained if $ISEF_{Vmax}$ or $ISEF_{CLint}$ were applied, respectively. Consequently, $CL_{hepatic}$ of 266 and 127 mL/min (16.0 and 7.62 L/h) were determined using $ISEF_{Vmax}$ or $ISEF_{CLint}$, respectively.

3.2.2.5 Metabolic stability of voriconazole *N*-oxide and hydroxyvoriconazole

NO and OH-VRC showed no depletion over time, when incubated directly with HLM. After 60 min at the low NO concentration, 110% and 105% NO compared to a control incubation without HLM were present in the two replicates. At the high NO concentration 96.9% and 109% NO compared to the control were determined. The same was observed for OH-VRC which yielded a recovery of 92.5% and 108% at the low as well as of 94.7% at the high OH-VRC concentration after 60 min. Additionally, no trend, i.e. decreasing concentrations over time, was observable, neither for the HLM containing incubation nor for the control (Figure 3.8).

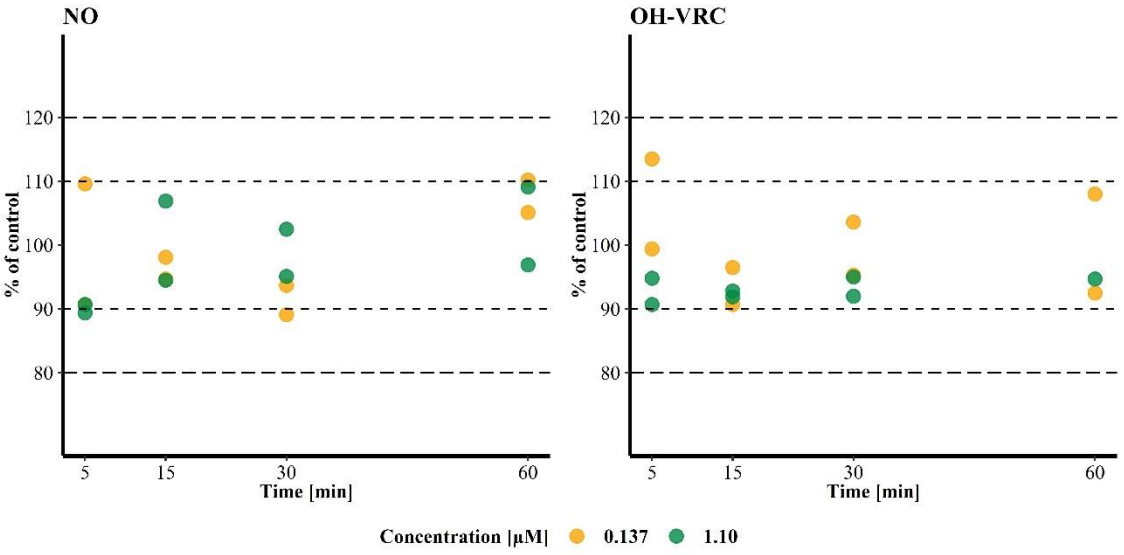

Figure 3.8: Stability of voriconazole *N*-oxide (NO) and hydroxyvoriconazole (OH-VRC) in human liver microsomes across time at two concentrations (n=1-2 each), presented as percentage of a control incubation (n=1). Dashed lines: ±10% and ±20% deviation from the control.

3.2.3 Voriconazole and its metabolites as enzyme inhibitors

In the following sections, the results of the investigations of the potential inhibitory effects of VRC, NO and OH-VRC on the CYP isoenzymes 2C19, 2C9 and 3A4 are presented. This includes the results of the determination of IC_{50} (chapter 3.2.3.1), the assessment of the occurrence of time-dependent inhibition (chapter 3.2.3.2) as well as the determination of the type of reversible inhibition and the corresponding K_i (chapter 3.2.3.3).

3.2.3.1 Inhibitory potential of voriconazole, voriconazole *N*-oxide and hydroxyvoriconazole

Aiming at a first assessment of the inhibitory potential of VRC, NO and OH-VRC, a determination of the IC_{50} of the three compounds on the enzymes also involved in the metabolism of VRC was performed. Therefore, reaction velocities of the marker reactions for CYP2C19, CYP2C9 and CYP3A4 (chapter 3.2.1) at substrate concentrations close to their K_M in the presence of different concentrations of VRC, NO and OH-VRC were evaluated.

Inhibitory effect on CYP2C19. VRC had a large effect on the 4-hydroxylation of S-mephenytoin by CYP2C19. Already a concentration of 0.1 µM caused a mean decrease in the reaction velocity of 11.7% compared to the uninhibited control. At a concentration of 1, 5 and 10 µM VRC, the reaction velocity dropped by 23.9%, 53.3% and 68.2% compared to the uninhibited control, respectively. The highest inhibition was observed at a VRC concentration of 100 µM with only 5.27% mean activity remaining compared to the uninhibited control (Figure 3.9). The precision of the assessment was high with a maximum CV of 16.3%, determined by duplicate incubation replicates, that were sampled twice each (n=4). Based on those data, via equation 2.17 an IC_{50} of 3.72 µM (95% CI: 2.85-4.78 µM) was determined for VRC.

Also NO inhibited CYP2C19 indicated by the reduction in reaction velocity of S-mephenytoin 4-hydroxylation. However, NO was a less potent inhibitor than VRC. At a concentration of 0.0958 µM the mean reaction velocity was decreased by 9.7% but a further increase in NO concentration did not entail a steep decrease in enzyme activity as observed for VRC. At concentrations of 0.958, 3.83 and 9.58 µM the mean reaction velocities of the 4-hydroxylation of S-mephenytoin remained at a high level with 89.3%, 81.2% and 77.9% compared to the uninhibited control. Even the highest concentration of NO (34.2 µM) only caused a reduction of activity to 61.8% compared to the control (Figure 3.9). The imprecision was comparable to those of VRC with a maximum of 12.4% CV (n=4). The determined IC_{50} of 288 µM (95% CI: 65.0 – 31623 µM) was 77-fold higher than for VRC but exceeded the experimentally applied concentrations. Consequently, a precise estimation of IC_{50} was precluded.

The inhibitory effect of OH-VRC on CYP2C19 was intermediate between the effects of VRC and NO. At lower concentrations of 0.0958 and 0.958 µM the influence on the reaction velocity of OH-MEP formation was minor with 98.0% and 92.1% mean activity remaining compared to the

uninhibited control. However, higher concentrations of 3.83 and 9.58 µM led to relevant inhibition indicated by a mean decrease in activity to 83.6% and 73.0%. The highest concentration of 34.2 µM caused an inhibition of 47.9% (Figure 3.9). The precision was in the same order of magnitude as in previous investigations with VRC and NO and resulted in a CV of ≤14.4% (n=4). Overall, an IC_{50} of 41.7 µM (95% CI: 26.9 – 89.1 µM) was estimated, which, besides the lower limit of the CI, exceeded the experimentally applied concentrations and resulted similarly to NO, in imprecise estimations of IC_{50}. Compared to VRC, OH-VRC was a 11-fold weaker inhibitor on CYP2C19.

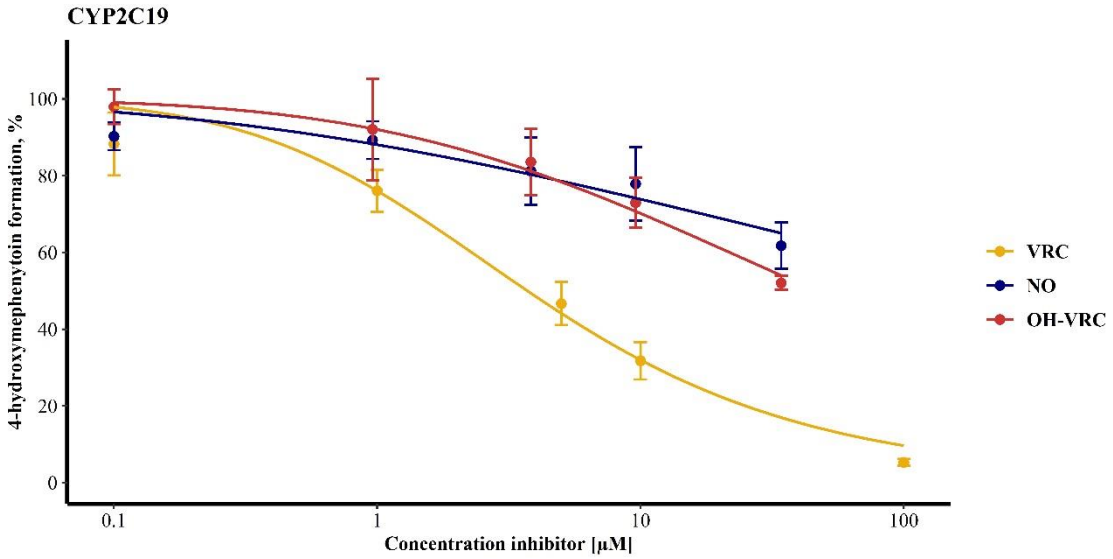

Figure 3.9: Inhibitory potential of voriconazole (VRC), voriconazole *N*-oxide (NO) and hydroxyvoriconazole (OH-VRC) on CYP2C19 presented as the remaining activity of the 4-hydroxylation of S-mephenytoin in dependence of the inhibitor concentration (n=4).
Data points: mean activity; error bars: standard deviation of activity; solid lines: estimated correlation between activity and inhibitor concentration.

Further evaluation focussed on the impact of the assumptions made for the IC_{50} determination, i.e. setting the potential minimum activity observed in the presence of inhibitor to 0% and maximum activity in the absence of inhibitor to 100%. Hence, A_0 and A_{max} were estimated one at a time or simultaneously together with the IC_{50} and steepness of the inhibition curve. For VRC this led to comparable results regarding IC_{50} and H (Table 3.8), as CI for all different model settings were overlapping. However, the 95% CI were relevantly broader, indicating a less precise estimation. Furthermore, estimations of A_0 resulted in values <0% with CI not always including zero, which was experimentally impossible.

Due to the low inhibitory effect of NO and OH-VRC on CYP2C19 estimations were already imprecise when two parameters were fixed. Extending the number of parameters to be estimated thus increased the imprecision of the parameters as indicated by the wide CI or the impossibility

to determine CI at all. Consequently, a comparison of the different parameter estimates was inconclusive.

Table 3.8: Overview of the parameter estimates (IC_{50}, H, A_{max}, A_0) of the inhibition model (chapter 2.3.5.1) for voriconazole (VRC), voriconazole *N*-oxide (NO) and hydroxyvoriconazole (OH-VRC) on CYP2C19, when either both A_{max} and A_0 were fixed to 100% and 0%, respectively, or only one of the two was fixed or all parameters were estimated by the model.

Inhi-bitor	**Setting**	**IC_{50} (95% CI) [µM]**	**H (95% CI)**	**A_{max} (95% CI), %**	**A_0 (95% CI), %**
VRC	Fixed A_{max}=100 and A_0=0	3.72 (2.85 – 4.78)	6.64 (5.19 – 8.49)	-	-
	Fixed A_{max}=100	10.4 (3.72 – 8411)	4.47 (2.68 – 7.00)	-	-31.5 (-234 – -1.72)
	Fixed A_0=0	5.50 (2.29 – 6.95)	8.75 (6.94 – 11.5)	88.2 (82.7 – 94.1)	-
	No fixed parameters	5.93 (4.17 – 11.8)	8.06 (5.14 – 12.0)	88.8 (NA – 95.9)	-3.40 (-27.0 – 6.92)
NO	Fixed A_{max}=100 and A_0=0	288 (65.0 – 31623)	3.34 (1.76 – 5.69)	-	-
	Fixed A_{max}=100	6.22 (1.75 – NA)	14.6 (NA)	-	75.0 (NA)
	Fixed A_0=0	118 (55.5 – 974)	6.98 (3.21 – 15.3)	90.5 (84.7 – 98.7)	-
	No fixed parameters	5.51 (2.46 – NA)	14.8 (NA)	73.3 (68.8 – 78.0)	49.5 (NA)
OH-VRC	Fixed A_{max}=100 and A_0=0	41.7 (26.9 – 89.1)	6.27 (4.30 – 4.95)	-	-
	Fixed A_{max}=100	11.8 (6.42 – NA)	12.3 (NA – 24.1)	-	38.7 (NA – 55.4)
	Fixed A_0=0	42.9 (27.2 – 90.9)	6.94 (4.10 – 4.96)	97.6 (90.6 – 106)	-
	No fixed parameters	107647 (NA)	4.84 (NA)	98.9 (NA)	-693 (NA)

A_0, minimum activity; A_{max}, maximum activity; CI, confidence interval; H, Hill factor, i.e. steepness of the inhibition curve; IC_{50}, Half maximum inhibitory concentration; NA, not assessable.

Inhibitory effect on CYP2C9. The inhibition by VRC on the 4-hydroxylation of diclofenac by CYP2C9 was very distinct. At a concentration of 0.1 µM the reaction velocity was decreased by a mean of 14.0%. With increasing VRC concentrations, the mean reaction velocity of OH-DIC formation decreased further with a drop of 15.7%, 54.1% and 70.8% at VRC concentrations of 1, 5 and 10 µM compared to the uninhibited control, respectively. The highest VRC concentration of 100 µM caused a nearly complete inhibition of the CYP2C9 mediated reaction of OH-DIC formation with a mean reaction velocity of only 6.85% compared to the uninhibited control (Figure 3.10). Overall, the two performed replicates, that were sampled each at two points in time, were in good agreement with each other indicated by an imprecision of ≤14.2% CV (n=4). There was only one exception at a VRC concentration of 0.1 µM where the two replicates were not alike entailing a large imprecision of 36.1% CV. The obtained data were fitted to the inhibition model (chapter 2.3.5.1) and resulted in an IC_{50} of 4.17 µM (95% CI: 2.54 – 6.51 µM) for VRC on the CYP2C9 catalysed reaction of the 4-hydroxylation of diclofenac.

NO showed a lower inhibitory potential than VRC on CYP2C9. At a concentration of 0.0958 µM no inhibition was observable with mean reaction velocities being identical to the uninhibited control. Higher NO concentrations of 0.958, 3.83 and 9.58 µM caused greater inhibition as alluded by mean reaction velocities of OH-DIC formation decreased by 5.1%, 27.9% and 42.3%, respectively. The largest reduction in reaction velocity was observed at a NO concentration of 34.2 µM with a decrease by 67.0% (Figure 3.10). The imprecision at all NO concentration levels was ≤16.2% CV (n=4). Based on those observations, an IC_{50} value of 13.4 µM (95% CI: 9.90 – 19.1 µM) was estimated, which was 3.2-fold higher than the IC_{50} for VRC on the 4-hydroxylation of diclofenac by CYP2C9.

The inhibitory effects of OH-VRC on CYP2C9 were intermediate between the effects of VRC and NO. No inhibition was observed at the very low concentration of 0.0958 µM OH-VRC with a determined mean reaction velocity of OH-DIC formation of 103% compared to the uninhibited control. However, a further increase in OH-VRC concentration led to a steep decrease in reaction velocities of the 4-hydroxylation of diclofenac by CYP2C9. At concentrations of 0.958, 3.83 and 9.58 µM OH-VRC, reaction velocities were decreased to a mean remaining activity of 76.1%, 51.6% and 29.9% compared to the uninhibited control. The maximum inhibition caused by OH-VRC at a concentration of 34.2 µM was 14.4% reaction velocity remaining compared to the uninhibited control (Figure 3.10). The two performed replicates, as well as the two sampled time points, yielded in good agreement regarding the determined reaction velocities, which was indicated by an imprecision of ≤11.5% CV. The estimated IC_{50} value of OH-VRC on the CYP2C9 mediated reaction of the 4-hydroxylation of diclofenac was with 3.67 µM (95% CI: 3.16 – 4.26 µM) 1.14-fold lower than the IC_{50} value of VRC on the same reaction.

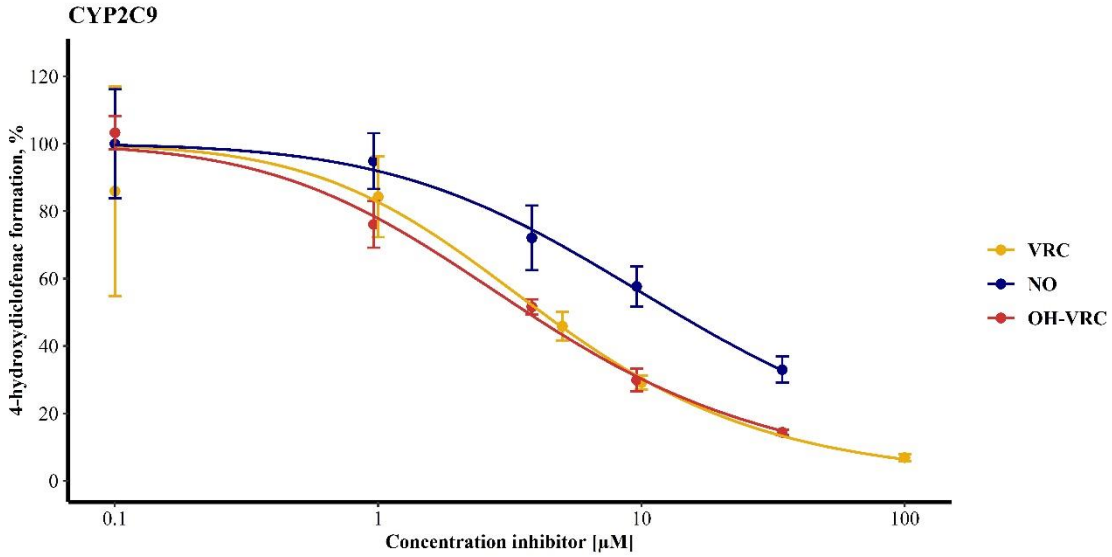

Figure 3.10: Inhibitory potential of voriconazole (VRC), voriconazole *N*-oxide (NO) and hydroxyvoriconazole (OH-VRC) on CYP2C9 presented as the remaining activity of the 4-hydroxylation of diclofenac in dependence of the inhibitor concentration (n=4).
Data points: mean activity; error bars: standard deviation of activity; solid lines: estimated correlation between activity and inhibitor concentration.

Additionally, the estimated parameters were evaluated for their consistency if the original assumptions in the model were changed. Thus, in a stepwise approach, the model was applied to estimate besides the IC_{50} and H, A_{max} or A_0, as well as all four parameters simultaneously. Overall, this resulted in a good agreement of all parameter estimates for VRC, NO and OH-VRC (Table 3.9). The maximum differences in the estimated IC_{50} were 2.25 µM for VRC (40.0%), 3.10 µM for NO (23.1%) and 1.31 µM for OH-VRC (29.2%). However, in all cases CI were overlapping, suggesting insignificant differences. Also the estimates for A_{max} and A_0 were mostly plausible. On the one hand, estimations of A_{max} were always close to 100% with a maximum difference of -12.7% with the CI always including 100% (if assessable). On the other hand, estimations of A_0 were always close to 0% with the CI always including 0% (if assessable). Here, a maximum difference of -14.8% was observed. Estimations of A_{max} >100% and A_0 <0% were experimentally implausible, however taking the imprecision of the determination into account, the differences were most likely negligible.

Regarding the precision of the estimations, it was observed, that parameter estimates were in general accompanied by larger 95% CI when more parameters were to be estimated. In some cases, based on the data CI were not assessable at all (Table 3.9). Thus, although the parameter estimates were in good agreement, due to the wide CI, a meaningful comparison of the conformity was precluded. In particular for A_0, CI stretched well into the negative range, which was implausible from an experimental point of view.

Table 3.9: Overview of the parameter estimates (IC_{50}, H, A_{max}, A_0) of the four-parameter inhibition model (chapter 2.3.5.1) for voriconazole (VRC), voriconazole *N*-oxide (NO) and hydroxyvoriconazole (OH-VRC) on CYP2C9, when either both A_{max} and A_0 were fixed to 100% and 0%, respectively, or only one of the two was fixed or all parameters were estimated by the model.

Inhi-bitor	Setting	IC_{50} (95% CI) [µM]	H (95% CI)	A_{max} (95% CI), %	A_0 (95% CI), %
VRC	Fixed A_{max}=100 and A_0=0	4.17 (2.54 – 6.51)	8.32 (4.77 – 15.6)	-	-
	Fixed A_{max}=100	3.38 (2.39 – 5.60)	7.67 (5.52 – 10.2)	-	-0.890 (-17.5 – 9.52)
	Fixed A_0=0	5.63 (3.19 – 9.39)	11.1 (5.89 – 24.7)	88.2 (75.6 – 103)	-
	No fixed parameters	5.14 (2.57 – 22.3)	13.1 (4.40 – NA)	87.3 (74.9 – 103)	5.67 (-45.9 – 22.6)
NO	Fixed A_{max}=100 and A_0=0	13.4 (9.90 – 19.1)	7.62 (5.60 – 10.2)	-	-
	Fixed A_{max}=100	10.3 (4.34 - 622)	6.47 (4.23 – 9.33)	-	-0.817 (-176 – 24.7)
	Fixed A_0=0	12.8 (8.30 – 20.2)	7.39 (4.98 – 10.6)	101 (92.5 – 112)	-
	No fixed parameters	10.6 (3.69 – NA)	7.92 (NA – 18.4)	101 (91.7 – NA)	6.96 (NA – 38.8)
OH-VRC	Fixed A_{max}=100 and A_0=0	3.67 (3.16 – 4.26)	7.26 (6.32 – 8.34)	-	-
	Fixed A_{max}=100	4.00 (2.62 – 9.07)	6.98 (5.26 – 9.00)	-	-3.05 (-31.2 – 10.7)
	Fixed A_0=0	3.17 (2.48 – 3.96)	6.71 (5.69 – 7.88)	105 (99.2 – 111)	-
	No fixed parameters	4.48 (2.56 – 187)	5.48 (2.70 – 7.80)	107 (100 – 124)	-14.8 (-154 – 5.66)

A_0, minimum activity; A_{max}, maximum activity; CI, confidence interval; H, Hill factor, i.e. steepness of the inhibition curve; IC_{50}, half maximum inhibitory concentration; NA, not assessable.

Inhibitory effect on CYP3A4. VRC was revealed to be a strong inhibitor of the 1-hydroxylation of midazolam catalysed by CYP3A4. The low concentration of 0.1 µM caused a decrease in the mean reaction velocity of 14.8%, while concentrations of 1, 5 and 10 µM VRC resulted in a reduction in the mean velocity of OH-MDZ formation of 22.2%, 73.1% and 77.9% compared to

an uninhibited control, respectively. A concentration of 100 µM VRC almost completely inhibited CYP3A4 as it yielded a decrease in the reaction velocity of 91.8% compared to the uninhibited control (Figure 3.11). A maximum imprecision of 16.7% CV was observed for the determination of the mean reaction velocity (n=4). Overall, this resulted in an estimated IC_{50} of VRC on the 1-hydroxylation of midazolam by CYP3A4 of 1.76 µM (95% CI: 1.26 – 2.36 µM).

Comparable to observations made with CYP2C19 and CYP2C9, NO showed the least inhibitory effect on CYP3A4. At low concentrations of 0.0958 and 0.958 µM NO inhibited the reaction velocity of OH-MDZ formation by 6.1% and 8.8% compared to an uninhibited control, respectively. A further increase in NO concentrations, i.e. 3.83 and 9.58 µM, resulted in a reduction in the mean reaction velocity of 48.1% and 68.7%, respectively. The largest impact was achieved with the highest NO concentration (34.2 µM) and resulted in a decrease in the mean reaction velocity of 88.9% compared to the uninhibited control (Figure 3.11). The maximum imprecision observed was 18.5% CV at a NO level of 100 µM (n=4). The resulting IC_{50} of NO on the CYP3A4 mediated reaction of the 1-hydroxylation of midazolam was 4.48 µM (95% CI: 3.78 – 5.29 µM) and thus 2.5-fold higher than IC_{50} of VRC on the same reaction.

OH-VRC showed similar strong inhibitory properties as VRC. Already at low concentrations of 0.0958 and 0.958 µM OH-VRC the reaction velocity of OH-MDZ formation was reduced by 11.1% and 46.9%, respectively. A further reduction of the mean reaction velocity by 73.9% and 83.9% was achieved with OH-VRC concentrations of 3.83 and 9.58 µM, respectively. At a concentration of 34.2 µM OH-VRC a decrease in OH-MDZ formation by 92.9% compared to the uninhibited control was determined (Figure 3.11). This was the same degree of inhibition observed for VRC on CYP3A4 at a concentration of 100 µM. The precision of the determined reaction velocity at the respective inhibitor levels was comparable to previous investigations with CV ≤22.4% (n=4). All in all, the investigation yielded an IC_{50} value of 1.02 µM (95% CI: 0.796 – 1.27 µM) for OH-VRC on the 1-hydroxylation of midazolam mediated by CYP3A4. This was 1.7-fold lower than the IC_{50} of VRC on the same reaction.

Furthermore, also for CYP3A4 the consistency of the parameter estimates was evaluated when only A_{max} or A_0 were fixed to 100% or 0%, respectively, as well as when all parameters were estimated at the same time. Overall, the estimation of IC_{50} for VRC, NO and OH-VRC on CYP3A4 was independent of the chosen setting, i.e. the a priori included assumptions in the model, indicating the justification of these assumptions (Table 3.10). For VRC, NO and OH-VRC the maximum difference in the estimated IC_{50} was 1.0 (36.2%), 0.78 (16.1%) and 0.26 µM (20.3%), respectively. Additionally, all CI were overlapping reinforcing the conclusion, that the observed differences were negligible. The estimation of H showed a higher variability, however also here CI were widely overlapping, which suggested non-significant differences. Estimations of A_{max} and A_0 were predominantly plausible, with A_{max} values reaching 100% and A_0 values

approaching 0%. The largest observed deviation was -14.2% for A_{max} with all CI including 100% except for the estimations of VRC. The estimation of A_0 showed a maximum deviation of +7.84%, however all CI (if assessable) included 0%.

Nevertheless, as observed before, the more parameters were estimated simultaneously, the wider the CI became, indicating a decreasing precision in the estimation, suggesting an overparametrisation of the model. Some CI were not assessable at all or resulted in implausible high or low estimations, e.g. A_{max} of 214% (Table 3.10). Consequently, conclusions about the most suitable model setting had to be handled with care.

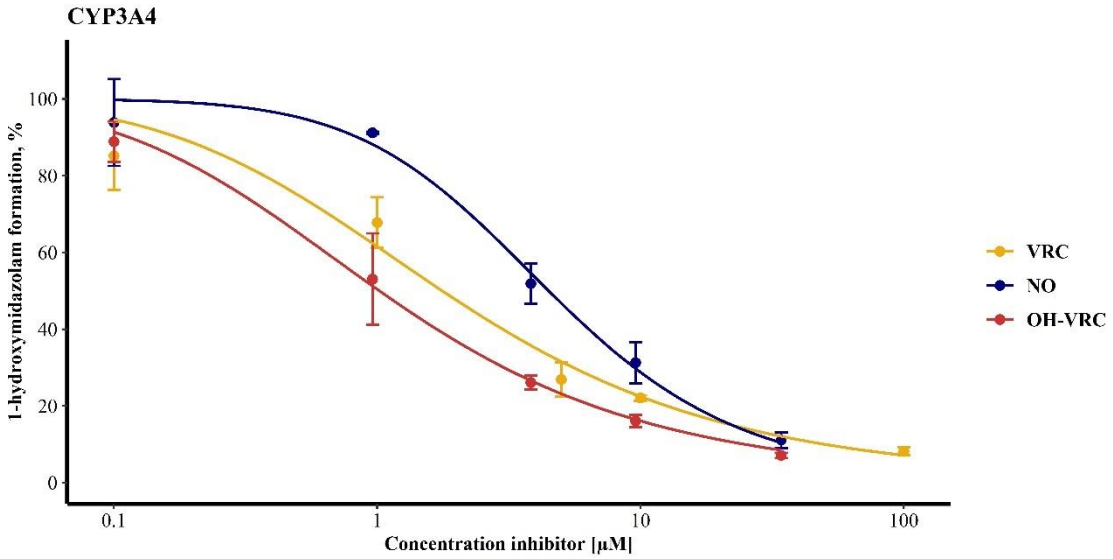

Figure 3.11: Inhibitory potential of voriconazole (VRC), voriconazole *N*-oxide (NO) and hydroxyvoriconazole (OH-VRC) on CYP3A4 presented as the remaining activity of the 1-hydroxylation of midazolam in dependence of the inhibitor concentration (n=4).
Data points: mean activity; error bars: standard deviation of activity; solid lines: estimated correlation between activity and inhibitor concentration.

Table 3.10: Overview of the parameter estimates (IC_{50}, H, A_{max}, A_0) of the inhibition model (chapter 2.3.5.1) for voriconazole (VRC), voriconazole *N*-oxide (NO) and hydroxyvoriconazole (OH-VRC) on CYP3A4, when either both A_{max} and A_0 were fixed to 100% and 0%, respectively, or only one of the two was fixed or all parameters were estimated by the model.

Inhibitor	Setting	IC_{50} (95% CI) [µM]	H (95% CI)	A_{max} (95% CI), %	A_0 (95% CI), %
VRC	Fixed A_{max}=100 and A_0=0	1.76 (1.26 – 2.36)	5.92 (4.47 – 8.00)	-	-
	Fixed A_{max}=100	1.92 (1.14 – 7.20)	5.46 (3.30 – 10.0)	-	-3.29 (-38.4 – 12.3)
	Fixed A_0=0	2.76 (2.01 – 3.68)	8.04 (6.14 – 10.5)	87.2 (80.4 – 94.6)	-
	No fixed parameters	2.30 (1.68 – 3.18)	10.2 (7.24 – 14.0)	85.8 (79.7 – 92.2)	7.84 (-0.56 – 14.6)
NO	Fixed A_{max}=100 and A_0=0	4.48 (3.78 – 5.29)	9.92 (8.13 – 12.2)	-	-
	Fixed A_{max}=100	4.06 (2.99 – 7.11)	10.8 (7.30 – 15.6)	-	4.57 (-19.0 – 16.2)
	Fixed A_0=0	4.84 (3.90 – 5.99)	10.5 (8.40 – 13.3)	96.5 (90.5 – 103)	-
	No fixed parameters	4.23 (3.16 – 6.56)	12.3 (8.09 – 18.9)	95.7 (89.7 – 102)	6.98 (-12.4 – 17.6)
OH-VRC	Fixed A_{max}=100 and A_0=0	1.02 (0.796 – 1.27)	5.75 (4.84 – 6.94)	-	-
	Fixed A_{max}=100	1.25 (0.789 – 3.06)	5.08 (3.71 – 7.02)	-	-7.00 (-32.5 – 5.71)
	Fixed A_0=0	1.28 (0.792 – 1.77)	6.50 (4.98 – 8.20)	93.7 (85.7 – 105)	-
	No fixed parameters	1.28 (0.698 – 6.52)	6.46 (NA – 10.7)	93.8 (84.8 – 214)	-0.202 (NA – 11.3)

A_0, minimum activity; A_{max}, maximum activity; CI, confidence interval; H, Hill factor, i.e. steepness of the inhibition curve; IC_{50}, Half maximum inhibitory concentration; NA, not assessable.

3.2.3.2 Time-dependent inhibition

Time-dependent inhibition was investigated by determination of the influence of a 30 min pre-incubation period of inhibitor with HLM in the presence and absence of NADPH re-generating system on the IC_{50} of the respective isoenzymes CYP2C19, CYP2C9 and CYP3A4.

Time-dependent inhibition on CYP2C19. The inhibitory effect of VRC on the CYP2C19 mediated reaction of the 4-hydroxylation of S-mephenytoin with a pre-incubation time of 30 min was as pronounced as without. Also, the absence or presence of the NADPH re-generating system did not show an impact (Figure 3.12). Precision for both investigations including a pre-incubation time was high with CV ≤16.4% (n=4). IC_{50} were estimated as 5.59 µM (95% CI: 4.61 – 6.74 µM) in the absence and as 5.02 µM (95% CI: 4.12 – 6.08 µM) in the presence of NADPH re-generating system. Thus, no relevantly increased inhibitory properties were observed compared to the IC_{50} determination without a pre-incubation period (Table 3.11).

The influence of NO on the OH-MEP formation by CYP2C19 was minor, as described before (chapter 3.2.3.1). Also a pre-incubation time of 30 min in the absence and presence of NADPH re-generating system did not change this observation (Figure 3.12). Imprecision was on all inhibitor levels for both investigations including a pre-incubation period ≤15.9% CV (n=4). Regarding the impact of NO on CYP2C19, IC_{50} values of 450 µM (95% CI: 93.3 – 339557 µM) and 320 µM (95% CI: 52.0 – 364870 µM) were determined in the absence and presence of NADPH re-generating system during the 30 min pre-incubation period, respectively (Table 3.11). As described for the IC_{50} determination (chapter 3.2.3.1), the overall inhibitory effect of NO was low, with IC_{50} exceeding the applied experimental NO concentrations, and hence a precise estimation of IC_{50} was precluded.

Lastly, inhibition on CYP2C19 by OH-VRC was not increased by the pre-incubation period, neither without nor with the presence of NADPH re-generating system (Figure 3.12). The precision of the determination was high with a CV of ≤9.27% (n=4). The IC_{50} of OH-VRC on CYP2C19 resulted in 35.5 µM (95% CI: 26.8 – 53.6 µM) in the absence and 33.6 µM (95% CI: 17.0 – 160 µM) in the presence of the NADPH re-generating system during pre-incubation (Table 3.11).

Consequently, no IC_{50} shift >1.5-fold was detectable indicating a time-independent inhibition of VRC, NO and OH-VRC on CYP2C19.

Time-dependent inhibition on CYP2C9. The inhibitory profiles of VRC on the CYP2C9 mediated reaction of the 4-hydroxylation of diclofenac observed without and with a pre-incubation period of 30 min were very similar (Figure 3.12). All determinations were precise as CV was in all cases ≤14.1% (n=4). The obtained IC_{50} of VRC on CYP2C9 including a 30 min pre-incubation was 3.31 µM (95% CI: 2.70 – 4.01 µM) in the absence and 3.16 µM (95% CI: 2.71 – 3.67 µM) in the presence of NADPH re-generating system (Table 3.11).

The inhibitory potential of NO on the 4-hydroxylation of diclofenac by CYP2C9 was not enhanced by the 30 min pre-incubation period, neither in the absence nor in the presence of the NADPH re-generating system (Figure 3.12). In both settings, precision was demonstrated by a

CV of ≤12.9% (n=4). The observations, that inhibition was not increased by the pre-incubation period was confirmed by the estimated IC_{50} values of 10.1 µM (95% CI: 8.28 – 12.4 µM) and 14.9 µM (95% CI: 11.1 – 21.3 µM) in the absence and presence of NADPH re-generating system during the pre-incubation period, respectively (Table 3.11).

The 30 min pre-incubation period of OH-VRC with HLM in the absence or presence of NADPH re-generating system did not influence the inhibitory effect on OH-DIC formation by CYP2C9. The trajectories of the CYP2C9 inhibition in dependence of OH-VRC concentration were almost identical in all settings (Figure 3.12). The imprecision of the investigations were for all OH-VRC concentrations ≤22.0% CV (n=4). Based on these data, an IC_{50} value of 3.68 µM (95% CI: 2.91 – 4.59 µM) was determined when NADPH re-generating system was absent during the pre-incubation. Furthermore, in the presence of NADPH re-generating system an IC_{50} of 3.64 µM (95% CI: 3.01 – 4.39 µM) was determined (Table 3.11).

Overall, VRC, NO and OH-VRC did not show time-dependent inhibition, as IC_{50} values determined from the three settings, i.e. no pre-incubation and 30 min pre-incubation without or with NADPH re-generating system, were comparable indicated by IC_{50} shifts of <1.5-fold and widely overlapping CI (Table 3.11).

Time-dependent inhibition on CYP3A4. VRC did not cause time-dependent inhibition on the 1-hydroxylation of midazolam by CYP3A4. Inhibitory effects were comparable to those observed when no pre-incubation was performed (Figure 3.12). In particular, for investigations with NADPH re-generating system during the pre-incubation, higher imprecisions of 37.4% (VRC concentration of 10 µM) and 20.6% CV (uninhibited control) were observed (n=4 each). However, the remaining determinations revealed imprecisions ≤11.9% CV (n=4). The estimated IC_{50} values based on the described observations resulted in 2.90 µM (95% CI: 2.13 – 3.85 µM) and 2.63 µM (95% CI: 1.97 – 3.40 µM) in the absence and presence of NADPH re-generating system during the pre-incubation period, respectively (Table 3.11).

The inhibitory potential of NO on the formation of OH-MDZ by CYP3A4 was partly increased when a pre-incubation with NADPH re-generating system was performed (Figure 3.12). However, also the observed variability was large, demonstrated by the imprecision reaching a maximum of 39.9% CV. Apart from that, CV was ≤25.0% (n=4). The estimated IC_{50} values were 6.96 µM (95% CI: 4.63 – 10.2 µM) and 2.91 µM (95% CI: 1.36 – 6.19 µM) in the absence and presence of NADPH re-generating system, respectively (Table 3.11).

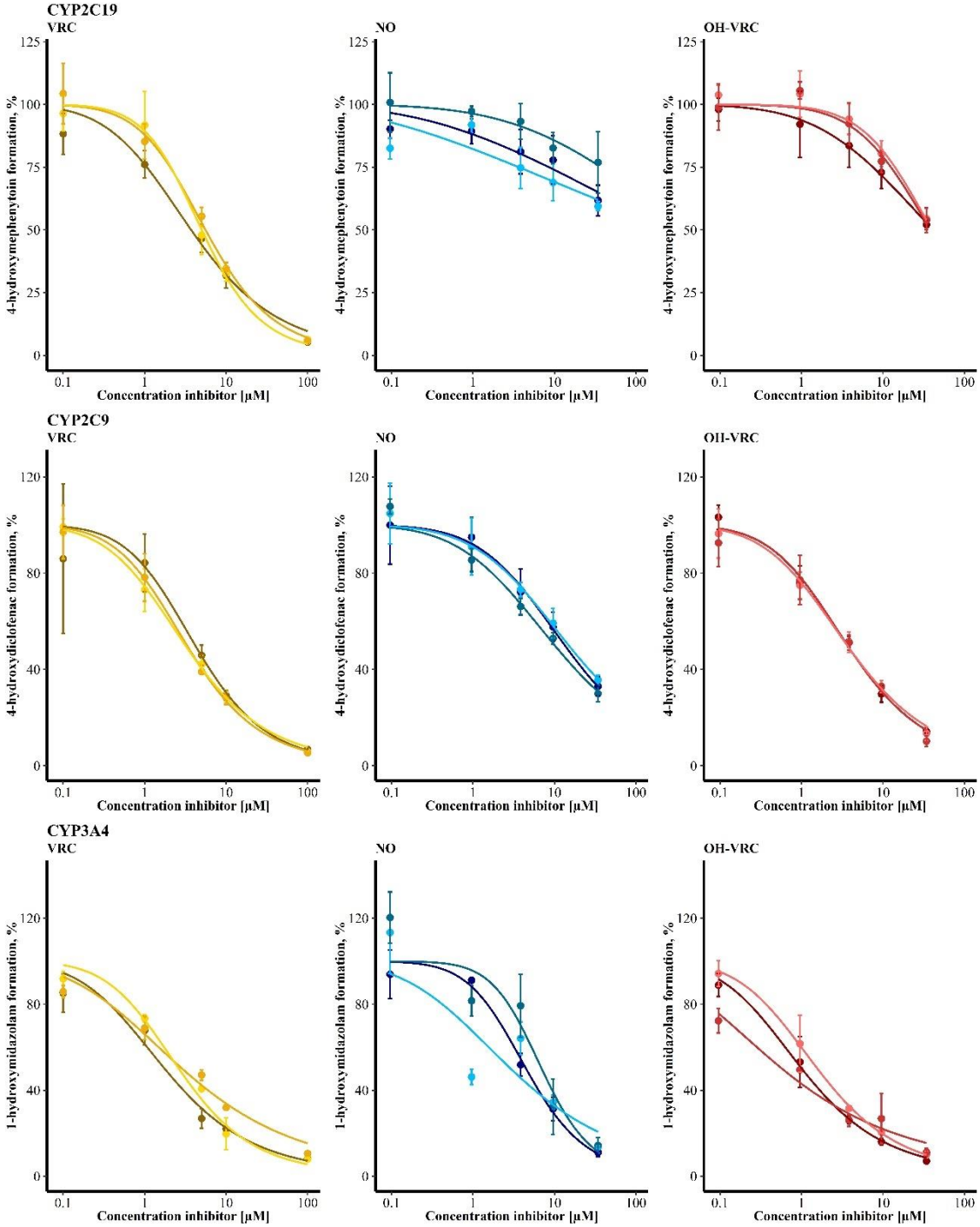

Figure 3.12: Inhibitory effect on the CYP2C19 mediated reaction of S-mephenytoin 4-hydroxylation (top), the CYP2C9 mediated 4-hydroxylation of diclofenac (middle) and the CYP3A4 mediated reaction of the 1-hydroxylation of midazolam (bottom) as function of the concentration of voriconazole (VRC, left), voriconazole *N*-oxide (NO, middle) and hydroxyvoriconazole (OH-VRC, right) without a pre-incubation period of human liver microsomes and inhibitor (dark colours) and with a pre-incubation period of 30 min in the absence (medium colours) and presence (light colours) of NADPH re-generating system (n=2-4). Data points: mean activity; error bars: standard deviation of activity; solid lines: model prediction of the activity in dependence of the inhibitor concentration.

Also for OH-VRC, the trajectory of the reduction of the reaction velocity of OH-MDZ formation with increasing concentrations differed slightly when a pre-incubation was performed (Figure 3.12). The imprecision observed during these investigations was again high with a maximum CV of 43.8% (n=4). As for the rest, CV was ≤20.8% (n=4). The consequently estimated IC_{50} values amounted to 0.579 µM (95% CI: 0.323 – 0.966 µM) and 1.57 µM (95% CI: 1.25 – 1.95 µM) in the absence and presence of NADPH re-generating system during pre-incubation, respectively (Table 3.11).

Table 3.11: Summary on the concentrations of voriconazole (VRC), voriconazole *N*-oxide (NO) and hydroxyvoriconazole (OH-VRC) causing a half maximum inhibitory effect (IC_{50}) on the CYP isoenzymes 2C19, 3A4 and 2C9 without a pre-incubation period (IC_{50}) and with a 30 min pre-incubation in the absence (IC_{50}(-)) or the presence (IC_{50}(+)) of NADPH re-generating system. The respective IC_{50} shift is given as ratio of IC_{50} to IC_{50}(-) or IC_{50}(+), respectively.

Enzyme	Inhibitor	IC_{50} (95% CI) [µM]	IC_{50} (-) (95% CI) [µM]	IC_{50} shift (-)	IC_{50} (+) (95% CI) [µM]	IC_{50} shift (+)
CYP2C19	VRC	3.72 (2.85 – 4.78)	5.59 (4.61 – 6.74)	0.667	5.02 (4.12 – 6.08)	0.741
	NO	288 (65.0 – 31623)	450 (93.3 – 339557)	0.641	320 (52.0 – 364870)	0.900
	OH-VRC	41.7 (26.9 – 89.1)	35.5 (26.8 – 53.6)	1.17	33.6 (17.0 – 160)	1.24
CYP2C9	VRC	4.17 (2.54 – 6.51)	3.31 (2.70 – 4.01)	1.26	3.16 (2.71 – 3.67)	1.32
	NO	13.4 (9.90 – 19.1)	10.1 (8.28 – 12.4)	1.34	14.9 (11.1 – 21.3)	0.899
	OH-VRC	3.67 (3.16 – 4.26)	3.68 (2.91 – 4.59)	0.997	3.64 (3.01 – 4.39)	1.01
CYP3A4	VRC	1.76 (1.26 – 2.36)	2.90 (2.13 – 3.85)	0.607	2.63 (1.97 – 3.40)	0.669
	NO	4.48 (3.78 – 5.29)	6.96 (4.63 – 10.2)	0.644	2.91 (1.36 – 6.19)	1.54
	OH-VRC	1.02 (0.796 – 1.27)	0.579 (0.323 – 0.966)	1.76	1.57 (1.25 – 1.95)	0.650

Overall, for the 1-hydroxylation of midazolam mediated by CYP3A4 in two cases an IC_{50} shift of >1.5-fold was observed as inhibition was more distinct when a 30 min pre-incubation period was performed. First, an IC_{50} shift of 1.54-fold was obtained when NO was pre-incubated with

HLM in the presence of NADPH re-generating system. However, the CI of the two IC_{50} determinations (without and with pre-incubation) were widely overlapping, challenging the assumption of time-dependent inhibition. Second, for OH-VRC an IC_{50} shift of 1.76-fold was determined when no NADPH re-generating system was present in the pre-incubation. However, also in this case, CI were overlapping, questioning the significance of this observation. Furthermore, the IC_{50} shift was not reproduced in the presence of NADPH re-generating system, provoking further considerations.

3.2.3.3 Type of reversible inhibition

In a next step, the inhibitory potential of VRC, NO and OH-VRC was assessed in HLM in a broader approach. Therefore, the effect of increasing inhibitor concentration was not only evaluated on one substrate concentration (chapter 3.2.3.1) but multiple substrate concentrations representative for all phases of the Michaelis-Menten kinetics. Consequently, the type of reversible inhibition was determinable and a K_i derivable.

Reversible inhibition on CYP2C19. Two major trends were observable, describing the impact of VRC on the reaction velocity of the CYP2C19 mediated OH-MEP formation. First, as described previously (chapter 3.2.3.1 and 3.2.3.2), with increasing VRC concentrations, reaction velocities of OH-MEP formation decreased when the substrate concentration of S-mephenytoin was constant. Second, the inhibitory effect of VRC decreased in the presence of increasing substrate concentrations (Figure 3.13). The inhibitory potential of VRC on the 4-hydroxylation of S-mephenytoin by CYP2C19 was in general high, leading partly to reductions in the reaction velocity of >90% at high VRC (100 µM) and low S-mephenytoin (9.16, 13.7 and 18.3 µM) concentrations. Consequently, the OH-MEP concentration of the respective incubations was below the LLOQ (0.5 ng/mL) of the bioanalytical assay. At all VRC and S-mephenytoin concentrations, reaction velocities were determined precisely as indicated by a CV of ≤19.6% (n=4). Overall, a competitive inhibition for VRC on the reaction of 4-hydroxylation of S-mephenytoin was determined as the model of competitive inhibition revealed plausible and precise parameter estimates and the best fit with an AIC decrease of 143 and 216 to the models of non-competitive and uncompetitive inhibition, respectively. The corresponding K_i was determined as 1.89 µM (95% CI: 1.68 – 2.13 µM).

For NO the observation of tendencies was challenging, as the overall inhibitory potential was low (chapter 3.2.3.1 and 3.2.3.2). Nevertheless, decreases in the reaction velocity of OH-MEP formation were distinguishable when NO concentrations increased, although the effect was not as distinct as for VRC (Figure 3.13). The imprecision was in the same order of magnitude as for VRC with CV ≤21.1% (n=4). Based on those observations, a non-competitive type of reversible inhibition was determined for the effect of NO on the 4-hydroxylation of S-mephenytoin by

CYP2C19. However, the AIC decreases were with 9 and 23 compared to the models of competitive and uncompetitive inhibition, respectively, much smaller than for VRC. The derived K_i was 58.5 µM (95% CI: 46.8 – 75.0 µM).

OH-VRC revealed a similar inhibition pattern on the 4-hydroxylation of S-mephenytoin as VRC, although the overall inhibition was not as pronounced. As observed before (chapter 3.2.3.1 and 3.2.3.2) reaction velocities of OH-MEP formation gradually decreased with increasing OH-VRC concentrations. Concurrently, the inhibitory effect of OH-VRC on CYP2C19 decreased in the incubations with higher S-mephenytoin concentrations (Figure 3.13). All determinations were precise indicated by CV of ≤13.4% (n=4). As for OH-VRC the overall inhibition was not very distinct in the investigated concentration range, the best model to describe the data was obtained by AIC decreases of 5 and 63 favouring the competitive inhibition model over the non-competitive and uncompetitive inhibition model, respectively. The resulting K_i for competitive inhibition of OH-VRC on the CYP2C19 catalysed reaction of the 4-hydroxylation of S-mephenytoin was 11.6 µM (95% CI: 9.67 – 14.0 µM).

The inhibitory effects of VRC, NO and OH-VRC on CYP2C19 were assessed using the same marker reaction of the 4-hydroxylation of S-mephenytoin under the same conditions. Thus, the resulting parameter estimates for K_M and V_{max}, that were simultaneously assessed together with the K_i in all cases, were compared for their consistency between these experiments. As a reference, K_M and V_{max} were determined based on the pooled experimental data of the control incubations (without inhibitor) of the respective experiments by fitting the Michaelis-Menten model (Eq. 2.5). Although some fluctuations were observed, K_M ranged from 86.8% to 107% of the reference. For V_{max} a conformity of 88.5% to 102% was achieved (Table 3.12).

Furthermore, the type of reversible inhibition was explored by the Lineweaver-Burk linearisation. This graphical evaluation supported the mathematical findings of a competitive inhibition for VRC and OH-VRC, as the linear regressions derived per inhibitor concentration, all shared the same y-axis intersection (Figure 7.3). For NO the interpretation of the graphical result was ambiguous being in line with the nonlinear regression analysis.

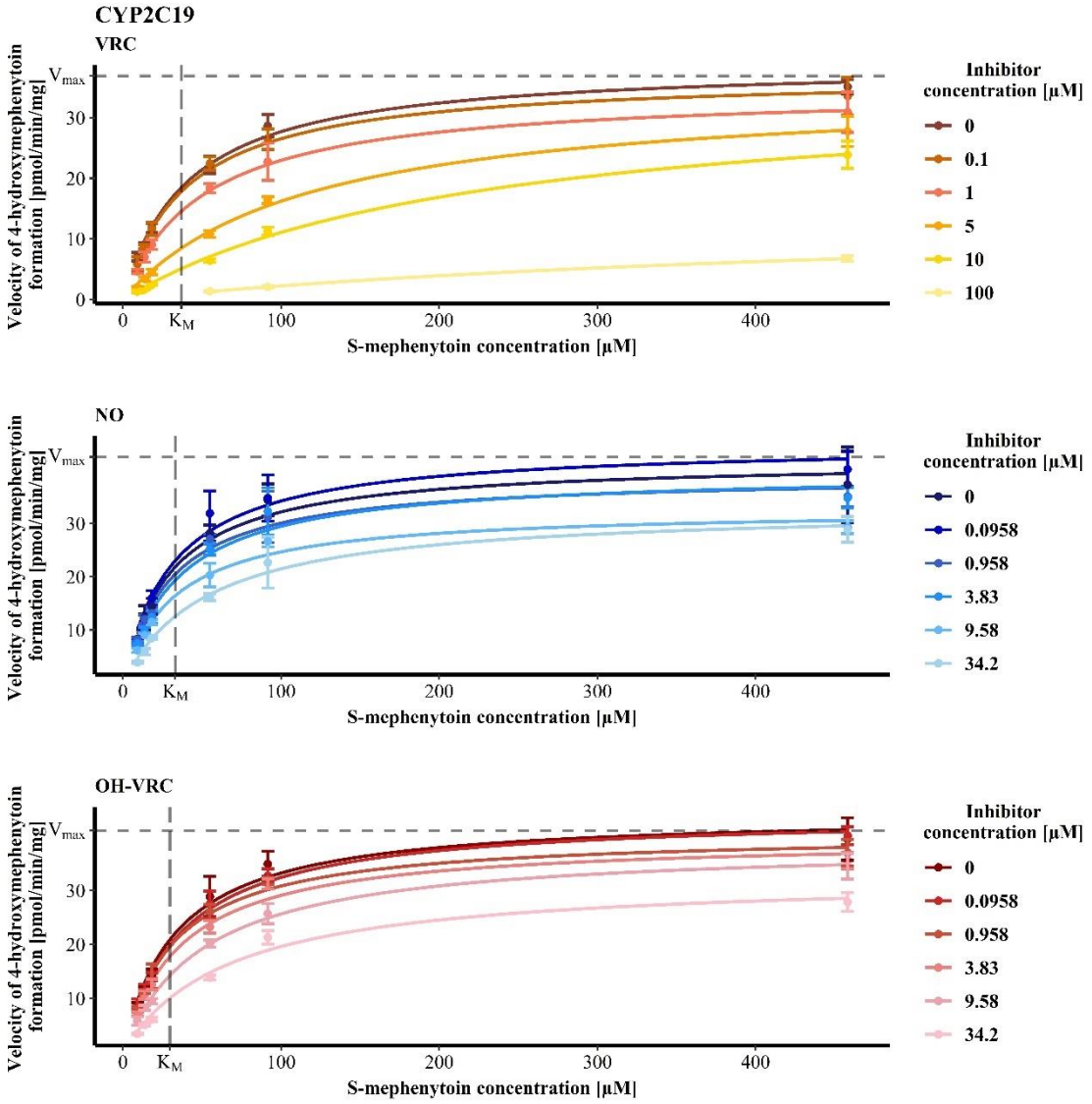

Figure 3.13: Reaction velocities of 4-hydroxymephenytoin formation by CYP2C19 in dependence of the S-mephenytoin concentration under the influence of increasing concentrations of the inhibitors voriconazole (VRC, top), voriconazole *N*-oxide (NO, middle) and hydroxyvoriconazole (OH-VRC, bottom) in human liver microsomes (n=4).

Data points: mean reaction velocity; error bars: standard deviation of reaction velocity; solid lines: estimated enzyme kinetics; dashed lines: Michaelis-Menten constant (K_M) and maximum reaction velocity (V_{max}) of the respective uninhibited control.

Reversible inhibition on CYP2C9. The inhibitory effect of VRC on the 4-hydroxylation of diclofenac by CYP2C9 was distinct. Confirming previous results (chapter 3.2.3.1 and 3.2.3.2), with increasing VRC concentrations, reaction velocities of the OH-DIC formation decreased, independent of the investigated substrate concentration. Furthermore, increasing substrate concentrations led to declining inhibitory effects of VRC on the reaction velocities of OH-DIC formation (Figure 3.14). The maximum determined imprecision was ≤25.0% CV (n=4). Overall, those observations matched the description of a competitive inhibition, which was confirmed by

comparison of the three inhibition models, revealing the competitive inhibition model as superior to the non-competitive and uncompetitive model with AIC decreases of 131 and 143, respectively. The consequently determined K_i amounted to 2.57 µM (95% CI: 2.12 – 3.14 µM).

The inhibitory effects of NO were most pronounced at low diclofenac substrate concentrations and increased with rising NO concentrations. In contrast, at high diclofenac concentrations almost no inhibition was detected, independent of the NO concentration (Figure 3.14). The imprecision was elevated for one investigated setting (diclofenac concentration of 27.0 µM and NO concentration of 0.0958 µM) with a CV of 24.2% (n=2). Apart from that, CV was at all times ≤18.4% (n=4). The evaluation of the data by the three inhibition models suggested a competitive mode of inhibition by NO on the 4-hydroxylation of diclofenac as AIC decreases were 113 and 145 compared to the non-competitive and uncompetitive inhibition model, respectively. The corresponding K_i resulted in a value of 5.47 µM (95% CI: 4.32 – 7.00 µM).

For OH-VRC two overall trends in the inhibitory profile on the 4-hydroxylation of diclofenac were distinguishable. First, increasing inhibitor concentrations entailed a decrease in reaction velocities compared to the uninhibited control when the substrate concentration was constant, as observed before (chapter 3.2.3.1 and 3.2.3.2). Second, identical OH-VRC concentrations caused less inhibition on incubations with higher diclofenac concentrations (Figure 3.14). The maximum observed imprecision was 34.3% CV (n=4). Overall, also for OH-VRC a competitive inhibition on the CYP2C9 mediated reaction of the 4-hydroxylation of diclofenac was observed. The competitive model was superior to the non-competitive and uncompetitive inhibition models indicated by AIC decreases of 104 and 142, respectively. The estimated K_i was consequently 2.80 µM (95% CI: 2.20 – 3.61 µM).

Independent of the investigated inhibitor, VRC, NO or OH-VRC, K_M and V_{max} values for the 4-hydroxylation of diclofenac were in all cases simultaneously assessed in the respective models (Table 3.12). Compared to the reference K_M and V_{max}, determined based on the pooled uninhibited control incubations of the three investigations, a conformity of 97.8% to 134% for K_M and of 98.2% to 106% of V_{max} was achieved. In all cases, the CI of the estimations were overlapping.

Moreover, the graphical evaluation by the Lineweaver-Burk linearisation supported the conclusion of a competitive mode of inhibition by VRC, NO and OH-VRC on CYP2C9. The derived linear functions all shared a common intersection on the y-axis of the plot (Figure 7.4).

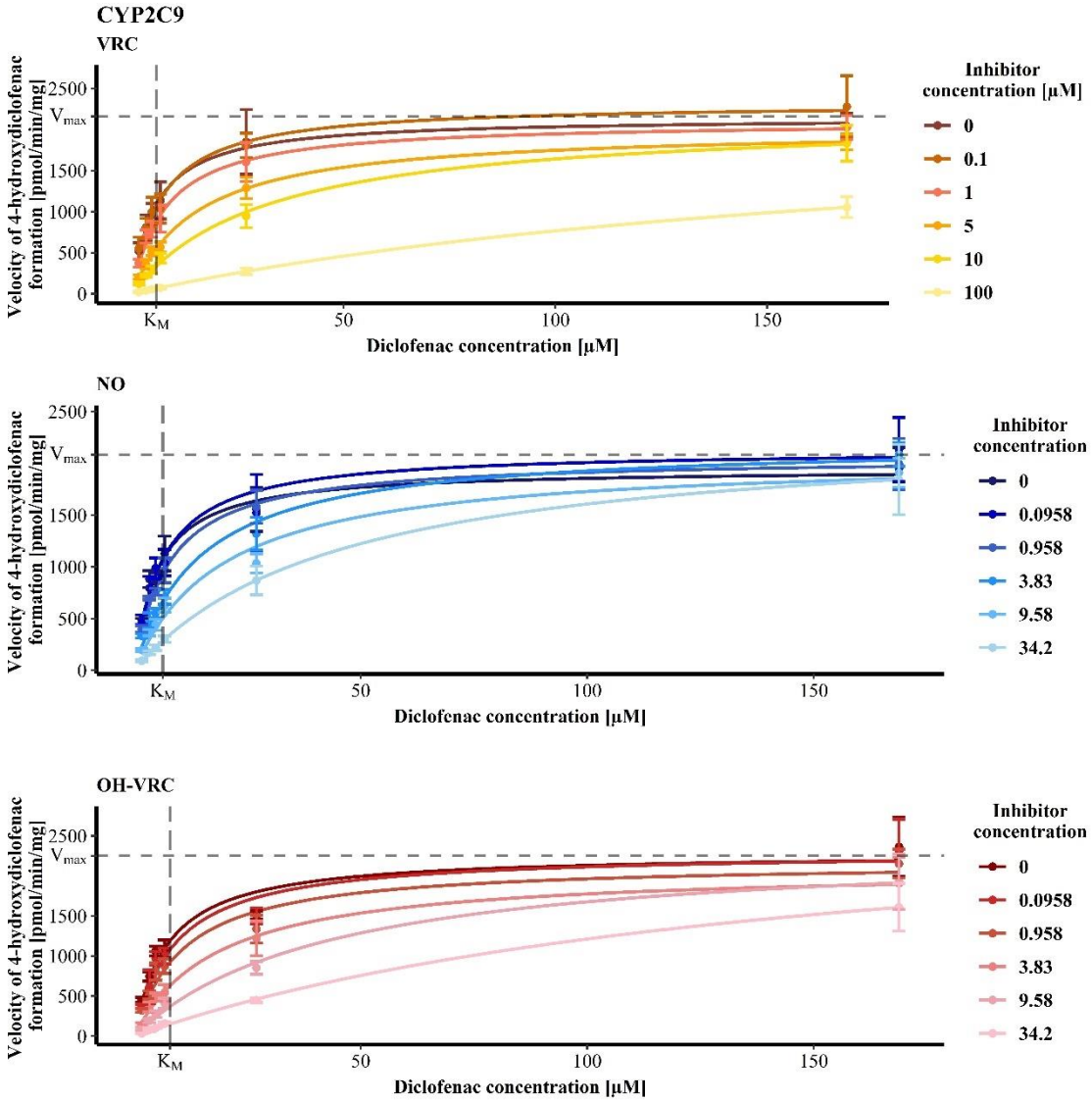

Figure 3.14: Reaction velocities of 4-hydroxydiclofenac formation by CYP2C9 in dependence of the diclofenac concentration under the influence of increasing concentrations of the inhibitors voriconazole (VRC, top), voriconazole *N*-oxide (NO, middle) and hydroxyvoriconazole (OH-VRC, bottom) in human liver microsomes (n=2-4).

Data points: mean reaction velocity; error bars: standard deviation of reaction velocity; solid lines: estimated enzyme kinetics; dashed lines: Michaelis-Menten constant (K_M) and maximum reaction velocity (V_{max}) of the respective uninhibited control.

Reversible inhibition on CYP3A4. The inhibitory effects of VRC on the 1-hydroxylation of midazolam by CYP3A4 increased with growing VRC concentrations when the substrate concentration was constant, as seen previously (chapter 3.2.3.1 and 3.2.3.2). However, in contrast to findings for CYP2C19 and CYP2C9, this inhibitory effect did not depend on the substrate, i.e. midazolam, concentration (Figure 3.15). In all possible combinations of substrate and inhibitor concentrations, imprecision was always ≤27.4% CV (n=4). Overall, those descriptions matched the profile of a non-competitive inhibition, which was confirmed by the evaluation of the three

inhibition models and revealing the non-competitive inhibition model as superior to the competitive and uncompetitive models with AIC decreases of 17 and 43, respectively. The corresponding K_i resulted in a value of 2.75 µM (95% CI: 2.35 – 3.22 µM).

For NO a comparable inhibitory profile on the 1-hydroxylatin of midazolam by CYP3A4 was observed. Again, with increasing NO concentrations also reaction velocities of OH-MDZ formation compared to an uninhibited control decreased at the same substrate level. Yet, this inhibitory potential did not decline when midazolam concentrations increased (Figure 3.15). The precision of the investigation was demonstrated by a CV of ≤18.2% (n=4). The described observations corresponded to a non-competitive mode of inhibition by NO on the CYP3A4 mediated reaction of the 1-hydroxylation of midazolam. Models of competitive and uncompetitive inhibition were inferior to the non-competitive model with AIC differences of 60 and 67, respectively. Based on this, a K_i of 5.23 µM (95% CI: 4.68 – 5.86 µM) was determined.

OH-VRC impacted the reaction velocities of the formation of OH-MDZ by CYP3A4 in a similar way as VRC and NO. While increasing OH-VRC concentrations resulted in a more distinct inhibition of CYP3A4 and consequently in lower reaction velocities of OH-MDZ formation, rising midazolam concentrations could not attenuate this phenomenon. Thus, depending on the concentration of OH-VRC, reaction velocities were, when compared relatively to the uninhibited control of the same substrate concentration, decreased to the same level (Figure 3.15). For investigations with OH-VRC on CYP3A4, the maximum observed imprecisions were 40.9% and 39.8% CV. Apart from that, CV was always ≤24.0% CV (n=4). On the whole, inhibitory effects of OH-VRC on the 1-hydroxylation of midazolam by CYP3A4 were demonstrated to be non-competitive as the obtained data best fitted the respective model. AIC decreases were 94 and 37 regarding the competitive and uncompetitive inhibition model, respectively. The corresponding Ki for the inhibition by OH-VRC on CYP3C4 was 2.53 µM (95% CI: 2.24 – 2.87 µM).

The simultaneously assessed model parameters of K_M and V_{max} are reported in Table 3.12. Overall, experiments revealed a good reproducibility with K_M ranging from 97.2% to 115% and V_{max} from 92.0% to 109% of the reference K_M and V_{max} values determined from the pooled data of the uninhibited control incubations.

Finally, also the Lineweaver-Burk linearisation reinforced the assessment of VRC, NO and OH-VRC being non-competitive inhibitors on CYP3A4. In contrast to investigations of CYP2C19 and CYP2C9 the derived linear functions showed a common intersection on the x-axis ($-1/K_M$) of the Lineweaver-Burk plot (Figure 7.5).

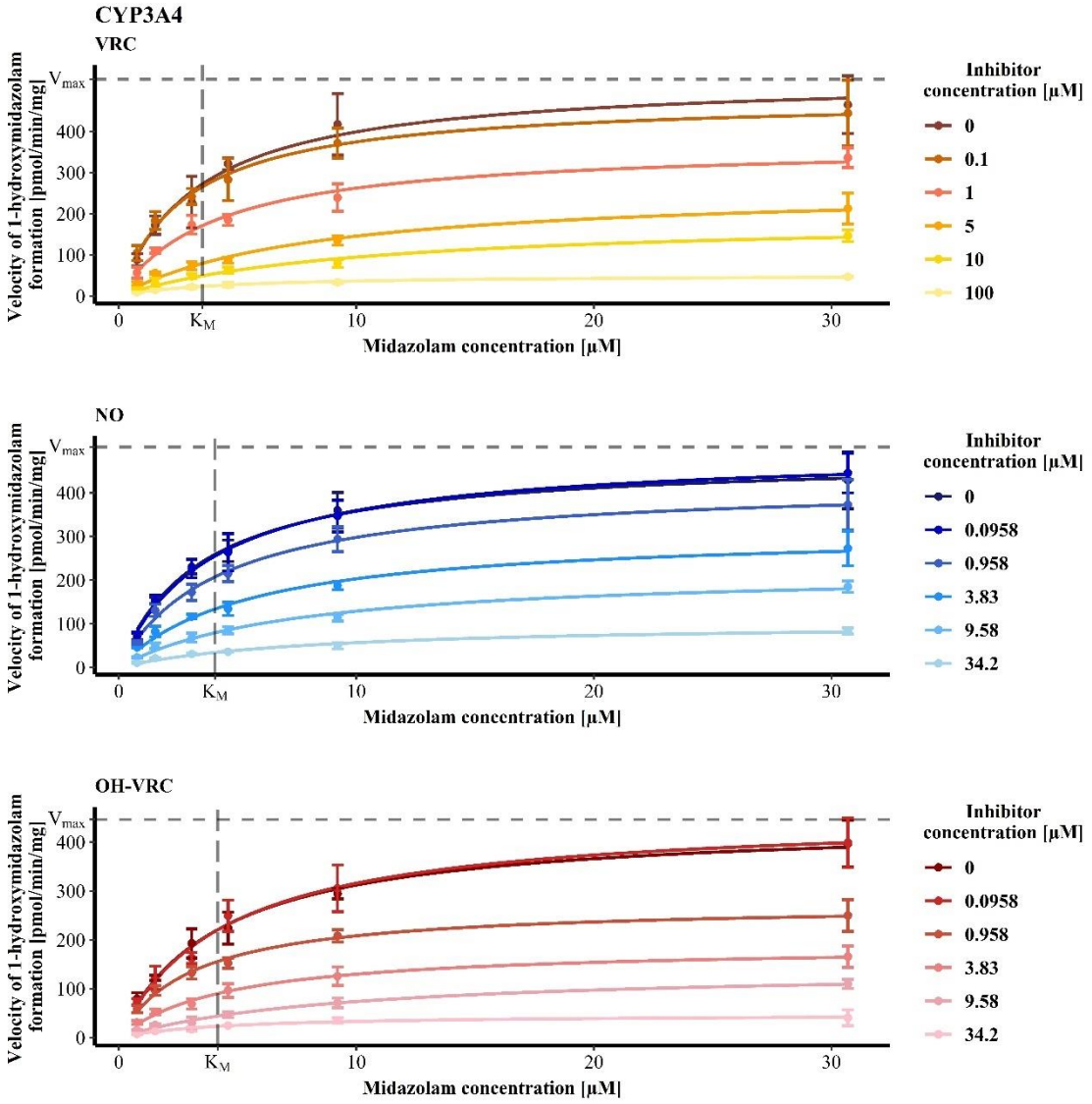

Figure 3.15: Reaction velocities of 1-hydroxymidazolam formation by CYP3A4 in dependence of the midazolam concentration under the influence of increasing concentrations of the inhibitors voriconazole (VRC, top), voriconazole *N*-oxide (NO, middle) and hydroxyvoriconazole (OH-VRC, bottom) in human liver microsomes (n=3-4).

Data points: mean reaction velocity; error bars: standard deviation of reaction velocity; solid lines: estimated enzyme kinetics; dashed lines: Michaelis-Menten constant (K_M) and maximum reaction velocity (V_{max}) of the respective uninhibited control.

Table 3.12: Overview on the type of inhibition caused by voriconazole (VRC), voriconazole *N*-oxide (NO) and hydroxyvoriconazole (OH-VRC) on the CYP isoenzymes 2C19, 3A4 and 2C9 and the associated inhibitory constants (K_i) as well as the Michaelis-Menten constants (K_M) and maximum reaction velocities (V_{max}). Reference K_M and V_{max} were determined by fitting the Michaelis-Menten model to the pooled experimental data of the control incubations (without inhibitor) only, which were included in each enzyme-inhibitor investigation.

Enzyme	**Inhibitor**	**Type of reversible inhibition**	**K_i (95% CI) [µM]**	**K_M (95% CI) [µM]**	**V_{max} (95% CI) [pmol/(min·mg)]**
CYP2C19	None	-	-	34.2 (29.1 – 39.3)	41.7 (39.6 – 43.8)
	VRC	Competitive	1.89 (1.68 – 2.13)	37.0 (34.2 – 40.1)	36.9 (36.0 – 37.9)
	NO	Non-competitive	58.5 (46.8 – 75.0)	33.2 (29.9 – 36.8)	42.4 (40.8 – 44.0)
	OH-VRC	Competitive	11.6 (9.67 – 14.0)	29.7 (27.3 – 32.2)	41.1 (40.1 – 42.1)
CYP2C9	None	-	-	5.93 (4.95 – 6.90)	2123 (2013 - 2232)
	VRC	Competitive	2.57 (2.12 – 3.14)	5.80 (5.14 – 6.52)	2159 (2089 – 2230)
	NO	Competitive	5.47 (4.32 – 7.00)	6.32 (5.60 – 7.13)	2084 (2016 – 2154)
	OH-VRC	Competitive	2.80 (2.20 – 3.61)	7.93 (6.81 – 9.23)	2251 (2158 – 2346)
CYP3A4	None	-	-	3.62 (2.88 – 4.36)	485 (451 - 520)
	VRC	Non-competitive	2.75 (2.35 – 3.22)	3.52 (3.05 – 4.05)	527 (500 – 554)
	NO	Non-competitive	5.23 (4.68 – 5.86)	4.05 (3.65 – 4.47)	505 (486 – 525)
	OH-VRC	Non-competitive	2.53 (2.24 – 2.87)	4.16 (3.71 – 4.66)	446 (427 – 466)

CI, confidence interval

3.3 *In vitro* microdialysis feasibility studies for voriconazole and its *N*-oxide metabolite

A comprehensive *in vitro* microdialysis study was performed to address the feasibility of microdialysis sampling of VRC, NO and their combination *in vitro* (chapter 3.3.2 and 3.3.3), including a LME modelling approach (chapter 3.3.4). Furthermore, potential influential factors of the determination of VRC and NO RR were explored (chapter 3.3.2.1, 3.3.2.2 and 3.3.2.3) and the performance of VRC retrodialysis for catheter calibration and determination of ISF concentrations of VRC *and* NO evaluated (chapter 3.3.5).

3.3.1 Stability of voriconazole *N*-oxide during *in vitro* microdialysis

NO was demonstrated to be stable under conditions relevant for *in vitro* microdialysis investigations. At a temperature of 37°C for 4 h, no degradation was observable. All determined concentrations ranged from 93.3% to 112% of their nominal concentration and were therefore within the required limits of the EMA guideline on bioanalytical method validation [139]. Additionally, no trend was detected across time suggesting bioanalytical variabilities for the above-mentioned deviations (Figure 3.16).

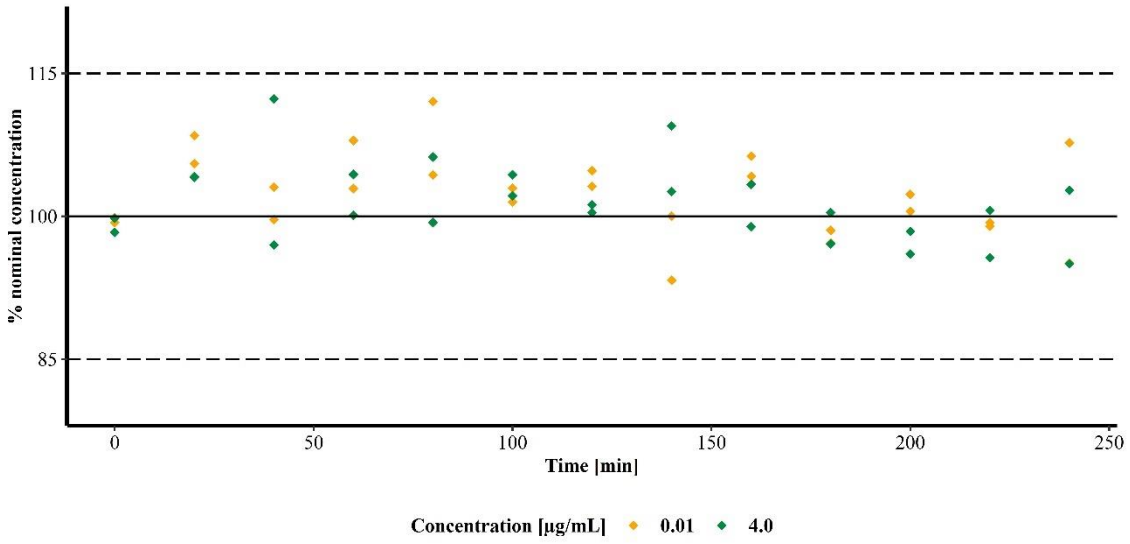

Figure 3.16: Stability of voriconazole *N*-oxide at a low and high concentration across time at 37°C presented as deviation to its nominal concentration. Dashed lines represent the accepted variabilities of ±15%.

3.3.2 Relative recovery of voriconazole and its *N*-oxide metabolite during individual microdialysis

First, RR of VRC and its *N*-oxide metabolite were explored in the absence of the respective other. Overall, both compounds revealed high and consistent RR. Pooling all RR values of VRC across all concentrations, study days and used microdialysis catheters, the median RR was 87.6% (95% CI: 86.5% – 88.8%, n=114). The observed minimum and maximum RR values were 77.4% and

101%, respectively. The median RR of NO across all concentrations, study days and microdialysis catheters was high and exceeded with 91.1% (95% CI: 88.4% – 94.5%, n=85) the median RR of VRC by an absolute difference of 3.5%. Minimum and maximum observed RR values for NO were 79.0% and 105%, respectively.

3.3.2.1 Relative recovery of voriconazole and its *N*-oxide metabolite as a function of concentration

The median RR of VRC in relation to its concentration (0.01 to 3 µg/mL) ranged from 85.6% (95% CI: 82.8% – 89.2%) at 0.20 µg/mL (n=10) to 90.3% (95% CI: 87.4% – 91.5%) at 0.50 µg/mL (n=15). Thus, no dependency on VRC concentration was observable as CI were overlapping. Moreover, no tendency, i.e. de- or increasing RR, with increasing VRC concentrations was observable (Figure 3.17). The variability of RR of VRC at the individual concentrations was comparably low indicated by IQR of a minimum of 3.93% points at a concentration of 0.50 µg/mL (n=15) and a maximum of 5.86% points at a concentration of 3 µg/mL (n=30).

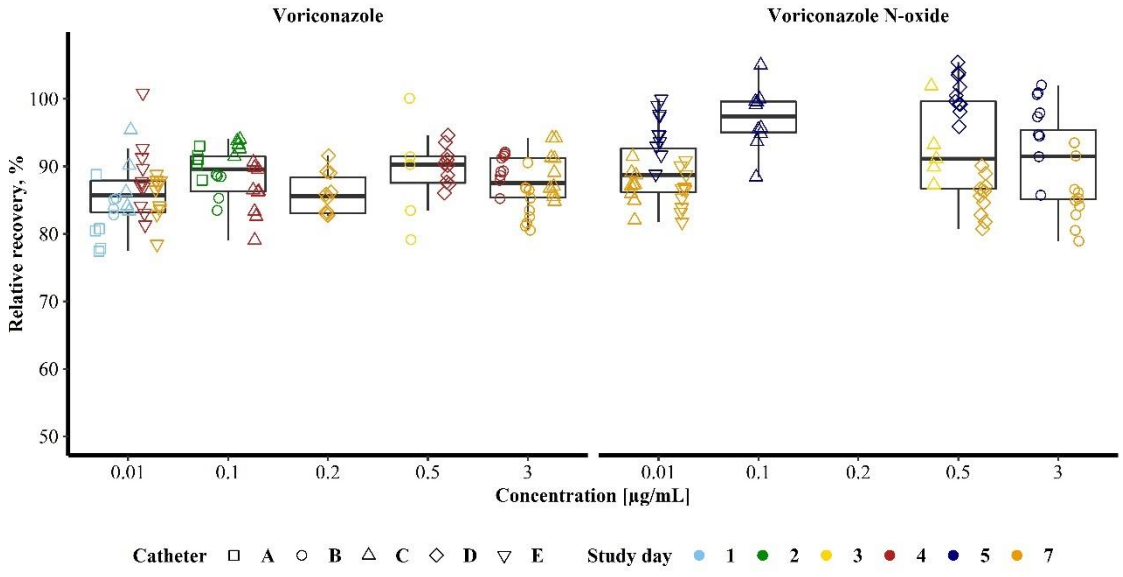

Figure 3.17: *In vitro* relative recoveries in percent of voriconazole (left panel) and its *N*-oxide metabolite (right panel) in relation to the nominal concentration. The boxes represent the interquartile ranges (IQR) including the respective median of all data points as a bold line. The upper whiskers extend to the largest value but no further than 1.5·IQR, the lower whiskers extend to the smallest value at most 1.5·IQR. Individual data points are overlaid (n=114 for voriconazole and n=85 for voriconazole *N*-oxide).

The lowest median RR for NO was observed at the lowest concentration of 0.01 µg/mL with 88.8% (95% CI: 86.7% – 91.5%, n=30) and the highest with 97.2% (95% CI: 93.7% – 100%) at the second lowest concentration of 0.10 µg/mL (n=10). Although CI were not overlapping, further

evaluations were needed to assess the significance of this observation (see chapter 3.3.4 Linear mixed-effects modelling), as all RR values at the concentration of 0.10 µg/mL derived from the same study day and the same microdialysis catheter. Moreover, no continuing trend for in- or decreasing RR with increasing NO concentrations was observable (Figure 3.17). The observed variability in RR was higher for NO than for VRC, indicated by an IQR of a minimum of 4.57% points at a concentration of 0.10 µg/mL (n=10) and a maximum of 13.0% points at a concentration of 0.50 µg/mL (n=25).

3.3.2.2 Relative recovery of voriconazole and its *N*-oxide metabolite in relation to the microdialysis catheter

For VRC, a minor influence of the used microdialysis catheter on RR was observable. Median RR were determined for every catheter, pooling data from different study days and concentrations. The catheter number was thereby allocated randomly not allowing to draw conclusions about tendencies. Median RR of VRC were 88.4% (95% CI: 77.9% – 91.6%, n=10), 86.8% (95% CI: 85.1% – 89.2%, n=34), 89.3% (95% CI: 86.2% – 91.2%, n=30), 88.2% (95% CI: 85.9% – 90.4%, n=20) and 87.1% (95% CI: 84.1% – 87.9%, n=20) for the catheters A to E, respectively (Figure 3.18).

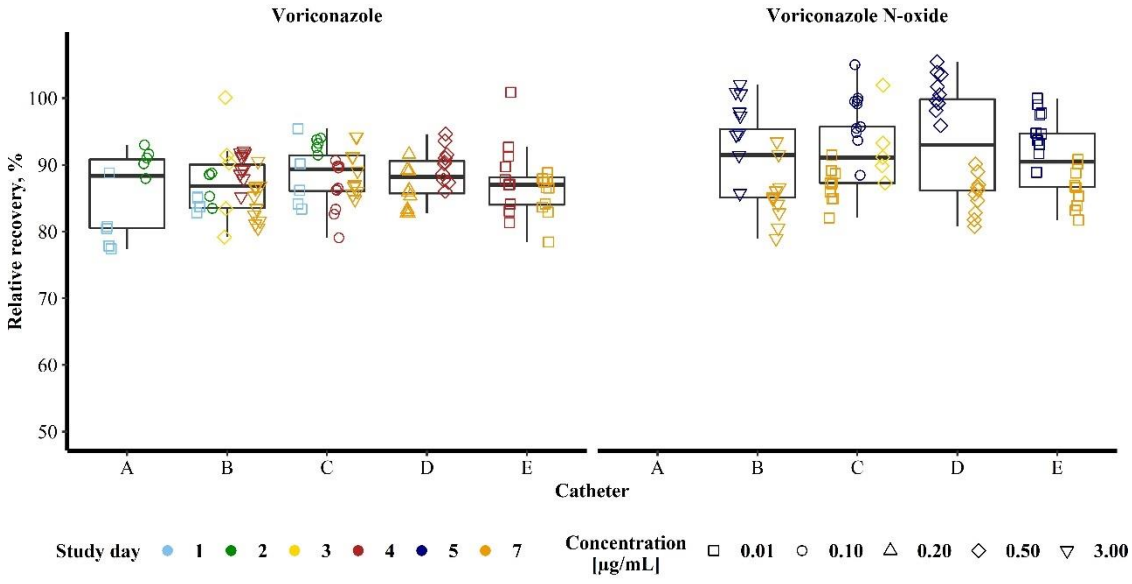

Figure 3.18: *In vitro* relative recoveries in percent of voriconazole (left panel) and its *N*-oxide metabolite (right panel) in relation to the individual microdialysis catheter. The boxes represent the interquartile ranges (IQR) including the respective median of all data points as a bold line. The upper whiskers extend to the largest value but no further than 1.5·IQR, the lower whiskers extend to the smallest value at most 1.5·IQR. Individual data points are overlaid (n=114 for voriconazole and n=85 for voriconazole *N*-oxide).

Thus, the maximum absolute detected difference in median RR between catheters was 2.5% points indicating a minor influence of the individual microdialysis catheter. Also the intracatheter variability of RR was mostly comparable with absolute IQR ranging from 4.15% (catheter E, n=20) to 6.50% (catheter B, n=34), with the exception of catheter A with an IQR of 10.3% (n=10).

For NO the observations were comparable. Here, median RR ranged from 90.5% in catheter E (n=20) to 93.0% in catheter D (n=20) (Figure 3.18), resulting in a maximum absolute difference in RR of 2.5%. Although the same microdialysis catheters were used as for VRC, intracatheter variability of RR was increased for NO with IQR of 10.2%, 8.45%, 13.7% and 7.99% points for the catheters B to E, respectively.

3.3.2.3 Relative recovery of voriconazole and its *N*-oxide metabolite in relation to the study day

Overall, the study day had the largest influence on VRC and NO RR. VRC RR was investigated on study days 1, 2, 3, 4 and 7 and resulted in median RR values of 83.9% (95% CI: 80.5% – 88.8%, n=14), 91.1% (95% CI: 88.5% – 93.1%, n=15), 90.3% (95% CI: not applicable, n=5) 89.3% (95% CI: 87.4% – 90.4%, n=40) and 86.4% (95% CI: 84.8% – 87.1%, n=40) on the respective day (Figure 3.19).

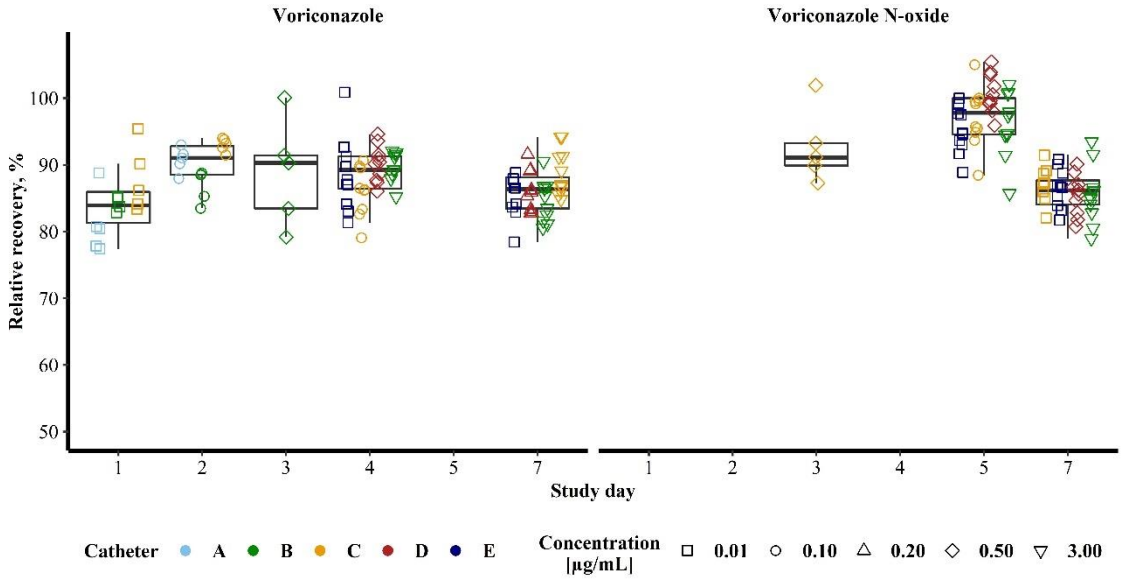

Figure 3.19: *In vitro* relative recoveries in percent of voriconazole (left panel) and its *N*-oxide metabolite (right panel) in relation to the study day. The boxes represent the interquartile ranges (IQR) including the respective median of all data points as a bold line. The upper whiskers extend to the largest value but no further than 1.5·IQR, the lower whiskers extend to the smallest value at most 1.5·IQR. Individual data points are overlaid (n=114 for voriconazole and n=85 for voriconazole *N*-oxide).

Consequently, the maximum observed absolute difference in RR between study days was 7.2%. However, within one study day RR of VRC was relatively constant and independent of catheter and VRC concentration. This was in agreement with IQR ranging from 4.26% (study day 2) to 7.95% points (study day 3).

RR of NO was investigated on study days 3, 5 and 7 and fluctuated with median RR of NO of 91.1% (95% CI: not applicable, n=5), 97.8% (95% CI: 94.9% – 99.5%, n=40) and 86.2% (95% CI: 85.0% – 87.05%, n=40), respectively, more than median RR of VRC (Figure 3.19). In particular as the variability was comparable with IQR of 3.36%, 5.39% and 3.61% points on study day 3, 5 and 7, respectively.

3.3.3 Relative recovery of voriconazole and its *N*-oxide metabolite during simultaneous microdialysis

In a second step, RR of VRC and its *N*-oxide metabolite were investigated in the presence of varying concentrations of the respective other. Pooling all data from different concentrations, catheters and study days, median RR of VRC in the presence of NO was 87.9% (95% CI: 85.3% – 90.5%, n=82). This was comparable to an absolute change in RR of 0.3% compared to RR determined in the absence of NO (Figure 3.20, A). Furthermore, not only the mere presence of NO was taken into consideration but also the respective concomitant NO concentration. An absolute decrease in VRC RR of 2.5% was observed when the combination of 0.01 µg/mL VRC plus 0.01 µg/mL NO was compared to the combination of 3 µg/mL VRC plus 3 µg/mL NO. This difference was classified as minor, as also CI were widely overlapping (Table 3.13).

Table 3.13: Median relative recovery of voriconazole and voriconazole *N*-oxide during simultaneous microdialysis of five different concentration combinations.

Concentration [µg/mL]		Median relative recovery voriconazole, %	Median relative recovery voriconazole *N*-oxide, %	n
Voriconazole	Voriconazole *N*-oxide	(95% confidence interval)	(95% confidence interval)	
0.01	0.01	87.9 (83.7 – 91.6)	86.3 (82.5 – 91.4)	18
0.20	0.50	86.4 (83.3 – 92.4)	89.1 (87.3 – 91.3)	20
0.50	0.50	95.1 (n.a.)	94.9 (n.a.)	5
3.0	0.01	87.9 (84.7 – 92.2)	95.0 (91.4 – 96.3)	19
3.0	3.0	85.4 (81.1 – 92.9)	87.4 (84.1 – 94.4)	20

n.a., not applicable due to low number of replicates

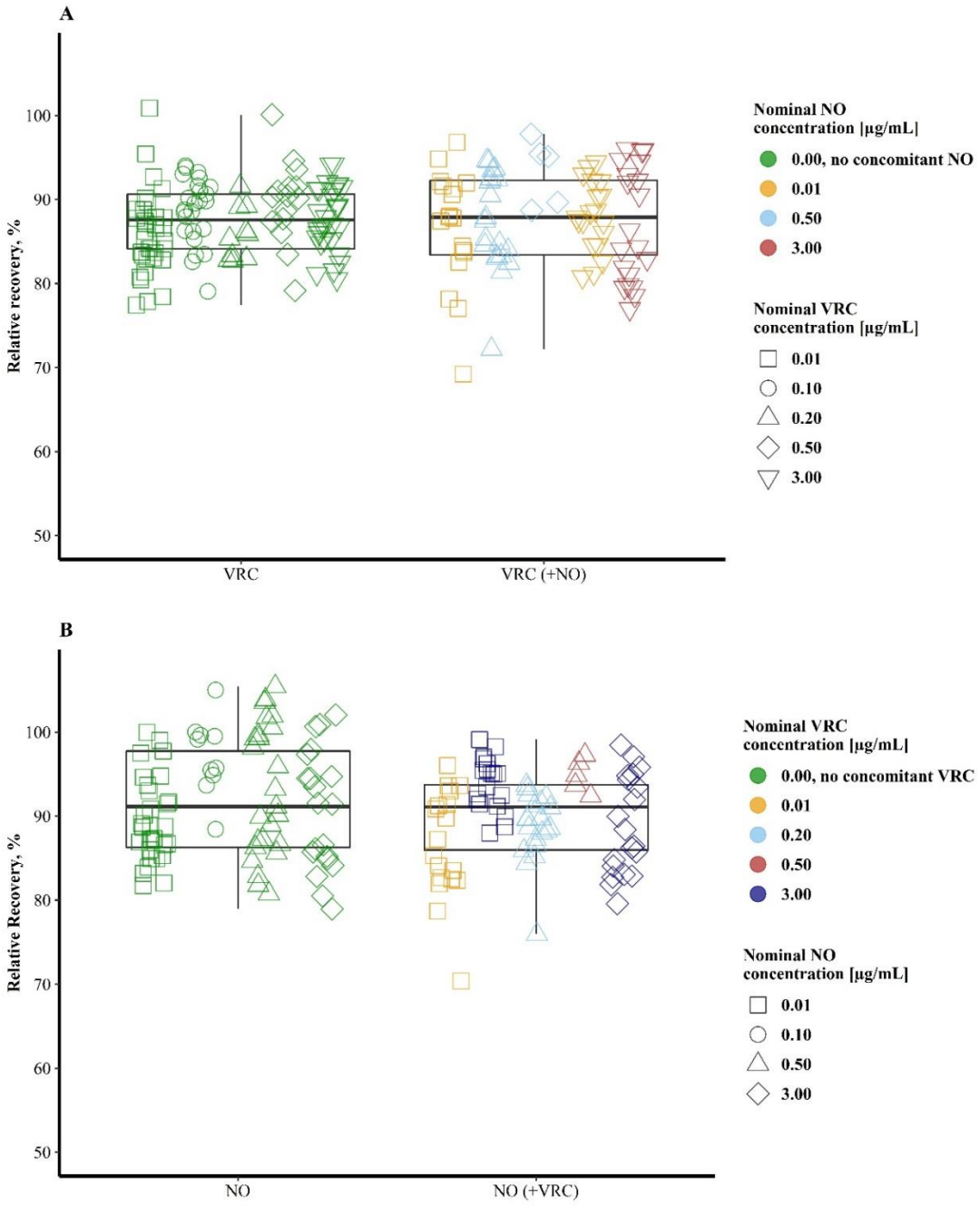

Figure 3.20: *In vitro* relative recovery of voriconazole (VRC, A) and voriconazole *N*-oxide (NO, B) in percent in the absence (left panel) and presence (right panel) of the respective other. The upper whiskers extend to the largest value but no further than 1.5·IQR, the lower whiskers extend to the smallest value at most 1.5·IQR. Individual data points are overlaid.

For NO, pooling data from all concentrations, microdialysis catheters and study days, median RR in the presence of VRC resulted in 91.1% (95% CI: 88.4% – 94.5%, n=82) and hence no shift was observed compared to determinations in individual microdialysis investigations (Figure 3.20, B).

The concomitant VRC concentration did not have a large impact on RR of NO. A difference in absolute RR of NO of +1.1% was observed when comparing the combination of 0.01 and 0.01 µg/mL to the combination of 3.0 and 3.0 µg/mL VRC and NO (Table 3.13). The combination of a high VRC concentration (3.0 µg/mL) with a low NO concentration (0.01 µg/mL) led to a slightly increased RR for NO of 95.0%. However, CI were still overlapping, indicating a negligible effect (Table 3.13).

3.3.4 Linear mixed-effects modelling

All exploratory and graphical assessments were confirmed and furthermore quantified by an LME model enabling the *simultaneous* consideration of all potentially influencing factors. In this model, RR of VRC in the absence of NO was set as the reference scenario, which resulted in an estimated RR of 89.7% (a_0, Table 3.14). No significant influence of compound concentration was revealed within the investigated concentration range with a small a_2 value (slope) and its 95% CI including zero ($p \geq 0.05$, Table 3.14). Moreover, the absolute deviations in RR of the other three scenarios in comparison to RR of VRC individual microdialysis were not significant with 95% CI including zero and p-values >0.05 (Table 3.14).

Table 3.14: Parameter estimates for the fixed effects of the linear mixed-effects model evaluating the dependence of the *in vitro* relative recovery (RR) on the nominal concentration and the investigated scenario, i.e. voriconazole (VRC) and its *N*-oxide metabolite (NO) in the absence of the respective other and the combination.

Parameter	Estimate	95% confidence interval of estimate	P-value
a_0			
RR of VRC	89.7%	86.2% – 93.3%	$1.8 \cdot 10^{-11}$
a_1			
ΔRR of VRC + NO	-1.56%	-3.18% – +0.113%	0.0636
ΔRR of NO	0.473%	-1.24% – +2.28%	0.5936
ΔRR of NO + VRC	0.868%	-0.757% – +2.54%	0.3014
a_2	0.309 mL/µg	-0.254 – +0.900 mL/µg	0.2840

a_0, intercept of the linear regression function corresponding to the estimated individual RR of voriconazole (= ”reference scenario”); a_1, absolute deviation in RR for the three scenarios; a_2, slope of the linear regression, i.e. change of RR in function of the concentration.

The random effects could explain in total 51.2% of the observed variance. Here, the study day was the most important factor, which explained a standard deviation (SD) of 4.10% points on RR and had a share of 46.3% in the total variance. In contrast, the individual microdialysis catheter only entailed an absolute variability of 1.25% (SD) and caused thus 4.33% of the total variance. A further SD of 4.23% points remained unexplained which equalled 49.4% of the total variance in the data.

3.3.5 *In vitro* retrodialysis

Concentrations of VRC and NO in catheter-surrounding medium were determined by direct measurement as well as by VRC retrodialysis. At a nominal concentration of 0.01 µg/mL VRC, median concentrations in catheter-surrounding medium determined by retrodialysis (n=8-10 each) at the two days of investigation were -12.8% and -9.2% lower than the median of directly measured concentrations (n=6 each). At a concentration of 0.02 µg/mL (n=10 each retrodialysis, n=6 each direct measurement) the deviation was -13.8% and -4.2%. For higher concentrations of VRC (3 µg/mL) four investigations were performed and resulted in deviations of -1.6%, +1.6%, -7.1% and -12.9% (n=9-10 each retrodialysis, n=6 each direct measurement) respectively.

Also for NO, retrodialysis of VRC was applied. At a nominal concentration of 0.01 µg/mL NO, median concentrations in catheter-surrounding medium determined by retrodialysis (n=8-10 each) were at the four investigations -14.9%, -3.0%, -5.0% and -1.5% lower than the median of directly measured concentrations (n=6 each). The deviation at a concentration of 0.50 µg/mL NO was -5.9% and -4.6% at the two study days (n=9-10 each retrodialysis, n=6 each direct measurement), respectively. Lastly, at a nominal concentration of 3.0 µg/mL NO retrodialysis resulted in median concentrations of -9.7% and +0.4% compared to direct measurements (n=10 each retrodialysis, n=6 each direct measurement).

3.4 Clinical microdialysis trial for the determination of voriconazole and its *N*-oxide metabolite concentrations in plasma, ultrafiltrate and interstitial space fluid

In the following sections, the results of the simultaneous determination of VRC and NO in samples of the clinical microdialysis trial in healthy volunteers will be presented. In detail, a PK data analysis was performed for VRC and NO in plasma, ultrafiltrate and microdialysate, focussing on the evaluation of the f_u in plasma (chapter 3.4.2.1), concentration-time profiles (chapter 3.4.2.2), the total exposure (chapter 3.4.2.3) and metabolic ratios (chapter 3.4.2.4) with regard to the CYP2C19 genotype-predicted phenotype of the individuals as well as the respective VRC dosing interval.

3.4.1 Bioanalysis of study samples

The developed and validated bioanalytical method described in chapter 3.1 was applied to overall 212 human plasma, 209 ultrafiltrate and 284 microdialysate clinical trial samples. The performance of the assay was investigated by the continuous evaluation of CAL and QC samples within the analytical runs as requested by the EMA guideline on bioanalytical method validation [139].

In total, four analytical runs were performed to simultaneously quantify VRC and NO concentrations in the matrices of plasma, ultrafiltrate and microdialysate, respectively. The seven CAL samples and the blank and zero sample, were prepared freshly in plasma, covering a range from 0.005 – 5 µg/mL, and microdialysate, covering a range from 0.004 – 4 µg/mL. VRC and NO concentrations were calculated using a linear regression model (chapter 2.2.2.2), which resulted in the calibration function parameters presented in Table 3.15.

Table 3.15: Parameters (slope, intercept, R^2) of voriconazole and voriconazole *N*-oxide calibration functions in human plasma and microdialysate of the different bioanalytical runs during the application of the liquid chromatography-tandem mass spectrometry assay to clinical trial samples.

Compound	**Run**	**Plasma**			**Microdialysate**		
		Slope	Intercept	R^2	Slope	Intercept	R^2
Vori-conazole	1	$7.66 \cdot 10^{-4}$	$0.0560 \cdot 10^{-4}$	0.9933	$9.00 \cdot 10^{-4}$	$2.15 \cdot 10^{-4}$	0.9931
	2	$11.5 \cdot 10^{-4}$	$8.32 \cdot 10^{-4}$	0.9897	$4.79 \cdot 10^{-4}$	$0.128 \cdot 10^{-4}$	0.9905
Vori-conazole *N*-oxide	1	$2.63 \cdot 10^{-4}$	$-0.275 \cdot 10^{-4}$	0.9960	$5.26 \cdot 10^{-4}$	$0.982 \cdot 10^{-4}$	0.9981
	2	$4.15 \cdot 10^{-4}$	$2.21 \cdot 10^{-4}$	0.9875	$2.19 \cdot 10^{-4}$	$1.21 \cdot 10^{-4}$	0.9939

For VRC and NO in plasma and microdialysate, overall, only 3.06% of CAL (n=98) and 7.87% of individual QC samples (n=89) were outside the allowed ±15% accuracy range (±20% at the LLOQ). For each of the four QC levels (>LLOQ) in plasma and microdialysate, mean accuracy and precision was determined across all analytical runs. In summary, the method performance conformed with the EMA guideline requirements with a mean accuracy in plasma (n=6 per level) ranging from 101% to 109% for VRC and from 94.8% to 105% for NO. In microdialysate, mean accuracy (n=5 per level) was between 100% and 109% for VRC and between 96.2 and 98.6% for NO (Figure 3.21). The imprecision determined as CV ranged from a minimum of 2.10% for NO in microdialysate at a concentration of 1.2 µg/mL (n=5) to a maximum of 12.4% for VRC in plasma at a concentration of 1.5 µg/mL (n=6). Based on these results all analytical runs were accepted for further evaluation of the study samples.

Due to the low LLOQ, from the total 705 samples, besides the baseline samples that were taken before VRC administration, only one microdialysate sample was below the LLOQ for VRC and NO and was thus not considered in the further analysis.

The difference in the number of evaluated plasma and ultrafiltrate samples was based on the unavailability of three of the original ultrafiltrate samples. Ultrafiltration of the respective plasma samples was not repeated for reasons of comparability. Furthermore, three microdialysate samples from the RM/PM in the fifth dosing interval were not available due to a necessary catheter replacement.

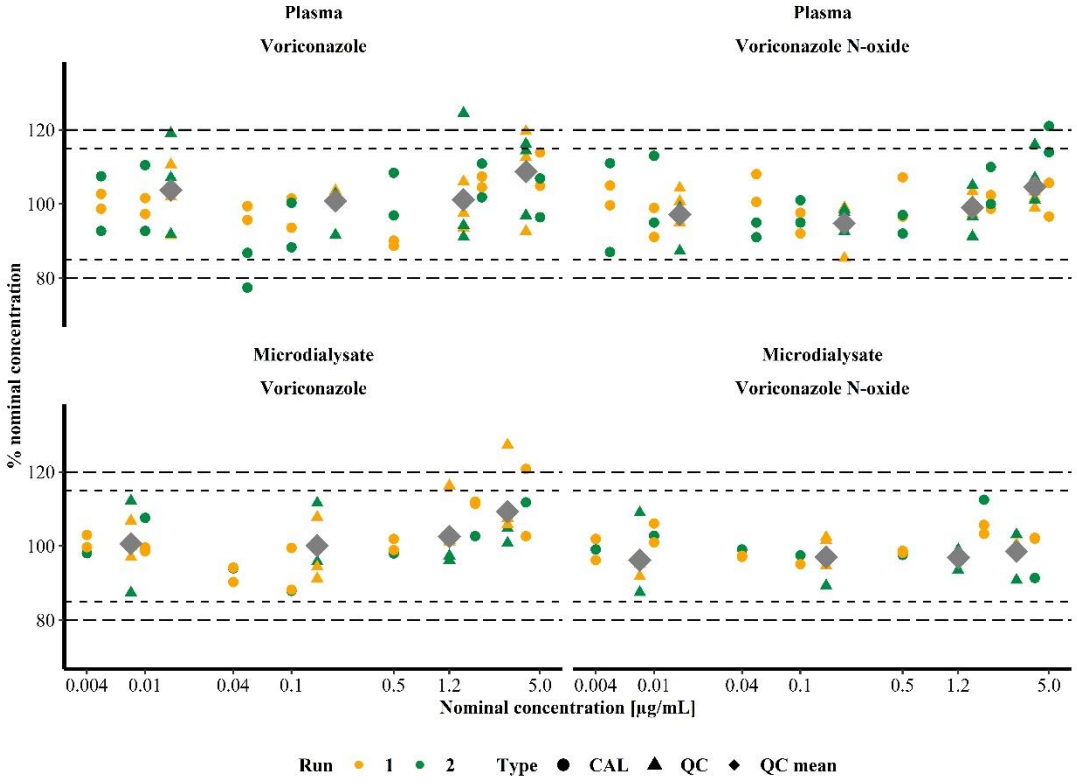

Figure 3.21: Accuracy of voriconazole (VRC) and voriconazole *N*-oxide calibrator (CAL) and quality control (QC) samples in plasma and microdialysate for the different bioanalytical runs during the application of the liquid chromatography-tandem mass spectrometry assay. The data is presented as percentage of its nominal concentration. Dashed lines indicate the accuracy limits of ±15% and ±20% for the lower limit of quantification, respectively.

3.4.2 Pharmacokinetic data analysis for clinical trial samples in plasma, ultrafiltrate and microdialysate

Subsequently to the bioanalysis of all available study samples, the individual PK of VRC and NO of the four healthy individuals was evaluated for total as well as unbound plasma (ultrafiltrate) and ISF concentrations. In detail, the f_u in plasma was investigated (chapter 3.4.2.1) as well as concentration-time profiles (chapter 3.4.2.2), the total exposure (chapter 3.4.2.3) and metabolic

ratios (chapter 3.4.2.4) were evaluated. The administered i.v. doses on day one ranged from 390 to 461 mg and on day two from 260 to 307 mg compared to the lower flat 200 mg p.o. doses on days three and four.

3.4.2.1 Fraction unbound in plasma of voriconazole and its *N*-oxide metabolite

Based on the concentrations determined for VRC and NO in plasma and ultrafiltrate the f_u for VRC and NO was determined. For VRC median f_u was 0.628 covering a range from 0.403 to 1.09. There was no considerable difference of f_u between the four healthy volunteers. The RM, NM, RM/PM and IM revealed median f_u for VRC of 0.649 (range: 0.555 – 0.765), 0.621 (range: 0.434 – 0.714), 0.643 (range: 0.512 – 1.09) and 0.607 (range: 0.403 – 0.847), respectively. No trend of changing f_u with increasing VRC concentrations was observable, as individual determinations of f_u scattered randomly around the median (Figure 3.22). Additionally, no tendencies of decreasing or increasing f_u over time were detectable (Figure 7.6).

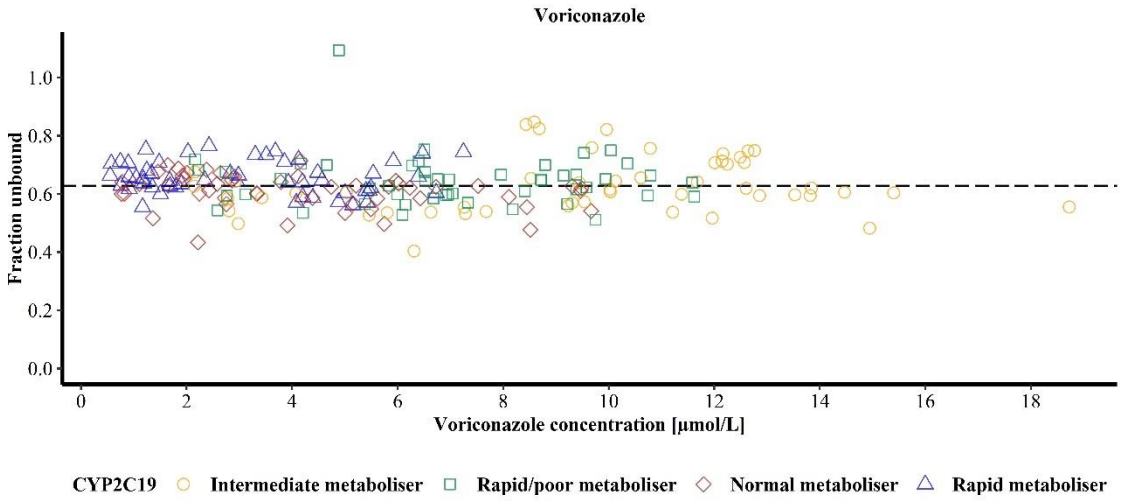

Figure 3.22: Fraction unbound of voriconazole in relation to the total voriconazole plasma concentration for four healthy volunteers determined by ultrafiltration. The dashed line represents the median fraction unbound of all volunteers and all samples.

For NO overall, a median f_u of 0.566 with a range from 0.251 to 0.908 was determined. The four individuals showed considerable differences in the determined f_u. For the CYP2C19 RM, RM/PM, NM and IM the assessment of median f_u resulted in 0.717 (range: 0.615 – 0.908), 0.704 (range: 0.555 – 0.790), 0.476 (range: 0.254 – 0.566) and 0.450 (range: 0.251 – 0.522), respectively. Also, for NO no trend of decreasing or increasing f_u across NO concentration was detectable (Figure 3.23). Furthermore, there were no trends in f_u of NO over time for all individuals (Figure 7.7).

However, it was noticeable, that the RM and NM as well as the RM/PM and IM showed very similar f_u whereas the differences in f_u between the two groups were distinct. Consequently,

potential reasons for the observed deviations were investigated. In this process, an anomaly was found in the bioanalysis of the study samples. All ultrafiltrate samples of the two individuals with lower f_u showed for NO a second larger peak in the chromatograms at a slightly later retention time (Figure 7.8). This peak was absent in chromatograms of ultrafiltrate samples of the RM and NM. Due to the application of a dMRM method, this peak had to have the same precursor as well as product ion as NO to be detected. Yet, because of the different retention time, a chemical modification was likely. Overall, it was concluded that ultrafiltrate samples of NO of the IM and RM/PM had to be evaluated with some caution. Thus, the f_u of NO was reassessed without the two individuals and resulted in a median of 0.713 (range: 0.555 – 0.908).

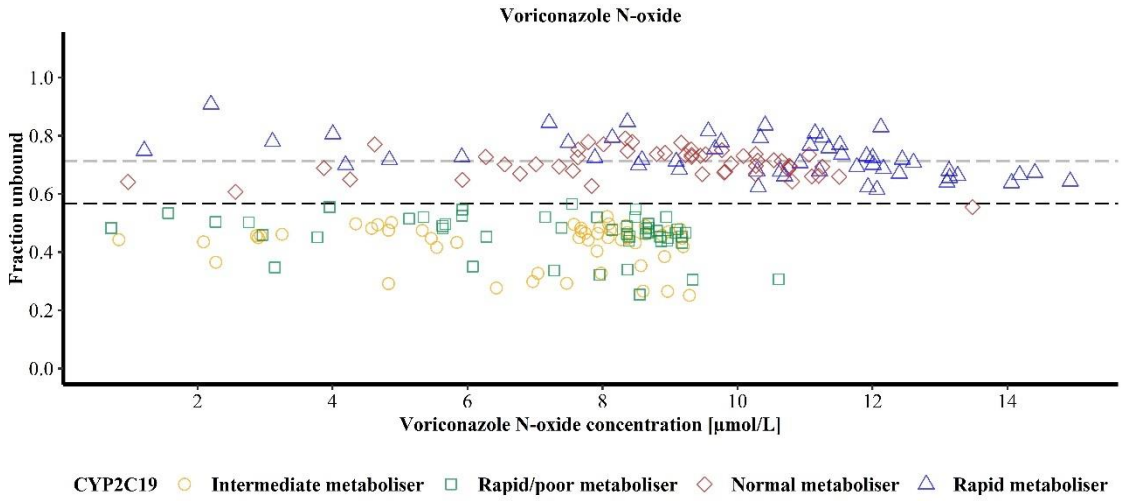

Figure 3.23: Fraction unbound of voriconazole *N*-oxide in relation to the total voriconazole *N*-oxide plasma concentration for four healthy volunteers determined by ultrafiltration. The black dashed line represents the median fraction unbound of all volunteers and all samples and the grey dashed line depicts the median fraction unbound of the CYP2C19 rapid and normal metaboliser (see text for explanation).

3.4.2.2 Concentration-time profiles and pharmacokinetic target attainment

Plasma. In total, across all dosing intervals VRC and NO plasma concentrations ranged from 0.553 to 18.7 µmol/L and from 0.720 to 14.9 µmol/L, respectively. Overall, the CYP2C19 IM showed the highest VRC and lowest NO concentrations, whereas the CYP2C19 RM revealed the lowest VRC and highest NO concentrations, respectively. Interindividual differences substantially increased for VRC plasma concentrations from the first to the last dose, while for NO it was relatively stable (Figure 3.24).

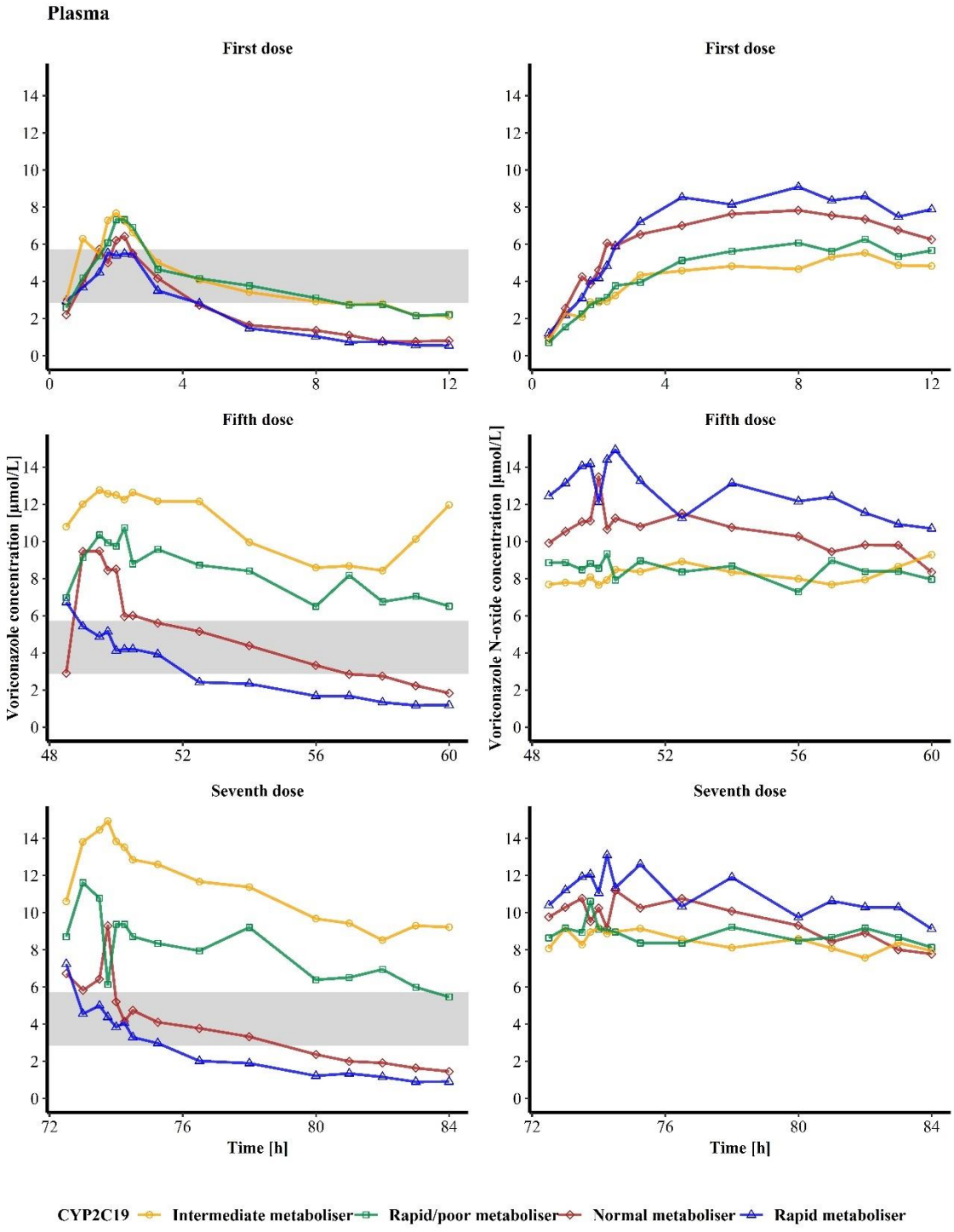

Figure 3.24: Concentration-time profiles of voriconazole (left) and its *N*-oxide metabolite (right) in plasma in the first, fifth and seventh dosing interval after continuous twice daily voriconazole administration to four healthy volunteers with different CYP2C19 genotype-predicted phenotypes. Time is presented as hours after the first VRC dose administration. The shaded area shows the recommended lower therapeutic target threshold of total voriconazole minimum plasma concentration (2.86 – 5.73 µmol/L) [174,180].

C_{max} values were assessed in dosing intervals with intensive sampling to ensure the correct capture over time and were influenced by the CYP2C19 genotype-predicted phenotype of the four volunteers (Table 3.16).

Maximum plasma concentrations of VRC and NO occurred at earlier times (t_{max}) after multiple dosing. After the first VRC administration, VRC C_{max} was reached after 1.75 to 2.25 h. After the fifth and seventh dosing, t_{max} for VRC declined to 0.5-2.25 h and 0.5-1.75 h, respectively.

NO C_{max} after the first VRC dose administration was observed considerably later with a t_{max} of 8 to 10 h, depending on the individual subject, reflecting the delayed metabolism of VRC. However, the plateau-like NO plasma concentrations after multiple dosing precluded a meaningful specification of t_{max} in the fifth and seventh dosing interval.

Table 3.16: Maximum plasma concentrations of voriconazole and voriconazole *N*-oxide of four healthy male adults with different CYP2C19 genotype-predicted phenotypes for the respective dosing interval.

CYP2C19 metaboliser	**Maximum plasma concentration [µmol/L]**					
	Voriconazole			**Voriconazole *N*-oxide**		
	Dosing interval			**Dosing interval**		
	1	**5**	**7**	**1**	**5**	**7**
Rapid metaboliser	5.54	6.73	7.24	9.09	14.9	13.1
Normal metaboliser	6.43	9.48	9.31	7.84	13.5	11.2
Rapid/poor metaboliser	7.33	10.7	11.6	6.28	9.33	10.6
Intermediate metaboliser	7.68	12.8	14.9	5.54	9.29	9.19

Regarding the PK target, the lower threshold was not met after the first VRC dose by any of the four volunteers with a maximum C_{min} of 2.22 µmol/L for the CYP2C19 RM/PM. After the second VRC dose, the IM and RM/PM exceeded the C_{min} threshold with 5.80 µmol/L and 5.83 µmol/L, respectively. The NM and RM did not reach the necessary C_{min} range in any of the dosing intervals (maximum observed C_{min}: for NM, 2.65 µmol/L after the fourth VRC dose; for RM, 1.79 µmol/L after the second dose). The upper limit of C_{min} of 12.9 – 17.2 µmol/L was never exceeded with a maximum observed C_{min} of 12.0 µmol/L in the CYP2C19 IM after the fifth VRC dose (Figure 3.25). No PK target range for C_{min} of NO has been defined yet. In the first dosing interval, C_{min} ranged from 4.83 (IM) to 7.89 µmol/L (RM) and increased for all individuals until the last i.v. dose before decreasing slightly again until the end of the trial. Overall, a general trend was observable, that the interindividual difference of VRC plasma C_{min} increased with multiple dosing, whereas the interindividual difference of C_{min} of NO reached the highest level after the second dose before decreasing until the sixth VRC dose administration (Figure 3.25).

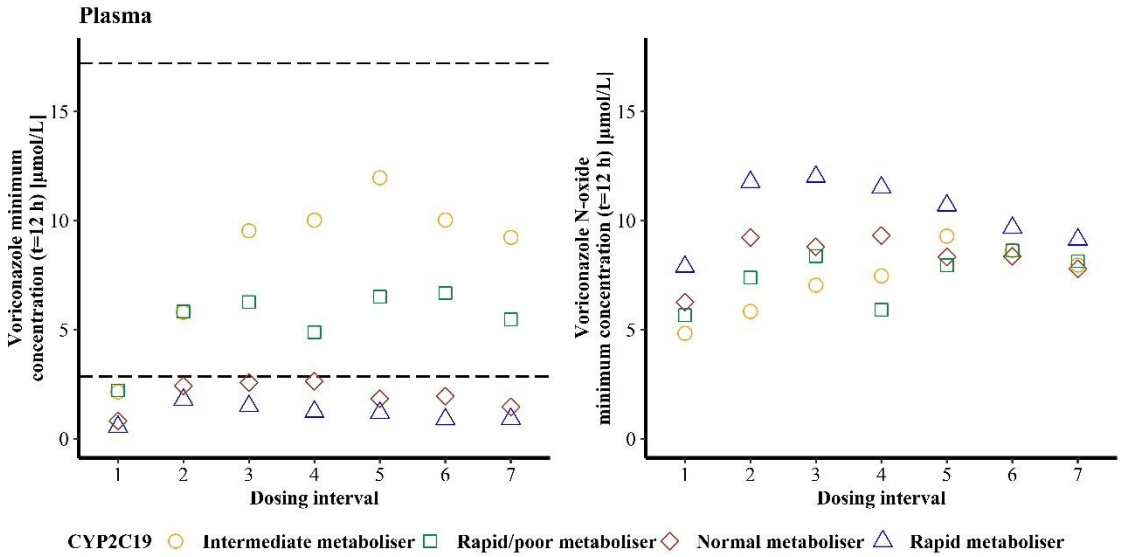

Figure 3.25: Voriconazole (left) and voriconazole *N*-oxide (right) minimum total plasma concentrations determined 12 h after voriconazole dose administration in function of the respective dosing interval (1 to 7) of four healthy volunteers with different CYP2C19 genotype-predicted phenotypes. The dashed lines indicate the recommended therapeutic target range of total voriconazole minimum plasma concentration (2.86 – 17.2 µmol/L) [174,180].

Ultrafiltrate. VRC and NO concentrations determined in ultrafiltrate, reflected the unbound plasma concentrations. Across all dosing intervals, concentrations in ultrafiltrate ranged from 0.366 to 10.4 µmol/L for VRC and from 0.348 to 10.1 µmol/L for NO. In the first dosing interval, the CYP2C19 RM and NM as well as the RM/PM and IM showed very similar VRC concentration-time profiles. However, for NO, similar concentrations were only observed for the RM/PM and IM but the RM exceeded the NM regarding NO concentrations. In the fifth and seventh dosing interval the IM showed the highest and the RM the lowest VRC concentrations, while for the RM the highest NO concentrations were observed. The RM/PM and IM revealed still similar NO concentrations in the fifth dosing interval before NO concentrations of the IM fell below those of the RM/PM in the seventh dosing interval. The interindividual differences in VRC concentration-time profiles increased substantially with multiple dosing, whereas for NO, only a slight rise was observable (Figure 3.26).

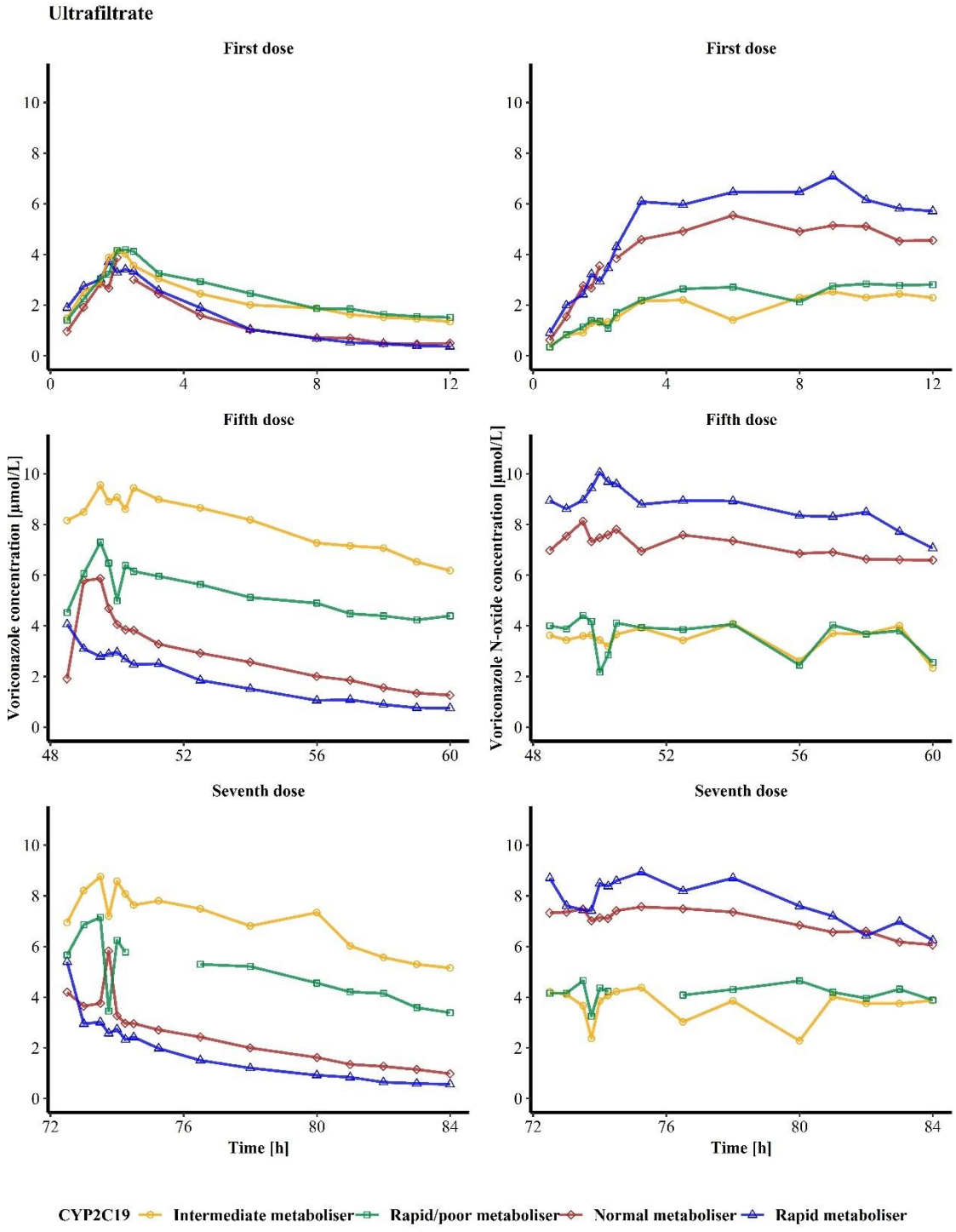

Figure 3.26: Concentration-time profiles of voriconazole (left) and its *N*-oxide metabolite (right) in ultrafiltrate in the first, fifth and seventh dosing interval after continuous twice daily voriconazole administration to four healthy volunteers with different CYP2C19 genotype-predicted phenotypes. Time is presented as hours after the first VRC dose administration.

In ultrafiltrate, C_{max} (Table 3.17) of VRC and NO occurred at comparable times after VRC dose administration as in plasma. For VRC t_{max} in the first dosing interval occurred between 1.75 and 2.25 h and for NO between 6 and 10 h. After multiple dosing t_{max} for VRC appeared at earlier times, i.e. after 0.5 – 1.75 h after VRC administration in the fifth and seventh dosing interval.

For NO, a plateau-like profile was observed in the fifth and seventh doing interval preventing a meaningful determination of t_{max} (Figure 3.26).

Table 3.17: Maximum concentrations of voriconazole and voriconazole *N*-oxide determined in ultrafiltrate of four healthy male adults with different CYP2C19 genotype-predicted phenotypes for the respective dosing interval.

CYP2C19 metaboliser	**Maximum ultrafiltrate concentration [µmol/L]**					
	Voriconazole			**Voriconazole *N*-oxide**		
	Dosing interval			**Dosing interval**		
	1	**5**	**7**	**1**	**5**	**7**
Rapid metaboliser	3.71	4.07	5.40	7.09	10.1	8.93
Normal metaboliser	3.89	5.87	5.83	5.55	7.81	7.57
Rapid/poor metaboliser	4.19	7.30	7.16	2.84	4.11	4.66
Intermediate metaboliser	4.14	9.56	8.76	2.53	4.09	4.38

C_{min} of VRC and NO in ultrafiltrate were lower compared to plasma. All individuals revealed the highest C_{min} for VRC after the fourth VRC dose administration, except for the CYP2C19 RM, who showed the highest VRC C_{min} in the second dosing interval. Thereby, C_{min} were increased 3.0-, 3.6-, 3.5-, and 4.6-fold for the RM, NM, RM/PM and IM compared to the first dosing interval, respectively. Until the end of the trial, C_{min} decreased again by a maximum of 44.4% (NM) compared to its maximum (Figure 3.27). For NO, C_{min} in ultrafiltrate revealed greater fluctuations. The maximum of C_{min} was reached after the fourth VRC dose administration for the CYP2C19 RM and NM, as well as after the sixth dose administration for the RM/PM and IM. This corresponded to a 1.6-, 1.5-, 1.4- and 1.8-fold increase in NO C_{min} for the RM, NM, RM/PM and IM compared to the first dosing interval, respectively. After the last VRC dose administration of this trial, C_{min} of NO was decreased by a maximum of 29.5% (RM) compared to its peak concentration (Figure 3.27).

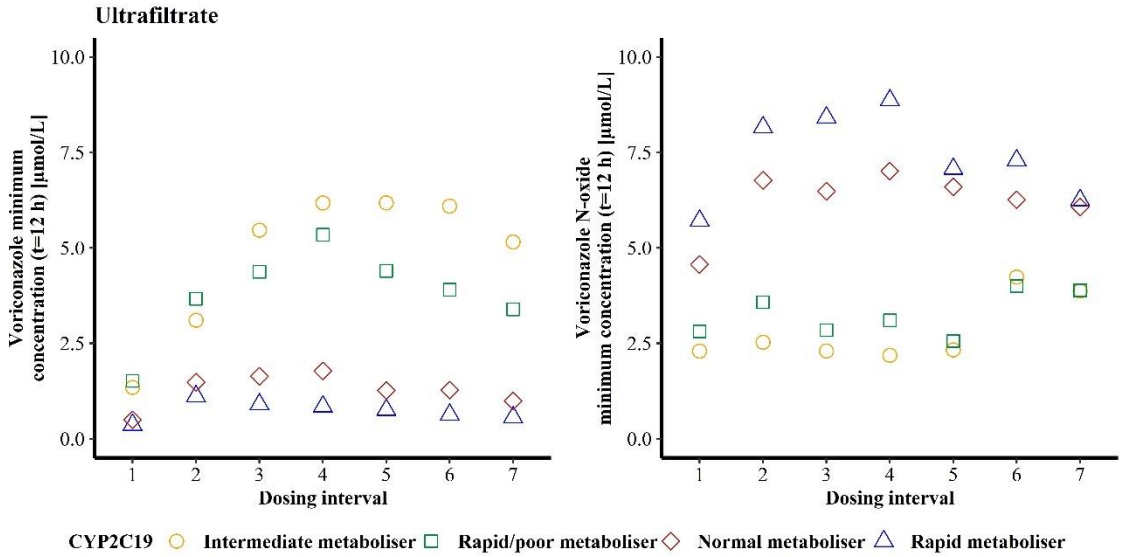

Figure 3.27: Voriconazole (left) and voriconazole *N*-oxide (right) minimum unbound plasma concentrations determined 12 h after voriconazole dose administration in function of the respective dosing interval (1 to 7) of four healthy volunteers with different CYP2C19 genotype-predicted phenotypes.

Interstitial space fluid. Microdialysate concentrations were transformed to ISF concentrations by taking RR into account, which was determined individually for all four volunteers subsequently to the third and seventh (last) dosing interval by VRC retrodialysis. Except for the CYP2C19 RM/PM, the mean of both RR determinations of each individual was applied to calculate ISF concentrations. As the microdialysis catheter of the RM/PM had to be replaced during the fifth dosing interval, RR determination for the individual catheter was used for ISF concentration determination. Overall RR was high and ranged from 75.2% to 96.8% for the individually performed retrodialysis investigations.

VRC, as well as NO, showed relevant distribution into ISF. Across all dosing intervals, ISF concentrations ranged from 0.0610 to 10.7 µmol/L for VRC and from 0.0231 to 5.47 µmol/L for NO, respectively. In the first dosing interval the CYP2C19 NM and RM showed very similar concentration-time curves, revealing the highest VRC concentrations until approximately four hours after VRC administration. Afterwards, the RM/PM exhibited the highest VRC concentrations. However, in the fifth and seventh dosing interval, it was the CYP2C19 IM revealing the highest and the RM showing the lowest VRC concentrations. For NO the CYP2C19 IM had the lowest concentrations at all times while the RM and NM showed comparable profiles in the first dosing interval before NO concentrations of the NM exceeded those of the RM in the fifth and seventh dosing interval. Similar to observations in plasma, in ISF the interindividual differences of VRC concentrations increased with multiple dosing. However, in ISF this observation was also true for NO (Figure 3.28).

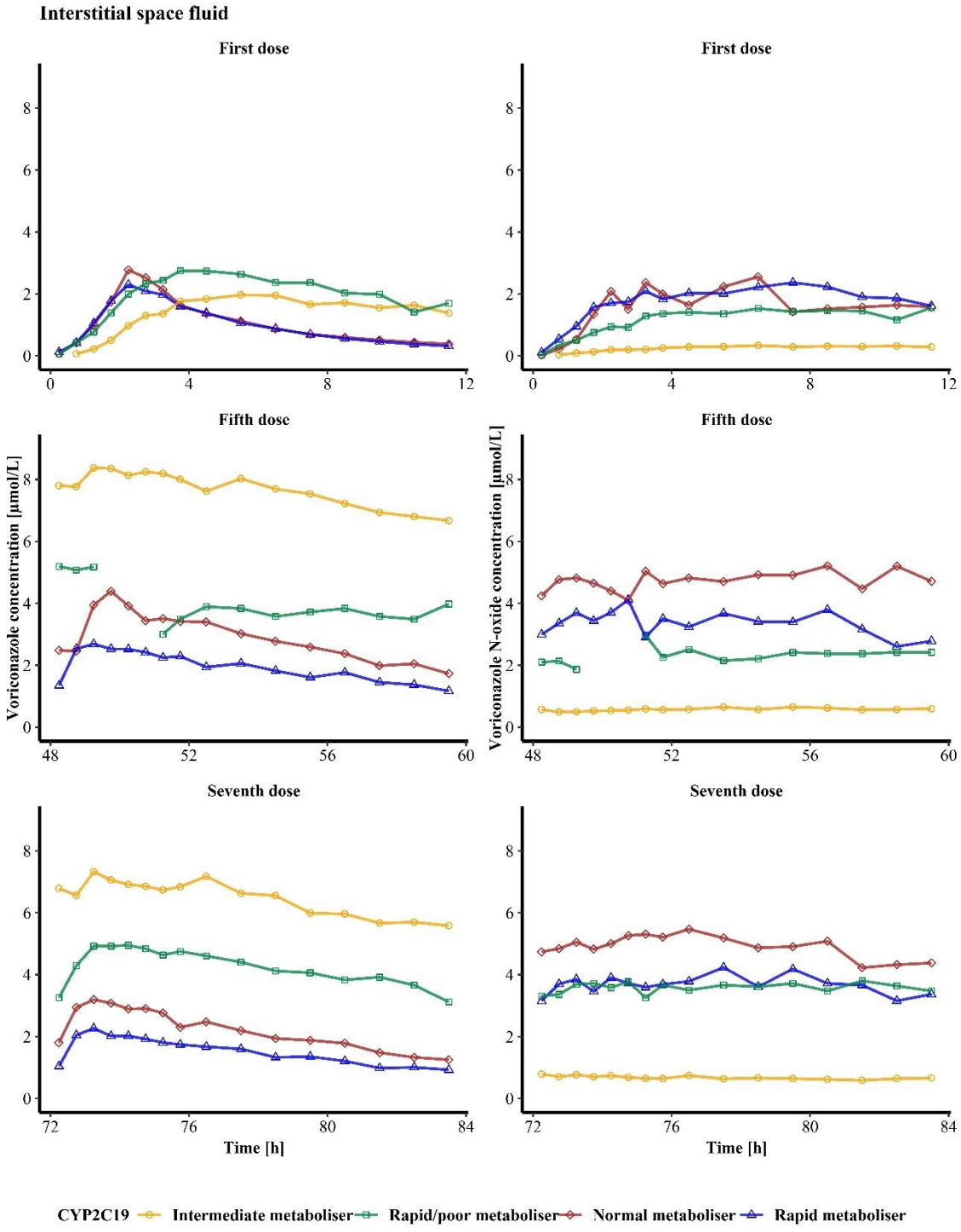

Figure 3.28: Concentration-time profiles of voriconazole (left) and its *N*-oxide metabolite (right) in interstitial space fluid in the first, fifth and seventh dosing interval after continuous twice daily voriconazole administration to four healthy volunteers with different CYP2C19 genotypes. Time is presented as hours after the first VRC dose administration. The data points are represented as midtime point of the microdialysis sampling interval.

In ISF, C_{max} (Table 3.18) of VRC occurred at earlier times after multiple dosing. Overall, the t_{max} of VRC ranged between 2.25 and 5.5 h for the four individuals in the first doing interval, from 0.25 to 1.75 h in the fifth and from 1.25 to 2.25 h in the seventh dosing interval. Some caution is required with the interpretation of t_{max} as midtime points of the sampling intervals were allocated to the respective concentrations. Additionally, for the RM/PM three samples in the fifth dosing interval were missing in the crucial time period. Overall, t_{max} of VRC did not differ substantially from plasma suggesting a fast distribution into ISF.

For NO, t_{max} in ISF was reached in the first dosing interval after 6 – 12 h indicating the time lag for the transformation of VRC. Furthermore, t_{max} of NO in ISF was similar to t_{max} in plasma, supporting a comparable fast distribution of NO into ISF as for VRC. In the fifth and seventh dosing interval, NO concentrations were plateau-like, impeding an assessment of t_{max} (Figure 3.28).

Table 3.18: Maximum interstitial space fluid (ISF) concentrations of voriconazole and voriconazole *N*-oxide of four healthy male adults with different CYP2C19 genotype-predicted phenotypes for the respective dosing interval.

CYP2C19 metaboliser	**Maximum ISF concentration [µmol/L]**					
	Voriconazole			**Voriconazole *N*-oxide**		
	Dosing interval			**Dosing interval**		
	1	**5**	**7**	**1**	**5**	**7**
Rapid metaboliser	2.30	2.69	2.27	2.37	4.12	4.24
Normal metaboliser	2.77	4.40	3.20	2.55	5.21	5.47
Rapid/poor metaboliser	2.75	5.20	4.95	1.56	2.97	3.81
Intermediate metaboliser	1.97	8.37	7.34	0.338	0.651	0.791

C_{min} of VRC and NO in ISF were available for the first, fifth and seventh dosing interval. Overall, C_{min} of VRC in ISF was lower compared to plasma and ultrafiltrate. In the fifth dosing interval, C_{min} were approximately 2- to 5-fold increased compared to the first dosing interval, before an approximately 16%-28% decrease in the seventh dosing interval compared to the fifth occurred (Figure 3.29). Similarly to VRC, C_{min} of NO in ISF increased 1.6- to 3-fold in the fifth dosing interval compared to the first. However, in the seventh dosing interval C_{min} of NO were increased by 10%-30% compared to the fifth, except for the CYP2C19 NM whose C_{min} decreased by 7% (Figure 3.29).

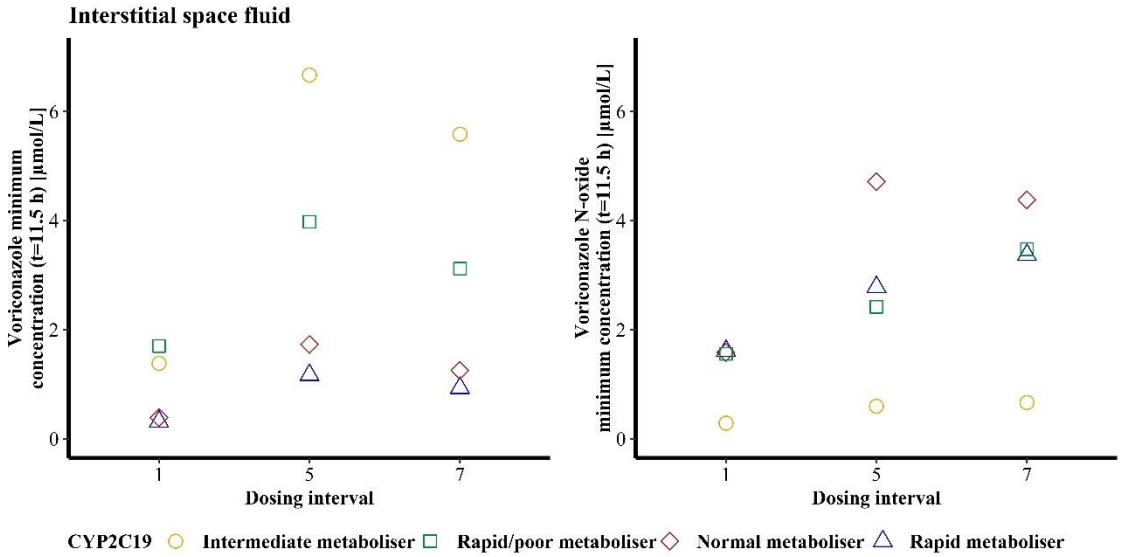

Figure 3.29: Voriconazole (left) and voriconazole *N*-oxide (right) minimum ISF concentrations determined 12 h after voriconazole dose administration in function of the respective dosing interval (1, 5 and 7) of four healthy volunteers with different CYP2C19 genotype-predicted phenotypes.

3.4.2.3 Total exposure of voriconazole and its *N*-oxide metabolite in plasma, ultrafiltrate and interstitial space fluid

VRC exposure in plasma, assessed by the AUC, was highest for the CYP2C19 IM and lowest for the RM. In the first dosing interval, the interindividual difference was the lowest with AUC ranging from 25.5 to 45.3 µmol·h/L, and consequently a 1.8-fold difference between the RM and NM was observed. In the fifth and seventh dosing interval, interindividual differences increased considerably with AUC of VRC ranging from 31.9 to 124 µmol·h/L and 27.2 to 130 µmol·h/L, respectively, indicating a 3.9- and 4.8-fold lower VRC exposure in plasma for the IM compared to the RM.

The NO exposure pattern in plasma was vice versa: the highest AUC were determined for the RM and the lowest for the IM. In contrast to VRC, the interindividual differences remained relatively constant across the dosing intervals. In the first dosing interval AUC of NO in plasma ranged from 50.4 to 84.3 µmol·h/L, which was equivalent to a 1.7-fold difference between the RM and the IM. In the fifth dosing interval, the AUC of NO overall increased, stretching from 96.9 to 146 µmol·h/L, yet the interindividual difference was comparable to the first dosing interval with a 1.5-fold difference between the RM and IM. The total exposure for NO in the seventh dosing interval changed only slightly with AUC ranging from 99.0 to 128 µmol·h/L, marking a 1.3-fold difference between the RM and IM (Figure 3.30).

In ultrafiltrate, the determined AUC of VRC were lower compared to plasma. However, except for the first dosing interval in which the NM revealed the lowest and the RM/PM the highest AUC, it was again the CYP2C19 IM who showed the highest and the RM who showed lowest

VRC exposure. In detail, AUC of VRC in ultrafiltrate ranged between 15.8 and 28.1 µmol·h/L in the first dosing interval, which was equivalent to a 1.8-fold difference between the NM and the RM/PM. In the fifth dosing interval, AUC of VRC as well as the interindividual difference increased, with AUC ranging from 20.4 to 93.2 µmol·h/L, revealing a 4.6-fold lower exposure of the RM compared to the IM. The overall exposure with VRC decreased slightly in the seventh dosing interval, with AUC of VRC spreading from 18.2 to 81.1 µmol·h/L and consequently the interindividual difference of a 4.5-fold difference between the RM and the IM was maintained.

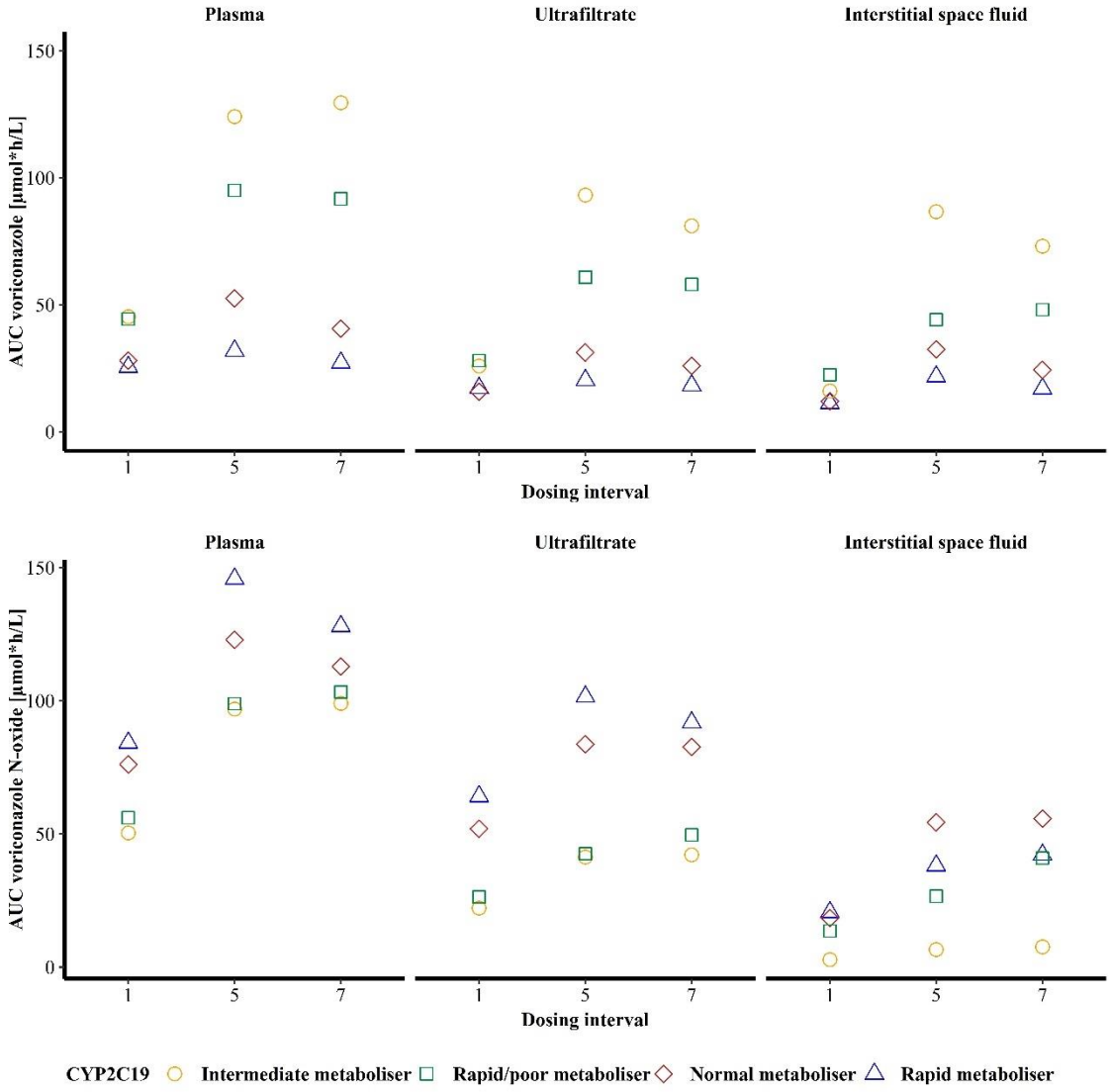

Figure 3.30: Area under the concentration-time curve (AUC) of voriconazole (top) and voriconazole *N*-oxide (bottom) in plasma (left), ultrafiltrate (middle) and interstitial space fluid (right) of four healthy volunteers with different CYP2C19 genotype-predicted phenotypes in relation to the respective dosing interval.

The AUC of NO in ultrafiltrate was in general lower compared to plasma, with the RM showing the highest and the IM showing the lowest exposures. In the first dosing interval, AUC of NO

ranged from 22.2 to 64.1 µmol·h/L, which equalled a 2.9-fold higher exposure with NO for the RM compared to the IM. In the fifth dosing interval AUC of NO increased and ranged from 41.4 to 102 µmol·h/L. However, the interindividual difference was relatively constant with a 2.5-fold difference between the RM and IM. In the seventh dosing interval AUC of NO were comparable to the fifth dosing interval and stretched from 42.2 to 91.8 µmol·h/L indicating a 2.2-fold higher exposure of NO for the RM in comparison to the IM (Figure 3.30).

In ISF, for all individuals AUC of VRC was lower compared to plasma and ultrafiltrate. In detail, in the first dosing interval, AUC of VRC was lowest for the CYP2C19 RM with 11.2 µmol·h/L and highest for the RM/PM with 22.2 µmol·h/L, resulting in a 2.0-fold higher exposure for the RM/PM. In the fifth dosing interval, the RM and IM showed the lowest and highest AUC of VRC with 21.8 and 86.7 µmol·h/L, respectively. Consequently, the interindividual difference was increased compared to the first dosing interval with a 4.0-fold difference between the RM and IM. In the last dosing interval, AUC of VRC in ISF ranged from 17.0 to 73.1 µmol·h/L, and thus, the interindividual difference was further increased to a 4.3-fold difference between the RM and IM.

For AUC of NO in ISF comparable observations were made: in the first dosing interval AUC of NO ranged from 2.84 to 20.7 µmol·h/L representing a 7.3-fold difference between the CYP2C19 RM and IM. In the fifth and seventh dosing interval, it was the IM showing the lowest AUC of NO with 6.61 and 7.62 µmol·h/L, respectively, and the NM revealing the highest AUC of NO with 54.4 and 55.8 µmol·h/L, respectively. This translated to an 8.2- and 7.3-fold higher NO exposure in the RM in comparison to the IM (Figure 3.30).

From the described observations the following results across matrices could be summarised: (i) exposure with VRC and NO was lowest in the first dosing interval, increased in the fifth dosing interval and remained relatively constant in the seventh; (ii) interindividual differences in AUC of VRC were comparable in plasma, ultrafiltrate and ISF, but were increased in the fifth and seventh dosing interval compared to the first; (iii) interindividual differences of AUC of NO were relatively constant within one matrix (independent of the dosing interval), but considerably increased in ISF.

Lastly, the distribution of VRC and NO into ISF was investigated by evaluating the AUC of VRC and NO in ISF in relation to their AUC in plasma or ultrafiltrate. Overall, VRC showed a relatively good distribution to ISF with observed exposure in ISF ranging from 35.5% to 68.2% compared to plasma exposure. When the unbound fraction was taken into account, the exposure in ISF ranged from 62.2% to 107% in comparison to ultrafiltrate. Furthermore, multiple dosing led for most individuals to an increase in the ratios of AUC in ISF to plasma and ultrafiltrate. The ratio of AUC in ISF to ultrafiltrate approached for most individuals after multiple dosing a value

of 1, indicating a comparable VRC exposure in the two matrices. Interindividual differences in the tissue penetration were minor (Table 3.19).

For NO the distribution into ISF was not as distinct as for VRC. The exposure with NO in ISF reached only 5.64% to 49.4% of the exposure in plasma as well as 12.8% to 82.4% of the exposure determined in ultrafiltrate. In particular, the CYP2C19 IM revealed low AUC ratios and protruded from the other individuals (Table 3.19).

Table 3.19: Distribution of voriconazole and voriconazole *N*-oxide into interstitial space fluid (ISF) assessed as ratios of area under the concentration-time curve (AUC) in ISF to plasma or ultrafiltrate (UF) in the three voriconazole dosing intervals with intensive sampling for four healthy volunteers with different CYP2C19 genotype-predicted phenotypes.

Compound	**CYP2C19 metaboliser**	**AUC_{ISF}/AUC_{Plasma}**			**AUC_{ISF}/AUC_{UF}**		
		Dosing interval			**Dosing interval**		
		1	**5**	**7**	**1**	**5**	**7**
Voriconazole	Rapid metaboliser	0.440	0.682	0.624	0.652	1.07	0.930
	Normal metaboliser	0.425	0.620	0.601	0.755	1.04	0.939
	Rapid/poor metaboliser	0.506	0.464	0.524	0.799	0.725	0.828
	Intermediate metaboliser	0.355	0.698	0.564	0.622	0.930	0.901
Voriconazole *N*-oxide	Rapid metaboliser	0.245	0.262	0.329	0.322	0.376	0.459
	Normal metaboliser	0.242	0.443	0.494	0.353	0.649	0.675
	Rapid/poor metaboliser	0.243	0.270	0.397	0.517	0.626	0.824
	Intermediate metaboliser	0.0564	0.0683	0.0769	0.128	0.160	0.180

3.4.2.4 Metabolic ratios

The individual ratios of NO to VRC molar concentrations in plasma showed the largest spread for all individuals after the first VRC dose. The intraindividual variability decreased for all individuals in the fifth dosing interval, i.e. the first p.o. dosing, before rising slightly again in the seventh dosing interval, i.e. after continued p.o. dosing. Continued VRC dosing led to an increase in the median metabolic ratios in all CYP2C19 genotype-predicted phenotypes, except for the IM whose median metabolic ratio was highest after the first VRC dose (Figure 3.31).

A similar pattern was observed for metabolic ratios in ultrafiltrate: the largest intraindividual variability was observed for all individuals after the first, i.v., VRC dose administration. However, intraindividual variability reached a minimum in the fifth dosing interval, before increasing again in the seventh. Overall, individual metabolic ratios were comparable to those determined in plasma with a maximum 1.5-fold difference. Median metabolic ratios increased with multiple

dosing for the CYP2C19 RM and NM. For the RM/PM and IM, median metabolic ratios decreased in the fifth dosing interval before rising again in the seventh (Figure 3.31).

In ISF, individual metabolic ratios showed the largest variability after the first VRC dose administration, while variability was reduced in the fifth dosing interval and rose again after the final VRC p.o. dose administration for all CYP2C19 genotype-predicted phenotypes. The only exception was the IM who showed a steady decrease in intraindividual variability with continued dosing (Figure 3.31). The median metabolic ratios were approximately 2-fold lower in ISF compared to plasma or ultrafiltrate for the CYP2C19 RM, NM and RM/PM and >5-fold decreased for the IM. Based on this, it could be assumed that distribution into ISF for NO was not as distinct as for VRC. Also in ISF, multiple dosing resulted in an increase of median metabolic ratios for all individuals, except for the CYP2C19 IM, who revealed the highest median metabolic ratio in the first dosing interval and the lowest in the fifth (Figure 3.31).

Overall, the observed difference in metabolic ratios between individuals within a matrix was higher in ISF compared to plasma and ultrafiltrate with the median ratios across all dosing intervals being 18- (ISF), 5- (plasma) and 9-fold (ultrafiltrate) lower in the CYP2C19 IM compared to the RM, respectively.

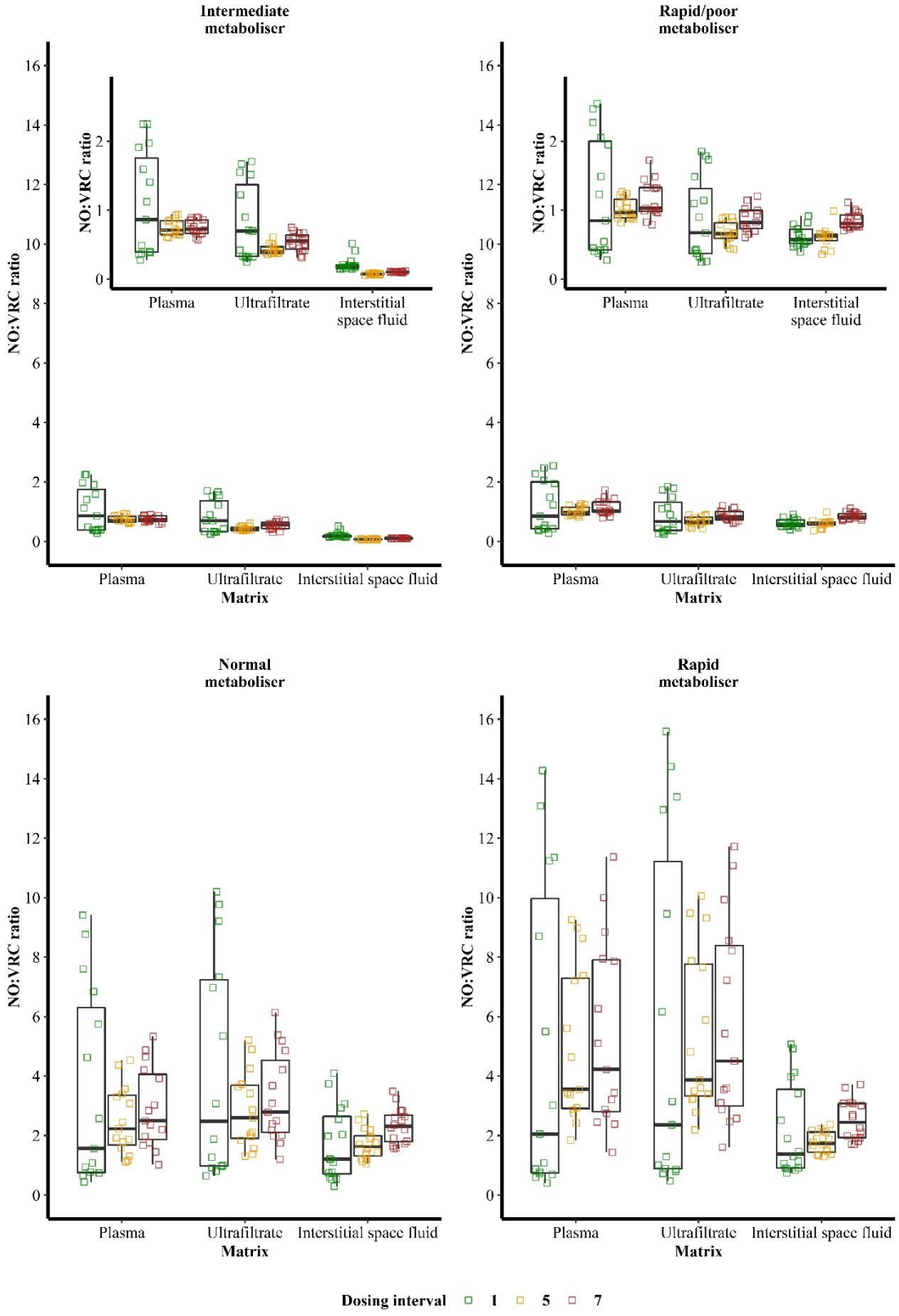

Figure 3.31: Variability of metabolic ratios of voriconazole *N*-oxide (NO) to voriconazole (VRC) in plasma, ultrafiltrate and interstitial space fluid in dependence of the CYP2C19 genotype-predicted phenotype of four healthy individuals in the first, fifth and seventh VRC dosing interval.

During one dosing interval, the individual metabolic ratios in plasma, ultrafiltrate and ISF increased steadily, illustrating the time-dependent transformation of VRC to NO. Overall, the differences in metabolic ratios at the beginning and the end of the dosing interval were largest after the first VRC dose administration and smallest after the fifth. Furthermore, the RM showed the steepest increase of metabolic ratios across time (within one dosing interval) and the IM the shallowest (Figure 3.32).

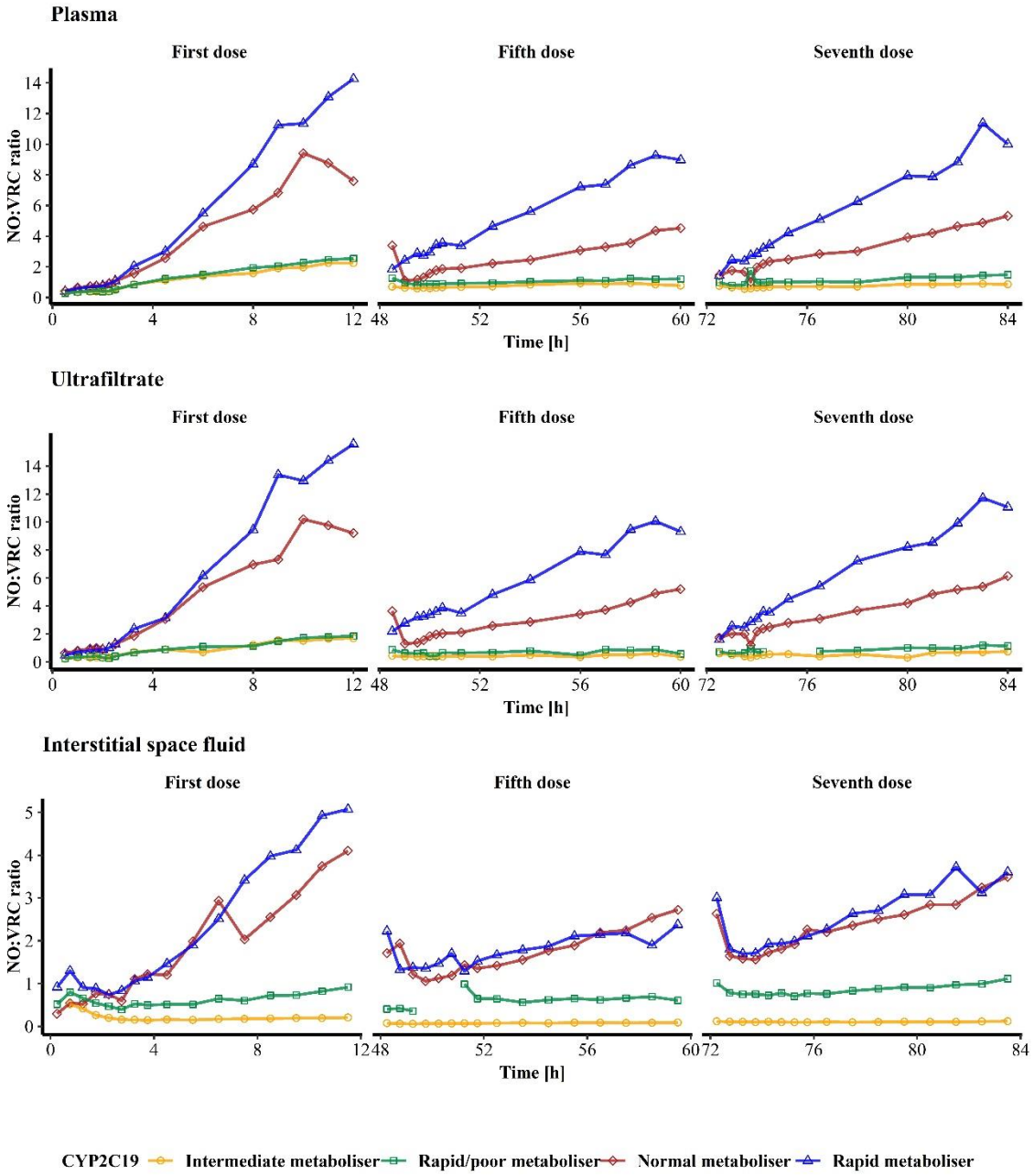

Figure 3.32: Metabolic ratios of voriconazole *N*-oxide (NO) to voriconazole (VRC) molar concentrations in plasma (top), ultrafiltrate (middle) and interstitial space fluid (bottom) across time in the first, fifth and seventh VRC dosing interval of four healthy volunteers with different CYP2C19 genotype-predicted phenotypes. Time is presented as hours after the first VRC dose administration.

The capacity of VRC metabolic transformation to NO was limited, indicated by a decreasing metabolic ratio with increasing VRC concentrations in plasma, ultrafiltrate and ISF, and was constrained depending on the CYP2C19 genotype-predicted phenotype of the individual. Independent of the CYP2C19 genotype, the decline of the metabolic ratio was not linear with regard to VRC concentration but appeared to approach a plateau at a particular VRC concentration (Figure 3.33).

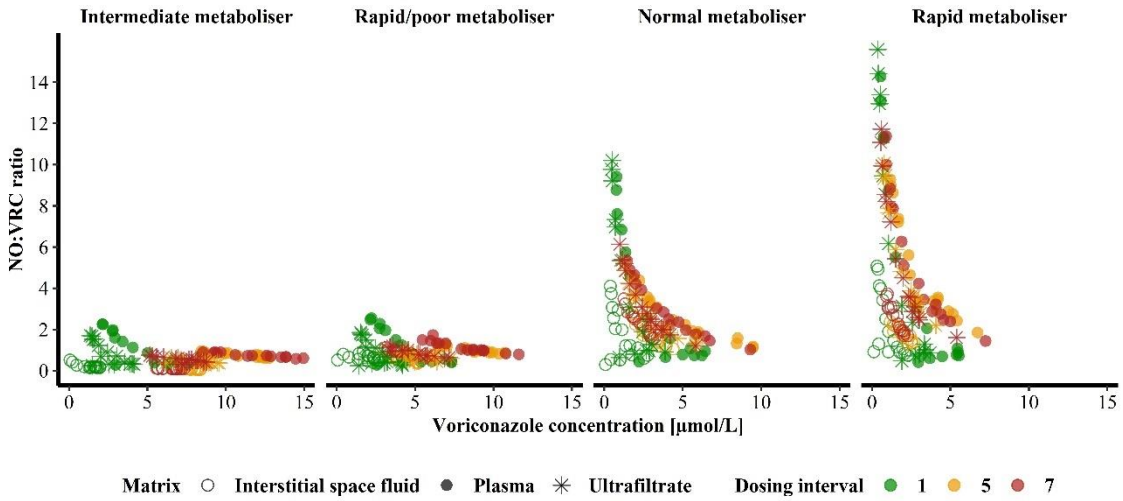

Figure 3.33: Metabolic ratios of voriconazole *N*-oxide (NO) to voriconazole (VRC) in plasma, ultrafiltrate and interstitial space fluid in the first, fifth and seventh VRC dosing interval in dependence of the VRC concentration stratified by CYP2C19 genotype-predicted phenotype of the four healthy volunteers.

The metabolic ratios of the AUC of NO to VRC were assessed in all matrices. In plasma, during the first dosing interval, interindividual differences were smallest with AUC ratios of 3.30, 2.71, 1.27 and 1.11 for the RM, NM, RM/PM and IM, respectively, resulting in a 3.0-fold difference between the RM and IM. The interindividual difference increased in the fifth dosing interval with AUC ratios of the RM, NM, RM/PM and IM of 4.57, 2.34, 1.04 and 0.780 and a 5.9-fold difference between the RM and IM. During the last dosing interval in plasma, the observed interindividual difference was the largest with an AUC ratio of the RM, NM, RM/PM and IM of 4.71, 2.78, 1.13 and 0.764 and consequently, a 6.2-fold difference between the RM and IM. Overall, the RM showed an increase in AUC ratios from the first to the last dosing interval, whereas the NM, RM/PM and IM revealed the lowest AUC ratios in the fifth dosing interval (Figure 3.34).

In ultrafiltrate, for the CYP2C19 RM, NM, RM/PM and IM AUC ratios of 3.72, 3.29, 0.939 and 0.857 were observed in the first dosing interval, representing a 4.4-fold difference between the CYP2C19 RM and IM. In the fifth dosing interval the interindividual difference was most distinctive as the RM, NM, RM/PM and IM revealed AUC ratios of 4.99, 2.68, 0.700 and 0.444,

respectively, resulting in an 11.2-fold difference between the largest and the lowest AUC ratio. In the seventh dosing interval AUC metabolic ratios amounted to 5.04, 3.17, 0.856 and 0.520 for the RM, NM, RM/PM and IM, respectively. Consequently, a 9.7-fold difference in AUC metabolic ratios between the RM and IM was determined. Similar to observations in plasma, AUC ratios increased from the first to the last dosing interval for the RM but decreased in the fifth dosing interval for the other three individuals before increasing again in the last dosing interval. Overall, AUC metabolic ratios in ultrafiltrate were slightly higher for the RM and NM (maximum 1.2-fold) and lower for the RM/PM and IM (max. 0.57-fold) compared to plasma (Figure 3.34).

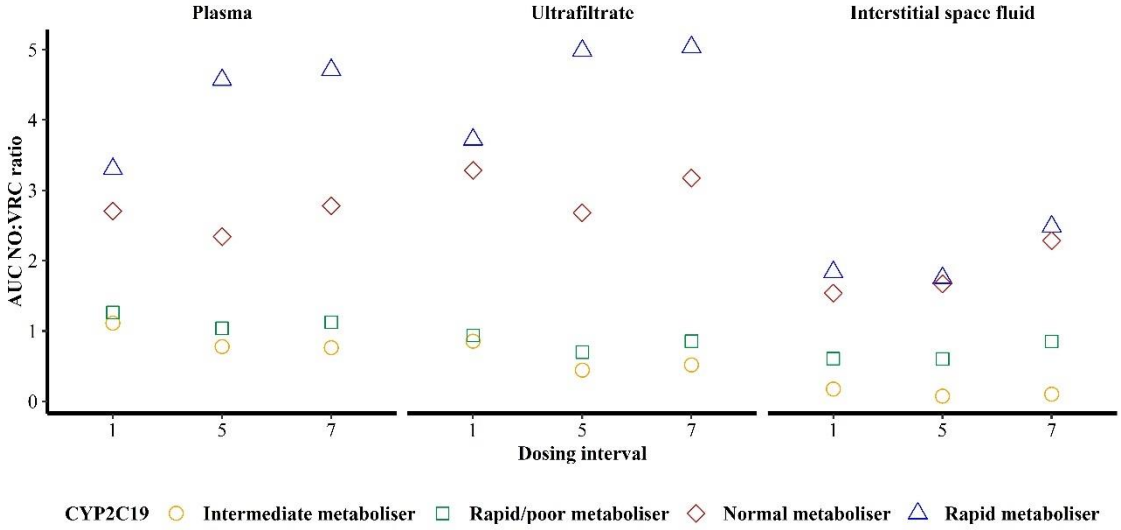

Figure 3.34: Ratio of the area under the concentration-time curve (AUC) of voriconazole *N*-oxide (NO) to voriconazole (VRC) in plasma (left), ultrafiltrate (middle) and interstitial space fluid (right) of four healthy volunteers with different CYP2C19 genotype-predicted phenotypes in dependence of the respective dosing interval.

The analysis of AUC ratios in ISF in the first dosing interval resulted in values of 1.84, 1.54, 0.608 and 0.177 for the RM, NM, RM/PM and IM, respectively, showing a 10-fold difference between the RM and IM. This observed interindividual difference increased with multiple dosing. In the fifth dosing interval AUC ratios were 1.75, 1.67, 0.604 and 0.0763 for the RM, NM, RM/PM and IM, respectively, with a maximum 23-fold difference between the RM and IM. Finally, in the seventh and last dosing interval, AUC metabolic ratios in ISF for the RM, NM, RM/PM and IM were 2.49, 2.28, 0.852 and 0.104, respectively. Consequently, a maximum 24-fold difference between the RM and IM was observed. The course of the AUC ratios across dosing intervals was different to those in plasma and ultrafiltrate: for the RM and RM/PM metabolic ratios were lowest in the fifth and highest in the seventh dosing interval, whereas for AUC ratios were smallest in the first and highest in the seventh dosing interval for the NM and

smallest in the fifth and highest in the first dosing interval for the IM. In total, AUC ratios in ISF were lower than in plasma or ISF. In detail, for the RM, NM and RM/PM the AUC ratio in ISF was a maximum of 2.6-, 1.8- and 2.1-fold lower compared to plasma, while for the IM, a maximum of a 10-fold difference was observed (Figure 3.34).

4 Discussion

4.1 Bioanalytical assay for the simultaneous quantification of voriconazole, voriconazole *N*-oxide and hydroxyvoriconazole

A bioanalytical LC-MS/MS for the simultaneous quantification of VRC, NO and OH-VRC in various biological matrices was developed and validated according to criteria of the EMA guideline on bioanalytical method validation [139].

The availability of a sensitive, fast and easy applicable bioanalytical assay was an essential prerequisite for all further investigations of this thesis [178]. Firstly, *in vitro* microdialysis studies for the feasibility testing of simultaneous sampling of VRC and NO were to be performed. Secondly, clinical study samples were to be analysed for VRC and NO concentrations in human plasma, ultrafiltrate and microdialysate. Thirdly, the formation of NO and OH-VRC in enzymatic incubations with VRC was to be monitored. As a consequence, the bioanalytical assay had to enable the simultaneous detection and quantification of VRC, NO and OH-VRC in plasma, ultrafiltrate and microdialysate as well as in incubations of HLM, HIM and rhCYP. Moreover, the analysis of small sample volumes was essential in particular for microdialysate. As microdialysis catheters are only perfused with a flow rate of 1-2 µL/min and shorter collecting intervals are preferable, high requirements are imposed on bioanalytical assays regarding the sample volume [127,129]. Simultaneously, analyte concentrations in microdialysate are often low, demanding a bioanalytical method with a low LLOQ but preferably also covering a large concentration range, to adequately quantify higher plasma concentrations. Lastly, also *in vitro* metabolism investigations benefit from a low LLOQ as shorter reaction times and lower enzyme concentrations can be applied, which is increasing the efficiency of those experiments. Overall, to meet those necessary requirements for a successful implementation of a bioanalytical assay the technique of LC-MS/MS with a QQQ mass detector was the method of choice.

Bioanalytical method development. During method development, in a first step, the detection of the three analytes, VRC, NO and OH-VRC, as well as the IS was ensured. Based on literature, the ESI source was operated in positive ionisation mode [181–185]. The fragmentation of the precursor ions ($[M+H]^+$) was monitored and product ions of high intensity and specificity for the respective compound with their corresponding collision energy were chosen. The finally selected fragmentations for quantification of *m/z* 350 → *m/z* 281 for VRC and *m/z* 366 → *m/z* 224 for NO have been previously applied in bioanalytical assays [181–185]. Although OH-VRC has been investigated in clinical analyses before, no fragmentation has been reported [48,67]. The great advantage of tandem MS is its large specificity, in particular when multiple reaction monitoring is applied. A highly targeted analysis can be performed by the selection of one precursor ion by the first quadrupole, which is subsequently fragmented in the second quadrupole, and the

selection of multiple product ions by the third quadrupole [138]. Consequently, for VRC, NO and OH-VRC as well as the IS a minimum of two fragmentation reactions were selected and implemented in the final method [186]. However, VRC and NO shared the same product ion of *m/z* 224 and the two hydroxylated metabolites of VRC had the same precursor ion (*m/z* 366) and additionally revealed a common product ion (*m/z* 143). Although other fragmentations, that were unique to the two metabolites (*m/z* 366 → *m/z* 224 for NO and *m/z* 366 → *m/z* 297 for OH-VRC), were chosen as the quantifier reaction, potential interferences with the qualifier reaction could not be excluded. Consequently, a chromatographic separation of NO and OH-VRC was aimed for, although this is usually not compulsory for tandem MS assays [138]. For this purpose, a phenyl-hexyl column was best suited, as all compounds (VRC, NO, OH-VRC and the IS diazepam) were characterised by multiple aromatic rings in their chemical structures. Compared to regularly used C_{18} columns [181,183,185,187–190] this promised a higher peak resolution and improved separation of NO and OH-VRC. In the following, a suitable gradient method for the elution and separation was developed. The most commonly used eluents are water and acetonitrile or MeOH with the addition of FA (usually 0.1% [V/V]), ammonium formate or acetate [182–185,191]. The highest detector responses and optimal chromatographic separation were achieved by the sole addition of FA (0.1% [V/V]) and the gradient method presented in Figure 3.1. All compounds were highly lipophilic and consequently eluted between 3.4 and 4.4 min, when the mobile phase was composed of 98% MeOH. Nevertheless, it was not feasible to shorten the retention times and thus the run time by a steeper methanolic gradient, because this prevented baseline separation of the NO and OH-VRC peaks. Furthermore, the initial high proportion of aqueous phase allowed the elution of polar matrix components and ions before the compounds of interest, avoiding potential ion suppression [192]. From a different perspective, it was also not possible to shorten the run time after the elution of all compounds as the postrun was essential to restore the initial conditions, i.e. composition of eluents and system pressure. The applied flow rate of 0.35 mL/min provided both, adequate chromatographic results as well as an acceptable backpressure, that was limited to 600 bar as a default parameter of the used column. Therefore, for a further reduction of run times, ultrahigh-performance liquid chromatography (UHPLC) methods must be developed. This would be advantageous for high-throughput analyses as run times can be reduced to <4 min, which enables the analysis of a high number of samples in a short time [181,193]. Lastly, after the successful implementation of detection and chromatography settings, ion source parameters were optimised to increase the signal strength of the detector for the final settings to enable quantification of low concentrations of VRC, NO and OH-VRC. For this purpose, a higher focus was put on the two VRC metabolites as their concentrations were expected to be lower [37,48,67].

The further method development was performed in a stepwise approach. First, the determination of VRC and NO in plasma, ultrafiltrate and microdialysate was targeted to proceed with method

validation. Aiming at the definition of an appropriate concentration range and an adequate sample pre-treatment, VRC and NO concentrations observed in clinical trials, during Therapeutic Drug Monitoring (TDM) as well as previously reported calibration ranges were considered. Regarding the latter most bioanalytical methods covered a calibration range between 10 ng/mL and 10 µg/mL for VRC and NO [182,183,193]. Yet, when clinical samples were investigated, only occasionally concentrations above 5 µg/mL were observed [48,65,67,132,181,188]. Exemplary, ter Avest et al. reported median VRC and NO concentrations of 2.5 µg/mL (IQR: 1.3-4.2 µg/mL, n=717) and 2.6 µg/mL (IQR: 1.6 – 3.7 µg/mL, n=590), respectively [181]. This was in line with Yoon et al., reporting a median VRC concentration of 2.63 µg/mL (range: 0.05 – 10.0 µg/mL, n=835) [188]. Additionally, also unbound plasma concentrations, determined by ultrafiltration, were of interest and considering the plasma protein binding of VRC, which has been reported as 50%-58% [57,60], a concentration range of 5 to 5000 ng/mL for plasma and ultrafiltrate samples was deemed appropriate. For microdialysis, only a few studies for VRC have been reported and none for NO [132,194,195]. However, overall a lower range as for plasma, i.e. 4 – 4000 ng/mL, was aimed for.

Based on this knowledge and the aforementioned objectives, a reasonable and easy applicable sample pre-treatment was developed. Plasma samples contain proteins that need to be removed before injection into the LC system to avoid e.g. column clogging. A simple approach, that is realisable in every laboratory, is the precipitation by an organic solvent, such as MeOH or acetonitrile, followed by a centrifugation step to separate the precipitate from the supernatant. Subsequently, the supernatant is used either directly [181–184,187,189] or further diluted before injection [185,191]. Due to the high sensitivity of the here presented assay, the latter approach was applied to attain a linear relation between concentration and detector signals. Indeed, a 1:40 dilution was necessary to avoid an overloading of the LC-MS/MS system. Consequently, also the previously intended calibration range for VRC and NO in plasma and ultrafiltrate was achievable without the use of more complex and time-intensive sample pre-treatment. This includes for instance LLE [196–198], SPE [199,200], additional evaporation steps [190,193] or even approaches using special instrumental set-ups [201], that have been previously described for the bioanalysis of VRC. Microdialysate is already protein-free and thus a simple dilution step was sufficient. To achieve comparable detector signals for a concentration range of 4 – 4000 ng/mL in microdialysate as for a concentration range of 5 – 5000 ng/mL in plasma, a 1+31 dilution step with IS solution was performed. The described dilutions were also beneficial regarding the sample volume. For less sensitive methods, potentially including an evaporation and reconstitution step to concentrate the sample, higher volumes of plasma or microdialysate are needed to obtain volumes after sample pre-treatment that are adequate for injection into the analytical system. However, due to the high dilution only 20 or 5 µL original plasma and microdialysate volume,

respectively, were necessary to achieve this aim in the here presented assay. Furthermore, only 2 µL were finally injected into the system. In case applications requiring a lower LLOQ become interesting in the future, the bioanalytical method could be further improved regarding the sensitivity by higher injection volumes. An additional advantage of the described sample pre-treatment was the associated dilution of matrix components that might cause ion suppression [192]. In combination with the setting of a 2.4 min period at the beginning of each sample run that led all eluents to waste, a contamination of the ion source and thus a decrease in sensitivity was successfully prevented also during longer analytical runs (>24 h).

Further considerations focussed on the IS. The described advantage of the high sensitivity in LC-MS/MS methods is at the expanse of its ruggedness. As a result, in particular for LC-MS/MS methods the use of an IS is recommended to detect and account for variations occurring during sample preparation or analysis [202,203]. For this purpose, structural analogues or stable isotope labelled (SIL) IS are added to all types of samples, i.e. CAL, QC as well as study samples, and the respective ratios of the detector signal of compound to IS are used in the regression analysis [202]. SIL IS have the advantage of having identical chemical features as the compound of interest and hence show co-elution, which is beneficial e.g. in case of occurring ion-suppression. However, SIL IS must be of highest purity and at least 4-5 Da higher in molecular mass to avoid interference with the analyte signal [203]. As a consequence, SIL IS are often expensive and structural analogues are used. For VRC and NO, triple deuterated SIL IS (VRC-D_3 and NO-D_3) are commercially available but were not used for this method as cross signal contribution from analyte to IS or from IS to analyte was likely based on the available purity levels [202,204,205]. Potential consequences include biases in the determined concentrations such as decreased accuracies in the higher concentration range when the analyte contributes to the IS signal [202,204]. These arise when the SIL IS is added to the samples at a low concentration and the respective detector signal is increased by the naturally occurring heavy atoms of the analyte at higher concentrations. Potentially this phenomenon was observed in the bioanalytical method validation published by Moorthy et al. [182]. The authors used VRC-D_3 at a low concentration (5 ng/mL) and the accuracy of their QC samples was constantly decreasing with increasing VRC and NO concentrations on most study days, although the required accuracy and precision limits were complied with. However, in the bioanalytical assay presented in this thesis an alternative for a SIL IS was chosen: diazepam. Diazepam shares identical chemical features with VRC, NO and OH-VRC such as aromatic, nitrogen substituted ring moieties, halogen substituents and an oxygen group. Moreover, samples of the various projects were not expected to contain diazepam, which was the reason for excluding other previously used IS, e.g. ketoconazole (used as *in vitro* CYP3A4 inhibitor) [206].

Bioanalytical method validation. The bioanalytical assay could be successfully validated for VRC and NO in plasma and microdialysate according to criteria of the EMA guideline on bioanalytical method validation [139]. The selectivity of the assay was expectedly high and no interfering peaks or noise were present at the retention times of VRC, NO or the IS. However, carry-over was a critical aspect of method validation. In particular VRC remained in the LC system and was detected in blank samples succeeding VRC samples close to the ULOQ. To minimise the effect, the composition of the needle wash solution was optimised by increasing the fraction of organic solvent, i.e. MeOH, to remove the lipophilic VRC. Simultaneously, the needle washing time was increased to 20 s. Furthermore, additional blank or solvent injections were processed after samples with expected high concentrations and samples were not fully randomised. Consequently, unbiased quantifications were feasible.

The desired calibration ranges for VRC and NO in plasma (5-5000 ng/mL) and microdialysate (4-4000 ng/mL) were maintainable during validation and thus covered clinically relevant concentrations [37,67,132,181,188]. Due to the large concentration range covered, a distinct heteroscedastic error was observed suggesting a higher SD and variance of the detector response at higher VRC or NO concentrations. Thus, the assumption of homoscedasticity in non-weighted linear regression analysis was not fulfilled and consequently non-weighted calibration functions did not allow the quantification of samples with the necessary accuracy [147]. For that reason, a weighting factor of $1/(\text{concentration})^2$ was implemented in the linear regression analysis to account for the different extent of measurement uncertainties at different concentration levels. Consequently, for both matrices and analytes reasonable linearity ($R^2>0.99$) and accuracy were observed.

The EMA guideline on bioanalytical method validation is not explicit about the procedure for multiple analytes, it only states, that "[i]n these cases the principles of validation and analysis apply to all analytes of interest" [139]. Thereon, in the here described method CAL and QC samples were prepared individually for VRC and NO and not pooled for shared CAL and QC solutions. To ensure the absence of interferences, in all validation runs also the respective other analyte was monitored and the occurrence of detector signals at the respective retention time was evaluated. Minor VRC peaks observed in NO CAL and QC samples of higher concentrations were potentially derived from the impurity of the reference substance, which the manufacturer reported to be 98.1% pure. Thus, this analytical artefact was not assumed to have an impact in study sample analysis. Nevertheless, this observation supported the decision for individual CAL and QC samples.

The LLOQ of VRC and NO of 5 ng/mL in plasma and 4 ng/mL in microdialysate achieved the necessary accuracy and precision required by the EMA guideline on bioanalytical method validation [139]. Indeed, within-run as well as between-run accuracy and precision at the LLOQ

were comparable to those of higher concentration levels and the higher allowances of the EMA guideline of ±20% at the LLOQ were not exhausted. The only exception here was the second validation run of VRC in microdialysate, which revealed an imprecision of 17.5% CV (Table 3.4, Table 7.3). Furthermore, also for the LLOQ the ratio of the detector response of the qualifier and quantifier transition was, within the allowed ±25% uncertainty, for the majority of samples maintained. Only three individual LLOQ samples did not fulfil this criterion. Different LC-MS/MS assays for VRC and NO have been developed and validated previously and hence in human plasma LLOQ of, e.g. 100 ng/mL [181,183,193], 10 ng/mL and 20 ng/mL [182] have been reported. VRC in microdialysate was quantified before only by a high-performance liquid chromatography (HPLC) ultraviolet (UV) detection method with a LLOQ of 150 ng/mL [194]. Compared to literature, the LLOQ in the newly developed assay was lowered 2- to 20-fold for plasma and approximately 38-fold for microdialysate and is therefore ideally suited for determinations of lower unbound plasma and ISF concentrations.

The calculated LOD of 0.914 ng/mL and 0.912 ng/mL for VRC and NO in plasma, and 1.70 ng/mL and 1.26 ng/mL in microdialysate, respectively, were highly plausible in comparison to the LLOQ and substantiated the definition of a highly sensitive bioanalytical assay. However, there is some controversy on the definition of a LOD. Firstly, the LOD was determined by calculations based on the calibration function of the four validation runs and thus represented rather a theoretical value that has not been confirmed by experiments. Secondly, as previously mentioned, the sensitivity of LC-MS/MS analytics comes at the expense of ruggedness. Thus, a LOD or even LLOQ value depends on the current instrument condition and might not always be transferrable from the validation process to analytical runs. Therefore, a continuous maintenance of all instruments and a continuous evaluation of method performance is essential. Thirdly, the definition of a LOD for LC-MS/MS MRM methods is more complex than its initial definition [148,186]. Originally, the LOD focussed only on one detector signal for each analyte. However, multiple product ions are monitored applying MRM methods, raising uncertainty about appropriate procedures for LOD determination. One suggestion that has been raised is to divide the LOD into three subcategories: the limit of suspicion, the limit of recognition and the limit of confirmation and hence, distinguish whether only the quantifier is detected, the quantifier and qualifier are detected but the ratio of the two is not corresponding, or both are detected and show the correct ratio, respectively [186]. Overall, this approach will entail the most reliable results, as the LOD is based on experimental verification. However, the LOD is of secondary significance for bioanalytical assays focussing on the quantification of (clinical) study samples and might be more relevant in toxicological research aiming at reliable statements about the presence or absence of compounds.

Further, accuracy and precision were demonstrated for VRC and NO in plasma and microdialysate within all validation runs as well as between runs by adhering to the EMA guideline requirements of a maximum ±15% (±20% at the LLOQ) deviation from the nominal concentration and imprecision determined as CV (Table 3.4, Table 7.3) [139]. Additionally, a random fluctuation of the individual deviations from the nominal concentration was observed, indicating unbiased measurements (Figure 3.3).

Occurring matrix effects for VRC and NO were investigated by determination of IS corrected MF, which ranged between 0.89 and 1.17 for both matrices, revealing an overall minor influence of the matrices. In an optimal setting, MF approach a value of 1 indicating identical detector responses in the presence and absence of matrix. Additionally, the variability between different lots of matrix, i.e. individual donors, was below the required 15% CV. There are three potential reasons for the absence of matrix effects in the validated assay [207]. First, a high dilution was applied during sample pre-treatment, substantially reducing the concentration of potentially co-eluting matrix components. This approach was feasible for the here presented assay as the sensitivity for the compounds was high. In cases of lower sensitivity, often sample pre-treatment by SPE or LLE is necessary to achieve cleaner sample extracts, especially for complex matrices such as plasma or urine. Second, a co-elution of compounds and matrix components was prevented by the settings for chromatography, in particular the gradient method. Third, the IS accounted for potentially occurring fluctuations in co-eluting matrix components. However, it must be recognised, that no six lots of microdialysate were available and instead six individually prepared replicates in RS were used for the investigation. Microdialysate is a rare matrix, available only in very small volumes, and therefore it was not feasible to obtain enough volume from six individuals for the performance of matrix effect investigations. Yet, matrix effects from microdialysate are mainly expected to be caused by ions able to diffuse across the microdialysis membrane [207]. Consequently, the approach with RS was reasonable and no effects for plasma were observed, which represented a more complex matrix.

The last investigated aspect of method validation was the stability of VRC and NO in plasma and microdialysate. In this regard, conditions relevant for the routine handling of samples were investigated: freeze-thaw stability, autosampler stability, short-term and long-term stability. VRC was demonstrated to be stable in both matrices under all conditions. This was in accordance with previously reported results [137,181,184,187,193,194]. For NO no instabilities were observed in the present investigation as the low recoveries observed after the third freeze-thaw cycle of <85% were probably a coincidence due to the low original concentration of the respective QC samples (87.5% of the nominal concentration). However, for NO instabilities have been described in literature [181,182,193], but the applied conditions were not identical to the present assay. Yamada et al. detected for instance decreased recoveries of NO after storage at 20°C for 4-24 h,

a condition not applied in the current study, but no reduction after 12 h at 4°C, which is comparable to the current investigation [193]. Similarly, ter Avest et al. observed reduced recoveries after storage at room temperature, yet they reported a decrease to 20% of the concentration after approximately 96 h and not after 12 h as Yamada et al [181,193]. Moreover, the instabilities ter Avest et al. observed at 10°C occurred after ≥72 h, an observation not contradictory to the present results as such time periods were not covered [181]. In contrast was however the observation of Moorthy et al., who determined recoveries of NO of only 74.6%-80.0% after one month storage at -80°C [182]. Nevertheless, Moorthy et al. investigated stability on loaded VAMS^{TM} devices, which contain whole blood instead of plasma. Overall, a rapid and targeted handling of all VRC and NO samples is recommended to forestall degradation processes. Wherever possible samples should be kept chilled, e.g. in the autosampler or the centrifuge, and on ice during preparation.

Application for ultrafiltrate and *in vitro* matrices. Subsequently to the full method validation for VRC and NO in plasma, approaches were explored to expand the application of the bioanalytical assays to further matrices. In a first step, a suitable surrogate for the standard preparation of CAL and QC samples in ultrafiltrate was searched for. In a reported HPLC-UV assay microdialysate, i.e. RS, was used to spike CAL and QC samples [137]. Yet, in LC-MS/MS analytics matrix effects are of higher importance. Therefore, plasma was deemed a better surrogate, as ultrafiltrate can be viewed as macromolecule-free, most importantly protein-free, plasma. Hence, the conformity of matrix effects was demonstrated by spiking ultrafiltrate with VRC and NO and determining their concentration by a calibration function prepared in plasma. This approach was demonstrated to be feasible and as a result no additional CAL and QC samples were needed for the quantification of unbound VRC as previously reported in literature [189], saving considerable time and material during bioanalysis.

A comparable approach for the quantification of NO in *in vitro* metabolism investigations was chosen. Overall, it was assumed that the majority of the results were transferable from plasma and microdialysate to the *in vitro* matrices of HLM, HIM and rhCYP. However, essential criteria from the EMA guideline, e.g. requirements for CAL and QC samples, were applied to continuously control the performance of the adapted assay. A reasonable surrogate matrix was necessary for the *in vitro* matrices to avoid the routine preparation of CAL and QC samples in the rare and expensive enzymatic matrix for the respective experiment. As the matrix effect was identified as the most influential factor, a surrogate incubation matrix was created comparable to the original HLM matrix. Thus, the respective protein content was replaced by BSA, essential co-factors were omitted and the overall ion strength was kept by the use of the authentic homogenisation and incubation buffers. Identical matrix effects, i.e. conforming detector signals, were shown for NO in this surrogate incubation matrix and original HLM and rhCYP incubation

matrix, respectively. Additionally, the bioanalytical method was adapted to allow for the quantification of lower NO concentrations. Therefore, the dilution after protein precipitation was minimised and the injection volume increased. In total, this led to comparable detector signals as for plasma or microdialysate, but now a concentration range from 0.1 to 500 ng/mL in the original incubations was covered. Similar *in vitro* analyses have been performed with LLOQ of 0.183 ng/mL [69] and 0.365 ng/mL [70]. A simultaneous quantification of VRC as a verification of the added nominal concentration to incubations was not feasible. Later applied VRC substrate concentrations ranged between 183 ng/mL and 36.5 µg/mL and were consequently in a different order of magnitude compared to NO concentrations. This prevented the simultaneous coverage of the linear calibration range for NO and VRC with the identical dilution step in sample pre-treatment. Nevertheless, VRC was semi-quantitatively monitored in all analyses, i.e. the signal strength detected without the inclusion of CAL and QC samples, to potentially detect major mistakes during preparation of the incubations or sample processing. Lastly, the advantage of an LC-MS/MS QQQ in this type of analysis should be highlighted: despite the complex matrix, including a variety of co-factors, ions and in particular high substrate concentrations, the selective quantification of low NO concentrations was feasible in particular due to the strong background noise reducing properties of the MRM method [138].

In summary, the developed and validated bioanalytical LC-MS/MS assay enabled the rapid quantification of VRC, NO and OH-VRC in small sample volumes of various matrices. Consequently, it allowed for further detailed PK investigations of VRC by enabling the generation of high-resolution concentration-time profiles at the target-site and an increased number of samples in animals [208] and vulnerable populations, such as infants. Furthermore, the assay enabled the optimisation of *in vitro* metabolism experiments, i.e. the usage low enzyme and substrate concentrations as well as short reaction times.

4.2 *In vitro* metabolism studies for voriconazole and its metabolites

In this work, a coherent, quantitative *in vitro* characterisation of VRC metabolism was presented to contribute to the elucidation of its complex PK to pave the way towards individualised VRC dosing regimen. Besides the precise description of Michaelis-Menten kinetics of VRC *N*-oxidation in HLM, rhCYP and HIM, CYP isoenzyme contributions were assessed by different approaches highlighting the relevance of the chosen experimental settings. Moreover, metabolic stability of NO and OH-VRC were demonstrated and IVIVE performed. Finally, this work for the first time assessed the inhibition kinetics not only of VRC but also its metabolites to explore their involvement in the observed nonlinear PK of VRC [179].

Experimental conditions for *in vitro* metabolism studies. *In vitro* metabolism investigations are an essential component in the preclinical development of drugs to obtain a mechanistic

understanding and collect important information for the design of future clinical trials. Moreover, also for established drugs, *in vitro* investigations can contribute to the knowledge about the PK by identification and quantification of the major routes of elimination, determination of individual enzyme contributions to these routes and assessment of interaction with enzymes and transporters to evaluate its drug-drug interaction potential [149,209]. However, for reliable inferences from *in vitro* observations, a thoroughly planning, execution and consideration of experiments is crucial as a variety of influential factors exist [110,141].

First, the chosen enzymatic system, its characteristics and challenges should be considered. Microsomes are derived from human tissues by homogenisation and differential centrifugation and represent the endoplasmic reticulum subcellular fraction containing CYP enzymes as well as UGT [110,210]. However, the quality of the tissue can vary widely, as tissues derive from discarded transplants, split liver transplants or waste material from partial hepatectomy and the treatment and storage of the tissue before the processing in the respective laboratory can have an impact on enzyme activity [110,115,211–213]. Furthermore, also the preparation procedure in the laboratory varies, which entails different abundances of CYP enzymes, variability in cytochrome b_5 content and NADPH-cytochrome c reductase activity that contribute to the observed different enzyme activities between vendors [141]. In addition, tissues obtained from individual donors express a different abundance of CYP isoenzymes [165,214] and differences between ethnicities have been described [114]. A meta-analysis of Achour et al. revealed for instance variabilities of up to 185% CV for CYP3A5 and 125% CV for CYP2B6 [165]. The variability observed between individual tissues is even expected to increase when activity is taken into account instead of the mere CYP isoenzyme abundance [215]. Overall, the impact by the described factors on kinetic determinations in microsomes cannot be circumvented. Yet, the awareness of those limitations can foster a better experimental planning and the correct interpretation of the results. For example, microsomes from the same manufacturer with identical lots can be used for the comparability of experimental results or the certificate of analysis provided by the manufacturer for each batch checked for CYP abundances, activities and more. Manufacturers of commercially available microsomes, e.g. Corning®, aim at addressing those impacts by pooling tissues from numerous donors (up to 150) with equal gender distribution and providing abundant information of the donors, e.g. age, ethnicity, social and medical history [216,217].

On the other hand, in rhCYP many of the described considerations for microsomes are negligible. Nevertheless, the artificial nature of the recombinant system involves limitations of its own [110]. This includes the use of different expression systems such as mammalian cells, insect cells, yeast and bacteria with a large variety of yielded expression levels [119,120]. Furthermore, depending on the expression system, often also the co-expression or addition of coenzymes such as P450 oxidoreductase and cytochrome b_5 are necessary whose individual concentration as well as ratio

were described to impact CYP activity [110,120,218]. Consequently, rhCYP lag the physiological conditions of microsomes regarding coenzymes but also the membrane composition, i.e. the lipid micro-environment surrounding the membrane-bound CYP enzymes [110].

Second, experimental conditions during incubation were described to impact CYP isoenzyme activity [110,219]. The experimental settings are standardised to some degree, this includes the incubation temperature of 37°C to mimic human body temperature as well as recommendation of a 50 to 100 mM PPB (pH 7.4) or TRIS (pH 7.5) buffer [110,141,143]. However, already within these narrow boundaries variations in kinetic investigations have been observed [220]. Moreover, the necessary co-factor NADPH is either added directly [70,110,221,222] or as NADPH re-generating system including glucose-6-phosphate, glucose-6-phosphate dehydrogenase and $NADP^+$ [110,162,223], for which concentrations vary. A depletion of NADPH would naturally alter enzyme kinetics and is to be avoided. Lastly, besides the necessary magnesium ions (mostly added as $MgCl_2$), sometimes further additives are used, e.g. ethylenediaminetetraacetic acid (EDTA) [110,162] or manganese chloride [71], whose specific impacts are less studied. Albeit their contribution to the ion strength of the incubation, which has been demonstrated to be relevant, should not be neglected [219].

Third and last, the content of organic solvents such as dimethyl sulfoxide (DMSO), MeOH, ethanol or acetonitrile, is to be minimised in enzymatic incubations as CYP inhibition can occur. Interestingly, the different solvents have varying effects on different CYP isoenzymes at different concentrations [110,224–226]. DMSO has for instance relevant effects on CYP3A4 at concentrations of 0.2% [V/V], but none on CYP2D6 at concentrations of ≤1% [V/V]. MeOH in contrast affects CYP2C19 at concentrations of ≤0.2% [V/V] but not CYP3A4 at concentrations ≤1% [V/V] [110,224]. Consequently, there is no ideal solvent for the preparation of substrate and inhibitor solutions used for enzymatic incubations, but MeOH or acetonitrile are preferred over DMSO and in general should be kept as low as possible [110].

In all investigations described in this thesis attention was paid to the mentioned aspects. Therefore, the same batch of the enzymatic source was used wherever individual experiments were to be compared with each other and freeze-thaw cycles avoided by prescient aliquoting of the enzyme stock solution. None of the enzymatic stock solutions was exposed to more than six freeze-that cycles, which was shown not to have an impact on CYP enzyme activity [211]. Furthermore, the experimental conditions, i.e. buffer (type, molarity, pH) and composition of co-factors, were kept constant throughout the work. For all kinetic investigations the MeOH content was <1%. However, due to the high lipophilicity of all used substrates and inhibitors, this limit was not maintainable in all inhibition investigations. In particular when high substrate concentrations were combined with high inhibitor concentrations the MeOH content reached a

maximum of 2.25% [V/V]. Thus, to assess and evaluate the inhibitory effect of the inhibitor alone, the same amount of MeOH was given to the control.

Also the experimental procedure was kept constant across the investigations. This included among others the storage of all solutions on ice to preserve enzyme activity and prevent instabilities of the substrate and inhibitor solutions. A maximum of 16 incubations were handled simultaneously, thus, if multiple iterations were performed, replicates were distributed accordingly to evenly account for potential variabilities. Besides, in case of inhibitory investigations, the uninhibited control was always performed simultaneously on the same day and wherever possible also in the same iteration. In this way, the same batch of buffers and co-factors was used and the above-described variabilities circumvented and comparability assured. Furthermore, from all incubations a minimum of two samples were taken. This was feasible as incubations represent a solution and no components are sedimenting. The homogenous distribution was additionally ensured by a gently shaking in the Eppendorf ThermoMixer®. As a consequence, besides replicate incubations further experimental replicates were obtained, which allowed the exploration of the reproducibility of determinations within one incubation and contributed to the number of observations for better statistical assessment. Lastly, it was aimed at starting the reaction by the addition of the respective enzyme source to evade a pre-incubation of enzyme with VRC, NO or OH-VRC to forestall precedent inhibitory effects. However, for investigations of IC_{50} shift a pre-incubation in the absence and presence of NADPH re-generating system was required and hence, the reaction started with the addition of NADPH re-generating system (solution A) after the 30 min pre-incubation period or with the substrate itself.

In different parts of this work, marker reactions for the activity of CYP2C19, CYP2C9 and CYP2C19 were needed. This included the assessment of VRC, NO and OH-VRC as CYP inhibitors, but also for the specificity testing of the CYP inhibitors loratadine (CYP2C19), sulfaphenazole (CYP2C9) and midazolam (CYP3A4) as well as the determination of ISEF. Marker reactions are characterised by CYP isoenzyme specificity and thus regularly used when effects on an individual enzyme are to be investigated. For this work, the marker reactions of the 4-hydroxylation of S-mephenytoin for CYP3C19, the 4-hydroxylation of diclofenac for CYP2C9 and the 1-hydroxylation of midazolam by CYP3A4 were chosen as recommended by FDA and EMA guidelines [149,150,209]. Although the reaction kinetics of those marker reactions have been frequently described in literature, due to the influences of experimental conditions as described above, a laboratory-individual determination was performed to ensure reliable results. In this work, for CYP2C19 in HLM a K_M and V_{max} of 53.0 µM and 44.7 pmol/(min·mg) were determined. Previously reported K_M and V_{max} values for the 4-hydroxylation of S-mephenytoin were 51 µM and 85 pmol/(min·mg) [227], 77.9 µM and 640 pmol/(min·mg) [85] and 56.8 µM and 78 pmol/(min·mg) (V_{max} normalised to HLM concentration of 0.5 mg/mL) [157]. For

CYP2C9 and the 4-hydroxylation of diclofenac in HLM K_M and V_{max} values of 8.28 µM and 155 pmol/(min·mg) [155], 17.7 µM and 1609 pmol/(min·mg) [228] as well as 22.4 µM and 80 pmol/(min·mg) (V_{max} normalised to HLM concentration of 0.5 mg/mL) [157] have been reported, while current investigations showed a K_M of 4.15 µM and a V_{max} of 1693 pmol/(min·mg), respectively. For CYP3A4 and the 1-hydroxylation of midazolam, in this work a K_M and V_{max} of 4.45 µM and 559 pmol/(min·mg) were presented, while in literature values of 2.1 µM and 1369 pmol/(min·mg) [85], 2.31 µM and 814 pmol/(min·mg) [155], 2.94 µM and 973 pmol/(min·mg) [228] as well as 4.8 µM and 7756 pmol/(min·mg) [157] were described.

In rhCYP, the following kinetic parameters have been reported: for rhCYP2C19 and the 4-hydroxylation of S-mephenytoin K_M and V_{max} values of 19.8 µM and 17.7 pmol/(min·pmol) (V_{max} normalised to rhCYP concentration of 50 pmol/mL) [157] were described, which were well in line with the K_M of 22.1 µM and V_{max} of 7.10 pmol/(min·pmol) of this work. For rhCYP2C9 and the 4-hydroxylation of diclofenac in the current investigation a K_M and V_{max} of 2.29 µM and 13.5 pmol/(min·pmol) were presented, while literature values were 9.7 µM and 29 pmol/(min·pmol) [228], 1.97 µM and 3.33 pmol/(min·pmol) [155] as well as 7.9 µM and 0.68 pmol/(min·pmol) (V_{max} normalised to rhCYP concentration of 50 pmol/mL) [157], respectively. Lastly, for the 1-hydroxylation of midazolam K_M and V_{max} of 2.89 µM and 21 pmol/(min·pmol) [228], 0.92 µM and 5.51 pmol/(min·pmol) [155] as well as 3.3 µM and 59.6 pmol/(min·pmol) (V_{max} normalised to rhCYP concentration of 50 pmol/mL) [157] were reported while the here presented investigations yielded a K_M of 1.96 µM and a V_{max} of 1.67 pmol/(min·pmol).

In conclusion, the kinetic parameters of the marker reactions determined in this work were within similar ranges of previously reported results. However, the large variability of reported kinetic parameters for the marker reactions highlight the importance of the decision to derive laboratory-individual results for *in vitro* investigations. Indeed, even in between repetitions of experiments in the same laboratory, some variation was observed, e.g. individual K_M and V_{max} determination of the marker reactions (chapter 3.2.1.2, Table 7.4) in comparison to K_M and V_{max} determination based on the uninhibited controls of inhibition experiments (chapter 3.2.3.3, Table 3.12). Potential reasons for the slight differences might lie in the experimental setup, i.e. the number and distribution of the investigated substrate concentrations, or (in this specific case) the use of different batches of HLM with varying CYP isoenzyme activities. Further sources of the observed variability will be discussed for the *N*-oxidation of VRC (see below) and are equally valid for the marker reactions.

Voriconazole and metabolites as substrates of CYP isoenzymes. As an essential prerequisite, linearity investigations for the formation of VRC metabolites with regard to reaction time and enzyme concentration were performed. In all kinetic investigations the reaction velocity depicts

the rate of metabolite formation per minute per milligram protein (in HLM and HIM) or picomole enzyme (in rhCYP) and thus would be distorted outside the linear range. Although the manufacturer often provides information on the assessed linearity over time in the certificates of analysis, there are two main reasons why it should be re-assessed: first, the transferability from one substrate to another is not always given and second, due to the influence of experimental conditions it should be evaluated under laboratory-specific circumstances. Besides, optimal reaction parameters, i.e. reaction time and enzyme concentration, compatible with the available bioanalytical assay regarding the metabolite concentration range can be determined, and the absence of substrate depletion precluded. In HLM linearity investigations were successful with quantifiable NO concentrations in all incubations (chapter 3.2.2.1). Thus, for future kinetic investigations an unrestricted choice (within the investigated settings) regarding protein concentration and reaction time was possible. Despite, some further considerations were made: firstly, a shorter reaction time was deemed beneficial in future experiments as potentially more replicates could be performed and the bench-top storage time of assay components could be decreased. Secondly, a low protein concentration was considered to be of advantage as consequently more experiments could be performed with the same HLM batch and nonspecific protein binding of substrate or inhibitor to proteins of the incubation could be minimised. Indeed, it has been described, that nonspecific binding of substrate or inhibitor can considerably distort the determined enzyme kinetics as the amount of free drug is decreased, which leads to higher K_M, IC_{50} and K_i [110,212,229–232]. Thirdly, in inhibitory investigations, when NO formation is impeded, concentrations still had to be in the quantifiable range of the bioanalytical assay. As a consequence, overall a protein concentration of 0.2 mg/mL in combination with reaction times of 10-30 min were chosen for future investigations.

Linearity assessment in rhCYP was more challenging. While for rhCYP2C19 the extent of formation of NO was as anticipated, for rhCYP3A4 and rhCYP2C9 turnover of VRC was unexpectedly low. As a result, enzyme concentrations of 5 pmol/mL rhCYP3A4 and ≤40 pmol/mL rhCYP2C9 could not be evaluated due to unquantifiable NO concentrations. Thus, for rhCYP2C9 linearity across enzyme concentration was not assessable. Additionally, for a full kinetic profile of VRC *N*-oxidation in rhCYP2C9 lower VRC concentrations as applied during linearity investigations (10 µM) were needed. Hence, for the assessment of Michaelis-Menten kinetics the highest possible rhCYP2C9 concentration of 100 pmol/mL was used and aliquots of the enzyme stock solution directly added to the incubation. Overall, this already hinted at the minor role of CYP2C9 in VRC metabolism. For rhCYP2C19 and rhCYP3A4 two enzyme concentrations each (5 and 15 pmol/mL rhCYP2C19, 20 and 40 pmol/mL rhCYP3A4) were brought forward to kinetic investigations to further investigate and confirm the independence of enzyme concentration on kinetic determinations.

Also for HIM, the VRC turnover was low, preventing an assessment of linearity across enzyme concentration. In particular, the enzyme concentrations should cover a sufficiently large range to enable the detection of potentially existing deviations from linearity.

Overall, in all linearity investigations also the formation of OH-VRC was monitored but could not be detected in any of the incubations. On the one hand, a rapid formation of the secondary metabolite dihydroxyvoriconazole was considered and consequently investigated by incubating OH-VRC directly with HLM monitoring for depletion. On the other hand, potentially a detection was hindered by the nonconformity of the analytical reference standard with the hydroxylated metabolite. In literature the position of the hydroxy group on the fluoropyrimidine moiety is not described [37,60] but was predefined in this analysis by the available reference standard (Figure 4.1). Lastly, OH-VRC might be formed CYP- and FMO-independently resulting in its absence in HLM and rhCYP *in vitro* incubations. However, Scholz et al., found decreased metabolic clearances in CYP2C19 PM, indicating a CYP2C19 involvement, which is in contrast to the here presented observations [48]. Overall, however, a predominant role of CYP2C19 in OH-VRC formation can be excluded.

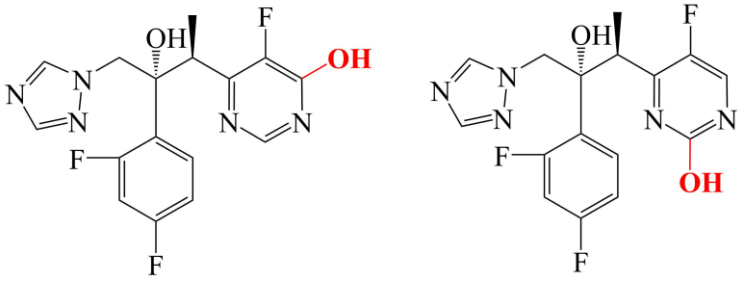

Figure 4.1: Positions of the hydroxylation (red) of the fluoropyrimidine moiety of voriconazole as described in literature [37,60]. The left molecule depicts the available analytical reference standard.

As a consequence, in further investigation focus was placed on the *N*-oxidation of VRC. In all enzymatic systems investigated, HLM, HIM, rhCYP2C19, rhCYP2C9 and rhCYP3A4, kinetics were described by the nonlinear Michaelis-Menten model. Derived kinetic parameters were compared to those previously reported in literature. In HLM, previously reported K_M and V_{max} reached values of 8.1±2.9 µM and 9.3±11.1 pmol/(min·mg), based on HLM derived from three individuals [71], as well as 9.3±3.6 µM and 40±13.9 pmol/(min·mg), based on HLM from six adults [233], respectively. Consequently, the deviations to the results of this thesis, i.e. K_M 2.98 µM (95% CI: 2.63 – 3.33 µM) and V_{max} 26.1 pmol/(min·mg) (95% CI: 25.4 – 26.8 pmol/(min·mg)), are distinct. In recombinant enzymes for CYP2C19, K_M and V_{max} values of 14±6 µM and 0.22±0.02 nmol/(min·nmol) [69], 3.5 µM and 0.39 pmol/(min·pmol) [71] as well as 4.31±0.31 µM and 4.85±0.08 pmol/(min·pmol) [234] have been described, representing an 11-, 3- and 3.3-fold higher K_M and a 7- and 4-fold lower as well as 3-fold higher V_{max} compared to here presented determinations. For rhCYP2C9, one study reported a K_M of 20 µM and a V_{max} of

0.056 pmol/(min·pmol) [71], which was 5- and 8-fold higher, respectively, than present determinations, while another one did not find metabolism mediated by CYP2C9 [69]. For rhCYP3A4, K_M and V_{max} of 16±10 µM and 0.05±0.01 nmol/(min·nmol) [69] and 235 µM and 0.14 pmol/(min·pmol) [71] were observed. In comparison, current results of a K_M of 1.20 µM and a V_{max} of 0.00893 pmol/(min·pmol) were 13- and 196-fold lower with regard to K_M and 6- and 16-fold lower with regard to V_{max}.

In particular the different magnitudes of reported parameters demonstrate the necessity of carefully planned and executed *in vitro* experiments to generate reliable results. However, previously reported studies carried some limitations, potentially resulting in discrepancies between *in vitro* predicted and *in vivo* observed PK properties. First, kinetic investigations were performed using HLM prepared from only a few individuals. Yet, individual predisposition for CYP enzymes is very heterogenic as discussed previously [114,165,214,215]. Therefore, kinetic parameters that are to be applied and interpreted in a wider context should be based on a larger pool of liver microsomes. Thus, the research presented in this thesis, relying on pooled microsomes from 150 donors with equal gender distribution, offers a better representation of the diversity of the human population and hence more reliable data. Second, according to regulatory agencies, *in vitro* kinetic investigations should be conducted at clinically relevant drug concentrations [149,209]. Although there is no generally recognized PK target for VRC, a recent position paper recommends VRC C_{min} of at least 1-2 mg/L for an efficient and at maximum of 4.5-6 mg/L for a safe therapy [174]. This translates approximately to a C_{min} target range of 2.86 to 17.2 µM VRC, a concentration range that was adequately covered in here presented investigations (0.5 – 100 µM). Surpassing the upper limit to a certain extent is certainly advisable as also individuals occasionally show unexpectedly high VRC plasma concentrations, e.g. >15 mg/L (43 µM) [181]. Yet, early *in vitro* studies of VRC applied concentrations as high as 2500 or 5000 µM [69,71]. This bridges to the third concern: the organic solvent concentrations in incubations. All kinetic determinations for the *N*-oxidation of VRC in this thesis had a maximum of 0.5% MeOH. As VRC is a lipophilic drug, it is difficult to reproduce how solubility as well as the organic solvent limit was maintained at VRC concentrations of 2500 or 5000 µM [69,71]. Fourth, the usage of high HLM (≥0.5 mg/mL) or rhCYP concentrations potentially increases nonspecific binding of the substrate to the protein or other components of the enzymatic system, thereby reducing the apparent substrate concentration [232]. Therefore, for unbiased kinetic determinations the unbound substrate concentration should be used for determinations of Michaelis-Menten kinetics [110]. However, if no data on the f_u in the respective enzymatic system is available, as it is the case for VRC, low HLM concentrations should be chosen, having a smaller influence on the free substrate concentration, and thus a smaller influence on the determined kinetics. Nevertheless, future research should evaluate the influence of the nonspecific binding

and the results be implemented in the kinetic determinations. Fifth and last, the observation of metabolite formation is generally favourable compared to substrate depletion [70]. Reaction kinetics change with decreasing substrate concentrations, however this is rarely accounted for and a depletion of 10% or 20% is defined as negligible.

Reaction kinetics of VRC metabolic processes in HIM have previously not been assessed. CL_{int} was approximately 6-fold lower than in HLM, which is probably due to the lower CYP enzyme abundance per gram microsomal protein in the small intestine compared to the liver. For CYP2C19, CYP2C9 and CYP3A4 in the small intestine abundances of 2.1, 11 and 58 pmol/mg have been described, which is 5.2-, 5.5- and 1.6-fold lower than in liver, respectively (Table 7.2) [165,235]. Nevertheless, the presented results suggest that metabolic transformation by the intestine should not be ignored. In addition to the first-pass effect in the liver, this is in line with clinical trials where p.o. and i.v. doses of 400 mg VRC resulted in similar maximum plasma concentrations and areas under the concentration-time curve but not doses of 50 mg. Moreover, bioavailability has been observed to increase in CYP2C19 PM (94% compared to 75% in NM) supporting the hypothesis of saturable CYP-dependent metabolic processes in the intestine [48]. Consequently, the variability in bioavailability might advise for a re-evaluation of the currently eligible switch from i.v. to p.o. dosing without adaptation in dose, which is permitted according to the summary of product characteristics [38]. For this purpose, PBPK modelling can be a beneficial tool. Additionally, in contrast to i.v. administration, no weight-adapted dosing is designated for p.o. administration of VRC, which is based on an ambiguous rational.

With regard to the contributions of the respective enzymes to the overall formation of NO, different approaches for the determination have been explored, yielding results with a mean contribution of 63.1% for CYP2C19, 13.2% for CYP2C9 and 29.5% for CYP3A4. Although this averaging approach is rather unusual, it might be able to compensate for the individual approaches under- or overpredictions. The determination by application of specific CYP inhibitors in HLM was interfered by cross-inhibition of the inhibitors loratadine and sulfaphenazole on the enzymes of the same subfamily, CYP2C19 and CYP2C9. This problem is not unknown and even the FDA and EMA state, that for CYP2C19 no specific inhibitor is yet available [149,150,209]. Additionally, the specificity is highly dependent on the concentration of the inhibitor with higher concentrations leading to increased cross-reactions [158]. In contrast, if inhibitor concentrations are too low, incomplete inhibition is the consequence. In the present study, based on data in literature, the best compromise was aimed for. Yet, ketoconazole concentrations might have been too low for a complete inhibition of CYP3A, potentially explaining the 11% remaining VRC metabolism when a combination of the CYP2C19, 2C9 and 3A4 inhibitors was used. Moreover, the magnitude of inhibition has been shown to be dependent on the probe substrate for CYP2C9 and CYP2C19 [159,161] indicating different binding modalities of different substrates. Further,

the question of an appropriate implementation of this inhibitor specificity testing arose. On the one hand, the optimal *in vitro* incubation conditions (protein concentration and reaction time) of the marker reactions can be applied. However, if incubation conditions deviate from those of the investigated compound, e.g. by lower protein concentrations and lower reaction time, it is challenging to predict whether the same concentration of inhibitor has the same influence under these different conditions. Potentially the respective inhibitor is metabolised itself and reveals depletion, which leads to an incomplete inhibition. On the other hand, if the same protein concentration and reaction times are applied for the marker reactions as for the compound of interest and inhibition is incomplete, a depletion of marker substrate might occur, which decreases the reaction velocity and causes a reduced metabolism independent of the inhibitor. The latter approach was chosen in the here presented results and indeed when the effect of ketoconazole on the 4-hydroxylation of diclofenac was investigated only 84.9% of metabolism remained and a slight depletion of diclofenac was observed. As substrate concentrations were only semiquantitatively assessed (as described for VRC and NO, see chapter 4.1) the full extent was not determinable but approximated 20%. In conclusion, also controls on well-established marker reactions for specificity testing of the inhibitor have to be considered with some limitations.

Due to the described limitations a second approach for the determination of enzyme contributions was used: the extrapolation from rhCYP. As seen by the results (chapter 3.2.2.3) the transformation from CL_{int} in rhCYP to CL_{int} in HLM, accounting for CYP abundance alone (without ISEF), did not yield satisfactory results. In particular for CYP2C19 implausible contributions of 157% were determined. Here, the artificial nature of rhCYP, i.e. the distinct overexpression of the respective enzyme, might play a role. Especially rhCYP derived from insect cells, which were used for all investigations of this thesis, reveal a high expression of the CYP isoenzyme being ideal for the identification of enzyme involvement but might be misleading for kinetic determinations [119,120]. In contrast, also the approach of relating the individual CL_{int} of each rhCYP to the sum of individual CL_{int} in the different rhCYP has a major limitation: it assumes that all involved CYP enzymes have been tested and no contribution neglected. Consequently, the ISEF approach is more promising, as laboratory-individual experimental conditions as well as the overexpression in rhCYP are accounted for using marker reactions [164,228]. However, also ISEF determination relied on marker reactions based on the assumption that substrates of the same CYP isoenzyme behave identically. That this is not always the case has been shown previously based on ISEF calculations with one marker substrate and the transfer to another, e.g. for CYP2C9 from the 4-hydroxylation of diclofenac to the hydroxylation of warfarin [155,236,237]. In particular for CYP3A4 this limitation is widely known and acknowledged in current guidelines for the identification of drug-drug interactions by the FDA and EMA [149,150,209]: besides the use of midazolam, it is recommended to also include

testosterone as an CYP3A4 substrate. A comparison of the determined ISEF with previously reported values is not meaningful, as ISEF are required to account for laboratory-individual factors, e.g. experimental conditions or the used enzymatic system (rhCYP expression system or source of HLM), and therefore inevitably exhibit a high variability. Lastly, it should be acknowledged, that also for the marker reactions the unbound substrate concentrations should be considered. In this work, total concentrations were studied for kinetic determinations and the influence by nonspecific binding deemed subordinate due to the low protein and enzyme concentrations used for incubations. However, differences in nonspecific binding in HLM and rhCYP based on varying protein concentrations are plausible and potentially lead to a distortion of the ISEF. Overall, by averaging different approaches for the determination, a compensation for the described limitations is conceivable. Yet, for a further validation of the observations an extension to other marker reactions could be performed.

Nevertheless, the results can be interpreted in context and summarised to the following major conclusions: (i) CYP2C19 plays the largest role in VRC *N*-oxidation, (ii) CYP2C9 contribution is negligible and (iii) besides CYP3A4, no further enzymes are relevantly contributing to NO formation. While (ii) is in accordance with the reported safety of VRC in a CYP2C9 PM in a clinical trial [238], (iii) contrasts with investigations of Yanni et al. who found a 25% contribution of FMO [70]. Furthermore, a clinical trial by Mikus et al. investigating potential reasons for differences in VRC clearance of CYP2C19 NM and PM in the absence and presence of the strong CYP3A4 inhibitor ritonavir came to the conclusion that CYP2C19 is responsible for 66% of metabolism and CYP3A4 for 34%. In case of CYP2C19 PM with ritonavir treatment, metabolism was decreased by 86% [239]. Overall, the *in vitro* results of this thesis regarding enzyme contributions, very well corresponded to those clinical observations, potentially even explaining the remaining 14% as CYP2C9 metabolism.

The performed IVIVE additionally confirmed the validity of the generated data. In clinical studies VRC clearance values of 244 mL/min (first dose, all genotypes) [67], 420 mL/min (first dose, NM), 194 mL/min (first dose, heterozygous NM), 149 mL/min (first dose, PM) [48] or 272 mL/min (multiple dose, all genotypes) [132] have been reported. Thus, the estimated $CL_{hepatic}$ of 127 –266 mL/min as derived from the here presented IVIVE represent a good approximation, if considering that only one metabolic pathway, VRC *N*-oxidation, was taken into account. The role of other pathways, e.g. (di-)hydroxylation of VRC at the fluoropyrimidine moiety, has been controversially discussed in literature. Although NO is the major *circulating* metabolite, the formation of (di-)hydroxy-VRC has been claimed to be the major pathway and low plasma concentrations explained by a higher renal clearance [37,48]. However, in the current investigations OH-VRC was not formed in incubations of HLM, HIM or rhCYP.

As described above, this might be due to a different pathway of formation, the hydroxylation on the second position of the fluoropyrimidine moiety or the rapid transformation to the secondary metabolite dihydroxyvoriconazole. The latter was consequently investigated by direct incubation of OH-VRC with HLM. However, as no depletion over time was observed this hypothesis seems unlikely. Also NO was demonstrated to be stable in HLM incubations, which confirmed the reliability of all kinetic determinations. However, this observation was in contrast to previously described continued metabolism of NO to an additionally hydroxylated metabolite and the loss of the fluoropyrimidine moiety [37,60].

Voriconazole and metabolites as inhibitors of CYP isoenzymes. In adults VRC exhibits nonlinear PK, an observation assumed to originate from saturation or auto-inhibition of its own metabolism [68,78]. The inhibitory potential of VRC has been described thoroughly in literature as observed drug-drug interactions *in vivo* [37,38,79,90,91,105,240,241] as well as based on *in vitro* experiments [79,83–88,242]. However, not many insights are available on the inhibitory potential of VRC metabolites. Aiming at the quantification of the inhibitory potential of VRC, NO *and* OH-VRC, investigations on IC_{50} and K_i were performed. IC_{50} was assessed by nonlinear regression using the four-parameter inhibition model (chapter 2.3.5.1, Eq. 2.17), fixing the parameters of maximum and minimum activity to 100% and 0%, respectively. This was found feasible as from a mechanistic point of view baseline activity, i.e. reaction velocity in the absence of inhibitor, should always be equal to 100% and deviations from this are most likely due to experimental variability. Further, if an inhibitory effect is observed at a fictive, infinitely high inhibitor concentration minimum activity is expected to decrease to 0%. Additionally, the sensitivity analysis showed, that the estimated IC_{50} did not change relevantly when either A_{max} or A_0 or all model parameters were estimated simultaneously, as CI were overlapping. However, A_0 and A_{max}, and the respective CI, occasionally resulted in physiologically implausible values, i.e. $A_0<0\%$ and $A_{max}>100\%$. Moreover, in some cases a precise estimation of parameters and CI were not achievable as the variability and quantity of observations were beyond the scope of the model and led to model overparametrisation. In conclusion, fixing the maximum and minimum activity was a justified assumption for IC_{50} estimations.

Previously *in vitro* determined IC_{50} values for VRC on CYP2C19 were 5.25 µM (S-mephenytoin 4-hydroxylation) [85], 5.29 µM (omeprazole 5-hydroxylation) [243], 8.7 µM (S-mephenytoin 4-hydroxylation) [83] and 17.1 µM (S-mephenytoin 4-hydroxylation) and thus 1.4-, 1.4-, 2.3- and 4.6-fold higher than the values determined in this work, respectively. For CYP2C9 IC_{50} values of 8.4 µM (tolbutamide 4-hydroxylation) [83] and 3.63 µM (tolbutamide 4-hydroxylation) [85] have been reported, which is 2.0- and 0.87-fold the value of the current investigation, respectively. Lastly, for CYP3A4 IC_{50} values of 0.5 µM (nifedipine oxidation) [83], 2.90 µM (midazolam 1-hydroxylation) [85], 2.10 µM (midazolam 1-hydroxylation) [242] and 6.04 µM (midazolam

1-hydroxylation) have been described, which amounts to 0.28-, 1.6-, 1.2- and 3.4-fold the IC_{50} values of the here described investigation, respectively. Despite the use of partially different marker reactions and varying substrate concentrations when the same marker reaction was applied, IC_{50} values are overall well corresponding.

However, as IC_{50} values are highly dependent on the substrate concentration used, a comparison of K_i is more reliable [112]. Here, Jeong et al. reported a K_i value of 2.79 µM and a competitive inhibition by VRC on CYP2C9, which is in good agreement with the findings of this thesis (2.57 µM, competitive inhibition) [85]. On CYP2C19, the authors also described a competitive inhibition, however their determined K_i of 5.07 µM was 2.7-fold higher than the here determined result [85]. Li et al. reported K_i of 1.08 and 1.26 µM when S-mephenytoin and omeprazole were used as marker substrates, respectively [243], which resembled the K_i of 1.90 µM of the current investigation. Lastly, on CYP3A4 Jeong et al. found a mixed competitive and non-competitive inhibition by VRC with K_i of 0.66 and 2.97 µM, respectively [85], while the present study demonstrated a non-competitive inhibition only (K_i 2.75 µM). A lower K_i was described by Li et al. with a value of 0.470 µM [243]. Deviations might arise from the different evaluation methods, Jeong et al. used a graphical tool, Dixon plots, which are based on a linear transformation of the data while in this thesis results were based on the best nonlinear model fit. A disadvantage of Dixon plots is the large influence of the lowest value as the reciprocal of the reaction velocity is plotted on the y-axis. The nonlinear modelling approach is thus less error prone. Furthermore, also here the choice of marker reactions might influence the determined parameters [159,161].

For the inhibitory potential of NO, only three investigations of IC_{50} have been published, resulting in different conclusions. In this work, a relevant inhibitory effect of NO on CYP3A4 was demonstrated (IC_{50} 4.48 µM) and, although to a lesser extent, on CYP2C9 (IC_{50} 13.4 µM), but only a minor one on CYP2C19 (IC_{50} 288 µM), which is in line with Giri et al. (IC_{50} of 11.2 and 8.7 µM on CYP2C9 and CYP3A4, marker substrates diclofenac and midazolam) [89]. Hohmann et al. found a higher inhibitory potential by NO on CYP2C19 (IC_{50} 40.2 µM, luminescence assay) than on CYP3A4 (IC_{50} 146 µM, luminescence assay) [68]. Furthermore, Li et al. reported IC_{50} values for NO of 3.52 µM on CYP3A4 as well as 119 and 40.4 µM on CYP2C19 when S-mephenytoin and omeprazole were used as marker substrate [243]. Previously determined K_i values of NO amounted to 0.894 µM on CYP3A4 (midazolam 1-hydroxylation) as well as 9.0 and 7.43 µM on CYP2C19 when S-mephenytoin and omeprazole were used, respectively, which is 5.9-, 6.- and 7.9-fold lower than K_i determined in this work [243]. OH-VRC has not been investigated previously, but in the present studies partly showed higher inhibitory potential than VRC (1.1-fold higher K_i for CYP3A4). The clinical relevance of the investigated inhibition is challenging to predict. Although plasma concentrations of OH-VRC are up to 30-fold lower than those of NO [37,48,67], local liver concentrations are of higher interest. In this context, especially

the transport in and out of the hepatocytes after the formation of the metabolite is crucial and needs further investigations, e.g. by applying PBPK modelling.

As an additional verification, IC_{50} and K_i were compared by the scientific basis that K_i values of competitive inhibitors represent half of the determined IC_{50}, and K_i values of non-competitive inhibitors are equal to IC_{50} [110,112]. For the competitive inhibition of VRC on CYP2C19 this assumption was met with an IC_{50} of 3.72 µM and a K_i of 1.90 µM. However, for NO and OH-VRC on CYP2C19 this evaluation was less informative, as overall inhibition was low and the estimated IC_{50} values exceeded the applied experimental inhibitor concentrations. Consequently, IC_{50} of the non-competitive inhibitor NO, 288 µM (65.0 – 31623 µM), was only equal to K_i, 58.6 µM (46.8 – 75.2 µM), if the CI were considered. For CYP2C9 the approach fitted well as VRC, NO and OH-VRC were determined as competitive inhibitors and revealed IC_{50} of 4.17, 13.4 and 3.67 µM and K_i of 2.57, 5.47 and 2.80 µM, respectively. Lastly, for CYP3A4 and the non-competitive inhibitors VRC, NO and OH-VRC the IC_{50} values of 1.76, 4.48 and 1.02 µM were overall comparable to the K_i values of 2.75, 5.24 and 2.53 µM, respectively.

Time-dependent inhibition can be observed when (i) reactive intermediates are formed from the substrate that covalently bind to the enzyme, which leads to its inactivation (typically named as "suicide inhibition" or "mechanism-based inhibition"), (ii) tight-binding complex are formed between the enzyme and the metabolite (typically named as "quasi-irreversible inhibition") or (iii) a more potent inhibitory metabolite is formed [111,112,244]. Consequently, time-dependent inhibitors in particular as described under (i) are likely to cause severe and long-lasting drug-drug interactions *in vivo* as CYP enzyme activity can only be restored by re-synthesis of the enzyme [112]. The investigations described in this thesis revealed no time-dependent inhibition on CYP2C19, CYP2C9 and CYP3A4. This is in line with two previously reported findings [83,85], but in contrast to another one, that described a time-dependent inhibition of VRC on CYP3A4 [243]. However, on a closer look, the determined IC_{50} and K_i values from the latter comprised large CI, which casts doubt in the significance of the findings. Additionally, the authors applied the IC_{50} shift dilution method, which has been critically evaluated to highly depend on the approach of data processing [245]. A particular strength of the investigations presented in this thesis is the direct assessment of the inhibitory potential of NO and OH-VRC. This is usually not possible during early drug development as authentic reference standards of metabolites are not yet available. Thus, the detection of inhibitory metabolites relies on the *in situ* formation. However, if the turnover of the substrate is low, a 30 min pre-incubation might not be sufficient to cause quantifiable effects. Hence, direct incubation of the metabolites yields more reliable results and if time-dependent inhibition is observed, allows the precise quantification and distinction of the inhibitory effect of substrate and metabolite. Lastly, it should be acknowledged, that it is usually recommended to keep the reaction time relatively short in comparison to the pre-

incubation period [110]. This was for the marker reactions of CYP2C9 and CYP3A4 rather abided by with 5 and 10 min as well as 7 and 12 min reaction time, but not for CYP2C19 with 15 and 25 min reaction time. Consequently, the inactivation could have continued during the substrate transformation. However, as no inhibitory effect was observed and consequently also no kinetic constants for time-dependent inhibition were derived, this limitation was ranked as negligible.

Overall, *in vitro* metabolism experiments have many pitfalls if not designed and performed with diligence. This work focussed, as discussed, on many of them, however for future approaches further aspects might be considered. First, as mentioned previously, the assumption of negligible nonspecific binding in incubations with low protein concentrations should be confirmed [230–232,246]. Second, not only local liver concentrations should be evaluated for the prediction of clinically relevant drug-drug interactions, but also intracellular concentrations [247]. Third, phase II metabolism should be investigated and quantified as the glucuronidation of VRC has been described previously [37,48,60,72]. Fourth, the interaction of VRC, NO and OH-VRC with transporters might play a role in the distribution and elimination of VRC. Previous investigations showed no interaction of VRC with P-glycoprotein [81], however the elimination of the OH-VRC has been described to exceed glomerular filtration [48]. Fifth, the transferability of kinetic determinations to the system of human hepatocytes might be considered [115,213]. Sixth and last, molecular modelling might contribute to a better justified choice of marker reactions as well as prediction of relevant drug-drug interactions by evaluation of binding modalities and interaction between enzyme, substrate and the respective inhibitor [248,249].

Indeed, for prospective predictions of VRC exposure in humans, developing a PBPK model is suggested to provide a mechanistic framework to integrate VRC physicochemical properties, the presented *in vitro* hepatic metabolism data, and other physiological processes and parameters [250,251]. The increasing availability of *in silico* and *in vitro* systems that act as easy-accessible surrogates for *in vivo* determinations of absorption, distribution, metabolism, and excretion (ADME) processes and advancements in the IVIVE techniques are crucial reasons why PBPK modelling is becoming more appealing [252]. An IVIVE-PBPK linked model is considered a valuable tool for hypothesis testing for investigating the impact of individual, drug-related PK assumptions, which can be confirmed by existing *in vivo* observations. Thus, ultimately knowledge gaps in VRC PK can be unveiled through a learn-predict-confirm-paradigm [253].

Furthermore, IVIVE-PBPK linked models enable extrapolation of VRC PK to vulnerable patient populations, e.g. paediatrics [254,255], to support dosing decisions. However, as a prerequisite the metabolic and elimination pathways and the contribution of different enzymes to each pathway have to be well-characterized using validated and reliable *in vitro* experiments [256]. For VRC several PBPK models have been published recently, which mostly included data from *in vitro* metabolism investigations performed in the early phases of VRC marketing [39,92,243].

However, those experiments were not designed for future applications in PBPK modelling and the knowledge on VRC PK as well as the execution of *in vitro* metabolism experiments has since increased.

Ultimately, the combination of a VRC PBPK model with a PD model, could be used to estimate the time course of drug response for various dosing regimens in different populations or disease states [250,257]. Simulations based such a model could then be used to i) inform and qualify the model using clinically observed data, and ii) recommend optimal dosing regimens for individual patients who have developed invasive fungal infections.

4.3 *In vitro* microdialysis feasibility studies for voriconazole and its *N*-oxide metabolite

The comprehensive *in vitro* analysis presented in this thesis demonstrated the feasibility of the simultaneous microdialysis of VRC and its major circulating metabolite NO, as would be the case in a patient during voriconazole treatment. Furthermore, potential sources of the variability regularly observed in microdialysis data were identified and a convenient approach for the simultaneous catheter calibration for VRC *and* NO presented.

Microdialysis is a valuable, minimally-invasive sampling technique for the assessment of unbound drug concentrations continuously over time in ISF, i.e. the residence of many pathogens and thus the target site of most antiinfectives. This contrasts with biopsy samples, which represent tissue homogenates and thus preclude a differentiation between blood, intra- or extracellular, bound and unbound drug concentrations. Additionally, the collection of biopsies is invasive and prevents the acquisition of multiple samples over time, which is necessary for PK investigations [127,128]. As a result, also regulatory agencies such as the EMA recommend PK investigations based on non-homogenate tissues, e.g. using microdialysis [125]. However, for the design and execution of high quality clinical microdialysis trials knowledge of the behaviour of the drug in microdialysis sampling is crucial. Consequently, reliable results and derivation of plausible conclusions in clinical trials rely on a thorough *in vitro* characterisation [129].

As an essential prerequisite, before the first *in vitro* investigations were performed, the stability of NO under *in vitro* microdialysis conditions were explored. Although during bioanalytical method development and validation the stability of VRC and NO was investigated and demonstrated (chapter 3.1.2.6), this did not cover temperatures of 37°C as applied in the sIVMS. However, the performed pre-investigations showed the stability of NO for 4 h at 37°C at a low (0.01 µg/mL) and a high (4.0 µg/mL) concentration. Based on this bracketing approach, as recommended by the EMA guideline on bioanalytical method validation [139], also concentrations in between were considered as stable under the applied conditions. Also the investigation of stability for longer than 4 h was not deemed necessary as due to the newly developed bioanalytical assay, requiring only 5 µL of microdialysate for analysis, sampling

periods could be considerably shortened. For VRC at a concentration of 10 µg/mL stability at 37°C for 10 h had been previously demonstrated and investigations thus not repeated for the current work [134,137]. In all investigations a VRC analytical reference substance was used and not the approved drug formulation (Vfend®). The major difference of the drug product is the presence of the solubilising agent sulfobutyl ether β-cyclodextrin sodium [38]. Yet no difference between RR of VRC drug substance and drug product has been seen previously, potentially due to the large dilution [137]. Thus, also for NO no impact was expected.

Aiming at reproducible and informative *in vitro* investigations a previously developed and validated sIVMS was used for all investigations [137]. The sIVMS ensured a secure setup of all components of the investigation, i.e. the even positioning of the microdialysis pumps, the stable mounting of the medium containers in the heating block as well as the centred position of the catheter membrane in the catheter-surrounding medium. To mimic physiological-like conditions, the catheter-surrounding medium consisted of RS, was heated to 37°C and constantly stirred to avoid local concentration gradients. Furthermore, for catheter perfusion a clinically relevant fluid (RS) and flow rate of 2 µL/min was chosen [132,146].

The presented *in vitro* investigations revealed high RR of 87.6% of VRC and confirmed the previously reported RR of VRC of 91.5% and 87.0% as well as its independence of concentration [134,135]. Additionally, these observations could be extended to 100-fold lower VRC concentrations, covering a more clinically relevant range [132]. This consistency of RR demonstrated an unhindered diffusion of drug molecules across the catheter membrane and thus was the foundation of reliable results. However, in *in vivo* applications by nature various compounds are simultaneously present in the ISF, potentially interacting, e.g. by competition for the diffusion across the microdialysis membrane, which might have an impact on RR. In the context of drug therapy this might be the case for other concomitantly administered drugs [258] but also the drug's metabolites. Therefore, feasibility of simultaneous microdialysis sampling of VRC and its major metabolite, NO, was to be assessed.

The slightly more hydrophilic metabolite does not differ largely from VRC in terms of molecular mass (349 versus 365 g/mol) and physical-chemical properties, i.e. water solubility, logP and pKa, providing good reason for the very similar behaviour in microdialysis [60,259,260]. RR of NO was also high with 91.1% and independent of concentration when sampled individually. The combination of VRC and NO in *in vitro* microdialysis did not lead to changes in their RR, again demonstrating their unsaturated and unhindered diffusion. The often observed nonspecific binding of lipophilic compounds to components of the microdialysis catheter did not play a role for NO [129,135]. No specific investigations were conducted for that matter, as VRC itself has been successfully applied in microdialysis sampling before, thereby it was unlikely that the more hydrophilic metabolite would show a different behaviour. Additionally, no unexpected

fluctuations in RR were observed during repeated sampling suggesting the absence of adsorption processes. One limitation of the presented investigations is that no combination of a high NO and a low VRC concentration were evaluated as might be observed *in vivo*. This was due to the impurity of the analytical reference standard. Although a purity of >98% was documented in the certificate of analysis, this was not enough as at a concentration of 3 µg/mL this resulted in a content of approximately 0.06 µg/mL VRC. Consequently, only the combination of 0.02 µg/mL VRC and 0.05 µg/mL NO was investigated. *In vivo* no interference of NO on VRC is expected independent of the concentrations as this observation most likely derived from the route of synthesis of the analytical reference standard.

Joint statistical evaluations of potentially impacting experimental factors and scenarios were performed applying an LME modelling approach as graphical evaluations indicated that RR values derived consecutively on the same study day with the same catheter were clustered around one central value. Thus, by mere statistical testing between data subsets, using e.g. t-tests, results could be biased by experimental parameters, potentially resulting in non-existing significant differences. The analyses demonstrated that RR of VRC and its *N*-oxide metabolite in the absence of the respective other was not significantly different to RR determined in the presence of the respective other. Furthermore, no significant differences between VRC and NO RR were detected. Instead, experimental factors were revealed as sources of variability. On the one hand, although microdialysis catheters are assembled by hand, no major variability originated from there, which was in agreement with a clinical trial investigating RR of several antiinfectives [261]. On the other hand, the study day played a large role. As a strict protocol was followed, this was unexpected and might originate from further unidentified factors, e.g. instruments such as the microdialysis pumps causing fluctuations in the flow rate. Also analysis of clinical data revealed interindividual variability as a large source of variability [261]. In the present study, almost 50% of variance in the data remained unexplained (being equal to a SD of 4.23% points) but are likely to include intracatheter variability as well as bioanalytical imprecision, which is allowed to amount to 15% CV [139,209]. A further extension or adaptation of the LME model by inclusion of the concomitant concentration of the combination partner was not possible due to overparametrisation. Consequently, more experiments would be needed. However, based on the exploratory analyses an influence is unlikely.

For catheter calibration, a variety of different methods has been applied, e.g. the method of flow rate variation, (dynamic) no-net-flux method and retrodialysis [127,129,262]. As it is less time intense and hence most applicable, retrodialysis is frequently used in clinical practice [127,261]. Retrodialysis is commonly performed compound-specific for individual catheter calibration *in vivo* [263]. Yet, metabolites are to be considered as chemical substances that are not licensed for the use in humans and hence are not allowed as supplement in retroperfusate solutions.

Consequently, a different approach for the determination of RR was required. The result, that the RR values of VRC and NO were not significantly different *in vitro* allowed for the hypothesis of using VRC retrodialysis for both the parent compound and its metabolite. The feasibility of this hypothesis was confirmed *in vitro* resulting in marginal deviations between VRC and NO. However, overall retrodialysis rather overestimated RR for both compounds resulting in a deviation of +1.6% to -14.9% of the determined concentration of catheter-surrounding medium compared to direct measurement, which indicated a slight imprecision in the method itself. For VRC, this observation has been described previously, with a mean RR of 87.0% at concentrations ranging from 0.5 to 4 µg/mL but a mean rD of 95.3% and 96.0% at concentrations of 20 and 200 µg/mL, respectively [135]. However, this contrasts with another report that did not find a difference in RR and rD for VRC with both values exceeding 95% at a flow rate of 1.5 µL/min across a concentration range from 1.0 to 50.0 µg/mL [134,137]. In context of the large total variability often observed in clinical microdialysis trials the occasionally observed deviation between RR and rD might be negligible and the use of retrodialysis still more convenient and the obtained results more accurate and precise compared to other catheter calibration procedures [127]. Nevertheless, further refinement of existing catheter calibration methods to derive tissue fluid concentrations is desirable. An interesting approach applied an IS in perfusate observing simultaneously the loss of the standard and recovery of the drug of interest saving the time and effort of retrodialysis altogether [127,261,264,265]. Either way, individual *in vivo* RR determinations are essential and a transfer of *in vitro* RR data insufficient as the presence of cells and extracellular matrix leads to a different movement of molecules, i.e. tortuosity [127,129]. As a consequence of tortuosity, RR determined *in vivo* are mostly lower than *in vitro* RR. For VRC this observation was confirmed, although not very distinct, with *in vivo* RR of 84.9% and 85.2% [132,146] compared to 87.6% *in vitro*. Nevertheless, the findings of identical behaviour and comparable RR of VRC and NO *in vitro* are assumed to be applicable also to the *in vivo* situation, justifying the utilisation of VRC retrodialysis for determination of tissue fluid concentrations of NO.

Although NO is not contributing to the antifungal activity of VRC, it has been suspected to contribute to adverse events, in particular to the emergence of phototoxicity and photocarcinogenicity occurring in patients with long-term VRC treatment [65,66,266,267]. A plausible mechanism of the sensitisation of keratinocytes to UV A light by NO and its photoproduct, has been presented based on *in vitro* investigations [66]. Thus, TDM and individualised dosing strategies might not only need to target certain VRC concentrations, but also limit NO concentrations [174]. Here, target-site exposures of VRC and NO, instead of total plasma concentrations, might yield more informative relationships between VRC PK and its pharmacodynamics (PD) to guide the optimisation of VRC dosing regimen [268].

The sIVMS, as it was used in this work, is a useful tool for first investigations of new compounds in microdialysis sampling. However, to further characterise the behaviour of VRC and NO in microdialysis sampling, additional efforts should be made towards a better mimicry of physiological-like conditions. This comprises two major aspects: first, RS is an isotonic and thus osmotically neutral solution, however the true ISF is more complex. Thus, future research should focus on identification of ISF composition and its mimicry for *in vitro* investigation as well as ideally incorporating the *in vivo* observed effect of tortuosity [127–129]. Second, in the sIVMS the concentration of the compounds is constant over time, which is not representative for the *in vivo* situation. Consequently, *in vitro* microdialysis investigations of VRC and NO in a dynamic setting would be of interest. Such dynamic *in vitro* microdialysis systems have been developed and validated [135] and could be applied also for mimicking VRC and NO concentration-time profiles. Thus, microdialysis sampling including also retrodialysis investigations could be performed closer to a real-life scenario.

Overall, it was demonstrated that comprehensive *in vitro* investigations are not only important components but necessary prerequisites on the path to meaningful clinical microdialysis trials. The demonstrated feasibility of simultaneous microdialysis of VRC and its major metabolite in clinically relevant concentrations as well as the applicability of VRC retrodialysis for both, depicts the essential framework for reliable *in vivo* investigations.

4.4 Clinical microdialysis trial for the determination of voriconazole and its *N*-oxide metabolite concentrations in plasma, ultrafiltrate and interstitial space fluid

In this work, the *in vivo* feasibility and clinical applicability of the simultaneous microdialysis of VRC and its *N*-oxide metabolite in humans was demonstrated. Moreover, the exploratory PK analysis enabled the leveraging of knowledge from target-site distribution and concentration-dependent metabolism processes and highlighted the large intra- and interindividual variabilities observed in VRC treatment. Additionally, the results revealed the substantial differences between plasma and ISF PK investigations of VRC and NO. Finally, the CYP2C19 genotype-predicted phenotype plausibly related to the observed VRC and NO concentrations in plasma, ultrafiltrate and ISF.

The comprehensive *in vitro* investigations demonstrated the feasibility of the simultaneous sampling of VRC and NO via microdialysis. Moreover, the analysis showed that RR of VRC and NO were not significantly different, and hence VRC retrodialysis could be applied for the determination of ISF concentrations of both compounds. For all *in vitro* investigations, identical microdialysis conditions as in the clinical trial were used. This included the same microdialysis catheter type (CMA 60) as well as the perfusion of the catheters with RS at a flow rate of

2 µL/min. Hence, it was concluded that the *in vitro* observations formed the necessary prerequisite to continue with the evaluation of the *in vivo* feasibility.

As a consequence, plasma, ultrafiltrate and microdialysate samples of a clinical trial were evaluated for their VRC and NO concentrations. The clinical trial was performed between 2009 and 2013 at the Medical University Vienna, aiming at the assessment of target-site PK of VRC in healthy volunteers. Therefore, ten healthy individuals were enrolled in the study, of which nine completed it, and received a VRC standard dosing regimen of 6 mg/kg bodyweight i.v. as a 2 h infusion on day one, 4 mg/kg i.v. as a 1.3 h infusion on day two and 200 mg tablets on day three and four [38]. Microdialysis catheters were placed in subcutaneous adipose tissue and ISF sampled according to a fixed schedule (chapter 2.5.1). Besides, plasma samples were taken and processed via ultrafiltration to obtain the unbound VRC fraction. The preceding first evaluation of the clinical study investigated VRC concentrations only in ultrafiltrate and microdialysate [132,137,146,173]. However, due to the newly gained knowledge from *in vitro* microdialysis investigations as well as information about the potential toxicity of NO [66], the analysis of the remaining sample volumes was considered as a viable approach for the initial assessment of the feasibility and clinical applicability of the simultaneous *in vivo* microdialysis sampling of VRC and NO.

Thus, plasma, ultrafiltrate and microdialysate samples from four individuals, that were fully genotyped for their CYP2C19 metaboliser status, were quantified using the newly developed and validated bioanalytical LC-MS/MS assay (chapters 2.2 and 3.1). As for the new assay only low sample volumes, i.e. 5 µL microdialysate and 20 µL plasma or ultrafiltrate, were required; all samples except three ultrafiltrate samples could be analysed. A renewed ultrafiltration of plasma samples was abstained from as potential alterations in the plasma proteins due to the long storage period could not be excluded, and thus the comparability might have been impeded.

Ultrafiltration is a commonly used method for the determination of unbound plasma concentrations of drugs [269–274]. Ultrafiltrate samples of this study were acquired by Centrifree® (ultracel regenerated cellulose membrane with 30 kDa molecular mass cut-off) ultrafiltration devices and centrifugation at 2000 × *g* for 20 min at room temperature [173]. However, for a variety of antiinfective drugs it has been described that the determined f_u is relevantly impacted by the experimental design of the ultrafiltration investigation. First, the choice of the ultrafiltration device with regard to the material of the ultrafiltration membrane, the material of the tube itself and the molecular-mass cut-off is essential. As an example, for fluconazole, linezolid and vancomycin, variability between different ultrafiltration devices has been shown [272,275]. In this context, to obtain reliable results also the nonspecific binding to the ultrafiltration membrane or the material of the tube needs to be investigated, e.g. by ultrafiltration of a protein-free test solution of the drug [272,275–277]. Second, experimental

conditions such as the temperature during ultrafiltration, the time and centrifugal force applied, were suspected and partially demonstrated to alter the determined f_u [272,275–277]. Third, the pH of plasma is influenced by storage and processing, potentially due to a loss of carbon dioxide, and hence is increasing over time [278,279]. Consequently, also plasma protein binding was observed to change with pH [272,273,277]. For VRC and NO no comprehensive investigations have been published, which systematically considered the impact of the described experimental conditions applied in ultrafiltration on the determination of VRC and NO unbound plasma concentrations. Hence, the influence of the chosen or uncontrolled experimental conditions and potential variations in these between individual analytical runs, e.g. pH and room temperature, on the determined f_u in the here evaluated study is difficult to assess. Overall, the gold standard for the determination of plasma protein binding is considered to be equilibrium dialysis [269–271]. The approach is based on the separation of the protein-containing sample and a puffer solution without proteins by a selective-permeable membrane. Similar to ultrafiltration, the unbound drug can cross the membrane while plasma proteins and the protein-bound drug cannot. Thus, after a period of 2 to 6 h, an equilibrium is reached and by quantification of the respective fraction of the drug in the two cavities the plasma protein binding can be determined [269,270]. However, it must be acknowledged that equilibrium dialysis is often time-consuming and challenging to implement in clinical practice. Thus, ultrafiltration is a beneficial method but a prior comparison of the two methods, i.e. equilibrium dialysis and ultrafiltration, or a systematic exploration of the impact of the described experimental conditions could have increased the validity of the study's evaluation of unbound plasma VRC and NO concentrations.

Nevertheless, in this study for VRC the nonspecific binding to the ultrafiltration device was investigated before the clinical trial and the absence of interferences demonstrated [137], which contrasts with another study [58]. Overall, for VRC a variety of different f_u have been reported in literature [57–60,276]. The manufacturer Pfizer reported in the summary of product characteristics a f_u of 42% [38], which is based on a triplicate determination of one VRC concentration by equilibrium dialysis [60]. Comparable results were obtained by Vanstraelen et al. who reported a f_u of 52.4% *in vitro* and of 50.4% *in vivo* in samples of patients of the intensive care unit [57] as well as Resztak et al., who found a f_u of 47.0% and 41.7% using two different ultrafiltration devices [58]. In contrast, Florent et al. reported a f_u of 32.3% and 22.95% determined *in vitro* and in plasma of patients, respectively [59]. However, the latter determination was critically commented as several experimental conditions might have led to the underestimation of f_u of VRC [276]. In comparison, the f_u of VRC determined in this work was 62.8% and thus higher than literature data. Potentially also here experimental conditions, e.g. the centrifugation at room temperature in contrast to 37°C, played a role. Nevertheless, to the best of knowledge, for the first time also a f_u of NO was reported. Overall, a slightly lower protein binding

of the more hydrophilic metabolite and hence a higher f_u was expected. This hypothesis was only confirmed for two individuals, the CYP2C19 RM and NM, with a median f_u of 71.3%. However, the remaining two individuals revealed considerably lower f_u. As in the respective chromatograms of the samples also an emerging second peak was observed, an instability of NO was assumed. In this case, potentially more freeze-thaw cycles of the ultrafiltrate samples of those two individuals might have played a role. All in all, ultrafiltrate data, in particular of the CYP2C19 IM and RM/PM, should be handled with some care when interpreting the presented results.

The first relevant observation during bioanalysis of microdialysate samples was the presence of NO in these samples. To the best knowledge, there are neither previous reports of the distribution of NO into ISF nor the extent. Based on the *in vitro* demonstrated feasibility of VRC retrodialysis for VRC *and* NO, tissue fluid concentrations were determined for subsequent PK evaluations.

In a first step, the concentration-time profiles in the respective matrices were explored. Therefore, for ISF, VRC and NO concentrations were allocated to a specific time point, the midtime point of the microdialysis sampling interval, despite originating from a collection period. Although this approach is commonly used for the evaluation of microdialysis data [132,280,281], the accuracy decreases the longer the collection intervals are and the more pronounced the concentration changes during this time. Moreover, it was shown that it had some limitations when the interindividual variability of PK parameters was investigated [282]. However, the proposed evaluation with an integral nonlinear mixed-effects compartmental analysis approach is associated with higher complexity and effort. Consequently, given the very intensive sampling as well as omitting the determination of the terminal elimination rate constant (λ_z) and dependent PK parameters, e.g. $t_{1/2}$, for a first exploratory PK analysis also the midtime point approach was justifiable. Nevertheless, for more extensive clinical studies, e.g. dose-finding studies, the more sophisticated integral nonlinear mixed-effects compartmental analysis approach might yield more reliable results and conclusions.

Overall, concentration-time profiles of VRC and NO in all matrices were highly plausible. In plasma and ultrafiltrate, one sample in the seventh dosing interval at 1.75 h might have been confused between the CYP2C19 RM/PM and NM as the concentration-time profiles for VRC suddenly fluctuate intensely and also for NO the respective concentrations would be replaceable. As the same fluctuation is observed in plasma and ultrafiltrate and the handling of the samples for bioanalysis (samples of the two individuals were processed in different analytical runs) eliminates the probability that samples were mixed up during analysis, it is likely that they were wrongly labelled already in the clinic. Despite this observation, concentration-time profiles of NO showed in general, a more pronounced fluctuation than those of VRC. Moreover, fluctuation of concentration-time profiles was more distinct in ultrafiltrate than in plasma and least in ISF. In all investigated matrices, in the first dosing interval C_{max} of NO occurred at later time points than

C_{max} of VRC, which was highly plausible as the formation of NO by metabolic processes in the liver is time delayed. Potentially also the saturation or autoinhibition of metabolising enzymes, displayed by VRC and its metabolites, contributed to the extent of the naturally expected time delay (chapter 4.2). Interestingly, VRC t_{max} was observed at earlier time points in the fifth and seventh dosing interval compared to the first, although i.v. dosing was switched to p.o. dosing and thus was expected to delay t_{max} due to dissolution and subsequent absorption processes in the digestive system. Lastly, C_{max} of VRC and NO occurred in plasma/ultrafiltrate and ISF at comparable time points, indicating a rapid distribution into ISF. For NO, concentration-time profiles in all matrices were plateau-like in the fifth and seventh dosing interval and thus precluded a meaningful definition of t_{max}.

For VRC as a PK target total plasma C_{min} of 1-2 µg/mL (equal to 2.86 – 5.73 µmol/L) have been described for efficacy and C_{min} of 4.5-6 µg/mL (equal to 12.9 – 17.2 µmol/L) as a threshold of toxicity [174,180]. The four individuals of this study did not exceed the lower threshold after the first VRC dose and only the CYP2C19 IM and RM/PM from the second dosing onwards. In the context of antifungal treatment, the probability of therapy failure would be high in the CYP2C19 RM and NM. Therefore, TDM is recommended to assess C_{min} [174]. This recommendation is based on a clinical trial that showed a larger treatment response in the TDM group compared to the non-TDM group (81% versus 57%) as well as a lower proportion of discontinuation of VRC due to adverse events in the TDM group [283]. For the implementation of TDM for VRC in clinical routine, a recent position paper advises for the evaluation of one TDM sample, taken maximum 30 min before the next dosing two to five days after initiation of VRC therapy [174]. However, often the successful performance of TDM is challenging due to the clinical infrastructure. This includes for instance, the correct timing of sample collection to enable correct decisions on dose adaptations or the bioanalytical process and the subsequent report of the results back to the clinicians. Often only a few samples for TDM of one drug are available and assays therefore run only once or twice a week, which delays the time until dose adaptation immensely [284,285].

Further evaluations focussed on the total exposure to VRC and NO. Therefore, AUC was assessed based on all available concentrations without extrapolation. An extended noncompartmental analysis was not found feasible for VRC as in the terminal elimination phase a linear decline, on a logarithmically scaled y-axis, was not consistently recognisable for all four individuals. Additionally, the plateau-like concentration-time profiles in particular of NO precluded a determination of a meaningful terminal elimination rate constant, which would lead to a large extrapolation of AUC and thus very imprecise PK parameter estimations. Not all concentration-time profiles of all individuals were complete, there were two unavailable ultrafiltrate concentrations of the CYP2C19 RM/PM in the seventh dosing interval and three missing

microdialysate samples of the same individual in the fifth dosing interval. As a result, AUC determinations were probably in those cases less precise in comparison to the other determinations. However, as in none of the trajectories of the other individuals at those time periods distinctly in- or decreasing concentrations were observed, the resulting error in AUC calculation was expected to be negligible.

Overall, VRC showed a relatively good distribution to ISF with observed exposure in ISF ranging from 35.5% to 68.2% compared to plasma exposure (Table 3.19). As the VRC AUC ratio of ISF to ultrafiltrate approached 1, an unimpeded diffusion of VRC into extravascular spaces was suggested because only the protein unbound fraction is unhindered in its diffusion. For NO, the AUC ratios of ISF to plasma were lower than for VRC, indicating a less distinct distribution of NO to ISF. In this context, a potentially higher renal excretion of the more hydrophilic metabolite might play a role [259,260]. This hypothesis is supported by the renal clearances (CL_R) determined by Geist et al. who reported a slightly lower CL_R of 1.39±1.04 mL/min for VRC compared to 1.60±1.08 mL/min for NO [67]. Interestingly, in particular the CYP2C19 IM revealed a very low NO exposure in ISF and consequently low AUC ratios of ISF to plasma and ultrafiltrate in comparison to the other individuals. The reasons for this remain to be elucidated. Furthermore, VRC and NO PK should be investigated in a statistically relevant number of CYP2C19 IM, as well as PM, as the described observation might be an individual variation.

Based on the total exposure of the metabolite in comparison to the parent drug, *current* guidelines by regulatory agencies, such as the FDA, recommend additional *in vitro* investigations to evaluate the toxicity as well as the interaction potential of the metabolite with CYP enzymes and transporters during drug development [209,286,287]. Firstly, toxicity studies, i.e. the assessment of genotoxicity, embryo-fetal development toxicity and carcinogenicity can become relevant when the metabolite exposure in humans is greater than 10% of the total drug-related exposure at steady-state [287]. However, these investigations are only essential if a metabolite is present in high levels in humans but not in any of the tested animal species during drug development. For VRC and its *N*-oxide metabolite, this was not the case, as tested species such as rat and dog revealed relevant NO concentrations as well [60]. Therefore, possibly adverse events, such as phototoxicity and photocarcinogenicity observed in patients with long-term VRC treatment, could be related to the *N*-oxide metabolite only after market authorisation and continued research [65,66,266,267]. Should the assumptions of the toxicity of NO be confirmed, distribution of NO into the skin might play an important role. In this context, the presented results of the distribution of NO into subcutaneous adipose tissue could provide first insights. Secondly, according to the current FDA guideline on *in vitro* drug interaction studies [209], additional *in vitro* investigations should be performed during drug development based on the *in vivo* total exposure and the polarity of the respective metabolite. The key elements to be explored are the metabolites inhibitory

potential on transporters and metabolising enzymes. In the case of less polar metabolites (compared to the parent drug) investigations should be performed if the AUC of the metabolite is ≥25% of the AUC of the parent. If the metabolite is more polar than the parent, *in vitro* analyses are required if the AUC of the metabolite is equal to or greater than the AUC of the parent [209]. For VRC the attainment of the latter described limit would be, based on the results of the four individuals of this study, dependent on the CYP2C19 genotype, an aspect not covered by the FDA guideline. However, regardless of the potential regulatory requirement for such studies nowadays, in this thesis the described investigations on the inhibitory potential of the VRC metabolites NO and OH-VRC were performed and presented in chapter 3.2.3. The *in vivo* relevance of the observed inhibitory potential of a drug or metabolite is evaluated considering local organ concentrations [149]. Consequently, PBPK modelling and simulation can be helpful to assess local concentrations of VRC and its metabolites to elucidate their influence in the characteristic PK of VRC (see also chapter 4.2) [149]. Prospectively, this knowledge might help to develop more precise individual VRC dose recommendations.

Furthermore, the extent of metabolism was evaluated by the assessment of metabolic ratios, i.e. the ratio of NO to VRC as concentrations in individual samples of the different matrices or AUC. When the individual metabolic ratios were observed in dependence of the VRC concentration a nonlinear decrease with increasing VRC concentrations was revealed in all matrices and all individuals (Figure 3.33). This was in line with a saturation process of VRC *N*-oxidation or with an onset of inhibition by VRC or a metabolite on its own biotransformation [65,68,288], which could also explain the observed nonlinear PK of VRC [60,104,132,288,289]. Additionally, metabolic ratios summarised the information on both compounds and thus a simultaneous evaluation of the observed effects was feasible. In particular the intra- and interindividual variability was easily assessable.

Based on the individual metabolic ratios, the observed intraindividual variability was largest during the first doing interval. This was not unanticipated as VRC metabolism in the liver delayed the occurrence of NO in blood and consequently also in ISF. Thus, in particular at the beginning of the first dosing interval NO:VRC ratios were small and did not decrease at any other time point of the study again to these initial values. The largest intraindividual variability was observed in all matrices for the CYP2C19 RM potentially due to the largest fluctuations in the concentration-time profiles caused by the rapid VRC metabolism.

As all healthy individuals had similar demographic characteristics, i.e. male, aged between 22 and 28 years, BMI of 20.5 – 23.4 kg/m², their CYP2C19 genotype-predicted phenotype was presumably the most influential parameter for the observed interindividual differences [239,290]. CYP2C19 is a highly polymorphic enzyme with 35 defined variants (so-called star alleles, e.g. *2 and *17). The most common loss of function allele is the *2 allele as well as the *3 allele in

the Asian population. The *17 gain of function allele is most common in African populations [63,291]. Depending on the combination of the two CYP2C19 alleles (CYP2C19 genotype), five different CYP2C19 phenotypes are defined according to the CPIC® [63]: UM (*17/*17), RM (*1/*17), NM (*1/*1), IM (*1/*2, *1/*3, *2/*17) and PM (*2/*2, *3/*3, *2/*3). As routinely only the presence of the *2, *3 and *17 alleles are searched for and the *1 allele assumed in their absence, differences between the CYP2C19 genotype and phenotype are possible on the rare occasion of the presence of a less frequent allelic variant. In the context of this study, it was plausible that the CYP2C19 RM showed the lowest VRC but highest NO concentrations while it was reversed for the IM. Interestingly, profiles of the PM/RM (CYP2C19 *2/*17) were closer to the IM than the RM, suggesting a high influence of the *2 and a minor impact of the *17 allele on NO formation, which justified the classification of the CPIC® as an IM [63].

The observed interindividual differences in this study increased when besides plasma VRC concentrations also NO concentrations were considered. This was indicated by a maximum 4.8-fold observed difference in plasma AUC between the CYP2C19 RM and IM when only VRC was assessed, compared to a maximum 6.2-fold difference when the AUC ratios of VRC to NO of the RM and IM were considered. Moreover, the interindividual difference was elevated further when ultrafiltrate and ISF concentrations were examined. As variability in ultrafiltrate might originate from the observed NO instability, no further conclusions should be drawn here. However, in ISF, a maximum 4.3-fold difference between the RM and IM was observed when VRC AUC was investigated, which increased to a 24-fold difference between the two individuals when VRC to NO AUC ratios were considered. In short, VRC and NO plasma concentrations did not represent a reasonable surrogate parameter for target-site PK and disregarded important subsequent PK processes that might be essential to draw conclusions on an appropriate VRC dosing regimen. Yet, when comparing interindividual differences in plasma and ISF, the large method-related variability of microdialysis has to be taken into account. Recent studies thoroughly explored this methodology-related variability and inferred clinical trial recommendations, e.g. determination of individual RR for each patient as well as multiple determinations per patient [261]. As the present study complied to these essential settings the made comparison of the interindividual differences in the two matrices seem appropriate. In total, in a larger and more diverse *patient* population, in contrast to the four healthy adults in this study, variability is expected to increase even further, outlining the challenges in safe and effective VRC dosing.

Currently, only VRC and NO total plasma concentrations were assessed for the deduction of efficacy and/or toxicity, a relationship that some studies could confirm [292–296] and others not [65,295]. In particular, the occurrence of neurotoxicity and hepatotoxicity were recently associated with increased VRC concentrations in a meta-analysis [296]. Yet, most studies

observed high intra- and interindividual variability in VRC concentrations impeding relations between less frequent adverse reactions. Overall, the assessment to target-site exposure of VRC and NO might lead to a better understanding of its PK relationship to observed PD effects.

Regarding the observed intra- and interindividual variabilities, also the switch in VRC dose administration from i.v. to p.o. and the simultaneously discarded weight-adaptation are a plausible source for observed variability. In the here analysed clinical trial a switch from i.v. to p.o. dosing was performed on day three. Consequently, distinct differences in the investigated PK parameters, e.g. AUC and C_{max}, were observed between the first (first weight-adapted i.v. loading dose of 6 mg/kg), fifth (first p.o. 200 mg dose) and seventh (last p.o. 200 mg dose) dosing interval. This was in general expected as the switch to p.o. dosing was accompanied by a decrease in VRC dose for all individuals and hence a new steady-state condition was progressing.

Finally, the analysis of the study samples demonstrated the suitability of the established concentration range of the bioanalytical assay. For microdialysate only one sample was below the LLOQ for VRC and NO while for plasma and ultrafiltrate concentrations did not fall below the LLOQ. However, individual samples were above the ULOQ of VRC. As none exceeded the limit of more than +15%, which reflects the accuracy criterium defined by the EMA guideline on bioanalytical method validation [139] of QC and CAL samples, evaluation was deemed feasible.

Lastly, it should be acknowledged that for this exploratory PK analysis study samples were evaluated that were stored for approximately 8 years at -80°C. Despite the very plausible results and the thorough investigations during bioanalytical method validation and responsible handling, stability should be considered with caution. Moreover, only four healthy individuals were investigated. For confirmation of the established hypotheses a larger study is required linking VRC and NO ISF concentrations to efficacy and toxicity while ensuring a reasonable distribution of CYP2C19 genotype-predicted phenotypes.

The use of microdialysis provides an excellent approach for the determination of unbound concentrations in ISF, i.e. the target site of antifungals such as VRC. In the presented proof-of-concept investigation the feasibility of simultaneous microdialysis of VRC and its *N*-oxide metabolite was demonstrated *in vivo*. Additionally, in an exploratory PK analysis, the clinical applicability of the concomitant observation of VRC and NO in different matrices was shown. The assessment of ISF as well as metabolite concentrations increased the knowledge of the PK of VRC by demonstrating the full extent of interindividual differences as well as its potential source.

5 Conclusions and perspectives

The present thesis successfully generated quantitative and mechanistic insights into VRC distribution and metabolism processes in humans by leveraging *in vitro* and *in vivo* approaches to advance the elucidation of the complex PK of VRC. For this purpose, research in three major areas was performed and presented. First, a bioanalytical LC-MS/MS assay was developed, validated and implemented to allow the quantification of VRC and its two metabolites, NO and OH-VRC, in a large variety of matrices enabling detailed PK investigations in humans. Second, *in vitro* metabolism studies were performed, characterising VRC and its metabolites comprehensively as substrates and inhibitors of the CYP isoenzymes 2C19, 2C9 and 3A4. Third, microdialysis, as a powerful technique for the assessment of target-site concentrations, was thoroughly characterised *in vitro* for the simultaneous sampling of VRC and NO. Finally, the obtained knowledge was applied to investigate the *in vivo* feasibility and clinical applicability of the simultaneous microdialysis of VRC and NO by quantification of clinical trial samples and a subsequent exploratory PK analysis (Figure 5.1).

The developed and validated **bioanalytical LC-MS/MS assay** enabled the rapid quantification of VRC, NO and OH-VRC in small sample volumes of various matrices. Thus, it laid the foundation for consecutive research in two main areas: (i) VRC PK investigations in human *in vivo* studies and (ii) mechanistic and quantitative understanding of VRC metabolism through *in vitro* analyses. The simultaneous quantification of VRC and its major circulating metabolite VRC *N*-oxide in plasma, ultrafiltrate and microdialysate (i) allowed the determination of the unbound, and thus pharmacologically active, fraction in plasma and in ISF, the target site of antiinfectives, respectively. The small sample volumes and the low LLOQ expand the performance of PK investigations by enabling high resolution concentration-time profiles and allowing for an increased number of samples in vulnerable populations, such as infants. At the same time, the simple and rapid sample pre-treatment is ideally suited for measurements in the clinical setting. The assessment of additional metabolite concentrations thereby supports the understanding of intra- and interindividual variability in VRC PK and the contribution in causing therapy failures or adverse events. Finally, the explanatory power of *in vitro* metabolism investigations (ii) is improved as the low LLOQ and small sample volumes enable the optimisation of experimental parameters, such as low enzyme and substrate concentrations as well as short reaction times.

***In vitro* investigations in different enzymatic systems** such as HLM, HIM and rhCYP are an effective tool for the assessment and evaluation of human drug metabolism not only during drug development but also for well-established drugs. In this work, the Michaelis-Menten kinetics of the *N*-oxidation of VRC were quantified, revealing the polymorphic CYP2C19 as main contributor to the observed CL_{int}, CYP3A4 with a secondary and CYP2C9 with a negligible role.

Time-independent inhibition by VRC, NO and OH-VRC was observed on all three enzymes with NO being the weakest and VRC and OH-VRC comparably strong inhibitors of CYP2C9 and CYP3A4. CYP2C19 was significantly inhibited by VRC only. Thus, the presented coherent framework of VRC metabolism assessing and quantifying relevant aspects of its properties as a substrate and inhibitor allows for a better understanding of clinical observations in VRC PK, e.g. its nonlinear kinetics, drug-drug interactions and interindividual variability. Future perspectives in VRC dose optimisation as well as individualisation lie within *in silico* approaches such as PBPK modelling. PBPK modelling enables the simultaneous integration of a wide range of human (patho)physiological parameters and physicochemical properties of a drug to overall predict the systemic or tissue exposure of the drug over time. As a consequence, observations from one population, e.g. adults, can be extrapolated to another, e.g. children, to guide safe and effective VRC treatment. In this work, high quality quantitative data of VRC metabolism were presented, which are ideally suited as input parameters for PBPK modelling and an essential prerequisite for reliable predictions. Overall, this approach could translate the presented research results from *in vitro* over *in silico* to clinical practice, supporting future therapeutic decisions.

Microdialysis is a powerful method for the determination of unbound drug concentrations in ISF, i.e. the target site of antifungals such as VRC. However, implementation of microdialysis sampling is associated with certain challenges as a variety of influential parameters can affect experimental results and thus the thereon based conclusions. Consequently, *in vitro* feasibility investigations were performed to ensure an unbiased *in vivo* application. For this purpose, RR of VRC and its major circulating metabolite, NO, were assessed in the absence and presence of the respective other and the insignificance of the deviations demonstrated by LME modelling concurrently quantifying the impact of the microdialysis catheter and the study day on RR. Moreover, VRC retrodialysis was demonstrated to be feasible for determination of ISF concentrations from microdialysate of both compounds. Hence, it relevantly facilitated *in vivo* applications as NO as a metabolite is not approved for human use preventing the usual compound-specific catheter calibration. Overall, it was demonstrated that comprehensive *in vitro* investigations are not only important components but necessary prerequisites on the path to meaningful clinical microdialysis trials.

Based on the knowledge gained *in vitro*, clinical plasma, ultrafiltrate and microdialysate samples from four healthy male individuals were evaluated for their VRC and NO concentrations in a proof-of-concept investigation. As a result, the distribution of NO into ISF was for the first time observed and quantified and hence also the feasibility of simultaneous microdialysis of VRC and its *N*-oxide metabolite *in vivo* was demonstrated. The exploratory PK analysis highlighted the knowledge on interindividual differences that can be gained by amalgamating information of target-site distribution and simultaneous drug and metabolite assessment and that total plasma

concentrations are not in all cases suitable surrogates. Further research is required to link VRC and NO ISF concentrations to efficacy and toxicity in relation to the CYP2C19 phenotype, e.g. by generating a joint drug and metabolite PK model linked to PD parameters.

Overall, this thesis fostered the quantitative understanding of VRC distribution and metabolism processes in humans by combining different research areas. Further, it unveiled and described sources of intra- and interindividual variability in the context of the PK of VRC. Ultimately, the elucidation of VRC PK, in particular the understanding of its complex metabolism and distribution to the target site will guide the development of individualised, metabolism-based dosing regimens for VRC.

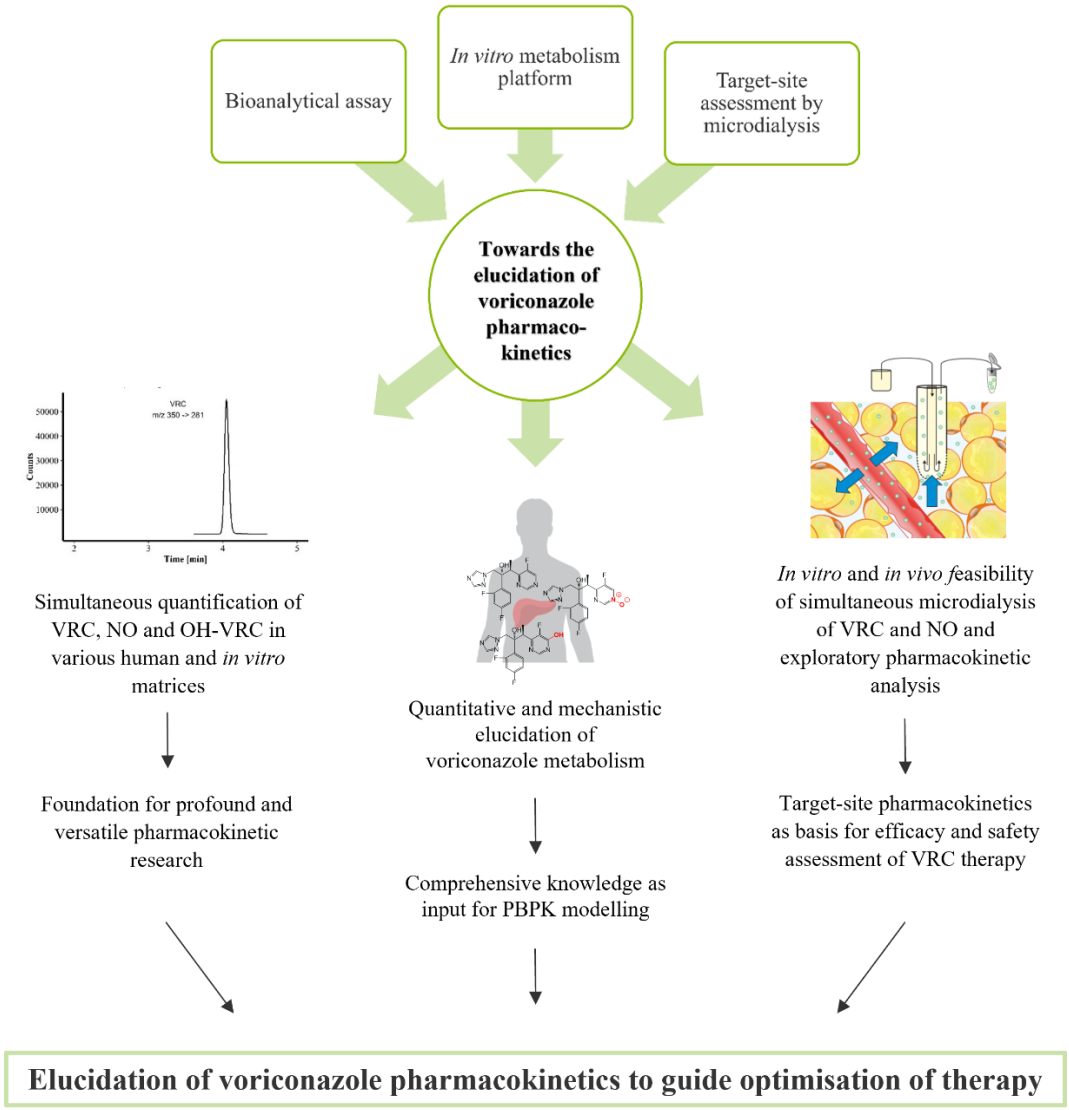

Figure 5.1: Overview of the applied methodologies, the objective, the main results and the perspectives of this thesis. NO, voriconazole *N*-oxide, OH-VRC, hydroxyvoriconazole; PBPK, physiologically-based pharmacokinetic; VRC, voriconazole

6 Bibliography

[1] V. Raleigh. Trends in world population: how will the millenium compare with the past? Human Reproduction Update 5: 500–505 (1999).

[2] S. Haensch, R. Bianucci, M. Signoli, M. Rajerison, M. Schultz, S. Kacki, M. Vermunt, D.A. Weston, D. Hurst, M. Achtman, E. Carniel, B. Bramanti. Distinct Clones of Yersinia pestis Caused the Black Death. PLoS Pathogens 6: e1001134 (2010).

[3] K.I. Mohr. History of Antibiotics Research. In: Current Topics in Microbiology and Immunology. Springer Verlag, 237–272 (2016).

[4] M.I. Hutchings, A.W. Truman, B. Wilkinson. Antibiotics: past, present and future. Current Opinion in Microbiology 51: 72–80 (2019).

[5] K.D. Kochanek, J. Xu, Arias Elizabeth. Mortality in the United States. https://www.cdc.gov/nchs/data/databriefs/db395-H.pdf (last access 14 Dec 2021).

[6] Centers for Disease Control and Prevention. Achievements in Public Health, 1900-1999: Control of Infectious Diseases. https://www.cdc.gov/mmwr/preview/mmwrhtml/mm4829a1.htm (last access 14 Dec 2021).

[7] Statistisches Bundesamt. Todesursachen in Deutschland. https://www.destatis.de/DE/Themen/Gesellschaft-Umwelt/Gesundheit/Todesursachen/_inhalt.html (last access 12 Mar 2022).

[8] Tackling drug-resistant infections globally. https://amr-review.org/sites/default/files/160518_Final%20paper_with%20cover.pdf (last access 14 Dec 2021).

[9] World Health Organization. Antimicrobial resistance. https://www.who.int/news-room/fact-sheets/detail/antimicrobial-resistance (last access 14 Dec 2021).

[10] F. Prestinaci, P. Pezzotti, A. Pantosti. Antimicrobial resistance: a global multifaceted phenomenon. Pathogens and Global Health 109: 309–318 (2015).

[11] C.L. Ventola. The antibiotic resistance crisis. Pharmacy & Therapeutics 40: 277–283 (2015).

[12] M.C. Fisher, N.J. Hawkins, D. Sanglard, S.J. Gurr. Worldwide emergence of resistance to antifungal drugs challenges human health and food security. Science (1979) 360: 739–742 (2018).

[13] World Health Organization. Global Action Plan on Antimicrobial Resistance. https://apps.who.int/iris/rest/bitstreams/864486/retrieve (last access 8 Dec 2021).

[14] G.D. Brown, D.W. Denning, N.A.R. Gow, S.M. Levitz, M.G. Netea, T.C. White. Hidden Killers: Human Fungal Infections. Science Translational Medicine 4: 165rv13-165rv13 (2012).

[15] World Health Organization. Tuberculosis. https://www.who.int/en/news-room/fact-sheets/detail/tuberculosis (last access 14 Sep 2021).

[16] F. Bongomin, S. Gago, R. Oladele, D. Denning. Global and Multi-National Prevalence of Fungal Diseases—Estimate Precision. Journal of Fungi 3: 57 (2017).

[17] World Health Organization. First Meeting of the WHO Antifungal Expert Group on Identifying Priority Fungal Pathogens. https://apps.who.int/iris/rest/bitstreams/1279936/retrieve (last access 8 Dec 2021).

[18] B. Pathakumari, G. Liang, W. Liu. Immune defence to invasive fungal infections: A comprehensive review. Biomedicine & Pharmacotherapy 130: 110550 (2020).

[19] J.D. Jenks, O.A. Cornely, S.C.A. Chen, G.R. Thompson, M. Hoenigl. Breakthrough invasive fungal infections: Who is at risk? Mycoses 63: 1021–1032 (2020).

[20] L. Ostrosky-Zeichner, M. Al-Obaidi. Invasive Fungal Infections in the Intensive Care Unit. Infectious Disease Clinics of North America 31: 475–487 (2017).

[21] D.C. Cole, N.P. Govender, A. Chakrabarti, J. Sacarlal, D.W. Denning. Improvement of fungal disease identification and management: combined health systems and public health approaches. The Lancet Infectious Diseases 17: e412–e419 (2017).

[22] M.C. Dignani. Epidemiology of invasive fungal diseases on the basis of autopsy reports. F1000Prime Reports 6: 81 (2014).

[23] M. Sanguinetti, B. Posteraro, C. Beigelman-Aubry, F. Lamoth, V. Dunet, M. Slavin, M.D. Richardson. Diagnosis and treatment of invasive fungal infections: looking ahead. Journal of Antimicrobial Chemotherapy 74: ii27–ii37 (2019).

[24] R. van Daele, I. Spriet, J. Wauters, J. Maertens, T. Mercier, S. van Hecke, R. Brüggemann. Antifungal drugs: What brings the future? Medical Mycology 57: S328–S343 (2019).

[25] N.P. Wiederhold. The antifungal arsenal: alternative drugs and future targets. International Journal of Antimicrobial Agents 51: 333–339 (2018).

[26] M. von Lilienfeld-Toal, J. Wagener, H. Einsele, O.A. Cornely, O. Kurzai. Invasive Fungal Infection. Deutsches Ärzteblatt international 116: 271–278 (2019).

[27] D.S. Perlin, R. Rautemaa-Richardson, A. Alastruey-Izquierdo. The global problem of antifungal resistance: prevalence, mechanisms, and management. The Lancet Infectious Diseases 17: e383–e392 (2017).

[28] A. Arastehfar, T. Gabaldón, R. Garcia-Rubio, J.D. Jenks, M. Hoenigl, H.J.F. Salzer, M. Ilkit, C. Lass-Flörl, D.S. Perlin. Drug-Resistant Fungi: An Emerging Challenge Threatening Our Limited Antifungal Armamentarium. Antibiotics 9: 877 (2020).

[29] K. Benedict, M. Richardson, S. Vallabhaneni, B.R. Jackson, T. Chiller. Emerging issues, challenges, and changing epidemiology of fungal disease outbreaks. The Lancet Infectious Diseases 17: e403–e411 (2017).

[30] European Committee on Antimicrobial Susceptibility Testing. Clinical breakpoints for fungi. https://www.eucast.org/fileadmin/src/media/PDFs/EUCAST_files/AFST/Clinical_breakpoints/Antifungal_breakpoints_v_9.0_180212.pdf (last access 9 Dec 2021).

[31] European Committee on Antimicrobial Susceptibility Testing. EUCAST method for susceptibility testing of yeasts. https://www.eucast.org/fileadmin/src/media/PDFs/EUCAST_files/AFST/Files/EUCAST_E_Def_7.3.2_Yeast_testing_definitive_revised_2020.pdf (last access 9 Dec 2021).

[32] European Committee on Antimicrobial Susceptibility Testing. EUCAST method for susceptibility testing of moulds. https://www.eucast.org/fileadmin/src/media/PDFs/EUCAST_files/AFST/Files/EUCAST_E_Def_9.3.2_Mould_testing_definitive_revised_2020.pdf (last access 9 Dec 2021).

[33] N.P. Wiederhold. Review of the Novel Investigational Antifungal Olorofim. Journal of Fungi 6: 122 (2020).

[34] C. Mota Fernandes, D. Dasilva, K. Haranahalli, J.B. McCarthy, J. Mallamo, I. Ojima, M. del Poeta. The Future of Antifungal Drug Therapy: Novel Compounds and Targets. Antimicrobial Agents and Chemotherapy 65: e01719-20 (2021).

[35] World Health Organization. WHO model list of essential medicines. https://apps.who.int/iris/rest/bitstreams/1237479/retrieve (last access 27 Jul 2021).

[36] World Health Organization. WHO model list of essential medicines for children. https://apps.who.int/iris/rest/bitstreams/1374783/retrieve (last access 24 Sep 2021).

[37] J. Schulz, F. Kluwe, G. Mikus, R. Michelet, C. Kloft. Novel insights into the complex pharmacokinetics of voriconazole: a review of its metabolism. Drug Metabolism Reviews 51: 247–265 (2019).

[38] Pfizer. VFEND: EPAR - product information. https://www.ema.europa.eu/documents/product-information/vfend-epar-product-information_en.pdf (last access 27 Jul 2021).

[39] B. Damle, M. v. Varma, N. Wood. Pharmacokinetics of voriconazole administered concomitantly with fluconazole and population-based simulation for sequential use. Antimicrobial Agents and Chemotherapy 55: 5172–5177 (2011).

[40] A.J. Ullmann, J.M. Aguado, S. Arikan-Akdagli, D.W. Denning, A.H. Groll, K. Lagrou, C. Lass-Flörl, R.E. Lewis, P. Munoz, P.E. Verweij, A. Warris, F. Ader, M. Akova, M.C. Arendrup, R.A. Barnes, C. Beigelman-Aubry, S. Blot, E. Bouza, R.J.M. Brüggemann, D. Buchheidt, J. Cadranel, E. Castagnola, A. Chakrabarti, M. Cuenca-Estrella, G. Dimopoulos, J. Fortun, J.-P. Gangneux, J. Garbino, W.J. Heinz, R. Herbrecht, C.P. Heussel, C.C. Kibbler, N. Klimko, B.J. Kullberg, C. Lange, T. Lehrnbecher, J. Löffler, O. Lortholary, J. Maertens, O. Marchetti, J.F. Meis, L. Pagano, P. Ribaud, M.

Richardson, E. Roilides, M. Ruhnke, M. Sanguinetti, D.C. Sheppard, J. Sinkó, A. Skiada, M.J.G.T. Vehreschild, C. Viscoli, O.A. Cornely. Diagnosis and management of Aspergillus diseases: executive summary of the 2017 ESCMID-ECMM-ERS guideline. Clinical Microbiology and Infection 24: e1–e38 (2018).

[41] A. Warris, T. Lehrnbecher, E. Roilides, E. Castagnola, R.J.M. Brüggemann, A.H. Groll. ESCMID-ECMM guideline: diagnosis and management of invasive aspergillosis in neonates and children. Clinical Microbiology and Infection 25: 1096–1113 (2019).

[42] T.J. Walsh, E.J. Anaissie, D.W. Denning, R. Herbrecht, D.P. Kontoyiannis, K.A. Marr, V.A. Morrison, B.H. Segal, W.J. Steinbach, D.A. Stevens, J.-A. van Burik, J.R. Wingard, T.F. Patterson. Treatment of Aspergillosis: Clinical Practice Guidelines of the Infectious Diseases Society of America. Clinical Infectious Diseases 46: 327–360 (2008).

[43] H. Sanati, P. Belanger, R. Fratti, M. Ghannoum. A new triazole, voriconazole (UK-109,496), blocks sterol biosynthesis in Candida albicans and Candida krusei. Antimicrobial Agents and Chemotherapy 41: 2492–2496 (1997).

[44] J. Zhang, L. Li, Q. Lv, L. Yan, Y. Wang, Y. Jiang. The Fungal CYP51s: Their Functions, Structures, Related Drug Resistance, and Inhibitors. Frontiers in Microbiology 10: 691 (2019).

[45] K. Han, B. Capitano, R. Bies, B.A. Potoski, S. Husain, S. Gilbert, D.L. Paterson, K. McCurry, R. Venkataramanan. Bioavailability and Population Pharmacokinetics of Voriconazole in Lung Transplant Recipients. Antimicrobial Agents and Chemotherapy 54: 4424–4431 (2010).

[46] A. Veringa, S. Geling, L.F.R. Span, K.M. Vermeulen, J.G. Zijlstra, T.S. van der Werf, J.G.W. Kosterink, J.-W.C. Alffenaar. Bioavailability of voriconazole in hospitalised patients. International Journal of Antimicrobial Agents 49: 243–246 (2017).

[47] X. Lin, Z. Li, M. Yan, B. Zhang, W. Liang, F. Wang, P. Xu, D. Xiang, X. Xie, S. Yu, G. Lan, F. Peng. Population pharmacokinetics of voriconazole and *CYP2C19* polymorphisms for optimizing dosing regimens in renal transplant recipients. British Journal of Clinical Pharmacology 84: 1587–1597 (2018).

[48] I. Scholz, H. Oberwittler, K.-D. Riedel, J. Burhenne, J. Weiss, W.E. Haefeli, G. Mikus. Pharmacokinetics, metabolism and bioavailability of the triazole antifungal agent voriconazole in relation to CYP2C19 genotype. British Journal of Clinical Pharmacology 68: 906–915 (2009).

[49] M.O. Karlsson, I. Lutsar, P.A. Milligan. Population Pharmacokinetic Analysis of Voriconazole Plasma Concentration Data from Pediatric Studies. Antimicrobial Agents and Chemotherapy 53: 935–944 (2009).

[50] L. Purkins, N. Wood, D. Kleinermans, K. Greenhalgh, D. Nichols. Effect of food on the pharmacokinetics of multiple-dose oral voriconazole. British Journal of Clinical Pharmacology 56: 17–23 (2003).

[51] T. Felton, P.F. Troke, W.W. Hope. Tissue Penetration of Antifungal Agents. Clinical Microbiology Reviews 27: 68–88 (2014).

[52] I. Lutsar, S. Roffey, P. Troke. Voriconazole Concentrations in the Cerebrospinal Fluid and Brain Tissue of Guinea Pigs and Immunocompromised Patients. Clinical Infectious Diseases 37: 728–732 (2003).

[53] S. Weiler, D. Fiegl, R. MacFarland, E. Stienecke, R. Bellmann-Weiler, S. Dunzendorfer, M. Joannidis, R. Bellmann. Human Tissue Distribution of Voriconazole. Antimicrobial Agents and Chemotherapy 55: 925–928 (2011).

[54] E. Denes, A. Boumediene, H. Durox, A. Oksman, F. Saint-Marcoux, M.-L. Darde, J.-M. Gaulier. Voriconazole concentrations in synovial fluid and bone tissues. Journal of Antimicrobial Chemotherapy 59: 818–819 (2007).

[55] J.-B. Stern, P. Girard, R. Caliandro. Pleural Diffusion of Voriconazole in a Patient with *Aspergillus fumigatus* Empyema Thoracis. Antimicrobial Agents and Chemotherapy 48: 1065–1065 (2004).

[56] J.C. Poupelin, F. Philit, J.C. Richard, M. Badet, S. Lemasson, F. Bayle, C. Guérin. Pericardial and pleural diffusion of voriconazole during disseminated invasive aspergillosis: report of a case with successful outcome. Intensive Care Medicine 32: 939–940 (2006).

[57] K. Vanstraelen, J. Wauters, H. de Loor, I. Vercammen, P. Annaert, K. Lagrou, I. Spriet. Protein-Binding Characteristics of Voriconazole Determined by High-Throughput Equilibrium Dialysis. Journal of Pharmaceutical Sciences 103: 2565–2570 (2014).

[58] M. Resztak, K. Kosicka, P. Zalewska, J. Krawiec, F.K. Główka. Determination of total and free voriconazole in human plasma: Application to pharmacokinetic study and therapeutic monitoring. Journal of Pharmaceutical and Biomedical Analysis 178: 112952 (2020).

[59] A. Florent, P. Gandia, P. Seraissol, E. Chatelut, G. Houin. Determination of Plasma Unbound Fraction of Voriconazole in Patients Treated With a Prophylactic or a Curative Treatment. Therapeutic Drug Monitoring 36: 752–758 (2014).

[60] S.J. Roffey, S. Cole, P. Comby, D. Gibson, S.G. Jezequel, A.N.R. Nedderman, D.A. Smith, D.K. Walker, N. Wood. The Disposition of Voriconazole in Mouse, Rat, Rabbit, Guinea Pig, Dog, and Human. Drug Metabolism and Disposition 31: 731–741 (2003).

[61] A.N. Werk, I. Cascorbi. Functional Gene Variants of CYP3A4. Clinical Pharmacology & Therapeutics 96: 340–348 (2014).

[62] K.E. Caudle, H.M. Dunnenberger, R.R. Freimuth, J.F. Peterson, J.D. Burlison, M. Whirl-Carrillo, S.A. Scott, H.L. Rehm, M.S. Williams, T.E. Klein, M. v. Relling, J.M. Hoffman. Standardizing terms for clinical pharmacogenetic test results: Consensus terms from the Clinical Pharmacogenetics Implementation Consortium (CPIC). Genetics in Medicine 19: 215–223 (2017).

[63] B. Moriyama, A.O. Obeng, J. Barbarino, S. Penzak, S. Henning, S. Scott, J. Agúndez, J. Wingard, H. McLeod, T. Klein, S. Cross, K. Caudle, T. Walsh. Clinical Pharmacogenetics Implementation Consortium (CPIC) Guidelines for *CYP2C19* and Voriconazole Therapy. Clinical Pharmacology & Therapeutics 102: 45–51 (2017).

[64] D. van Booven, S. Marsh, H. McLeod, M.W. Carrillo, K. Sangkuhl, T.E. Klein, R.B. Altman. Cytochrome P450 2C9-CYP2C9. Pharmacogenetics and Genomics 20: 277–281 (2010).

[65] D. Zonios, H. Yamazaki, N. Murayama, V. Natarajan, T. Palmore, R. Childs, J. Skinner, J.E. Bennett. Voriconazole Metabolism, Toxicity, and the Effect of Cytochrome P450 2C19 Genotype. The Journal of Infectious Diseases 209: 1941–1948 (2014).

[66] K. Ona, D.H. Oh. Voriconazole N-oxide and its ultraviolet B photoproduct sensitize keratinocytes to ultraviolet A. British Journal of Dermatology 173: 751–759 (2015).

[67] M.J.P. Geist, G. Egerer, J. Burhenne, K.-D. Riedel, J. Weiss, G. Mikus. Steady-state pharmacokinetics and metabolism of voriconazole in patients. Journal of Antimicrobial Chemotherapy 68: 2592–2599 (2013).

[68] N. Hohmann, R. Kreuter, A. Blank, J. Weiss, J. Burhenne, W.E. Haefeli, G. Mikus. Autoinhibitory properties of the parent but not of the N-oxide metabolite contribute to infusion rate-dependent voriconazole pharmacokinetics. British Journal of Clinical Pharmacology 83: 1954–1965 (2017).

[69] N. Murayama, N. Imai, T. Nakane, M. Shimizu, H. Yamazaki. Roles of CYP3A4 and CYP2C19 in methyl hydroxylated and N-oxidized metabolite formation from voriconazole, a new anti-fungal agent, in human liver microsomes. Biochemical Pharmacology 73: 2020–2026 (2007).

[70] S.B. Yanni, P.P. Annaert, P. Augustijns, A. Bridges, Y. Gao, D.K. Benjamin, D.R. Thakker. Role of Flavin-Containing Monooxygenase in Oxidative Metabolism of Voriconazole by Human Liver Microsomes. Drug Metabolism and Disposition 36: 1119–1125 (2008).

[71] R. Hyland, B.C. Jones, D.A. Smith. Identification of the Cytochrome P450 Enzymes Involved in the *N* -Oxidation of Voriconazole. Drug Metabolism and Disposition 31: 540–547 (2003).

[72] K. Bourcier, R. Hyland, S. Kempshall, R. Jones, J. Maximilien, N. Irvine, B. Jones. Investigation into UDP-glucuronosyltransferase (UGT) enzyme kinetics of imidazole- and triazole-containing antifungal drugs in human liver microsomes and recombinant UGT enzymes. Drug Metabolism and Disposition 38: 923–929 (2010).

[73] T. Wang, H. Zhu, J. Sun, X. Cheng, J. Xie, H. Dong, L. Chen, X. Wang, J. Xing, Y. Dong. Efficacy and safety of voriconazole and CYP2C19 polymorphism for optimised dosage regimens in patients with invasive fungal infections. International Journal of Antimicrobial Agents 44: 436–442 (2014).

[74] L.E. Friberg, P. Ravva, M.O. Karlsson, P. Liu. Integrated population pharmacokinetic analysis of voriconazole in children, adolescents, and adults. Antimicrobial Agents and Chemotherapy 56: 3032–3042 (2012).

[75] K. Eljaaly, D.E. Nix. Voriconazole Dosing in Obese Patients. Clinical Infectious Diseases 63: 286–287 (2016).

[76] M.J.P. van Wanrooy, L.F.R. Span, M.G.G. Rodgers, E.R. van den Heuvel, D.R.A. Uges, T.S. van der Werf, J.G.W. Kosterink, J.-W.C. Alffenaar. Inflammation Is Associated with Voriconazole Trough Concentrations. Antimicrobial Agents and Chemotherapy 58: 7098–7101 (2014).

[77] A. Veringa, M. ter Avest, L.F.R. Span, E.R. van den Heuvel, D.J. Touw, J.G. Zijlstra, J.G.W. Kosterink, T.S. van der Werf, J.-W.C. Alffenaar. Voriconazole metabolism is influenced by severe inflammation: a prospective study. Journal of Antimicrobial Chemotherapy 72: 261–267 (2017).

[78] N. Hohmann, F. Kocheise, A. Carls, J. Burhenne, J. Weiss, W.E. Haefeli, G. Mikus. Dose-Dependent Bioavailability and CYP3A Inhibition Contribute to Non-Linear Pharmacokinetics of Voriconazole. Clinical Pharmacokinetics 55: 1535–1545 (2016).

[79] T. Niwa, Y. Imagawa, H. Yamazaki. Drug Interactions between Nine Antifungal Agents and Drugs Metabolized by Human Cytochromes P450. Current Drug Metabolism 15: 651–679 (2015).

[80] A.C. Pasqualotto, M.O. Xavier, H.F. Andreolla, R. Linden. Voriconazole therapeutic drug monitoring: focus on safety. Expert Opinion on Drug Safety 9: 125–137 (2010).

[81] V.J.C. Lempers, J.J.M.W. van den Heuvel, F.G.M. Russel, R.E. Aarnoutse, D.M. Burger, R.J. Brüggemann, J.B. Koenderink. Inhibitory Potential of Antifungal Drugs on ATP-Binding Cassette Transporters P-Glycoprotein, MRP1 to MRP5, BCRP, and BSEP. Antimicrobial Agents and Chemotherapy 60: 3372–3379 (2016).

[82] T. Niwa, S. Inoue-Yamamoto, T. Shiraga, A. Takagi. Effect of Antifungal Drugs on Cytochrome P450 (CYP) 1A2, CYP2D6, and CYP2E1 Activities in Human Liver Microsomes. Biological and Pharmaceutical Bulletin 28: 1813–1816 (2005).

[83] T. Niwa, T. Shiraga, A. Takagi. Effect of Antifungal Drugs on Cytochrome P450 (CYP) 2C9, CYP2C19, and CYP3A4 Activities in Human Liver Microsomes. Biological and Pharmaceutical Bulletin 28: 1805–1808 (2005).

[84] H. Yamazaki, M. Nakamoto, M. Shimizu, N. Murayama, T. Niwa. Potential impact of cytochrome P450 3A5 in human liver on drug interactions with triazoles. British Journal of Clinical Pharmacology 69: 593–597 (2010).

[85] S. Jeong, P.D. Nguyen, Z. Desta. Comprehensive in vitro analysis of voriconazole inhibition of eight cytochrome P450 (CYP) enzymes: Major effect on CYPs 2B6, 2C9, 2C19, and 3A. Antimicrobial Agents and Chemotherapy 53: 541–551 (2009).

[86] R. Venkataramanan, S. Zang, T. Gayowski, N. Singh. Voriconazole Inhibition of the Metabolism of Tacrolimus in a Liver Transplant Recipient and in Human Liver Microsomes. Antimicrobial Agents and Chemotherapy 46: 3091–3093 (2002).

[87] S. Zhang, V.C. Pillai, S.R. Mada, S. Strom, R. Venkataramanan. Effect of voriconazole and other azole antifungal agents on CYP3A activity and metabolism of tacrolimus in human liver microsomes. Xenobiotica 42: 409–416 (2012).

[88] D.E. Moody, F. Liu, W.B. Fang. Azole antifungal inhibition of buprenorphine, methadone and oxycodone in vitro metabolism. Journal of Analytical Toxicology 39: 374–386 (2015).

[89] P. Giri, S. Naidu, N. Patel, H. Patel, N.R. Srinivas. Evaluation of In Vitro Cytochrome P450 Inhibition and In Vitro Fate of Structurally Diverse N-Oxide Metabolites: Case Studies with Clozapine, Levofloxacin, Roflumilast, Voriconazole and Zopiclone. European Journal of Drug Metabolism and Pharmacokinetics 42: 677–688 (2017).

[90] A.H. Groll, R. Townsend, A. Desai, N. Azie, M. Jones, M. Engelhardt, A.H. Schmitt-Hoffman, R.J.M. Brüggemann. Drug-drug interactions between triazole antifungal agents used to treat invasive aspergillosis and immunosuppressants metabolized by cytochrome P450 3A4. Transplant Infectious Disease 19: 1–11 (2017).

[91] L. Purkins, N. Wood, D. Kleinermans, D. Nichols. Voriconazole potentiates warfarin-induced prothrombin time prolongation. British Journal of Clinical Pharmacology 56: 24–29 (2003).

[92] M. Li, L. Zhu, L. Chen, N. Li, F. Qi. Assessment of drug–drug interactions between voriconazole and glucocorticoids. Journal of Chemotherapy 30: 296–303 (2018).

[93] N. Li, L. Zhu, F. Qi, M. Li, G. Xu, T. Ge. Prediction of the effect of voriconazole on the pharmacokinetics of non-steroidal anti-inflammatory drugs. Journal of Chemotherapy 30: 240–246 (2018).

[94] L. Chen, L. Zhu, M. Li, N. Li, F. Qi, N. Wang. Predicting the Effects of Different Triazole Antifungal Agents on the Pharmacokinetics of Tamoxifen. AAPS PharmSciTech 20: 24 (2019).

[95] K.L. Niece, N.K. Boyd, K.S. Akers. In vitro study of the variable effects of proton pump inhibitors on voriconazole. Antimicrobial Agents and Chemotherapy 59: 5548–5554 (2015).

[96] F. Qi, L. Zhu, N. Li, T. Ge, G. Xu, S. Liao. Influence of different proton pump inhibitors on the pharmacokinetics of voriconazole. International Journal of Antimicrobial Agents 49: 403–409 (2017).

[97] N.K. Boyd, C.L. Zoellner, M.A. Swancutt, K.P. Bhavan. Utilization of Omeprazole To Augment Subtherapeutic Voriconazole Concentrations for Treatment of Aspergillus Infections. Antimicrobial Agents and Chemotherapy 56: 6001–6002 (2012).

[98] M.J. Ferguson, M.L. Randles, D.G. de Freitas. A suspected case of autoinduction of voriconazole metabolism in a patient with cerebral aspergillosis. Drug, Healthcare and Patient Safety 9: 89–91 (2017).

[99] J. Rengelshausen, M. Banfield, K.D. Riedel, J. Burhenne, J. Weiss, T. Thomsen, I. Walter-Sack, W.E. Haefeli, G. Mikus. Opposite effects of short-term and long-term St John's wort intake on voriconazole pharmacokinetics. Clinical Pharmacology and Therapeutics 78: 25–33 (2005).

[100] M.J.P. Geist, G. Egerer, J. Burhenne, K.-D. Riedel, G. Mikus. Induction of Voriconazole Metabolism by Rifampin in a Patient with Acute Myeloid Leukemia: Importance of Interdisciplinary Communication To Prevent Treatment Errors with Complex Medications. Antimicrobial Agents and Chemotherapy 51: 3455–3456 (2007).

[101] L. Purkins, N. Wood, P. Ghahramani, E.R. Love, M.D. Eve, A. Fielding. Coadministration of voriconazole and phenytoin: pharmacokinetic interaction, safety, and toleration. British Journal of Clinical Pharmacology 56: 37–44 (2003).

[102] T. Li, W. Liu, K. Chen, S. Liang, F. Liu. The influence of combination use of CYP450 inducers on the pharmacokinetics of voriconazole: a systematic review. Journal of Clinical Pharmacy and Therapeutics 42: 135–146 (2017).

[103] A.J. Hsu, A. Dabb, R. Arav-Boger. Autoinduction of voriconazole metabolism in a child with invasive pulmonary aspergillosis. Pharmacotherapy 35: e20–e26 (2015).

[104] U. Theuretzbacher, F. Ihle, H. Derendorf. Pharmacokinetic/pharmacodynamic profile of Voriconazole. Clinical Pharmacokinetics 45: 649–663 (2006).

[105] A.C. Pasqualotto, M.O. Xavier, H.F. Andreolla, R. Linden. Voriconazole therapeutic drug monitoring: focus on safety. Expert Opinion on Drug Safety 9: 125–137 (2010).

[106] K. Venkatakrishnan, L.L. von Moltke, D.J. Greenblatt. Human drug metabolism and the cytochromes P450: Application and relevance of in vitro models. Journal of Clinical Pharmacology 41: 1149–1179 (2001).

[107] J. Vrbanac, R. Slauter. ADME in Drug Discovery. In: A Comprehensive Guide to Toxicology in Preclinical Drug Development. Elsevier, 3–30 (2013).

[108] U.M. Zanger, M. Schwab. Cytochrome P450 enzymes in drug metabolism: Regulation of gene expression, enzyme activities, and impact of genetic variation. Pharmacology & Therapeutics 138: 103–141 (2013).

[109] P. Manikandan, S. Nagini. Cytochrome P450 Structure, Function and Clinical Significance: A Review. Current Drug Targets 19: 38–54 (2018).

[110] S. Nagar, U.A. Argikar, D. J. Tweedie (eds.). Enzyme Kinetics in Drug Metabolism: Fundamentals and Applications. Humana Press, (2014).

[111] M. Deodhar, S.B. al Rihani, M.J. Arwood, L. Darakjian, P. Dow, J. Turgeon, V. Michaud. Mechanisms of CYP450 Inhibition: Understanding Drug-Drug Interactions Due to Mechanism-Based Inhibition in Clinical Practice. Pharmaceutics 12: 846 (2020).

[112] S. Fowler, H. Zhang. In vitro evaluation of reversible and irreversible cytochrome P450 inhibition: Current status on methodologies and their utility for predicting drug-drug interactions. AAPS Journal 10: 410–424 (2008).

[113] S.-F. Zhou, J.-P. Liu, B. Chowbay. Polymorphism of human cytochrome P450 enzymes and its clinical impact. Drug Metabolism Reviews 41: 89–295 (2009).

[114] J. McGraw, D. Waller. Cytochrome P450 variations in different ethnic populations. Expert Opinion on Drug Metabolism and Toxicology 8: 371–382 (2012).

[115] M. Gomez-Lechon, M. Donato, J. Castell, R. Jover. Human Hepatocytes in Primary Culture: The Choice to Investigate Drug Metabolism in Man. Current Drug Metabolism 5: 443–462 (2004).

[116] A.P. Li. Human hepatocytes: Isolation, cryopreservation and applications in drug development. Chemico-Biological Interactions 168: 16–29 (2007).

[117] N.J. Hewitt. Optimisation of the cryopreservation of primary hepatocytes. In: Hepatocytes. Methods in Molecular Biology. Humana Press, 83–105 (2010).

[118] S.J. Richardson, A. Bai, A.A. Kulkarni, M.F. Moghaddam. Efficiency in Drug Discovery: Liver S9 Fraction Assay As a Screen for Metabolic Stability. Drug Metabolism Letters 10: 83–90 (2016).

[119] K. Schroer, M. Kittelmann, S. Lütz. Recombinant human cytochrome P450 monooxygenases for drug metabolite synthesis. Biotechnology and Bioengineering 106: 699–706 (2010).

[120] J. Hausjell, H. Halbwirth, O. Spadiut. Recombinant production of eukaryotic cytochrome P450s in microbial cell factories. Bioscience Reports 38: BSR20171290 (2018).

[121] K.A. Rodvold, L. Yoo, J.M. George. Penetration of Anti-Infective Agents into PulmonaryEpithelial Lining Fluid. Clinical Pharmacokinetics 50: 689–704 (2011).

[122] U. Theuretzbacher. Tissue penetration of antibacterial agents: how should this be incorporated into pharmacodynamic analyses? Current Opinion in Pharmacology 7: 498–504 (2007).

[123] M. Müller, A. dela Peña, H. Derendorf. Issues in Pharmacokinetics and Pharmacodynamics of Anti-Infective Agents: Distribution in Tissue. Antimicrobial Agents and Chemotherapy 48: 1441–1453 (2004).

[124] I.K. Minichmayr, A. Schaeftlein, J.L. Kuti, M. Zeitlinger, C. Kloft. Clinical Determinants of Target Non-Attainment of Linezolid in Plasma and Interstitial Space Fluid: A Pooled Population Pharmacokinetic Analysis with Focus on Critically Ill Patients. Clinical Pharmacokinetics 56: 617–633 (2017).

[125] European Medicines Agency. Guideline on the use of pharmacokinetics and pharmacodynamics in the development of antibacterial medicinal products. (2017). https://www.ema.europa.eu/documents/scientific-guideline/guideline-use-pharmacokinetics-pharmacodynamics-development-antimicrobial-medicinal-products_en.pdf (last access 27 Jul 2021).

[126] J.W. Mouton, U. Theuretzbacher, W.A. Craig, P.M. Tulkens, H. Derendorf, O. Cars. Tissue concentrations: Do we ever learn? Journal of Antimicrobial Chemotherapy 61: 235–237 (2008).

[127] N. Plock, C. Kloft. Microdialysis—theoretical background and recent implementation in applied life-sciences. European Journal of Pharmaceutical Sciences 25: 1–24 (2005).

[128] M. Stahl, R. Bouw, A. Jackson, V. Pay. Human Microdialysis. Current Pharmaceutical Biotechnology 3: 165–178 (2002).

[129] M. Hammarlund-Udenaes. Microdialysis as an Important Technique in Systems Pharmacology—a Historical and Methodological Review. The AAPS Journal 19: 1294–1303 (2017).

[130] M.K. Kit Lee. Crosstalk the Microdialysis in Scientific Research: from Principle to its Applications. Pharmaceutica Analytica Acta 5: 1000276 (2013).

[131] C. Buerger, N. Plock, P. Dehghanyar, C. Joukhadar, C. Kloft. Pharmacokinetics of Unbound Linezolid in Plasma and Tissue Interstitium of Critically Ill Patients after Multiple Dosing Using Microdialysis. Antimicrobial Agents and Chemotherapy 50: 2455–2463 (2006).

[132] C. Kirbs, F. Kluwe, F. Drescher, E. Lackner, P. Matzneller, J. Weiss, M. Zeitlinger, C. Kloft. High voriconazole target-site exposure after approved sequence dosing due to nonlinear pharmacokinetics assessed by long-term microdialysis. European Journal of Pharmaceutical Sciences 131: 218–229 (2019).

[133] M Dialysis AB. Catheters for clinical use. https://www.mdialysis.com/products/catheters-for-clinical-use/ (last access 17 Dec 2021).

[134] F. Simmel, C. Kloft. Microdialysis feasibility investigations with the non-hydrophilic antifungal voriconazole for potential applications in nonclinical and clinical settings. Int. Journal of Clinical Pharmacology and Therapeutics 48: 695–704 (2010).

[135] C. Weiser. Principle in vitro microdialysis investigation to characterise the feasibility for antifungals. Freie Universitaet Berlin. (2018).

[136] C.S. Chaurasia, M. Müller, E.D. Bashaw, E. Benfeldt, J. Bolinder, R. Bullock, P.M. Bungay, E.C.M. DeLange, H. Derendorf, W.F. Elmquist, M. Hammarlund-Udenaes, C. Joukhadar, D.L. Kellogg, C.E. Lunte, C.H. Nordstrom, H. Rollema, R.J. Sawchuk, B.W.Y. Cheung, V.P. Shah, L. Stahle, U. Ungerstedt, D.F. Welty, H. Yeo. AAPS-FDA Workshop White Paper: Microdialysis Principles, Application and Regulatory Perspectives. Pharmaceutical Research 24: 1014–1025 (2007).

[137] F. Simmel. Development, optimisation and application of in vitro and in vivo microdialysis methods contributing to characterise drug disposition processes. Martin-Luther-Universitaet Halle-Wittenberg. (2010).

[138] J.J. Pitt. Principles and applications of liquid chromatography-mass spectrometry in clinical biochemistry. Clin Biochem Rev 30: 19–34 (2009).

[139] European Medicines Agency. Guideline on bioanalytical method validation. (2012). https://www.ema.europa.eu/documents/scientific-guideline/guideline-bioanalytical-method-validation_en.pdf (last access 27 Jul 2021).

[140] U. S. Food and Drug Administration. Bioanalytical Method Validation - Guidance for Industry. (2018). https://www.fda.gov/files/drugs/published/Bioanalytical-Method-Validation-Guidance-for-Industry.pdf (last access 18 Dec 2021).

[141] L. Jia, X. Liu. The Conduct of Drug Metabolism Studies Considered Good Practice (II): In Vitro Experiments. Current Drug Metabolism 8: 822–829 (2007).

[142] K.M. Knights, D.M. Stresser, J.O. Miners, C.L. Crespi. In Vitro Drug Metabolism Using Liver Microsomes. Current Protocols in Pharmacology 74: 7.8.1-7.8.24 (2016).

[143] Corning. Mammalian Liver Microsomes Guidelines for Use. https://certs-ecatalog.corning.com/life-sciences/product-descriptions/452117.pdf (last access 6 Aug 2021).

[144] Clinical and Laboratory Standards Institute. Methods for Dilution Antimicrobial Susceptibility Tests for Bacteria That Grow Aerobically: Approved Standard-Ninth Edition. (2012).

[145] Agilent Technologies. Agilent MassHunter Optimizer - Quick Start Guide.

[146] F. Simmel, C. Kirbs, Z. Erdogan, E. Lackner, M. Zeitlinger, C. Kloft. Pilot Investigation on Long-Term Subcutaneous Microdialysis: Proof of Principle in Humans. The AAPS Journal 15: 95–103 (2013).

[147] H. Gu, G. Liu, J. Wang, A.-F. Aubry, M.E. Arnold. Selecting the Correct Weighting Factors for Linear and Quadratic Calibration Curves with Least-Squares Regression Algorithm in Bioanalytical LC-MS/MS Assays and Impacts of Using Incorrect Weighting Factors on Curve Stability, Data Quality, and Assay Performance. Analytical Chemistry 86: 8959–8966 (2014).

[148] International Conference On Harmonisation (ICH). Validation on analytical procedures: Text and Methodology. https://www.gmp-navigator.com/files/guidemgr/Q2(R1).pdf (last access 27 Jul 2021).

[149] European Medicines Agency. Guideline on the investigation of drug interactions. (2013). http://www.ema.europa.eu/docs/en_GB/document_library/Scientific_guideline/2012/07/WC500129606.pdf (last access 18 Aug 2021).

[150] U.S. Food and Drug Administration. Drug Development and Drug Interactions | Table of Substrates, Inhibitors and Inducers. https://www.fda.gov/drugs/drug-interactions-labeling/drug-development-and-drug-interactions-table-substrates-inhibitors-and-inducers#table1-2 (last access 18 Aug 2021)

[151] A. Thomas. Assessing the enzyme inhibitory potential of voriconazole and two of its metabolites using in vitro metabolism experiments. Martin-Luther-Universitaet Halle-Wittenberg. (2021).

[152] Corning. Human CYP2C9*1 (Arg144) + P450 Reductase SUPERSOMES, batch 9277002. https://certs-ecatalog.corning.com/life-sciences/certs/456218_9277002.pdf (last access 20 Aug 2021).

[153] Corning. Human CYP3A4 + P450 Reductase SUPERSOMES, batch 9023001. https://certs-ecatalog.corning.com/life-sciences/certs/456207_9023001.pdf (last access 20 Aug 2021).

[154] Corning. Human CYP2C19 + P450 Reductase SUPERSOMES, batch 9275001. https://certs-ecatalog.corning.com/life-sciences/certs/456219_9275001.pdf (last access 20 Aug 2021).

[155] S. Wang, X. Tang, T. Yang, J. Xu, J. Zhang, X. Liu, L. Liu. Predicted contributions of cytochrome P450s to drug metabolism in human liver microsomes using relative activity factor were dependent on probes. Xenobiotica 49: 161–168 (2019).

[156] Corning. UltraPool HLM 150 Characterization. https://www.corning.com/catalog/cls/documents/application-notes/CLS-DL-AN-GT-236_DL.pdf (last access 20 Aug 2021).

[157] Y.A. Siu, W.G. Lai. Impact of Probe Substrate Selection on Cytochrome P450 Reaction Phenotyping Using the Relative Activity Factor. Drug Metabolism and Disposition 45: 183–189 (2017).

[158] S.C. Khojasteh, S. Prabhu, J.R. Kenny, J.S. Halladay, A.Y.H. Lu. Chemical inhibitors of cytochrome P450 isoforms in human liver microsomes: a re-evaluation of P450 isoform selectivity. European Journal of Drug Metabolism and Pharmacokinetics 36: 1–16 (2011).

[159] V. Kumar, J.L. Wahlstrom, D.A. Rock, C.J. Warren, L.A. Gorman, T.S. Tracy. CYP2C9 Inhibition: Impact of Probe Selection and Pharmacogenetics on in Vitro Inhibition Profiles. Drug Metabolism and Disposition 34: 1966–1975 (2006).

[160] M.E. Barecki, C.N. Casciano, W.W. Johnson, R.P. Clement. In vitro characterization of the inhibition profile of loratadine, desloratadine, and 3-OH-desloratadine for five human cytochrome P-450 enzymes. Drug Metabolism and Disposition 29: 1173–1175 (2001).

[161] R.S. Foti, J.L. Wahlstrom. CYP2C19 inhibition: The impact of substrate probe selection on in vitro inhibition profiles. Drug Metabolism and Disposition 36: 523–528 (2008).

[162] S.J. Dekker, F. Dohmen, N.P.E. Vermeulen, J.N.M. Commandeur. Characterization of kinetics of human cytochrome P450s involved in bioactivation of flucloxacillin: inhibition of CYP3A-catalysed hydroxylation by sulfaphenazole. British Journal of Pharmacology 176: 466–477 (2019).

[163] Y. Chen, L. Liu, K. Nguyen, A.J. Fretland. Utility of intersystem extrapolation factors in early reaction phenotyping and the quantitative extrapolation of human liver microsomal intrinsic clearance using recombinant cytochromes P450. Drug Metabolism and Disposition 39: 373–382 (2011).

[164] N.J. Proctor, G.T. Tucker, A. Rostami-Hodjegan. Predicting drug clearance from recombinantly expressed CYPs: Intersystem extrapolation factors. Xenobiotica 34: 151–178 (2004).

[165] B. Achour, J. Barber, A. Rostami-Hodjegan. Expression of hepatic drug-metabolizing cytochrome P450 enzymes and their intercorrelations: A meta-analysis. Drug Metabolism and Disposition 42: 1349–1356 (2014).

[166] J. Yang, M. Jamei, K.R. Yeo, A. Rostami-Hodjegan, G.T. Tucker. Misuse of the Well-Stirred Model of Hepatic Drug Clearance. Drug Metabolism and Disposition 35: 501–502 (2007).

[167] K.S. Pang, Y.R. Han, K. Noh, P.I. Lee, M. Rowland. Hepatic clearance concepts and misconceptions: Why the well-stirred model is still used even though it is not physiologic reality? Biochem Pharmacol 169: 113596 (2019).

[168] L. Berry, Z. Zhao. An Examination of IC50 and IC50-Shift Experiments in Assessing Time-Dependent Inhibition of CYP3A4, CYP2D6 and CYP2C9 in Human Liver Microsomes. Drug Metabolism Letters 2: 51–59 (2008).

[169] H. Akaike. A new look at the statistical model identification. IEEE Transactions on Automatic Control 19: 716–723 (1974).

[170] D. Bates, M. Mächler, B. Bolker, S. Walker. Fitting Linear Mixed-Effects Models Using lme4. Journal of Statistical Software 67: 1–48 (2015).

[171] A. Kuznetsova, P.B. Brockhoff, R.H.B. Christensen. lmerTest Package: Tests in Linear Mixed Effects Models. Journal of Statistical Software 82: 1–26 (2017).

[172] World Medical Association. Declaration of Helsinki – Ethical Principles for Medical Research involving human Subjects. https://www.wma.net/wp-content/uploads/2018/07/DoH-Oct2008.pdf (last access 12 Nov 2021).

[173] C. Kirbs. Development and application of in vitro and in vivo microdialysis methods contributing to biomarker profiling and characterisation of drug distribution processes. Freie Universitaet Berlin. (2015).

[174] M.H. Abdul-Aziz, J.-W.C. Alffenaar, M. Bassetti, H. Bracht, G. Dimopoulos, D. Marriott, M.N. Neely, J.-A. Paiva, F. Pea, F. Sjovall, J.F. Timsit, A.A. Udy, S.G. Wicha, M. Zeitlinger, J.J. de Waele, J.A. Roberts. Antimicrobial therapeutic drug monitoring in critically ill adult patients: a Position Paper. Intensive Care Medicine 46: 1127–1153 (2020).

[175] Kyun-Seop Bae, Jee Eun Lee. pkr: Pharmacokinetics in R. https://CRAN.R-project.org/package=pkr (last access 16 Sep 2021).

[176] K.R. Choi, J.Y. Ryu, S.Y. Lee. Revisiting Statistical Design and Analysis in Scientific Research. Small 14: 1802604 (2018).

[177] Peter L. Bonate (ed.). Pharmacokinetic-Pharmacodynamic Modeling and Simulation. Springer US, (2011).

[178] J. Schulz, R. Michelet, J.F. Joseph, M. Zeitlinger, F. Schumacher, G. Mikus, C. Kloft. A versatile high-performance LC-MS/MS assay for the quantification of voriconazole and its N-oxide metabolite in small sample volumes of multiple human matrices for biomedical applications. Journal of Pharmaceutical and Biomedical Analysis 210: 114551 (2022).

[179] J. Schulz, A. Thomas, A. Saleh, G. Mikus, C. Kloft, R. Michelet. Towards the Elucidation of the Pharmacokinetics of Voriconazole: A Quantitative Characterization of Its Metabolism. Pharmaceutics 14: 477 (2022).

[180] M.-L. Luong, M. Al-Dabbagh, A.H. Groll, Z. Racil, Y. Nannya, D. Mitsani, S. Husain. Utility of voriconazole therapeutic drug monitoring: a meta-analysis. Journal of Antimicrobial Chemotherapy 71: 1786–1799 (2016).

[181] M. ter Avest, A. Veringa, K. van Hateren, R.A. Koster, D.J. Touw, J.-W. Alffenaar. Method for Therapeutic Drug Monitoring of Voriconazole and its Primary Metabolite Voriconazole-N-oxide in Human Serum using LC-MS/MS. Journal of Applied Bioanalysis 4: 114–123 (2018).

[182] G.S. Moorthy, C. Vedar, N. Zane, J.L. Prodell, A.F. Zuppa. Development and validation of a volumetric absorptive microsampling assay for analysis of voriconazole and voriconazole N-oxide in human whole blood. Journal of Chromatography B 1105: 67–75 (2019).

[183] H. Mei, X. Hu, J. Wang, R. Wang, Y. Cai. Determination of voriconazole in human plasma by liquid chromatography-tandem mass spectrometry and its application in therapeutic drug monitoring in Chinese patients. Journal of International Medical Research 48: 1–10 (2020).

[184] K.Y. Beste, O. Burkhardt, V. Kaever. Rapid HPLC–MS/MS method for simultaneous quantitation of four routinely administered triazole antifungals in human plasma. Clinica Chimica Acta 413: 240–245 (2012).

[185] L.A. Decosterd, B. Rochat, B. Pesse, T. Mercier, F. Tissot, N. Widmer, J. Bille, T. Calandra, B. Zanolari, O. Marchetti. Multiplex Ultra-Performance Liquid Chromatography-Tandem Mass Spectrometry Method for Simultaneous Quantification in Human Plasma of Fluconazole, Itraconazole, Hydroxyitraconazole, Posaconazole, Voriconazole, Voriconazole- *N* -Oxide, Anidulafungin, and Caspofungin. Antimicrobial Agents and Chemotherapy 54: 5303–5315 (2010).

[186] T. Delatour, P. Mottier, E. Gremaud. Limits of suspicion, recognition and confirmation as concepts that account for the confirmation transitions at the detection limit for quantification by liquid chromatography–tandem mass spectrometry. Journal of Chromatography A 1169: 103–110 (2007).

[187] J.W.C. Alffenaar, A.M.A. Wessels, K. van Hateren, B. Greijdanus, J.G.W. Kosterink, D.R.A. Uges. Method for therapeutic drug monitoring of azole antifungal drugs in human serum using LC/MS/MS. Journal of Chromatography B 878: 39–44 (2010).

[188] S.J. Yoon, K. Lee, J. Oh, H.I. Woo, S.-Y. Lee. Experience with therapeutic drug monitoring of three antifungal agents using an LC-MS/MS method in routine clinical practice. Clinical Biochemistry 70: 14–17 (2019).

[189] J. Li, J. Ma, E.A. Wagar, D. Liang, Q.H. Meng. A rapid ultra-performance LC-MS/MS assay for determination of serum unbound fraction of voriconazole in cancer patients. Clinica Chimica Acta 486: 36–41 (2018).

[190] S. Prommas, A. Puangpetch, N. Jenjirattithigarn, S. Chuwongwattana, T. Jantararoungtong, N. Koomdee, S. Santon, M. Chamnanphon, C. Sukasem. Development and Validation of Voriconazole Concentration by LC-MS-MS: Applied in Clinical Implementation. Journal of Clinical Laboratory Analysis 31: e22011 (2017).

[191] A.J. McShane, S. Wang. Development and validation of a liquid chromatography-tandem mass spectrometry assay for the simultaneous quantitation of 5 azole antifungals and 1 active metabolite. Clinica Chimica Acta 474: 8–13 (2017).

[192] T.M. Annesley. Ion Suppression in Mass Spectrometry. Clinical Chemistry 49: 1041–1044 (2003).

[193] T. Yamada, Y. Mino, T. Yagi, T. Naito, J. Kawakami. Rapid simultaneous determination of voriconazole and its N-oxide in human plasma using an isocratic high-performance liquid chromatography method and its clinical application. Clinical Biochemistry 45: 134–138 (2012).

[194] F. Simmel, J. Soukup, A. Zoerner, J. Radke, C. Kloft. Development and validation of an efficient HPLC method for quantification of voriconazole in plasma and microdialysate reflecting an important target site. Analytical and Bioanalytical Chemistry 392: 479–488 (2008).

[195] D.M. Saunte, F. Simmel, N. Frimodt-Moller, L.B. Stolle, E.L. Svejgaard, M. Haedersdal, C. Kloft, M.C. Arendrup. In vivo efficacy and pharmacokinetics of voriconazole in an animal model of dermatophytosis. Antimicrobial Agents and Chemotherapy 51: 3317–3321 (2007).

[196] X. Xiong, S. Zhai, J. Duan. Validation of a fast and reliable liquid chromatography-tandem mass spectrometry (LC-MS/MS) with atmospheric pressure chemical ionization method for simultaneous quantitation of voriconazole, itraconazole and its active metabolite hydroxyitraconazole in human plasma. Clinical Chemistry and Laboratory Medicine (CCLM) 51: 339–346 (2013).

[197] L.J. Langman, F. Boakye-Agyeman. Measurement of voriconazole in serum and plasma. Clinical Biochemistry 40: 1378–1385 (2007).

[198] G.A. Khoschsorur, F. Fruehwirth, S. Zelzer. Isocratic high-performance liquid chromatographic method with ultraviolet detection for simultaneous determination of levels of voriconazole and itraconazole and its hydroxy metabolite in human serum. Antimicrobial Agents and Chemotherapy 49: 3569–3571 (2005).

[199] J.-B. Gordien, A. Pigneux, S. Vigouroux, R. Tabrizi, I. Accoceberry, J.-M. Bernadou, A. Rouault, M.-C. Saux, D. Breilh. Simultaneous determination of five systemic azoles in plasma by high-performance liquid chromatography with ultraviolet detection. Journal of Pharmaceutical and Biomedical Analysis 50: 932–938 (2009).

[200] G.J. Pennick, M. Clark, D.A. Sutton, M.G. Rinaldi. Development and Validation of a High-Performance Liquid Chromatography Assay for Voriconazole. Antimicrobial Agents and Chemotherapy 47: 2348–2350 (2003).

[201] S. Nakagawa, R. Suzuki, R. Yamazaki, Y. Kusuhara, S. Mitsumoto, H. Kobayashi, S. Shimoeda, S. Ohta, S. Yamato. Determination of the Antifungal Agent Voriconazole in Human Plasma Using a Simple Column-Switching High-Performance Liquid Chromatography and Its Application to a Pharmacokinetic Study. Chemical and Pharmaceutical Bulletin 56: 328–331 (2008).

[202] A. Tan, K. Awaiye. Use of Internal Standards in LC-MS Bioanalysis. In: Handbook of LC-MS Bioanalysis: Best Practices, Experimental Protocols, and Regulations. John Wiley & Sons Inc., 217–227 (2013).

[203] R. Bakhtiar, T.K. Majumdar. Tracking problems and possible solutions in the quantitative determination of small molecule drugs and metabolites in biological fluids using liquid chromatography-mass spectrometry. Journal of Pharmacological and Toxicological Methods 55: 227–243 (2007).

[204] A. Tan, I.A. Lévesque, I.M. Lévesque, F. Viel, N. Boudreau, A. Lévesque. Analyte and internal standard cross signal contributions and their impact on quantitation in LC–MS based bioanalysis. Journal of Chromatography B 879: 1954–1960 (2011).

[205] K. Duxbury, L. Owen, S. Gillingwater, B. Keevil. Naturally occurring isotopes of an analyte can interfere with doubly deuterated internal standard measurement. Annals of Clinical Biochemistry 45: 210–212 (2008).

[206] B.G. Keevil, S. Newman, S. Lockhart, S.J. Howard, C.B. Moore, D.W. Denning. Validation of an Assay for Voriconazole in Serum Samples Using Liquid Chromatography-Tandem Mass Spectrometry. Therapeutic Drug Monitoring 26: 650–657 (2004).

[207] A. van Eeckhaut, K. Lanckmans, S. Sarre, I. Smolders, Y. Michotte. Validation of bioanalytical LC–MS/MS assays: Evaluation of matrix effects. Journal of Chromatography B 877: 2198–2207 (2009).

[208] D.M. Saunte, F. Simmel, N. Frimodt-Moller, L.B. Stolle, E.L. Svejgaard, M. Haedersdal, C. Kloft, M.C. Arendrup. In Vivo Efficacy and Pharmacokinetics of Voriconazole in an Animal Model of Dermatophytosis. Antimicrobial Agents and Chemotherapy 51: 3317–3321 (2007).

[209] U.S. Food and Drug Administration. In Vitro Drug Interaction Studies: Cytochrome P450 Enzyme-and Transporter-Mediated Drug Interactions, Guidance for Industry. (2020). https://www.fda.gov/media/134582/download (last access 4 Dec 2021).

[210] S. J. Richardson, A. Bai, A. A. Kulkarni, M. F. Moghaddam. Efficiency in Drug Discovery: Liver S9 Fraction Assay As a Screen for Metabolic Stability. Drug Metabolism Letters 10: 83–90 (2016).

[211] R.E. Pearce, C.J. McIntyre, A. Madan, U. Sanzgiri, A.J. Draper, P.L. Bullock, D.C. Cook, L.A. Burton, J. Latham, C. Nevins, A. Parkinson. Effects of Freezing, Thawing, and Storing Human Liver Microsomes on Cytochrome P450 Activity. Archives of Biochemistry and Biophysics 331: 145–169 (1996).

[212] D. Hallifax, J.B. Houston. Methodological Uncertainty in Quantitative Prediction of Human Hepatic Clearance from In Vitro Experimental Systems. Current Drug Metabolism 10: 307–321 (2009).

[213] M.J. Gómez-Lechón, J.V. Castell, M.T. Donato. Hepatocytes—the choice to investigate drug metabolism and toxicity in man: In vitro variability as a reflection of in vivo. Chemico-Biological Interactions 168: 30–50 (2007).

[214] K. Rowland Yeo, A. Rostami-Hodjegan, G.T. Tucker. Abundance of cytochromes P450 in human liver: a meta-analysis. British Journal of Clinical Pharmacology 57: 687–688 (2004).

[215] H. Zhang, N. Gao, X. Tian, T. Liu, Y. Fang, J. Zhou, Q. Wen, B. Xu, B. Qi, J. Gao, H. Li, L. Jia, H. Qiao. Content and activity of human liver microsomal protein and prediction of individual hepatic clearance in vivo. Scientific Reports 5: 17671 (2015).

[216] Corning. UltraPool HLM 150, batch 38294. https://certs-ecatalog.corning.com/life-sciences/certs/452117_38294.pdf (last access 26 Nov 2021).

[217] Corning. Pooled human intestine microsomes, batch 8193001. https://certs-ecatalog.corning.com/life-sciences/certs/452210_8193001.pdf (last access 30 Sep 2021).

[218] H. Yamazaki, M. Nakamura, T. Komatsu, K. Ohyama, N. Hatanaka, S. Asahi, N. Shimada, F.P. Guengerich, T. Shimada, M. Nakajima, T. Yokoi. Roles of NADPH-P450 reductase and apo- and holo-cytochrome b5 on xenobiotic oxidations catalyzed by 12 recombinant human cytochrome P450s expressed in membranes of Escherichia coli. Protein Expression and Purification 24: 329–337 (2002).

[219] M. Hermann, T. Kase, E. Molden, H. Christensen. Evaluation of Microsomal Incubation Conditions on CYP3A4-Mediated Metabolism of Cyclosporine A by a Statistical Experimental Design. Current Drug Metabolism 7: 265–271 (2006).

[220] T. Kudo, Y. Ozaki, T. Kusano, E. Hotta, Y. Oya, S. Komatsu, H. Goda, K. Ito. Effect of buffer conditions on CYP2C8-mediated paclitaxel 6α-hydroxylation and CYP3A4-mediated triazolam α- and 4-hydroxylation by human liver microsomes. Xenobiotica 46: 241–246 (2016).

[221] Y. Yamamura, N. Koyama, K. Umehara. Comprehensive kinetic analysis and influence of reaction components for chlorzoxazone 6-hydroxylation in human liver microsomes with CYP antibodies. Xenobiotica 45: 353–360 (2015).

[222] R.A. Stringer, C. Strain-Damerell, P. Nicklin, J.B. Houston. Evaluation of recombinant cytochrome p450 enzymes as an in vitro system for metabolic clearance predictions. Drug Metabolism and Disposition 37: 1025–1034 (2009).

[223] T. Kudo, H. Goda, Y. Yokosuka, R. Tanaka, S. Komatsu, K. Ito. Estimation of the Contribution of CYP2C8 and CYP3A4 in Repaglinide Metabolism by Human Liver Microsomes Under Various Buffer Conditions. Journal of Pharmaceutical Sciences 106: 2847–2852 (2017).

[224] N. Chauret, A. Gauthier, D.A. Nicoll-Griffith. Effect of common organic solvents on in vitro cytochrome P450-mediated metabolic activities in human liver microsomes. Drug Metabolism and Disposition 26: 1–4 (1998).

[225] C. Tang, M. Shou, A.D. Rodrigues. Substrate-dependent effect of acetonitrile on human liver microsomal cytochrome P450 2C9 (CYP2C9) activity. Drug Metabolism and Disposition 28: 567–72 (2000).

[226] W.F. Busby, J.M. Ackermann, C.L. Crespi. Effect of methanol, ethanol, dimethyl sulfoxide, and acetonitrile on in vitro activities of cDNA-expressed human cytochromes P-450. Drug Metabolism and Disposition 27: 246–249 (1999).

[227] J.K. Coller, A.A. Somogyi, F. Bochner. Comparison of (S)-mephenytoin and proguanil oxidation *in vitro* : contribution of several CYP isoforms. British Journal of Clinical Pharmacology 48: 158–167 (1999).

[228] Y. Chen, L. Liu, K. Nguyen, A.J. Fretland. Utility of Intersystem Extrapolation Factors in Early Reaction Phenotyping and the Quantitative Extrapolation of Human Liver Microsomal Intrinsic Clearance Using Recombinant Cytochromes P450. Drug Metabolism and Disposition 39: 373–382 (2011).

[229] R.L. Walsky, R.S. Obach. Validated Assays for Human Cytochrome P450 Activities. Drug Metabolism and Disposition 32: 647–660 (2004).

[230] K. Grime, R. Riley. The Impact of In Vitro Binding on In Vitro - In Vivo Extrapolations, Projections of Metabolic Clearance and Clinical Drug-Drug Interactions. Current Drug Metabolism 7: 251–264 (2006).

[231] R.S. Obach. The importance of nonspecific binding in in vitro matrices, its impact on enzyme kinetic studies of drug metabolism reactions, and implications for in vitro-in vivo correlations. Drug Metabolism and Disposition 24: 1047–1049 (1996).

[232] J.A. McLure, J.O. Miners, D.J. Birkett. Nonspecific binding of drugs to human liver microsomes. British Journal of Clinical Pharmacology 49: 453–461 (2000).

[233] S.B. Yanni, P.P. Annaert, P. Augustijns, J.G. Ibrahim, D.K. Benjamin, D.R. Thakker. In Vitro Hepatic Metabolism Explains Higher Clearance of Voriconazole in Children versus Adults: Role of CYP2C19 and Flavin-Containing Monooxygenase 3. Drug Metabolism and Disposition 38: 25–31 (2010).

[234] R. Xu, E. Gu, T. Liu, Q. Ou-yang, G. Hu, J. Cai. The effects of cytochrome P450 2C19 polymorphism on the metabolism of voriconazole in vitro. Infection and Drug Resistance 11: 2129–2135 (2018).

[235] M.F. Paine, H.L. Hart, S.S. Ludington, R.L. Haining, A.E. Rettie, D.C. Zeldin. The Human Intestinal Cytochrome P450 "PIE." Drug Metabolism and Disposition 34: 880–886 (2006).

[236] Y.A. Siu, W.G. Lai. Impact of Probe Substrate Selection on Cytochrome P450 Reaction Phenotyping Using the Relative Activity Factor. Drug Metabolism and Disposition 45: 183–189 (2017).

[237] H.K. Crewe, Z.E. Barter, K. Rowland Yeo, A. Rostami-Hodjegan. Are there differences in the catalytic activity per unit enzyme of recombinantly expressed and human liver microsomal cytochrome P450 2C9? A systematic investigation into inter-system extrapolation factors. Biopharmaceutics and Drug Disposition 32: 303–318 (2011).

[238] M.J.P. Geist, G. Egerer, J. Burhenne, G. Mikus. Safety of Voriconazole in a Patient with CYP2C9*2/CYP2C9*2 Genotype. Antimicrobial Agents and Chemotherapy 50: 3227–3228 (2006).

[239] G. Mikus, V. Schöwel, M. Drzewinska, J. Rengelshausen, R. Ding, K.-D. Riedel, J. Burhenne, J. Weiss, T. Thomsen, W.E. Haefeli. Potent cytochrome P450 2C19 genotype-related interaction between voriconazole and the cytochrome P450 3A4 inhibitor ritonavir. Clinical Pharmacology & Therapeutics 80: 126–135 (2006).

[240] Z. Desta, I.F. Metzger, N. Thong, J.B.L. Lu, J.T. Callaghan, T.C. Skaar, D.A. Flockhart, R.E. Galinsky. Inhibition of cytochrome P450 2B6 activity by voriconazole profiled using efavirenz disposition in healthy volunteers. Antimicrobial Agents and Chemotherapy 60: 6813–6822 (2016).

[241] M. Fihlman, T. Hemmilä, N.M. Hagelberg, K. Kuusniemi, J.T. Backman, J. Laitila, K. Laine, P.J. Neuvonen, K.T. Olkkola, T.I. Saari. Voriconazole more likely than posaconazole increases plasma exposure to sublingual buprenorphine causing a risk of a clinically important interaction. European Journal of Clinical Pharmacology 72: 1363–1371 (2016).

[242] X. Luo, T. Li, Z. Yu, X. Xue, H. Zhao, N. Li, L. Ma, C. Yang, L. Huang, W. Feng. The impact of azole antifungal drugs on imatinib metabolism in human liver microsomes. Xenobiotica 49: 753–761 (2019).

[243] X. Li, S. Frechen, D. Moj, T. Lehr, M. Taubert, C. hsuan Hsin, G. Mikus, P.J. Neuvonen, K.T. Olkkola, T.I. Saari, U. Fuhr. A Physiologically Based Pharmacokinetic Model of Voriconazole Integrating Time-Dependent Inhibition of CYP3A4, Genetic Polymorphisms of CYP2C19 and Predictions of Drug–Drug Interactions. Clinical Pharmacokinetics 59: 781–808 (2020).

[244] C. Lu, L. Di. *In vitro* and *in vivo* methods to assess pharmacokinetic drug– drug interactions in drug discovery and development. Biopharmaceutics & Drug Disposition 41: 3–31 (2020).

[245] A. Parkinson, F. Kazmi, D.B. Buckley, P. Yerino, B.L. Paris, J. Holsapple, P. Toren, S.M. Otradovec, B.W. Ogilvie. An Evaluation of the Dilution Method for Identifying Metabolism-Dependent Inhibitors of Cytochrome P450 Enzymes. Drug Metabolism and Disposition 39: 1370–1387 (2011).

[246] S.K. Quinney, S. Knopp, C. Chang, S.D. Hall, L. Li. Integration of *In Vitro* Binding Mechanism Into the Semiphysiologically Based Pharmacokinetic Interaction Model Between Ketoconazole and Midazolam. CPT: Pharmacometrics & Systems Pharmacology 2: e75 (2013).

[247] A.M. Filppula, R. Parvizi, A. Mateus, P. Baranczewski, P. Artursson. Improved predictions of time-dependent drug-drug interactions by determination of cytosolic drug concentrations. Scientific Reports 9: 5850 (2019).

[248] H. Kato. Computational prediction of cytochrome P450 inhibition and induction. Drug Metabolism and Pharmacokinetics 35: 30–44 (2020).

[249] P.C. Nair, R.A. McKinnon, J.O. Miners. Cytochrome P450 structure–function: insights from molecular dynamics simulations. Drug Metabolism Reviews 48: 434–452 (2016).

[250] H. Jones, Y. Chen, C. Gibson, T. Heimbach, N. Parrott, S. Peters, J. Snoeys, V. Upreti, M. Zheng, S. Hall. Physiologically based pharmacokinetic modeling in drug discovery and development: A pharmaceutical industry perspective. Clinical Pharmacology & Therapeutics 97: 247–262 (2015).

[251] S.A. Peters, H. Dolgos. Requirements to Establishing Confidence in Physiologically Based Pharmacokinetic (PBPK) Models and Overcoming Some of the Challenges to Meeting Them. Clinical Pharmacokinetics 58: 1355–1371 (2019).

[252] A. Rostami-Hodjegan. Physiologically Based Pharmacokinetics Joined With In Vitro–In Vivo Extrapolation of ADME: A Marriage Under the Arch of Systems Pharmacology. Clinical Pharmacology & Therapeutics 92: 50–61 (2012).

[253] L.B. Sheiner. Learning versus confirming in clinical drug development. Clinical Pharmacology & Therapeutics 61: 275–291 (1997).

[254] R. Michelet, J. van Bocxlaer, K. Allegaert, A. Vermeulen. The use of PBPK modeling across the pediatric age range using propofol as a case. Journal of Pharmacokinetics and Pharmacodynamics 45: 765–785 (2018).

[255] R. Michelet, J. van Bocxlaer, A. Vermeulen. PBPK in Preterm and Term Neonates: A Review. Current Pharmaceutical Design 23: 5943–5954 (2018).

[256] Y. Chen, J.Y. Jin, S. Mukadam, V. Malhi, J.R. Kenny. Application of IVIVE and PBPK modeling in prospective prediction of clinical pharmacokinetics: strategy and approach during the drug discovery phase with four case studies. Biopharmaceutics & Drug Disposition 33: 85–98 (2012).

[257] F. Kluwe, R. Michelet, A. Mueller-Schoell, C. Maier, L. Klopp-Schulze, M. Dyk, G. Mikus, W. Huisinga, C. Kloft. Perspectives on Model-Informed Precision Dosing in the Digital Health Era: Challenges, Opportunities, and Recommendations. Clinical Pharmacology & Therapeutics 109: 29–36 (2021).

[258] D. Burau, D. Petroff, P. Simon, L. Ehmann, C. Weiser, C. Dorn, A. Kratzer, H. Wrigge, C. Kloft. Drug combinations and impact of experimental conditions on relative recovery in in vitro microdialysis investigations. European Journal of Pharmaceutical Sciences 127: 252–260 (2019).

[259] Drugbank. Voriconazole. https://go.drugbank.com/drugs/DB00582 (last access 22 Nov 2021).

[260] Drugbank. Metabolite Voriconazole N-Oxide. https://go.drugbank.com/metabolites/DBMET00071 (last access 22 Nov 2021).

[261] D. Busse, P. Simon, R. Michelet, L. Ehmann, F. Mehner, C. Dorn, A. Kratzer, W. Huisinga, H. Wrigge, D. Petroff, C. Kloft. Quantification of microdialysis related variability in humans: Clinical trial design recommendations. European Journal of Pharmaceutical Sciences 157: 105607 (2021).

[262] C.M. Kho, S.K. Enche Ab Rahim, Z.A. Ahmad, N.S. Abdullah. A Review on Microdialysis Calibration Methods: the Theory and Current Related Efforts. Molecular Neurobiology 54: 3506–3527 (2017).

[263] M. Cano-Cebrian, T. Zornoza, A. Polache, L. Granero. Quantitative In Vivo Microdialysis in Pharmacokinetic Studies: Some Reminders. Current Drug Metabolism 6: 83–90 (2005).

[264] Y. Yu, H. Chandasana, T. Sangari, C. Seubert, H. Derendorf. Simultaneous Retrodialysis by Calibrator for Rapid In Vivo Recovery Determination in Target Site Microdialysis. Journal of Pharmaceutical Sciences 107: 2259–2265 (2018).

[265] P. Hanberg, M. Bue, K. Öbrink-Hansen, J. Kabel, M. Thomassen, M. Tøttrup, K. Søballe, M. Stilling. Simultaneous Retrodialysis by Drug for Cefuroxime Using Meropenem as an Internal Standard—A Microdialysis Validation Study. Journal of Pharmaceutical Sciences 109: 1373–1379 (2020).

[266] O. Epaulard, M.-T. Leccia, S. Blanche, O. Chosidow, M.-F. Mamzer-Bruneel, P. Ravaud, A. Thiebaut, C. Villier, O. Lortholary. Phototoxicity and photocarcinogenesis associated with voriconazole. Médecine et Maladies Infectieuses 41: 639–645 (2011).

[267] O. Epaulard, C. Villier, P. Ravaud, O. Chosidow, S. Blanche, M.-F. Mamzer-Bruneel, A. Thiebaut, M.-T. Leccia, O. Lortholary. A Multistep Voriconazole-Related Phototoxic Pathway May Lead to Skin Carcinoma: Results From a French Nationwide Study. Clinical Infectious Diseases 57: e182–e188 (2013).

[268] A. Schaeftlein, I.K. Minichmayr, C. Kloft. Population pharmacokinetics meets microdialysis: Benefits, pitfalls and necessities of new analysis approaches for human microdialysis data. European Journal of Pharmaceutical Sciences 57: 68–73 (2014).

[269] K. Wanat, E. Brzezińska, A.W. Sobańska. Aspects of Drug-Protein Binding and Methods of Analyzing the Phenomenon. Current Pharmaceutical Design 24: 2974–2985 (2018).

[270] M. Howard, J. Hill, G. Galluppi, M. McLean. Plasma Protein Binding in Drug Discovery and Development. Combinatorial Chemistry & High Throughput Screening 13: 170–187 (2010).

[271] F. Zhang, J. Xue, J. Shao, L. Jia. Compilation of 222 drugs' plasma protein binding data and guidance for study designs. Drug Discovery Today 17: 475–485 (2012).

[272] A. Kratzer, F. Kees, C. Dorn. Unbound fraction of fluconazole and linezolid in human plasma as determined by ultrafiltration: Impact of membrane type. Journal of Chromatography B 1039: 74–78 (2016).

[273] M.G. Kees, S.G. Wicha, A. Seefeld, F. Kees, C. Kloft. Unbound fraction of vancomycin in intensive care unit patients. The Journal of Clinical Pharmacology 54: 318–323 (2014).

[274] M. Schleibinger, C.L. Steinbach, C. Töpper, A. Kratzer, U. Liebchen, F. Kees, B. Salzberger, M.G. Kees. Protein binding characteristics and pharmacokinetics of ceftriaxone in intensive care unit patients. British Journal of Clinical Pharmacology 80: 525–533 (2015).

[275] A. Kratzer, U. Liebchen, M. Schleibinger, M.G. Kees, F. Kees. Determination of free vancomycin, ceftriaxone, cefazolin and ertapenem in plasma by ultrafiltration: Impact of experimental conditions. Journal of Chromatography B 961: 97–102 (2014).

[276] K. Vanstraelen, S. Pauwels, M. Oyaert, J. Maertens, I. Spriet. Key Elements in Determining Voriconazole Protein Binding Characteristics. Therapeutic Drug Monitoring 37: 551–553 (2015).

[277] C. Dorn, A. Kratzer, U. Liebchen, M. Schleibinger, A. Murschhauser, J. Schlossmann, F. Kees, P. Simon, M.G. Kees. Impact of Experimental Variables on the Protein Binding of Tigecycline in Human Plasma as Determined by Ultrafiltration. Journal of Pharmaceutical Sciences 107: 739–744 (2018).

[278] A. Fura, T.W. Harper, H. Zhang, L. Fung, W.C. Shyu. Shift in pH of biological fluids during storage and processing: effect on bioanalysis. Journal of Pharmaceutical and Biomedical Analysis 32: 513–522 (2003).

[279] C.J. Kochansky, D.R. McMasters, P. Lu, K.A. Koeplinger, H.H. Kerr, M. Shou, K.R. Korzekwa. Impact of pH on Plasma Protein Binding in Equilibrium Dialysis. Molecular Pharmaceutics 5: 438–448 (2008).

[280] C. Dorn, D. Petroff, N. Neumann, A. Kratzer, N. El-Najjar, A. Dietrich, C. Kloft, M. Zeitlinger, M.G. Kees, F. Kees, H. Wrigge, P. Simon. Plasma and tissue pharmacokinetics of fosfomycin in morbidly obese and non-obese surgical patients: a controlled clinical trial. Journal of Antimicrobial Chemotherapy 74: 2335–2340 (2019).

[281] D. Hutschala, C. Kinstner, K. Skhirtladze, B.-X. Mayer-Helm, M. Zeitlinger, W. Wisser, M. Müller, E. Tschernko. The impact of perioperative atelectasis on antibiotic penetration into lung tissue: an in vivo microdialysis study. Intensive Care Medicine 34: 1827–1834 (2008).

[282] D. Busse, A. Schaeftlein, A. Solms, L. Ilia, R. Michelet, M. Zeitlinger, W. Huisinga, C. Kloft. Which Analysis Approach Is Adequate to Leverage Clinical Microdialysis Data? A Quantitative Comparison to Investigate Exposure and Response Exemplified by Levofloxacin. Pharmaceutical Research 38: 381–395 (2021).

[283] W.B. Park, N.-H. Kim, K.-H. Kim, S.H. Lee, W.-S. Nam, S.H. Yoon, K.-H. Song, P.G. Choe, N.J. Kim, I.-J. Jang, M. Oh, K.-S. Yu. The Effect of Therapeutic Drug Monitoring on Safety and Efficacy of Voriconazole in Invasive Fungal Infections: A Randomized Controlled Trial. Clinical Infectious Diseases 55: 1080–1087 (2012).

[284] J.-S. Kang, M.-H. Lee. Overview of Therapeutic Drug Monitoring. Korean J Intern Med 24: 1 (2009).

[285] D. Alihodzic, A. Broeker, M. Baehr, S. Kluge, C. Langebrake, S.G. Wicha. Impact of Inaccurate Documentation of Sampling and Infusion Time in Model-Informed Precision Dosing. Frontiers in Pharmacology 11: 172 (2020).

[286] S. Schadt, B. Bister, S.K. Chowdhury, C. Funk, C.E.C.A. Hop, W.G. Humphreys, F. Igarashi, A.D. James, M. Kagan, S.C. Khojasteh, A.N.R. Nedderman, C. Prakash, F. Runge, H. Scheible, D.K. Spracklin, P. Swart, S. Tse, J. Yuan, R.S. Obach. A Decade in the MIST: Learnings from Investigations of Drug Metabolites in Drug Development under the "Metabolites in Safety Testing" Regulatory Guidance. Drug Metabolism and Disposition 46: 865–878 (2018).

[287] U. S. Food and Drug Administration. Safety Testing of Drug Metabolites. Guidance for Industry. (2020). https://www.fda.gov/media/72279/download (last access 23 Nov 2021).

[288] T. Yamada, Y. Mino, T. Yagi, T. Naito, J. Kawakami. Saturated Metabolism of Voriconazole N-Oxidation Resulting in Nonlinearity of Pharmacokinetics of Voriconazole at Clinical Doses. Biological & Pharmaceutical Bulletin 38: 1496–1503 (2015).

[289] C. Shi, Y. Xiao, Y. Mao, J. Wu, N. Lin. Voriconazole: A Review of Population Pharmacokinetic Analyses. Clinical Pharmacokinetics 58: 687–703 (2019).

[290] A. Owusu Obeng, E.F. Egelund, A. Alsultan, C.A. Peloquin, J.A. Johnson. CYP2C19 Polymorphisms and Therapeutic Drug Monitoring of Voriconazole: Are We Ready for Clinical Implementation of Pharmacogenomics? Pharmacotherapy: The Journal of Human Pharmacology and Drug Therapy 34: 703–718 (2014).

[291] M. Biswas. Global distribution of CYP2C19 risk phenotypes affecting safety and effectiveness of medications. The Pharmacogenomics Journal 21: 190–199 (2021).

[292] Z. Hashemizadeh, P. Badiee, S.A. Malekhoseini, H. Raeisi Shahraki, B. Geramizadeh, H. Montaseri. Observational Study of Associations between Voriconazole Therapeutic Drug Monitoring, Toxicity, and Outcome in Liver Transplant Patients. Antimicrobial Agents and Chemotherapy 61: e01211 (2017).

[293] M. Hoenigl, W. Duettmann, R.B. Raggam, K. Seeber, K. Troppan, S. Fruhwald, F. Prueller, J. Wagner, T. Valentin, I. Zollner-Schwetz, A. Wölfler, R. Krause. Potential Factors for Inadequate Voriconazole Plasma Concentrations in Intensive Care Unit Patients and Patients with Hematological Malignancies. Antimicrobial Agents and Chemotherapy 57: 3262–3267 (2013).

[294] M.J. Dolton, J.E. Ray, S.C.-A. Chen, K. Ng, L.G. Pont, A.J. McLachlan. Multicenter Study of Voriconazole Pharmacokinetics and Therapeutic Drug Monitoring. Antimicrobial Agents and Chemotherapy 56: 4793–4799 (2012).

[295] M.J. Dolton, A.J. McLachlan. Voriconazole pharmacokinetics and exposure–response relationships: Assessing the links between exposure, efficacy and toxicity. International Journal of Antimicrobial Agents 44: 183–193 (2014).

[296] Y. Hanai, Y. Hamada, T. Kimura, K. Matsumoto, Y. Takahashi, S. Fujii, K. Nishizawa, Y. Miyazaki, Y. Takesue. Favorable Effects of Voriconazole Trough Concentrations Exceeding 1 μg/mL on Treatment Success and All-Cause Mortality: A Systematic Review and Meta-Analysis. Journal of Fungi 7: 306 (2021).

[297] D.K. Molina, V.J.M. DiMaio. Normal Organ Weights in Men. The American Journal of Forensic Medicine and Pathology 33: 368–372 (2012).

[298] B. Davies, T. Morris. Physiological Parameters in Laboratory Animals and Humans. Pharmaceutical Research 10: 1093–1095 (1993).

[299] K. Utsey, M.S. Gastonguay, S. Russell, R. Freling, M.M. Riggs, A. Elmokadem. Quantification of the Impact of Partition Coefficient Prediction Methods on Physiologically Based Pharmacokinetic Model Output Using a Standardized Tissue Composition. Drug Metabolism and Disposition 48: 903–916 (2020).

7 Appendix

7.1 Figures

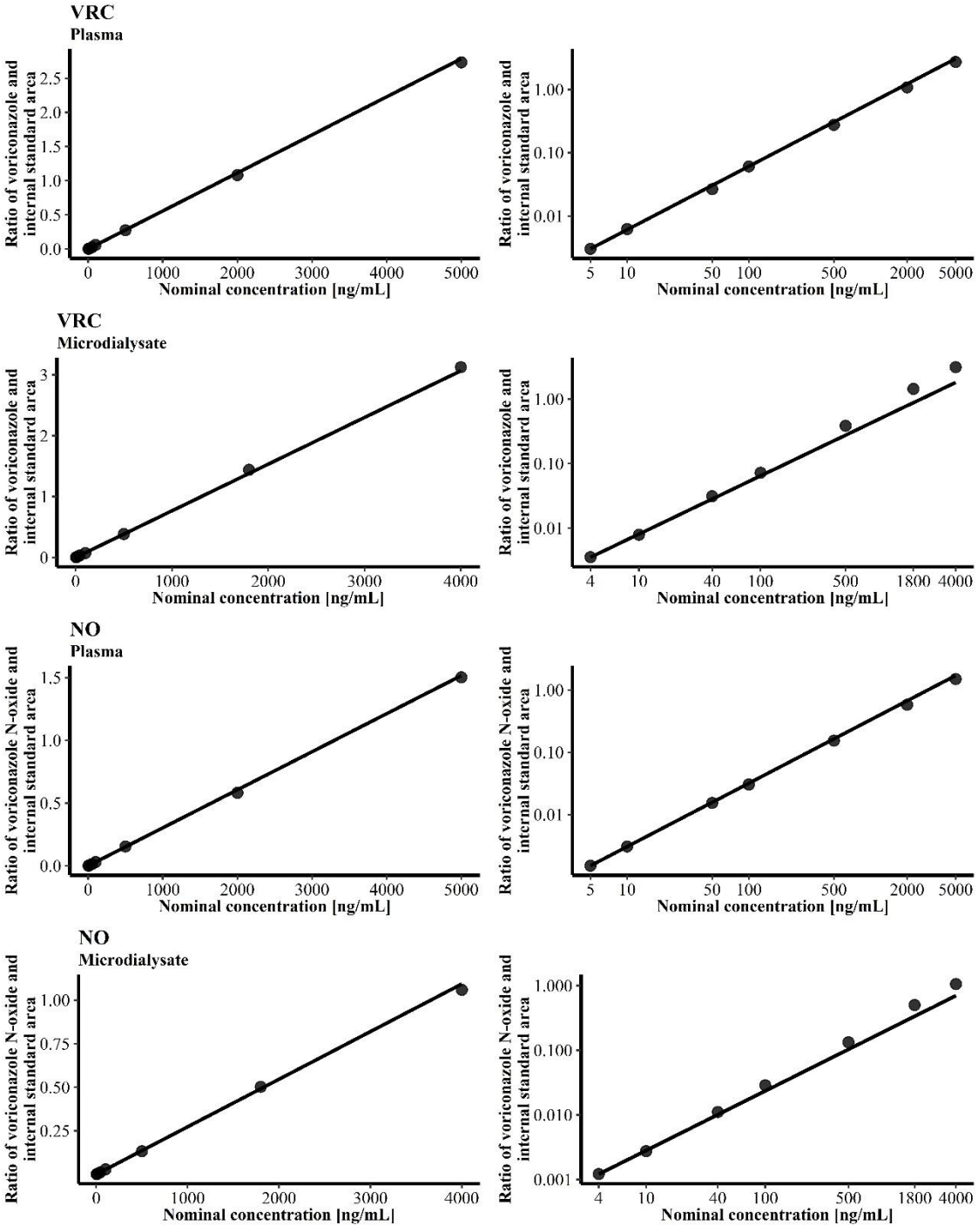

Figure 7.1: Representative calibration functions of voriconazole (VRC, top) and its *N*-oxide metabolite (NO, bottom) in plasma and microdialysate depicted on linear scale (left) and on log-log-transformed scale (right).

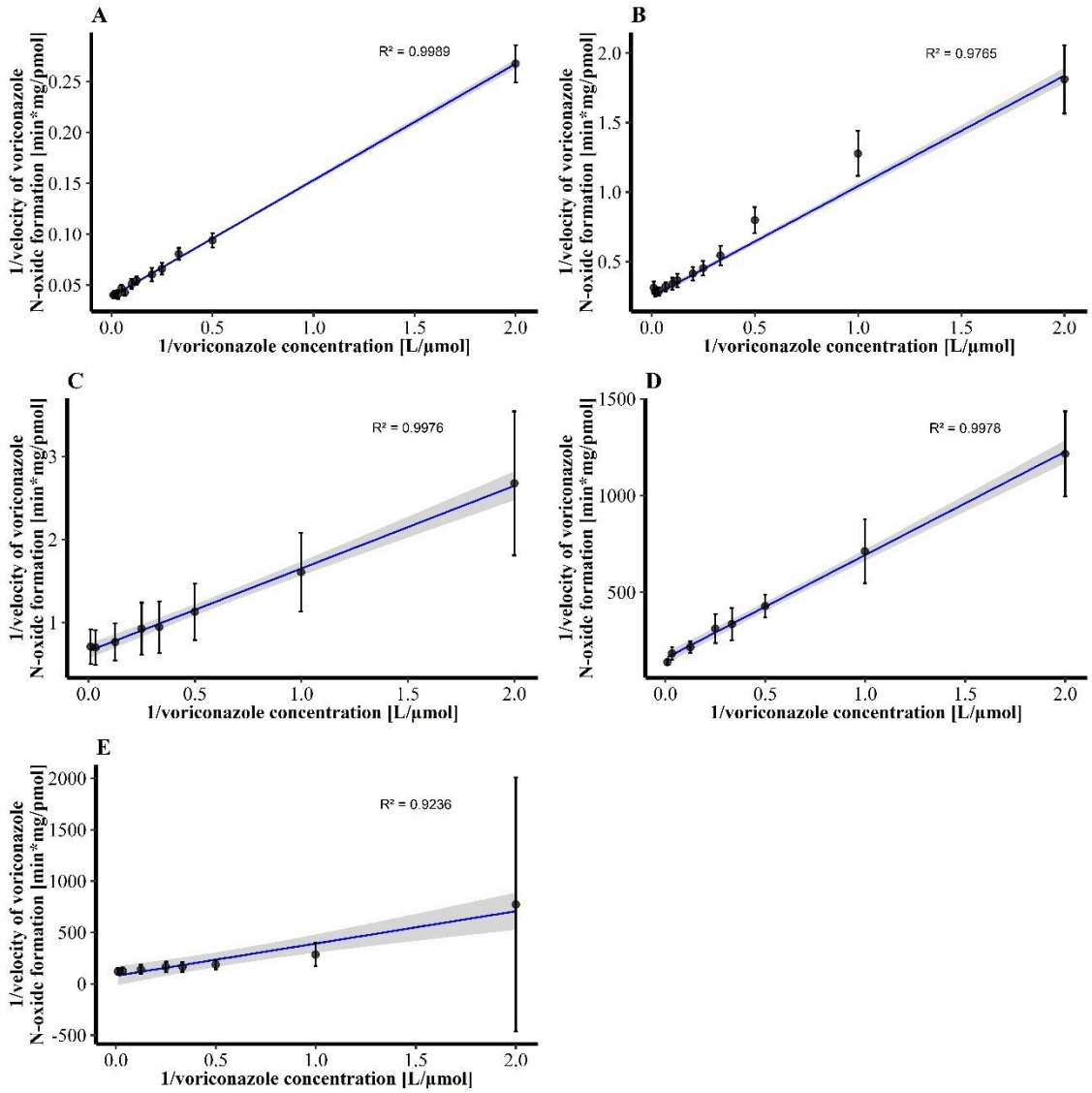

Figure 7.2: Lineweaver-Burk plots of the Michaelis-Menten kinetics of the *N*-oxidation of voriconazole in human liver microsomes (A, n=8-9), human intestine microsomes (B, n=9) and recombinant human cytochrome P450 isoenzymes 2C19 (C, n=18), 2C9 (D, n=10) and 3A4 (E, n=18). Coefficient of determination (R^2) based on linear regression of the mean reciprocal reaction velocity at the respective reciprocal substrate concentration.

Data points: mean reaction velocity; error bars: standard deviation of reaction velocity; solid line: linear regression; shaded area: standard error of the linear regression.

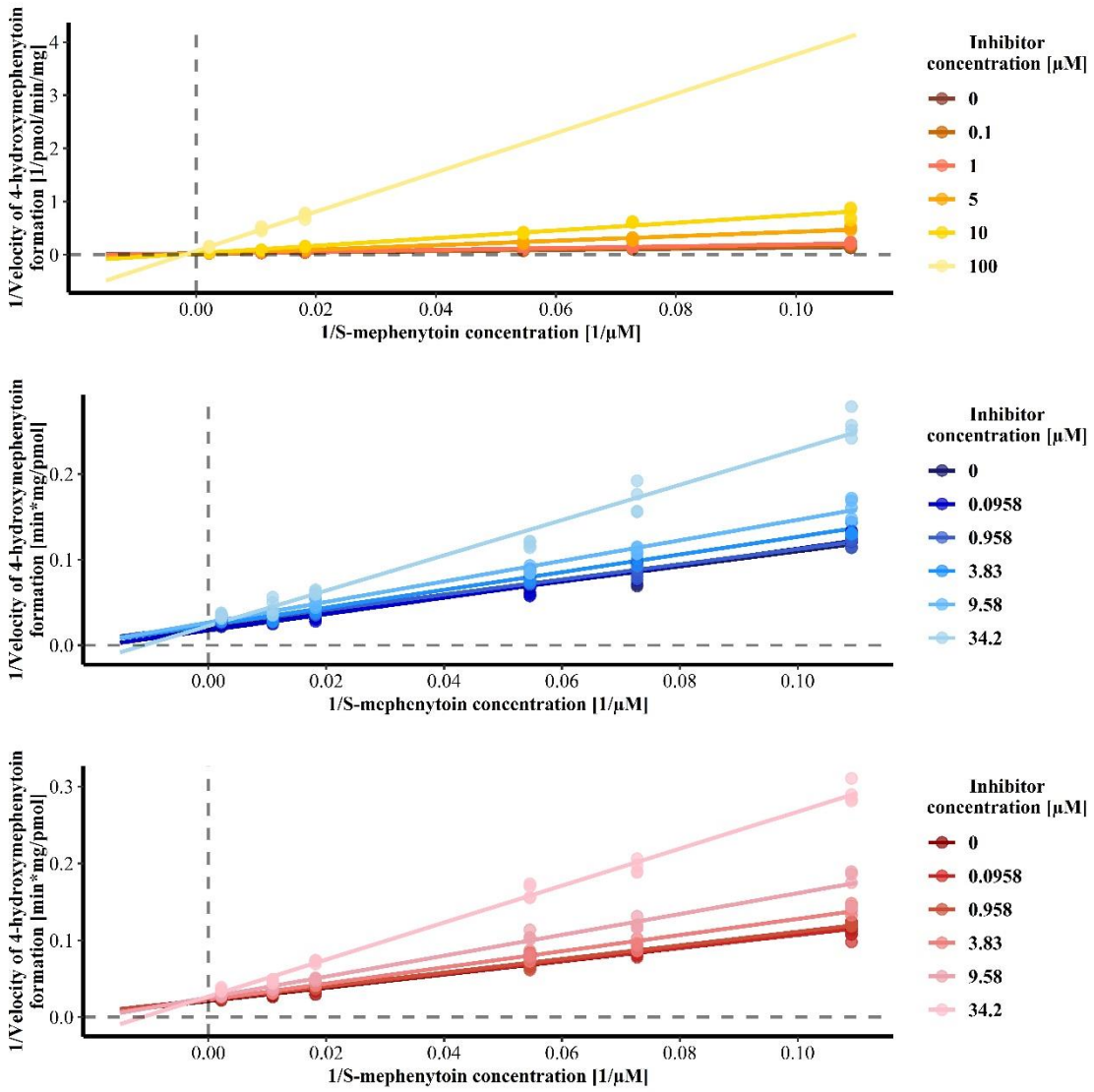

Figure 7.3: Lineweaver-Burk linearisation of the reciprocal reaction velocities of 4-hydroxymephenytoin formation by CYP2C19 in dependence of the reciprocal substrate concentration under the influence of increasing concentrations of the inhibitors voriconazole (VRC, top), voriconazole *N*-oxide (NO, middle) and hydroxyvoriconazole (OH-VRC, bottom) in human liver microsomes (n=4).
Data points: reciprocal reaction velocities; solid lines: linear regression; dashed lines: zero intercepts of the coordinate system.

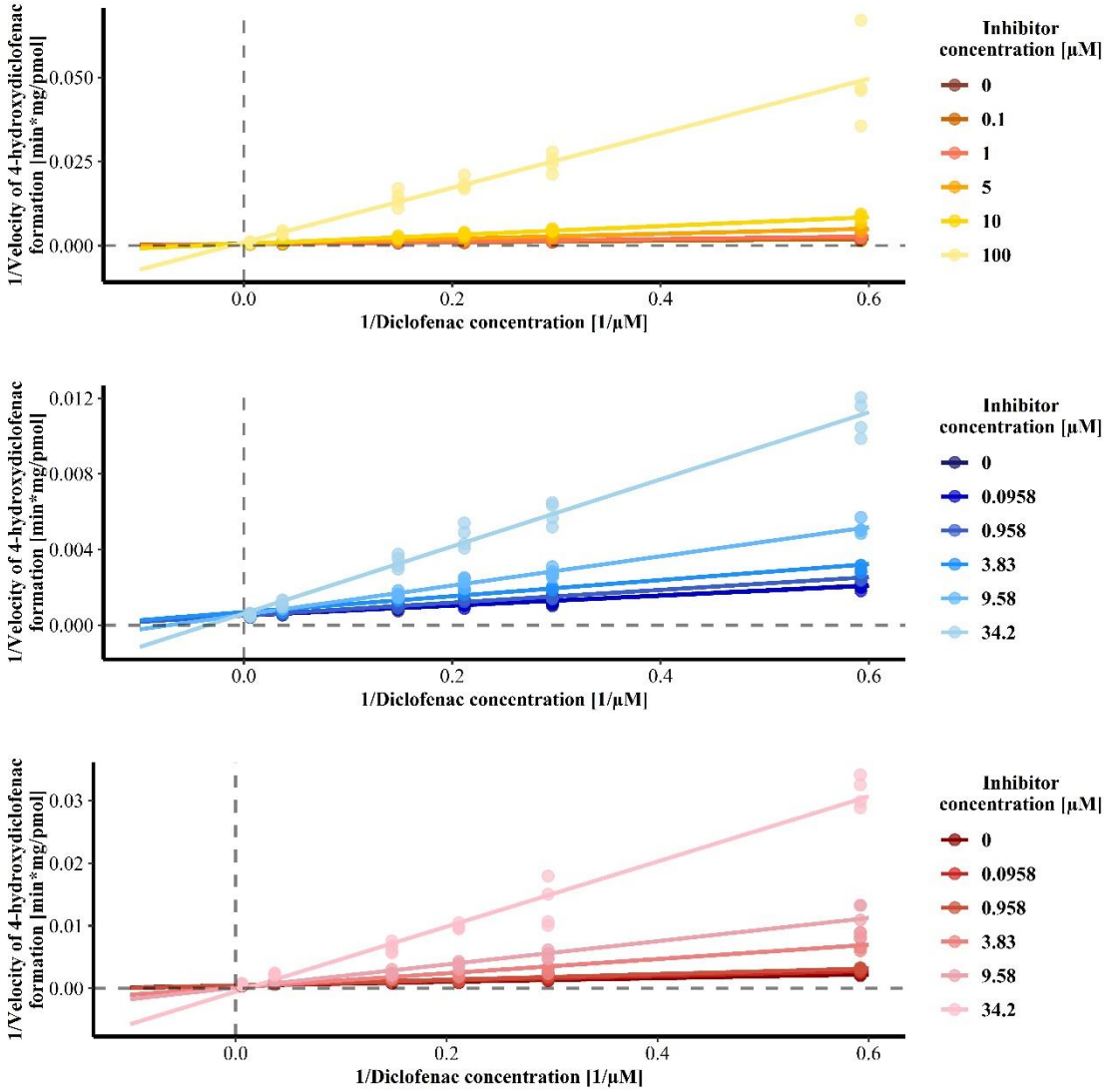

Figure 7.4: Lineweaver-Burk linearisation of the reciprocal reaction velocities of 4-hydroxydiclofenac formation by CYP2C9 in dependence of the reciprocal substrate concentration under the influence of increasing concentrations of the inhibitors voriconazole (VRC, top), voriconazole *N*-oxide (NO, middle) and hydroxyvoriconazole (OH-VRC, bottom) in human liver microsomes (n=2-4).

Data points: reciprocal reaction velocities; solid lines: linear regression; dashed lines: zero intercepts of the coordinate system

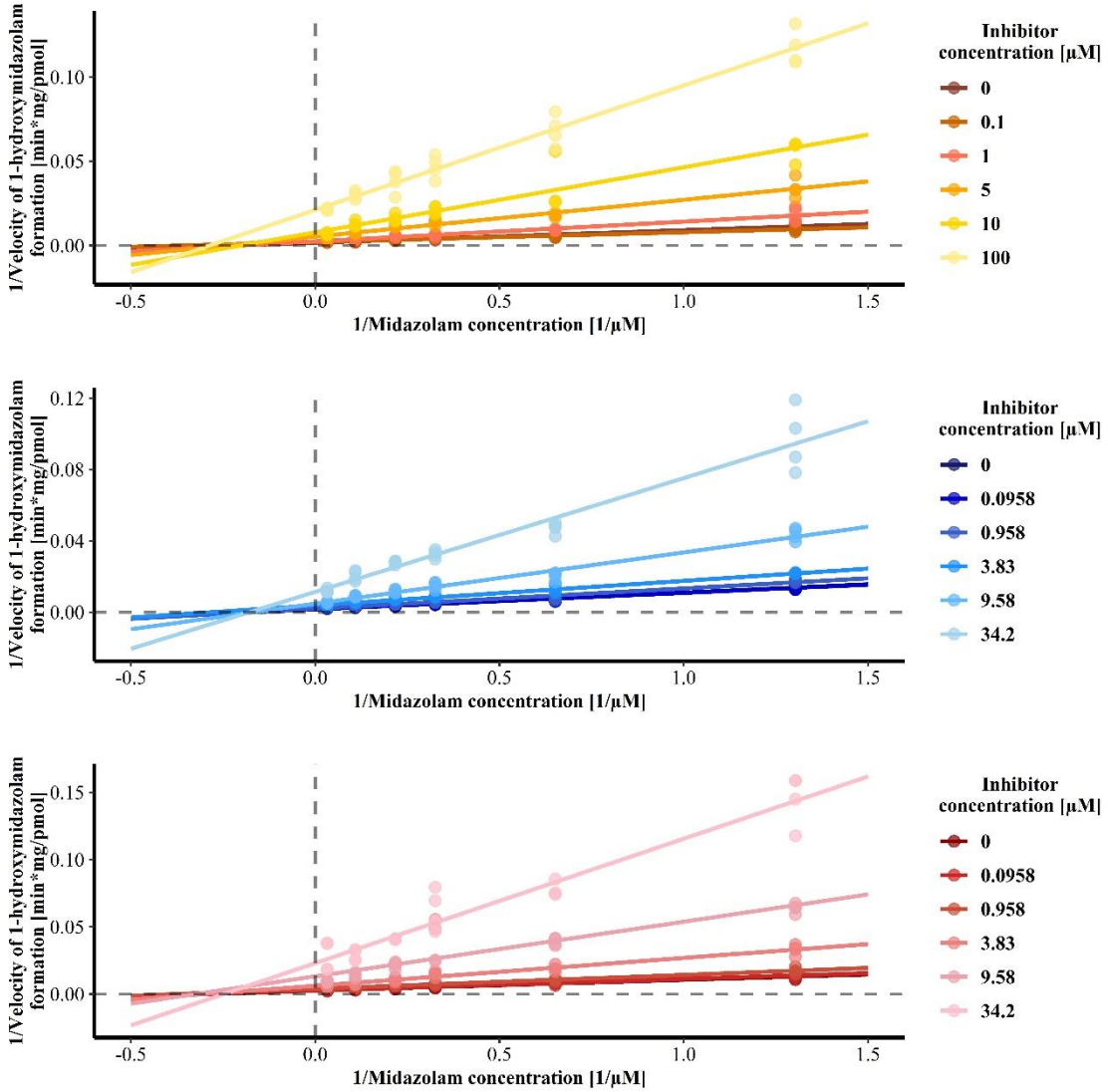

Figure 7.5: Lineweaver-Burk linearisation of the reciprocal reaction velocities of 1-hydroxymidazolam formation by CYP3A4 in dependence of the reciprocal substrate concentration under the influence of increasing concentrations of the inhibitors voriconazole (VRC, top), voriconazole *N*-oxide (NO, middle) and hydroxyvoriconazole (OH-VRC, bottom) in human liver microsomes (n=3-4).
Data points: reciprocal reaction velocities; solid lines: linear regression; dashed lines: zero intercepts of the coordinate system

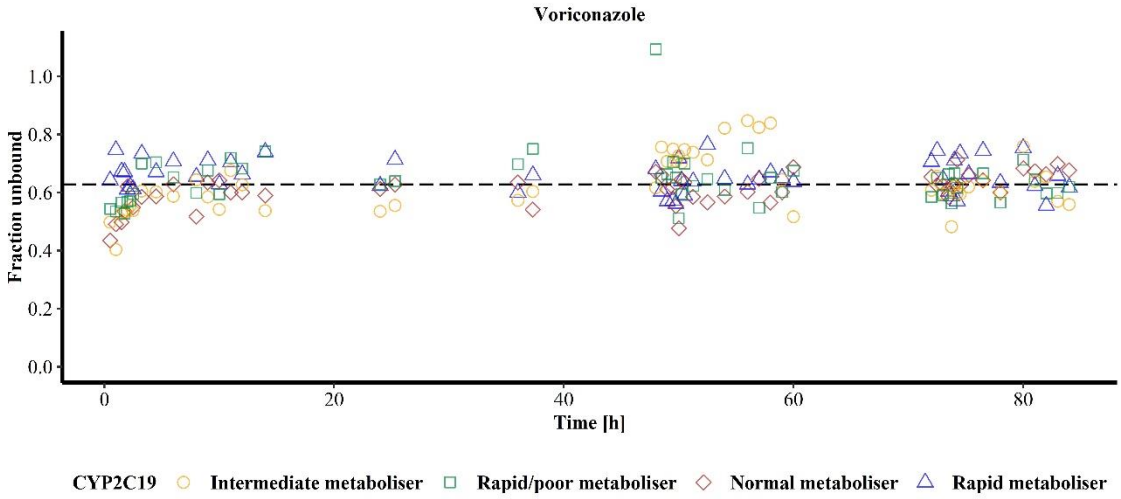

Figure 7.6: Fraction unbound of voriconazole over the duration of the clinical trial for four healthy volunteers determined by ultrafiltration. The black dashed line represents the median fraction unbound of all volunteers and all samples.

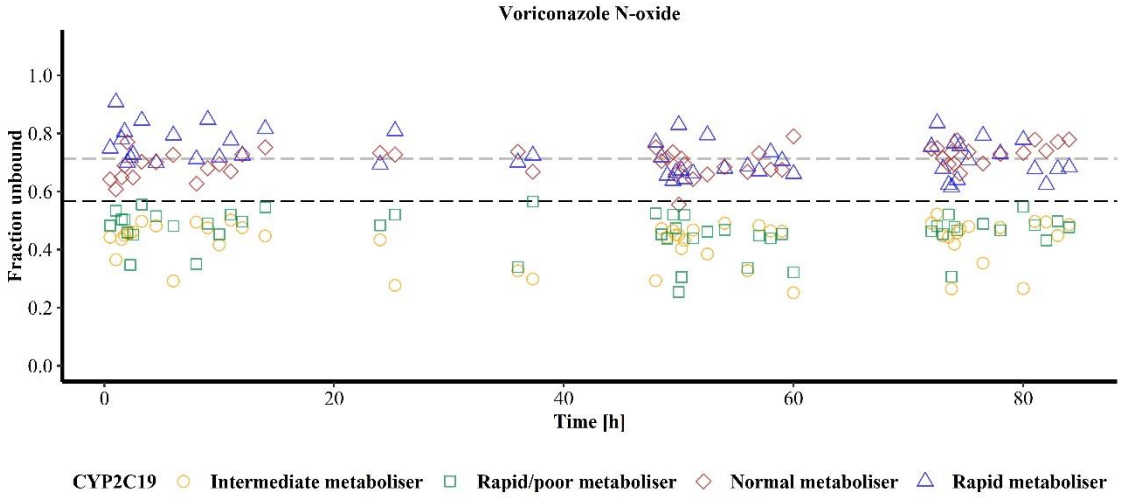

Figure 7.7: Fraction unbound of voriconazole *N*-oxide over the duration of the clinical trial for four healthy volunteers determined by ultrafiltration. The black dashed line represents the median fraction unbound of all volunteers and all samples and the grey dashed line depicts the median fraction unbound of the CYP2C19 rapid and normal metaboliser (see text for explanation).

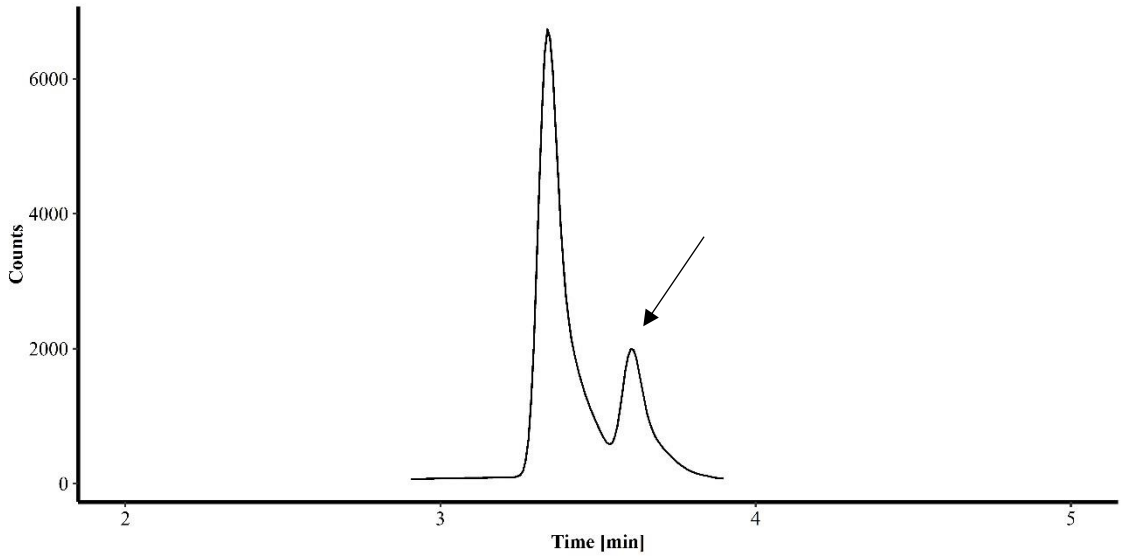

Figure 7.8: Representative chromatogram of voriconazole *N*-oxide as observed in ultrafiltrate samples of the CYP2C19 rapid/poor metaboliser and intermediate metaboliser during bioanalysis of clinical trial samples. The arrow indicates the evolving second peak.

Table 7.1: Overview of experimental settings (enzymatic system, protein/enzyme concentration, reaction times, substrate concentrations, inhibitor and inhibitor concentration) and replicate numbers of all performed *in vitro* metabolism experiments investigating voriconazole as substrate and inhibitor.

Experiment (chapter)	Enzyme system	Reaction monitored	Protein concentration (HLM/HIM) [mg/mL] or enzyme concentration (rhCYP) [pmol/mL]	Substrate concentration [µM]	Inhibitor and concentration [µM]	Sampling time points [min]	Number of performed replicates	Total number of performed incubations	Total number of samples
Michaelis-Menten kinetics MEP	HLM	MEP 4-hydroxy-lation	0.2	4.58, 9.16, 13.7, 18.3, 36.7, 45.8, 91.6, 458	No inhibitor	15, 25	3	24	48
(chapter 2.3.3.2 and 3.2.1.2)	rhCYP2C19	MEP 4-hydroxy-lation	2.5	4.58, 9.16, 13.7, 18.3, 36.7, 45.8, 91.6, 458	No inhibitor	15, 25	3	24	48
Michaelis-Menten kinetics DIC	HLM	DIC 4-hydroxy-lation	0.04	1.69, 3.38, 6.75, 10.1 13.5, 27.0, 67.5, 169	No inhibitor	5, 10	3	24	48
(chapter 2.3.3.2 and 3.2.1.2)	rhCYP2C9	DIC 4-hydroxy-lation	2	0.844, 1.69, 3.38, 6.75, 13.5, 27.0, 67.5, 169	No inhibitor	5, 10	6	48	96
Michaelis-Menten kinetics MID	HLM	MDZ 1-hydroxy-lation	0.05	0.307, 0.767, 1.53, 3.07, 6.14, 9.21, 20.0, 30.7	No inhibitor	7, 12	3	24	48
(chapter 2.3.3.2 and 3.2.1.2)	rhCYP3A4	MDZ 1-hydroxy-lation	12.5, 25	0.307, 0.767, 1.53, 3.07, 6.14, 9.21, 20.0, 30.7	No inhibitor	7, 12	3 for each rhCYP concentration	48	96

Table 7.1: continued.

Reaction linearity, voriconazole stability and substrate depletion (chapter 2.3.4.1 and 3.2.2.1)	HLM	VRC *N*-oxidation	0.05, 0.1, 0.2, 0.5	1, 10, 20, 100	No inhibitor	5, 10, 15, 20, 30, 60, 120	2	64	448
	rhCYP2C19	VRC *N*-oxidation	1, 5, 10, 20	1, 10, 100	No inhibitor	5, 10, 15, 20, 30, 60	2-4[*,#] (1 control)	39[*,#]	234[*,#]
	rhCYP2C9	VRC *N*-oxidation	5, 20, 40, 60, 80	1, 10, 100	No inhibitor	5, 10, 15, 20, 30, 60	2[*,°] (1 control)	35[*,°]	210[*,°]
	rhCYP3A4	VRC *N*-oxidation	5, 20, 40, 80	1, 10, 100	No inhibitor	5, 10, 15, 20, 30, 60	2[*] (1 control)	33[*]	198[*]
	HIM	VRC *N*-oxidation	0.5	1, 5, 10, 100	No inhibitor	5, 15, 25, 60	3[*] (1 control)	9[*]	52[*]
Michaelis-Menten kinetics of VRC *N*-oxidation (chapter 2.3.4.2 and 3.2.2.2)	HLM	VRC *N*-oxidation	0.2	0.5, 2, 3, 4, 5, 8, 10, 15, 20, 30, 60, 100	No inhibitor	10, 20, 30	3	36	108
	rhCYP2C19	VRC *N*-oxidation	5, 15	0.5, 1, 2, 3, 4, 8, 30, 100	No inhibitor	15, 25	3-6[a]	72	144
	rhCYP2C9	VRC *N*-oxidation	100	0.5, 1, 2, 3, 4, 8, 30, 100	No inhibitor	15, 25	5	40	80
	rhCYP3A4	VRC *N*-oxidation	20, 40	0.5, 1, 2, 3, 4, 8, 30, 100	No inhibitor	15, 25	3-6[b]	72	144
	HIM	VRC *N*-oxidation	0.5	0.5, 1, 2, 3, 4, 5, 8, 10, 15, 30, 60, 100	No inhibitor	5, 15, 25	3	36	108

Table 7.1: continued.

Contribution of individual CYP enzymes to voriconazole *N*-oxidation (chapter 2.3.4.3 and 3.2.2.3)	HLM	VRC *N*-oxidation	0.2	0.5, 1, 2, 3, 4, 8, 30, 100	Either: • No inhibitor, • Loratadine (10), • Sulfaphenazole (10), • Ketoconazole (0.1), or • Mixture of the above	15, 25	3	120	240
	HLM	MEP 4-hydroxylation	0.2	45.8		15, 25	2	6^{x}	12^{x}
	HLM	DIC 4-hydroxylation	0.2	10.1		15, 25	2	6^{x}	12^{x}
	HLM	MDZ 1-hydroxylation	0.2	6.14		15, 25	2	6^{x}	12^{x}
Metabolic stability NO and OH-VRC (chapter 2.3.4.5 and 3.2.2.5)	HLM	Depletion	0.2	0.137, 1.10	No inhibitor	5, 15, 30, 60	2 (1 control)	12	48
Inhibitory potential of VRC, NO and OH-VRC, IC_{50}-determination (chapter 2.3.5.1 and 3.2.3.1)	HLM	MEP 4-hydroxylation	0.2	55.0	• VRC (0, 0.1, 1.0, 5.0, 10, 100)	15, 25	2	36	72
	HLM	DIC 4-hydroxylation	0.08	4.73	• NO and OH-VRC (0, 0.0958, 0.958, 3.83, 9.58, 34.2)	5, 10	2	36	72
	HLM	MDZ 1-hydroxylation	0.05	4.60		7, 12	2	36	72

Table 7.1: continued.

Time-dependent inhibition, IC_{50}-shift assay (chapter 2.3.5.2 and 3.2.3.2)	HLM	MEP 4-hydroxy-lation	0.2	55.0	• VRC (0, 0.1, 1.0, 5.0, 10, 100)	15, 25	2	72	144
	HLM	DIC 4-hydroxy-lation	0.08	4.28	• NO and OH-VRC (0, 0.0958, 0.958, 3.83, 9.58, 34.2)	5, 10	2	72	144
	HLM	MDZ 1-hydroxy-lation	0.05	4.60		7, 12	2	72	144
Type of reversible inhibition, K_i-determination (chapter 2.3.5.3 and 3.2.3.3)	HLM	MEP 4-hydroxy-lation	0.2	9.16, 13.7, 18.3, 55.0, 91.6, 458	• VRC (0, 0.1, 1.0, 5.0, 10, 100)	15, 25	2	216	432
	HLM	DIC 4-hydroxy-lation	0.08	1.69, 3.38, 4.73, 6.75, 27.0, 169	• NO and OH-VRC (0, 0.0958, 0.958, 3.83, 9.58, 34.2)	5, 10	2	216	432
	HLM	MDZ 1-hydroxy-lation	0.05	0.767, 1.53, 3.07, 4.60, 9.21, 30.7		7, 12	2	216	432

[*] Controls without NADPH re-generating system were performed: at 1, 5 and 20 pmol/mL rhCYP2C19; 5, 20 and 40 pmol/mL rhCYP3A4; 5, 20 and 40 pmol/mL rhCYP2C9; for 100 µM voriconazole in HIM

[#] Experiment at 20 pmol/mL was repeated, thus four replicates were available

[°] Investigations at 60 and 80 pmol/mL rhCYP2C9 were only performed with 10 and 100 µM voriconazole

[a] n=3 for rhCYP2C19 concentration of 5 pmol/mL and n=6 for rhCYP2C19 concentration of 15 pmol/mL

[b] n=3 for rhCYP3A4 concentration of 20 pmol/mL and n=6 for rhCYP3A4 concentration of 40 pmol/mL

[x] No mixture of loratadine, sulfaphenazole and ketoconazole was applied to the marker reactions, controls of the uninhibited marker reactions belonged to the Michaelis-Menten kinetics determination experiment and are included in the sample count there

Abbreviations: DIC, diclofenac; HIM, human intestine microsomes; HLM, human liver microsomes; IC_{50}, half-maximum inhibitory concentration; K_i, inhibitory constant; MEP, S-mephenytoin; MID, midazolam; NO, voriconazole *N*-oxide; OH-VRC, hydroxyvoriconazole; rhCYP, recombinant human cytochrome P450; VRC, voriconazole.

Table 7.2: Physiological parameters taken from literature to perform *in vitro in vivo* extrapolation.

Parameter	**Value**	**Reference**
CYP enzyme abundance per milligram liver		
CYP2C19	11 pmol/mg	[165]
CYP2C9	61 pmol/mg	
CYP3A4	93 pmol/mg	
Microsomal protein per gram liver (MPPGL)	39.46 mg/g	[215]
Liver mass	1561 g	[297]
Hepatic blood flow (Q_H)	1450 mL/min	[298]
Fraction unbound in plasma (fu_P)	0.5	[57]
Blood to plasma ratio (BP)	1	[299]

Table 7.3: Within-run accuracy and precision of voriconazole and its *N*-oxide metabolite quality control samples prepared in plasma and microdialysate in four independent runs executed on four days (n=5-6 per level). Accuracy is presented as mean concentration compared to nominal concentration and precision as coefficient of variation.

Matrix and compound	**C_{Nom} [ng/mL]**	**Run 1**			**Run 2**			**Run 3**			**Run 4**		
		X_{mean} ± SD [ng/mL]	**CV, %**	**Accu-racy, %**	**X_{mean} ± SD [ng/mL]**	**CV, %**	**Accu-racy, %**	**X_{mean} ± SD [ng/mL]**	**CV, %**	**Accu-racy, %**	**X_{mean} ± SD [ng/mL]**	**CV, %**	**Accu-racy, %**
Plasma													
Vori-conazole	5	4.74 ± 0.598	12.6	94.7	5.14 ± 0.446	8.67	103	5.25 ± 0.290	5.52	105	5.14 ± 0.454	8.84	103
	15	15.1 ± 0.783	5.20	100	15.7 ± 1.07	6.84	105	16.1 ± 1.88	11.6	108	15.4 ± 0.928	6.05	102
	200	201 ± 2.42	1.20	101	202 ± 16.5	8.15	101	199 ± 18.5	9.34	99.3	190 ± 24.4	12.8	94.9
	1500	1543 ± 126	8.18	103	1553 ± 47.9	3.08	104	1620 ± 31.0	1.91	108	1473 ± 135	9.16	98.2
	4000	4228 ± 216	5.10	106	4229 ± 116	2.75	106	4409 ± 181	4.10	110	3998 ± 303	7.59	100
Vori-conazole *N*-oxide	5	4.60 ± 0.436	9.47	92.0	5.25 ± 0.503	9.58	105	4.82 ± 0.552	11.5	96.4	5.11 ± 0.319	6.24	102
	15	13.1 ± 0.577	4.40	87.5	14.0 ± 1.03	7.39	93.2	13.8 ± 0.690	5.00	92.0	14.9 ± 0.487	3.27	99.3
	200	169 ± 21.7	12.8	84.5	194 ± 10.7	5.51	96.8	186 ± 13.4	7.18	93.1	202 ± 20.9	10.3	101
	1500	1418 ± 65.9	4.65	94.6	1453 ± 42.0	2.89	96.8	1441 ± 35.9	2.49	96.1	1545 ± 56.7	3.67	103
	4000	3890 ± 306	7.88	97.2	3686 ± 233	6.31	92.1	3861 ± 270	6.99	96.5	4173 ± 276	6.62	104

Table 7.3: continued

Microdialysate													
Voriconazole	4	4.09 ± 0.262	6.41	102	4.39 ± 0.769	17.5	110	3.76 ± 0.123	3.26	94.1	3.71 ± 0.198	5.34	92.8
	8	7.72 ± 0.243	3.15	96.5	7.95 ± 0.650	8.18	99.4	7.76 ± 0.509	6.57	97.0	7.43 ± 0.393	5.29	92.9
	150	139 ± 9.07	6.54	92.5	143 ± 6.76	4.73	95.3	132 ± 5.45	4.13	88.0	147 ± 5.93	4.04	97.9
	1200	1199 ± 62.4	5.20	100	1226 ± 77.0	6.28	102	1169 ± 20.9	1.79	97.4	1227 ± 29.1	2.37	102
	3000	3192 ± 180	5.62	106	3172 ± 105	3.31	106	2893 ± 275	9.49	96.4	3193 ± 143	4.47	106
Voriconazole *N*-oxide	4	4.17 ± 0.408	9.77	104	4.36 ± 0.279	6.41	109	4.60 ± 0.523	11.4	115	3.95 ± 0.606	15.3	98.8
	8	8.61 ± 0.611	7.10	108	8.62 ± 0.442	5.13	108	8.62 ± 0.594	6.89	108	7.46 ± 0.788	10.6	93.3
	150	159 ± 8.05	5.08	106	156 ± 3.31	2.12	104	145 ± 7.75	5.33	97.0	146 ± 10.62	7.27	97.4
	1200	1241 ± 58.4	4.70	103	1263 ± 78.7	6.23	105	1128 ± 41.0	3.63	94.0	1195 ± 63.4	5.30	99.6
	3000	3121 ± 165	5.27	104	3337 ± 236	7.07	111	2932 ± 197	6.73	97.7	2916 ± 207	7.09	97.2

$C_{Nom,}$ nominal concentration; CV, coefficient of variation; X_{mean}±SD: arithmetic mean ± standard deviation

Table 7.4: Michaelis-Menten kinetic parameters for the marker reactions of CYP2C19, CYP2C9 and CYP3A4 in human liver microsomes (HLM) and recombinant human CYP2C19, CYP2C9 and CYP3A4 (rhCYP).

Enzyme	**Reaction**	**Enzy-matic system**	**K_M (95% CI) [µM]**	**$V_{max,HLM}$ (95% CI) [pmol/min/mg] or $V_{max,rhCYP}$ (95% CI) [pmol/min/pmol]**	**$CL_{int, HLM}$ [µL/min/mg] or $CL_{int, rhCYP}$ [µL/min/pmol]**
CYP2C19	S-mephenytoin 4-hydroxy-lation	HLM	53.0 (45.6 – 60.4)	44.7 (42.3 – 47.2)	0.845
		rhCYP 2C19	22.1 (17.2 – 27.3)	7.10 (6.59 – 7.62)	0.321
CYP2C9	Diclofenac 4-hydroxy-lation	HLM	4.15 (3.61 – 4.70)	1693 (1639 – 1746)	408
		rhCYP 2C9	2.29 (1.40 – 3.17)	13.5 (12.4 – 14.6)	5.89
CYP3A4	Midazolam 1-hydroxy-lation	HLM	4.45 (3.56 – 5.35)	559 (523 – 595)	126
		rhCYP 3A4	1.96 (1.49 – 2.44)	1.67 (1.56 – 1.78)	0.850

CI, confidence interval; CL_{int}; intrinsic clearance; CYP, cytochrome P450; K_M, Michaelis-Menten constant; V_{max}, maximum reaction velocity.

Table 7.5: Specificity of the CYP2C19, CYP2C9 and CYP3A4 inhibitors loratadine, sulfaphenazole and ketoconazole on the marker reactions of the respective enzymes (CYP2C19: 4-hydroxylation of S-mephenytoin, CYP2C9: 4-hydroxylation of diclofenac, CYP3A4: 1-hydroxylation of midazolam) determined as remaining reaction velocity compared to a control incubation without inhibitor in human liver microsomes (n=3-4). The colours illustrate the interpretation of the specificity: green, high degree of specificity; red: relevant cross-inhibition; orange: ambiguous results; see main text for further explanation.

Enzyme	**Marker reaction**	**Remaining reaction velocity in the presence of the inhibitor**		
		Loratadine, %	**Sulfaphenazole, %**	**Ketoconazole, %**
CYP2C19	S-mephenytoin 4-hydroxylation	<5.0*	77.2	92.2
CYP2C9	Diclofenac 4-hydroxylation	41.7	6.34	84.9
CYP3A4	Midazolam 1-hydroxylation	106	96.9	37.3

* 4-hydroxymephenytoin concentration below lower limit of quantification

8 Publications

Original articles

J. Schulz, R. Michelet, J.F. Joseph, M. Zeitlinger, F. Schumacher, G. Mikus, C. Kloft.
A versatile high-performance LC-MS/MS assay for the quantification of voriconazole and its *N*-oxide metabolite in small sample volumes of multiple human matrices for biomedical applications
J. Pharm. Biomed. Anal. 210: 114551 (2022).
doi: 10.1016/j.jpba.2021.114551

J. Schulz, A. Thomas, A. Saleh, G. Mikus, C. Kloft*, R. Michelet*.
Towards the elucidation of the pharmacokinetics of voriconazole: a quantitative characterization of its metabolism
Pharmaceutics 14: 477 (2022).
doi: 10.3390/pharmaceutics14030477
* shared senior authorship

J. Schulz, R. Michelet, M. Zeitlinger, G. Mikus, C. Kloft.
Microdialysis of drug and drug metabolite: a comprehensive *in vitro* analysis for voriconazole and voriconazole *N*-oxide
Accepted at Pharmaceutical Research

J. Schulz, R. Michelet, M. Zeitlinger, G. Mikus, C. Kloft.
Microdialysis of voriconazole and its *N*-oxide metabolite: amalgamating knowledge of distribution and metabolism processes in humans
Under review at Pharmaceutical Research

Review articles

J. Schulz, F. Kluwe, G. Mikus, R. Michelet, C. Kloft.
Novel insights into the complex pharmacokinetics of voriconazole: a review of its metabolism.
Drug Metab. Rev. 51: 247-265 (2019).
doi: 10.1080/03602532.2019.1632888

Conference abstracts (oral/poster)

J. Schulz, A. Thomas, G. Mikus, R. Michelet, C. Kloft.
Voriconazole metabolites can be clinically relevant: an investigation on their *in vitro* inhibitory potential on human CYP3A4, CYP2C9 and CYP2C19
Annual Meeting of the Deutsche Pharmazeutische Gesellschaft (DPhG), Virtual, 28 September-01 October 2021
(poster presentation)

J. Schulz, R. Michelet, F. Kluwe, C. Kirbs, F. Drescher, G. Mikus, M. Zeitlinger, C. Kloft.
Towards the elucidation of the complex pharmacokinetics of voriconazole: simultaneous microdialysis of drug and drug metabolite in humans
31st European Congress of Clinical Microbiology and Infectious Diseases (ECCMID), Virtual, 09-12 July 2021
(oral presentation)

J. Schulz, R. Michelet, F. Kluwe, C. Kloft.
Clinical feasibility of simultaneous microdialysis of voriconazole and its *N*-oxide metabolite at target site demonstrated by *in vitro* investigations
Young Investigator session of the annual meeting of the International Society of Anti-Infective Pharmacology (ISAP), Virtual, 18 September 2020.
(oral presentation)

J. Schulz, R. Michelet, F. Kluwe, C. Kloft.
Clinical feasibility of simultaneous microdialysis of voriconazole and its *N*-oxide metabolite at target site demonstrated by *in vitro* investigations
30th European Congress of Clinical Microbiology and Infectious Diseases (ECCMID),
Paris, France, 18-21 April 2020. Abstract book, 848, (2020).
(abstract only, cancelled due to COVID-19 pandemic)

F. Kluwe, **J. Schulz**, W. Huisinga, M. Zeitlinger, G. Mikus, R. Michelet, C.Kloft.
Amalgamating knowledge from translational bottom-up and top-down approaches to elucidate complex pharmacokinetics: The voriconazole example
3rd World Conference on Pharmacometrics (WCoP), Cape Town, South-Africa, 06-09 April 2020.
CPT: Pharmacometrics Syst. Pharmacol. 9: S9-S26 (2020).
doi: 10.1002/psp4.12497

J. Schulz, J.F. Joseph, C. Kloft.
Bioanalytical method validation for the quantification of voriconazole in microdialysate: An assay for small sample volumes and low concentrations.
Annual Meeting of the Deutsche Pharmazeutische Gesellschaft (DPhG), Heidelberg, Germany, 01-04 September 2019.
https://www.dphg.de/fileadmin/downloads/DPhG-ConferenceBook_2019.pdf, 131, (2019).

Further publications outside the topic of this dissertation

M. Petersen, **J. Schulz**, N. Zimmermann, J. Seeger, S. Gehrke-Beck, W. Herrmann, R. Behrend, C. Czimmek, N. Lauterbach, I. Siebenbrodt, A. Pevzner, U. Mueller, H. Peters, M.Schulz, C. Kloft.
Interprofessional Education – the First Step to Interprofessional Collaboration between Pharmacists and Physicians?
Annual Meeting of the Deutsche Pharmazeutische Gesellschaft (DPhG), Virtual, 28 September-01 October 2021

S. Gehrke-Beck, W. Herrmann, J. Seeger, **J. Schulz**, N. Zimmermann, C. Czimmek, A. Pevzner, M. Petersen, I. Siebenbrodt, H. Peters, C. Kloft, M. Schulz, R. Behrend.
Wieviel interprofessioneller Austausch kann unter Pandemiebedingungen in einem Lehr-/Lernprojekt erreicht werden?
55. Kongress für Allgemeinmedizin und Familienmedizin (DEGAM), Greifswald, Germany 15-17 September 2021

J. Seeger, **J. Schulz**. Patienten im Fokus. Klinische Pharmazie weitergedacht.
Deutsche Apotheker Zeitung 43: 86 (2020).

9 Curriculum vitae

According to the EU General Data Protection Regulation (GDPR) the curriculum vitae has been removed from the electronic version.